Exploring Localized Relationships Between Age-Related Bone Loss and Cortical Expansion in Diaphyseal Bone

A Dissertation Presented for the
Doctor of Philosophy
Degree
The University of Tennessee, Knoxville

Gregory James Wehrman
August 2023

ACKNOWLEDGEMENTS

I am forever grateful for the generosity of those who participated in this study, without whom this research would not be possible. I would also like to thank my doctoral committee and all the educators who have helped me get to this point. Thank you to my loving and supportive family, friends, and partner for being there for me throughout this process. Finally, thank you to the National Science Foundation for providing funding for this research through their Doctoral Dissertation Research Improvement Grant.

ABSTRACT

Humans experience age-related changes to bone geometry and material properties that impact bone strength and increase the risk of fracture. At a macrostructural level, resorption along the endosteal surface and deposition on the periosteal surface of cortical cross-sections result in expanded cross-sectional diameters and decreased cortical thickness. Additionally, intracortical porosity increases with age through a net-resorptive dysregulation of the remodeling process. The processes implicated in age-related bone loss are considered to be largely systemic, such as hormonal decline, accumulation of oxidative stress, and cellular senescence. However, previous research has demonstrated that age-related changes to bone geometry and bone mineral density (BMD) occur non-uniformly at different sites throughout the skeleton, suggesting that local factors (e.g. mechanical loading, soft tissue interactions) may mediate otherwise systemic aging processes.

This dissertation adopts a modified "whole bone" approach to assess local variation in age-related differences in cortical bone both within and between cross-sectional slices of the tibia, radius, and ulna within a living sample of adults between 40-80 years of age. Cross-sections at 20%, 35%, 50%, and 65% element length were examined. Within each cross-section, eight endosteal and periosteal semi-landmarks are established along anatomical directions to assess local variation in age-related cortical bone expansion. Corresponding sectors of the cross-section were then sampled for average cortical BMD to measure microstructural differences with age. Finally, the relationship between age-related differences in cortical bone macrostructure and microstructure were assessed using correlation analysis.

Results indicate that age-related differences in both cortical expansion and cortical BMD decline exhibit local variation both within and between cross-sections. Furthermore, the patterns

of local variation are not easily explained by biomechanical expectations, suggesting that age-related processes influencing cortical bone macro- and microstructure are multifactorial and likely overlapping. Additionally, the correlations between age-related differences in cortical geometry and those of cortical BMD are moderate at best, suggesting that these processes are not strongly coupled with age. Importantly, these results illustrate that aging does not affect bone uniformly, which has implications for both clinical approaches to bone loss and anthropological interpretations of the aging experience of past groups.

TABLE OF CONTENTS

LIST OF TABLES

LIST OF FIGURES

CHAPTER 1: INTRODUCTION, BACKGROUND, AND RESEARCH QUESTIONS

Decades of research on cortical bone geometry and porosity in limb long bones has revealed that patterns of changes in these properties coincide with sex, age, and habitual mechanical loading (Ruff and Hayes, 1982, 1983; Lazenby, 1986; McCalden et al., 1993; Feik et al., 2000; Gosman et al., 2011; Ireland et al., 2014; Razi et al., 2015; Vilayphiou et al., 2016; Javaheri and Pitsillides, 2019; Weaver and Peacock, 2019; Carina et al., 2020; Wang et al., 2022). As I review in this chapter, the information gleaned from experimental studies with model organisms and from clinical and nonclinical studies of humans, both living and deceased, has given researchers a general model of how cortical bone mass will change into older adulthood. However, much remains unknown about the relationship of changes in cortical bone properties in the limb long bones as individuals age.

Following acquisition of peak bone mass, humans gradually lose bone with advanced adult age. This loss is typically measured as bone mineral density (BMD), which accounts for the mass of bone in a region of bone divided by the region's area/volume. While BMD decline is sufficient to clinically assess bone health and fracture risk clinically (Melton et al., 1992; Melton et al., 1998; Lorentzon et al., 2021), bone loss occurs through several mechanisms throughout the skeleton. On a macro scale, cortical bone undergoes a geometric shift where bone loss on the endosteal surface is accompanied by addition of bone on the periosteal surface (Ruff and Hayes, 1982; Beck et al., 2001). Proportionally, age-related endosteal loss is greater than periosteal deposition, resulting in a diaphyseal cross-section that becomes wider, but with thinner walls and decreased cortical area, with age. From a biomechanical perspective, this reconfiguration of cortical bone geometry bolsters a bone's resistance to bending/torsional stress from loading because bone mass is distributed farther from the neutral axis. As a result, this shape change has

been characterized as having a compensatory relationship with age-related decline in bone mass. However, the interplay between geometric (cortical bone expansion) and microstructural changes (BMD loss) is not well characterized.

Therefore, this dissertation explores the relationship between age-related changes in cortical geometry and cortical BMD decline in long bones of the upper and lower limbs in living modern humans. Specifically, local variation in age-related changes of cortical bone expansion and BMD decline is assessed within and between cross-sections along the length of the tibia, radius, and ulna. Furthermore, given a proposed compensatory relationship between these age-related processes, I ask whether these changes locally correlate with each other.

The scope of this dissertation has implications for both the current understanding of bone loss in modern populations and the anthropological interpretation of past groups. Age-related bone loss, particularly among biological females, is a public health concern as it is predictive of fracture risk among elderly individuals (Kanis, 2002). Since bone fracture in advanced age can significantly impair mobility, considerable research has focused the etiology of bone loss with a goal of treatment and prevention (Percival, 1999; Kanis, 2002; Johnell and Kanis, 2005; Cauley, 2017; Khosla and Hofbauer, 2017). Additionally, biological anthropologists study skeletal remains of past groups to reconstruct aspects of their life histories. These interpretations must be grounded in a thorough understanding of skeletal biology across a lifetime, which requires an appreciation of the way in which age-related processes manifest in bone at both the macrostructural and microstructural level, and the interplay between these scales.

Before outlining the questions and hypotheses to be assessed in this research, I provide a review of the state of knowledge about cortical bone properties and factors that affect them in this chapter. A fundamental understanding of the way in which mechanical loading and other

factors influence diaphyseal shape of long bones is necessary to interpret bone structure. After discussing these, I focus on age-related changes in bone, both at the microscopic and macroscopic scales.

Bone Biomechanics

One of the principal roles of bone is its ability to withstand loads from weight-bearing, locomotion, injury, and the other myriad actions performed throughout an individual's life. For bone to successfully endure the demands placed on it, it must be both stiff enough to maintain its shape and elastic enough to undergo strain during loading. This balance is accomplished partly by the composite histological arrangement of bone, with the mineral hydroxyapatite providing stiffness and collagen fibers providing elasticity. At a larger scale, bone is configured into structurally distinct arrangements of cortical and trabecular bone. Cortical bone, forming the outer shell of an element, offers considerable stiffness given its compact arrangement of layers of bone called lamellae. Trabecular bone, meanwhile, is a network of interconnected bony struts and plates that traverse the marrow space, fill the subcortical space in epiphyses, and serve an important role in distributing loads of varying directions throughout the bone. Cortical and trabecular bone are primarily distinguished by their porosity, with cortical bone being around 5-15% and trabecular bone being about 40-95% porous (Martin et al., 2015; Morgan et al. 2018). Both types of bone, cortical and trabecular, offer unique mechanical properties for load bearing, however this dissertation will focus primarily on those of cortical bone.

Cross-sectional properties of cortical bone are assessed by adapting Euler-Bernoulli beam theory to model bones as hollow cylinders acting as levers and cantilevers (Martin et al., 2015). Through this approach, mechanical properties can be estimated through analysis of a bone's

cross-sectional geometry in relation to bone length and body mass (Ruff, 2000). Cross-sectional mechanical properties reflect the ability of a long bone to withstand the different loading patterns throughout life. Bones experience multiple loading modalities, with the main types being tension, compression, bending, and torsion. Tension occurs when bone is loaded along its longitudinal axis where the force directions are opposite and away from one another, going toward the proximal and distal ends of the bone respectively, while compression occurs when these forces travel towards each other along the same axis. Bending stress involves an off-axis load where one aspect of the bone is in tension and the opposite is in compression (Currey, 2006). When bone is loaded perpendicular to its longitudinal axis, it experiences shearing forces. One example of shearing is when bone is under torsion, when the ends of a bone are rotated in the opposite direction of each other. Human bones undergo a combination of all these modes of loading in varying degrees and directions, though they primarily experience compression and bending (Currey, 2012).

Loading results in stress, which is the force per unit of area (Martin et al., 2015). When bone is put under stress, it experiences strain, defined as the deformation or change of bone's shape under loading relative to its unloaded geometry (Martin et al., 2015). For example, a bone will shorten and widen in compression, while in tension it will elongate and narrow. The loading required to produce a given amount of strain is referred to as stiffness or rigidity, while the amount of loading a bone can withstand before failure (fracture) is referred to generally as strength (Martin et al., 2015; Currey, 2006).

As mentioned before, properties related to bone stiffness and strength can be estimated from cross-sectional geometry. Cortical area, or the area of a cross-section occupied by cortical bone, is a cross-sectional property that estimates the ability of a bone to withstand compressive and

tensile stress. Thus, low cortical area is associated with a higher buckling ratio, or its likelihood of failure under compressive loads (Beck et al., 2001). Cortical area and medullary area are summed in the measurement of total cross-sectional area; all three are typically reported. Another important set of cross-sectional properties in bone biomechanics are moments of area, which quantify the distribution of bone mass situated around a neutral axis. This neutral axis is thought to represent the neutral axis around which bending stresses (i.e., compressive and tensile loading) are thought to be zero (Currey, 2006; but see Pearson and Lieberman, 2004). These include the second moment of area (I) and polar moment of area (J), which describe resistance to bending stress in non-circular cross-sections. Second moments of area are axis-dependent and are typically measured along a bone's major (I_{max}), minor (I_{min}), anteroposterior (I_y), and mediolateral axes (I_x).

Muscle and joint reaction forces are the primary sources of loading experienced by bone (Currey, 2002; Martin et al., 2015; Wallace, 2019). Many muscle attachments are arranged such that the insertion site on the bone under movement is close to the axis of rotation, the joint where movement is taking place (Martin et al., 2015). This joint arrangement presents a mechanical disadvantage, where muscle/joint reaction forces are generally many times higher than those resulting from the load being moved (either the weight of the element or an object being moved) (Martin et al., 2015). Martin and colleagues (2015) explain that this arrangement, while mechanically disadvantageous, means that a short muscle contraction length can result in a proportionally large range of motion. Since muscle forces are the primary forces applied to bone (Martin et al., 2015), muscle strength is highly correlated with the strength of bone itself.

Bone Microstructure and Material Properties

Bone strength is a product of its geometric arrangement as well as its material properties, or those mechanical properties that are unrelated to shape and size. Material properties of bone refer to the microstructural arrangement of bone at a tissue level, its density, and its brittleness or elasticity. Cortical bone is arranged into structural units called osteons or Haversian systems which run approximately along the longitudinal axis of the bone. Osteons are made up of concentric layers of bone called lamellae that surround a Haversian canal, a channel occupied by capillaries for blood supply. The outermost circumference of a given osteon is bounded by a cement line, which is composed of a highly mineralized, low-collagen substance that separates the inner osteon from surrounding bone matrix (Skedros et al., 2005). Deep to the cement line, osteonal lamellae are arranged such that the collagen fibers and neighboring hydroxyapatite crystals of one lamella are oriented in a different direction than those of neighboring layers (Martin et al., 2015). Ascenzi and Bonucci (1967) classified three general osteon types based on collagen fiber direction patterns: transverse, longitudinal, or alternating, where fibers are roughly perpendicular across adjacent lamellar layers. This variable arrangement of lamellar direction makes bone anisotropic, that is having variable mechanical properties along different axes. Generally, cortical bone is stronger along the longitudinal axis of a skeletal element than transversely under both tension and compression, which corresponds to the average orientation of collagen and mineral in osteons (Reilly and Burstein, 1975; Adel-Wahab, 2011). Cortical bone's strength in compression is well-suited, given that loading of long bones is primarily in compression and bending (Currey, 2012).

The geometric configuration of bone throughout life is developed through modeling, where addition by osteoblasts and resorption by osteoclasts is uncoupled to favor a net addition of bone

along one surface and a net removal of bone on another (Burr and Allen, 2019). The new bone produced through modeling is referred to as primary bone (Martin et al., 2015). Modeling primarily occurs during growth to establish adult geometric configuration and to a lesser extent in adulthood to adapt to novel loading patterns (Goldman et al., 2009; Gosman et al., 2013). Maintenance of bone, on the other hand, is carried out through a process called remodeling where the actions of osteoblasts and osteoclasts, acting with bone lining cells as a basic multicellular unit (BMU), are tightly coordinated so that old primary bone is removed and new bone, called secondary bone, is deposited in roughly equal amounts within the same spaces. Briefly, remodeling consists of an activation phase where osteoclasts are recruited to a certain location to initiate bone resorption (Burr and Allen, 2019). Osteoclasts tunnel through primary bone in a direction approximately along the bone's longitudinal axis and are followed by osteoblasts, which gradually add layers of new bone through secretion of osteoid, or unmineralized bone matrix, to replace what was removed. Throughout the process of osteoid deposition and mineralization, these osteoblasts either die or become embedded in the surrounding bony matrix, where they mature as osteocytes. Over time, repetitive episodes of remodeling result in a tissue that is made up of majority secondary bone.

Remodeling introduces two unique mechanical properties to bone tissue. First, the newly deposited bone is inherently less mineralized than the primary bone it replaces, at least for a time (Currey, 2012). Mineralization of osteoid is hypothesized to occur in two phases. The primary phase of mineralization occurs about 5-10 days after osteoid is deposited by a osteoblasts in a BMU, while the secondary mineralization takes considerably longer over the span of 24-30 months (Boivin et al., 2009). Intuitively, bone rigidity is greater when bone is more completely mineralized compared to relatively new, partially mineralized bone (Follet et al., 2004). Second,

since the process of remodeling involves creating a new Haversian canal, (or widening existing ones; see Andreasen et al., 2018), this process will result in increased porosity of the bone tissue. High rates of remodeling, such as during growth and menopause, are associated with greater osteonal density (Ramchand and Seeman, 2018). Cortical porosity, along with the medullary space, provides a lightness to bone that makes it easier to move as well as more metabolically efficient to maintain (Martin et al., 2015). However, increased porosity can also negatively affect bone strength (McCalden et al., 1996; Vilayphiou et al., 2016)

While this dissertation is focused on cortical bone, it would be remiss to not briefly consider the mechanical properties of trabecular bone. Trabecular bone is most concentrated in the ends of long bones and irregularly shaped bones like the vertebrae and pelvis. The mechanical properties of trabecular bone can be quite variable because it exhibits considerable heterogeneity from location to location, even within the same general region of a bone (Keaveny et al., 2001). A major determinant of the mechanical properties of trabecular bone is apparent density (Martin et al., 2015; Keaveny et al., 2001). Apparent density is a product of the tissue density of trabecular bone and its bone volume fraction, or the proportion of bone in a volume. Additionally, trabecular bone exhibits anisotropy similarly to cortical bone, though at variable orientations based on the local trabecular arrangement.

Bone Functional Adaptation

Bone can adapt to typical loading patterns by responding with changes in its geometry and material properties. This adaptive capability, or bone functional adaptation (BFA), was first popularized as Wolff's law and later refined as Frost's mechanostat model (Frost, 1987; Ruff et al., 2006). The mechanostat model implicates strain as the primary signal to which bone adapts

(Frost, 1987, 2003). Above a certain strain threshold, new bone will be added at locations dependent on loading patterns so that the skeletal element will be more geometrically suited withstand similar loads in the future (Frost, 1987, 2003). Below a lower strain threshold, such as in disuse, bone is removed for better metabolic efficiency. In between these strain thresholds, there is a range of typical strain where bone is kept in homeostasis, with equal amounts being removed and replaced through remodeling. Somewhat complicating Frost's strain-based model is evidence that bone responds to loading signals other than strain magnitude, including strain rate, strain duration, number of loading cycles, and rest periods between loading (Skerry, 2006; Gardinier, 2021). Recent studies have also found that remodeling responses to strain across entire skeletal elements are nonlinear, where local functional adaptation occurs in response to strength requirements across the entire element and are not restricted to local strains (Javaheri et al., 2020). Despite these nuances, research using human subjects and animal models have broadly confirmed Frost's mechanostat or some variant of it (Robling et al., 2008; Nadell and Shaw, 2016; Birkhold et al., 2017; Yang et al., 2019). Thus, the geometry of bone is partly a product of its local and global loading history; other contributing factors include genetic background (Wallace et al., 2012; Agostini et al., 2018), sex (Duan et al., 2003), and body size (Ruff, 2000).

The mechanosensory mechanism(s) responsible for the ability of bone to detect strain from loading are still somewhat unclear, though osteocytes are generally accepted as the primary mechanosensory cell (Tatsumi et al., 2007; Hughes and Petit, 2010). Osteocytes are quiescent former osteoblasts that are embedded within the bone matrix. Situated in depressions called lacunae, osteocytes extend long dendritic processes through narrow fluid-filled channels called canaliculi which meet those of other osteocytes, creating an interconnected network throughout

the bone tissue. When a bone experiences load-induced strain, fluid shear stress occurs as canalicular fluid moves from areas of compression to areas of tension within the bone (Hughes and Petit, 2010). This shear stress causes perturbations along the plasma membrane of the osteocyte, which have been shown to initiate waves of increased intracellular calcium in the wounded cell (Yu et al., 2018). Calcium oscillations are also observable in neighboring osteocytes, which may indicate the amplification of the mechanosensory signal (Yu et al., 2018). These changes in intracellular calcium in osteocytes are associated with the release of several paracrine factors that influence osteoblasts and their precursors, like nitrous oxide and osteoprotegerin (OPG) (Hughes and Petit, 2010). Recent research has demonstrated that fluid shear stress is also associated with the release of extracellular vesicles from osteocytes that are capable of delivering molecular signals to other bone cells (Morrell et al., 2018). Furthermore, it appears that osteoblast progenitors also respond directly to fluid shear stress by differentiating into osteoblasts (Yan et al., 2016), while monocytes respond with reduced osteoclastogenesis (Kim et al., 2006; Ma et al., 2020).

Bone is most responsive to mechanical signals during adolescence and early adulthood (Rubin et al., 1992; Lieberman et al., 2003). During this time, a combination of elevated sex and growth hormones and generally greater levels of physical activity are responsible for the accrual of peak bone mass. Following skeletal maturity, however, bone geometry becomes less adaptive to loading (Lieberman et al., 2003; Javaheri and Pitsillides, 2019). There are several hypotheses as to why bone becomes less responsive to mechanical signals. At the cellular level, osteocyte density and sensitivity to mechanical signaling decreases with age, effectively impairing the skeletal mechanosensory system (Hughes and Petit, 2010; Hemmatian et al., 2017). Lanyon and Skeery (2001) posited a mechanostat-based explanation in which osteogenic strain thresholds

increase with age. Under this framework, greater mechanical loading is required to achieve geometric adaptation and maintenance of adapted shape compared to that required at younger ages, effectively making it more likely that bone is in a resorptive state during customary loading patterns from daily activity (Lanyon and Skeery, 2001). Razi and colleagues (2015) challenged the concept of age-related higher strain thresholds, instead suggesting that formation and resorption become dysregulated in advanced age. Their research showed that among mice, a transition range exists between low and high strains where bone formation and resorption activity overlaps (Razi et al., 2015). Younger mice have a narrower transition range, and strain-induced formation and resorption are separated, while older mice have a much wider transition range, suggesting that formation/resorption are not as tightly coupled during remodeling with age (Razi et al., 2015).

While bone is less plastic in response to loading with age, continually elevated levels of physical activity during aging maintain adapted cortical geometries acquired earlier in life (Korhonen et al., 2012; Warden et al., 2014; Biver et al., 2016). Warden and colleagues (2014) found that former minor league baseball players who continued training post-retirement experienced less BMD decline and endosteal resorption than their detrained counterparts. Similar results were found among sprinters who continued competition into advanced age (Korhonen et al., 2012). The preservative effects of continuous mechanical loading into advanced age are also observed through occupational activity, with individuals engaged in heavy-load occupations (e.g. farm workers, lumberjack) exhibiting reduced expansion of the medullary space and greater measures of bone strength compared to light-load occupations (e.g. office workers). Wilson and colleagues (2020) similarly found greater cross-sectional properties in the first metatarsal among rural medieval skeletons compared to an urban post-medieval sample, attributing this difference

to greater loading from agricultural work among the rural sample. Therefore, while capacity for geometric adaptation to loading is greatest at younger ages, bone is still responsive to loading in advanced age, though primarily through maintenance.

Age-Related Changes in Bone Mineral Density

Following skeletal maturity, humans experience a loss of bone mass that continues into advanced age. Bone loss is typically measured as a decline in bone mineral density (BMD), or the mass of bone divided by its area (g/cm^2) or volume (g/cm^3). After accrual of peak bone mass following puberty, young adulthood is characterized by a plateau period where mass is largely maintained (Frost, 1997; Agarwal, 2021). However, BMD begins to decline in both sexes during the early/mid-thirties and continues to decrease throughout life (Frost, 1997; Khosla, 2012). Females experience a marked decline in BMD during menopause due to the sudden decline of estrogen, while males experience a more gradual loss around the mid-sixties. Initial bone loss is diagnosed as osteopenia, and pronounced loss is categorized as osteoporosis, which is associated with increased risk of fragility fractures from routine activities.

For diagnostic purposes, BMD as a measure of bone mass is effective in predicting fracture risk (e.g., Melton et al., 1992; Melton et al., 1998; Lorentzon et al., 2021). Measures of BMD are typically evaluated using dual-energy X-ray absorptiometry (DEXA), a preferred method of BMD assessment that controls for variable soft tissue density between individuals. BMD values are then quantified as T-scores, which measure an individual's BMD against that of a 25–30-year-old healthy individual of the same sex and race, and as Z-scores which measure an individual's BMD against that of an age-matched peer. T-scores are used to diagnose osteopenia, defined as having a T-score between -1 and -2.5, and osteoporosis, defined as a T-score below -

2.5. While clinically useful, BMD is limited in that it is a coarse measure of bone mass that encompasses several different mechanisms for bone loss without distinguishing their relative contributions.

Regional variation in BMD declines have been observed, particularly at clinically relevant sites that are prone to fragility fractures like the lumbar vertebrae, femoral neck, and distal radius (Riggs et al, 2004). Initial declines of BMD are largely due to a loss of trabecular bone in the axial skeleton, such as vertebral bodies, and can be observed as early as the third decade (Riggs et al., 2004; Gosman et al., 2011; Khosla, 2012). Cortical bone, on the other hand, undergoes age-related changes in BMD comparatively later in life due to geometric changes that will be discussed in more depth below (Riggs et al., 2004; Nicks et al., 2012). Therefore, regional differences in the timing and rate of BMD decline are likely related in part to the differing proportions of trabecular to cortical bone between regions.

Another mechanism of bone loss encompassed by BMD decline is increased porosity in cortical bone. Age-related increases in intracortical cortical porosity occur due to increased cortical remodeling that favors resorption, resulting in in a greater number of Haversian canals with wider diameters (Gosman et al., 2011; Macdonald et al., 2011). Since greater amounts of bone are being removed than replaced, a developing osteon will have greater overall diameter of the cement line from increased osteoclastic activity as well as relatively incomplete closure of the resorption canal due to disrupted osteoblastic activity. Additionally, slower rates of remodeling lead to a longer duration of the process of mineralization, which further reduces the rigidity of bone. Finally, these resorption canals often merge to form even larger pores in the cortical bone, particularly along the endosteal surface where porosity can compound to the point

that the cortical bone is said to have “trabecularized”, adopting a structure akin to trabecular bone (Andreasen et al., 2020).

Conventional clinical methods assessing BMD, like DEXA, do not measure the true, volumetric density of bone. Instead, these methods are measuring areal BMD for either a specific region or the whole body (Golding, 2022). A reliance on area-specific BMD for assessment of bone loss is problematic for several reasons. First, since typical BMD imaging modalities generate two-dimensional superimposed images, like in X-ray, there is no way to accurately assess geometric changes associated with bone loss. Instead, areal BMD measurements are coarsely quantifying the overall mass of bone present at a given time. Beck and colleagues (1990) attempted to approximate bone geometry from DEXA scans of the proximal femur by developing a Hip Structural Analysis (HSA), which used the two-dimensional anteroposterior profile of the bone to infer cortical thickness and medullary area. However, the HSA method assumes circularity of the inferred cross-section, making it difficult to apply meaningfully in areas with more irregularly shaped cross-sections, like the tibial shaft. Additionally, medullary space is included in conventional BMD assessment imaging, potentially obscuring the true density values of the surrounding bone. Finally, as discussed above, loss of bone mass can be caused by several processes, including the thinning of trabecular bone, increased porosity from elevated remodeling rates, age-related resorption along the endosteal surface, or a transient period of partially mineralized bone. Thus, there is an ongoing unanswered question regarding how to apply a somewhat general assessment of bone loss to specific, localized concerns for fracture risk, such as in the femoral neck or the lumbar vertebrae.

An alternative to DEXA is peripheral quantitative computed tomography (pQCT), a smaller computed tomography (CT) scanner meant for peripheral structures like the limbs. As a form of

computed tomography, pQCT allows for three-dimensional visualization of bone geometry, distinguishes between trabecular and cortical bone, and accurately assesses volumetric BMD (Stagi et al., 2016). Standard pQCT software also includes analysis of muscle/bone ratio and cross-sectional properties such as cortical area, medullary area, and second moments of area. The radiation dose of a single pQCT scan (<0.001 mSV; Stratec Medizintechnik) is low compared to other CT modalities because the regions of interest (i.e., limbs) are not close to radiosensitive tissues in the thorax, abdomen, and pelvis (Damilakis et al., 2010). For these reasons, pQCT has gained popularity as a way to assess bone geometry and microarchitecture, particularly in pediatric and young adult populations (Cheng et al., 2009; Stagi et al., 2014) and to a lesser extent older populations (Lauretani et al, 2008).

Mechanisms of Age-Related Bone Loss

Age-related bone loss is related to the co-occurrence of a variety of interrelated factors, including sex hormone decline, loss of muscle strength, accumulation of oxidative stress, and cellular senescence. Much of the research on molecular and cellular processes of bone, however, has been conducted on animal models, primarily mice (cf., Carina et al., 2020). Mice are not humans, and there are several differences that prevent direct translation of the results from non-human research models to human anatomy and physiology. Despite genomic similarities between mice and humans, these two species diverged from a common ancestor some 85 million years ago and have since undergone distinct evolutionary histories (Springer and Murphy, 2007; Perlman, 2016). A major difference is body size, which is highly correlated with metabolic rate and life history (Perlman, 2016). Size difference between these two species is particularly relevant to bone biomechanics as it is an important determinant of the typical mechanical loading

a body experiences. Specifically, body size influences the ability to resist gravity as well as limb segment proportions (Beiwener, 1989; Schmidt and Fisher, 2008). Smaller species, like mice, tend to maintain more crouched, flexed limb configurations (Beiwener, 1989). Body mass and gravitational forces increase proportionally, and species tend to adopt a more extended limb configuration to maximize mechanical advantages of their moment arms (Schmidt and Fisher, 2008). In addition, while estrogen production can be artificially reduced in mouse models, mice do not naturally experience menopause and thus must be broadly simulated (Diaz Brinton, 2012). Thus, aging in mice does not occur in a process similar to humans. Therefore, while mice and other animal model research undoubtedly provides insight into biological processes that would be logistically and ethically fraught if applied to humans, species differences preclude direct translation of results to humans.

Given the rapid bone loss associated with menopause, estrogen has been a well-established relationship to bone mass and its decline (Carina et al., 2020). In fact, estrogen levels are the strongest hormonal predictor of BMD in both sexes, in part due to testosterone's aromatization into estrogen (Ho-Pham et al., 2013; Woo et al., 2012). Estrogen exerts its effects primarily on osteoclasts both directly and indirectly through other cell types (Manolagas et al., 2013). Direct action of estrogen on osteoclasts include inhibiting osteoclast differentiation from monocyte precursor cells, reducing resorptive activity, and promoting osteoclast apoptosis (Manolagas et al., 2013; Chen et al., 2014). Osteoclast differentiation has been shown to be suppressed by estrogen-induced activation of calcium channel mediators which limit the oscillations of intracellular calcium necessary for osteoclastogenesis in monocytes (Chen et al., 2014).

However, deletion of estrogen receptor-α (ERα) in osteoclasts had no effect on cortical bone mass in mice, which suggests that the cortical bone loss associated with estrogen decline is a

result of its actions on other cells (Manolagas et al., 2013). For example, estrogen appears to exert a dose-dependent suppressive effect on osteoclast differentiation via upregulation of regulatory T-cells, known to inhibit osteoclastogensis (Luo et al., 2011). Estrogen also interacts with other bone cells to further suppress osteoclast differentiation and activation. Osteoprotegerin (OPG) is a decoy ligand produced by osteoblasts and osteocytes that blocks RANKL from binding with its receptor protein, RANK. Estrogen increases OPG expression in osteoblasts (Bord et al., 2003) and osteocytes (Allison et al., 2020), providing another mechanism for limiting osteoclast differentiation. Additional evidence supports the idea that estrogen inhibits RANKL expression from bone lining cells which are thought to be involved in the activation stage of remodeling, though the mechanism by which estrogen-mediated RANKL suppression occurs is unclear (Streicher et al., 2017). Finally, estrogen's reaction with ERα in osteoblast progenitor cells enhances Wnt signalling, which promotes proliferation and differentiation of periosteal osteoblasts (Almeida et al., 2012).

Aside from their relation to estrogens through aromatization, androgens also exert protective effects on bone mass and are responsible for the accrual and expansion of periosteal bone among males during growth. Conversely, bone loss is associated with instances of androgen deficiency, for example in male hypogonadism or during androgen deprivation therapy for prostate cancer (Chen et al., 2019). Androgens' direct actions are primarily on cells of the osteoblast lineage and include promotion of osteoblast differentiation, osteoid production, and mineralization (Hofbauer and Khosla, 1999). Interestingly, deletion of androgen receptors in mice osteoblasts and osteocytes resulted in trabecular bone loss but did not affect cortical bone mass (Ucer et al., 2017). Thus, it is more likely that androgens exert osteogenic effects through their recruitment of

growth factors like transcription growth factor (TGF) and insulin-like growth factors (IGF) than through direct interactions with bone cells (Manolagas et al., 2013; Ucer et al., 2017)

In addition to hormonal decline, oxidative stress is also recognized for its role in age-related bone loss. In fact, the relative contributions of ovarectomy/orchidectomy and oxidative stress to age-related bone loss are distinct from each other (Ucer et al., 2017). Oxidative stress refers to the accumulation of reactive oxidative species (ROS) or free radicals, which are unstable molecules produced primarily by mitochondria that react with other cellular molecules. High levels of oxidative stress can result in damage to cell structures like proteins, lipids, and DNA, thereby impairing normal cellular processes and potentially leading to apoptosis (Almeida and O'Brien, 2013). Cells regulate ROS accumulation through the antioxidant actions of various enzymes, growth factors, and transcription factors (Almeida and O'Brien, 2013). Damaged cellular components are removed from the cell through a process called autophagy, where they are engulfed by a lysosome, degraded, and then exported from the cell (Almeida and O'Brien, 2013). Underlining the importance of autophagic processes, ROS are elevated and whole bone effects mimic age-related bone loss when genes responsible for autophagy are deleted from mouse osteocytes (Onal et al., 2013). While all cells experience oxidative stress, mesenchymal stem cells (MSCs) and osteocytes are especially susceptible due to their longer life spans compared to osteoblasts/osteoclasts and are therefore more likely to undergo cellular senescence (Almeida and O'Brien, 2013). Cellular senescence in MSCs is associated with decreased proliferation and differentiation capabilities toward the osteoblast lineage (Stenderup et al., 2003), while senescence within osteocytes impairs mechanotransduction from loading. When cellular senescence in bone cells is targeted using pharmaceutical interventions, resorption rates and osteoclast numbers are reduced in aged mice (Farr et al., 2017).

In the context of the cellular and molecular signaling summarized above, the effect of loading, especially from muscles, may be considered. As mentioned previously, muscle mass/strength and bone mass are intimately related given that muscle forces are the primary source of mechanical stress on bone (Bettis et al., 2018; Taaffe et al., 2001). This relationship of muscle strength to bone health is illustrated in extreme scenarios of unloading such as prolonged bed rest or spaceflight-induced microgravity, where muscle and bone mass decline almost in tandem (Tanaka et al., 2017). Similarly, sarcopenia, or low muscle mass, in older adults is generally followed by osteopenia/osteoporosis (Bettis et al., 2018). Beck and colleagues (2001) found that while increases in body weight marginally improved second moments of area and cortical thickness among older women through increased loading, frail individuals had lower bone parameters than non-frail individuals. Beyond simply a reduction in muscle-derived strains with sarcopenia, there is evidence for molecular cross-talk between muscle and bone (Bettis et al., 2018). Irisin is a myokine that promotes periosteal formation, while myostatin is a myokine that promotes osteoclastogenesis (Bettis et al., 2018). Accordingly, myostatin inhibitors have been targeted as a treatment for age-related bone loss (Bettis et al., 2018). Thus, many of the effects of loading, whether from muscular loads or resistances encountered from the environment, are potentially mediated by molecular signaling and differential induction of cellular processes based on availability and dosages of the many molecules noted here.

Age-Related Changes in Bone Geometry

With age-related changes in cellular and molecular processes, cortical geometry shifts to a thinner, more expanded configuration following menopause in females and somewhat later (mid-sixties) in males (Lauretani et al., 2008). This geometric change is a result of increased

resorption on the endosteal surface and, to a lesser extent, deposition on the periosteal surface (Ruff and Hayes, 1982; Beck et al., 2001). Despite a net loss of bone mass from endosteal resorption, the redistribution of bone farther away from the central (neutral) axis bolsters bending and torsional strength. Not surprisingly, Lauretani and colleagues (2008) reported only slight declines in second moments of area with age in females while these measures were essentially stable in males. Given this mechanical aspect and its temporal concurrence with BMD decline, cortical bone expansion has been characterized as being compensatory to age-related bone loss (Beck et al., 2001; Gosman et al., 2011; Martin et al., 2015), though the relationship between geometric changes and BMD remain unclear.

The patterns of age-related geometric changes of cortical bone differ between females and males due to disparate growth trajectories and the steep decline in estrogen among females following menopause. During puberty, greater proportions of estrogen in females promote accrual and maintenance of bone along the endosteal surface while restricting periosteal deposition (Duan et al., 2003; Manolagas et al., 2013). In contrast, increased androgens during male puberty promote periosteal as well as endosteal deposition (Manolagas et al., 2013). These differing hormonal environments result in sexually dimorphic bone sizes, with males having greater bone diameters than females while cortical thickness and cortical BMD are similar between the sexes (Duan et al., 2003). As a result of this dimorphism, males enter into advanced age with a cortical geometry that is already distributed farther away from the central axis compared to females. Additionally, post-menopausal declines of estrogen in females occur more rapidly than sex hormone declines experienced by older males, resulting in a greater rate of cortical expansion characterized by increased resorption among females. This rapid decline may

account for the relative age-related decline in bending strength among females compared to males (Lauretani et al., 2007).

Radial growth of cortical bone during development does not occur uniformly as an individual is establishing locomotive patterns (Goodman et al., 2009; Cowgill et al., 2010). In early childhood, individuals are transitioning from a waddling gait to more of a traditional forward oriented gait, which is correlated with femoral midshafts that are more mediolaterally reinforced compared to adult femoral geometry (Cowgill et al., 2010). Goodman and colleagues (2009) found that cortical drift occurred in the anterolateral direction of femoral midshaft cross-sections during adolescence as the bone approached typical adult morphology. It is unclear, however, if cortical bone expansion that occurs in advanced age is similarly mediated by factors like mechanical loading. Wilson and colleagues (2020) found that cortical bone expansion was more pronounced along the mediolateral axis of first metatarsal bones from a rural medieval British sample. Geometric analysis of femoral midshafts from a modern Australian sample showed greater expansion in mediolateral diameters compared to anteroposterior diameters (Feik et al., 2000). While these studies were cross-sectional in design, they suggest that cortical bone expansion does not occur uniformly across a cross-section and is instead mediated by local factors like strain distribution.

Synthesis and Research Questions

To summarize, age-related cortical bone expansion has been considered a compensatory geometric shift in response to declines in bone mass since this rearrangement of bone mass bolsters bending and torsional strength. While local variation in cortical bone expansion within a cross-section has been observed, the relationship between cortical geometry and microstructure

remains unclear. Furthermore, under the principles of the mechanostat hypothesis and bone functional adaptation, if cortical geometry compensates for loss in microstructure, both properties are expected to covary locally. Specifically, long bones should exhibit local variation and covariation in these processes both within a single cross-section along different directional axes (e.g. anteroposterior, mediolateral), between cross-sections at different locations down the length of a bone, and between elements. This research, therefore, seeks to explore local variation of and the relationship between cortical bone expansion and age-related decline of cortical BMD in the radius, ulna, and tibia of a living sample between 40-80 years of age.

This dissertation is organized into three interrelated manuscripts that correspond to the major questions of this research. These questions are addressed within each manuscript:

Manuscript 1 (Chapter 2): *Does age-related cortical bone expansion occur uniformly across a cross-section and along the length of long bone diaphyses? If not, does local variation in this geometric reconfiguration correspond with expected mechanical loading patterns within limb elements?*

Expectations: As reviewed above, osteogenic responses to loading are largely confined to younger ages, but continual loading in advanced age promotes maintenance of bone despite systemic causative factors of bone loss. Therefore, I expect that measures characterizing cortical bone expansion (endosteal/periosteal distance from centroid, cortical thickness) will exhibit local variation with age within and between diaphyseal cross-sections of the forearm and leg. Furthermore, I expect that areas of greatest difference in endosteal and periosteal distances will correspond

with both the direction of habitual loading as well as load-sharing within the leg (between the tibia and fibula) and within the forearm (between the raidus and ulna).

Manuscript 2 (Chapter 3): *Do age-related differences in cortical BMD occur evenly within regions of a cross-section or can local variation be observed in BMD differences with respect to age both within cross-sectional slices of the diaphysis as well as among cross-sectional slices?*

Expectations: Systemic factors are implicated as mechanisms for bone loss, especially for the loss of bone mineral density and increases in porosity. However, local factors such as loading patterns mediate remodeling and may therefore mitigate the decrease of density locally within the diaphyses both within and among slice locations. Furthermore, remodeling results in temporary intracortical porosity. Given these, I expect significant local variation in cortical BMD within and between cross-sections of the tibia, radius, and ulna, and for this variation to occur nonrandomly. Lower densities should occur along the axis of habitual mechanical loading (especially in the tibia) if remodeling in response to mechanical loads leads to increased BMD loss. Alternatively, higher cortical BMD may align with directional locations within the long bones where load sharing with other elements (e.g., the fibula for the tibia) occurs.

Manuscript 3 (Chapter 4): *Do directional differences among age groups in the distribution of bone in cortical cross-sections of diaphyses correspond with age-*

related differences in cross-sectional geometric properties (such as I *and* J*)? Do age group differences in the cortical bone distribution that occur in advanced age correlate with age group differences in intracortical BMD?*

Expectations: Cortical bone distribution within cross-sections may differ among age groups, and these differences can affect cross-sectional geometric properties. However, if periosteal expansion and endosteal resorption are observed in the sample, which I expect, then age-related differences in the distribution of cortical bone may not correspond with significant differences in cross-sectional geometric properties because the bone distribution changes are compensatory. That is, *I*, *J*, and *Z* will not significantly differ among age groups if the differences in cortical bone distribution are working to maintain bone strength in response to bending and torsion. Further, if cortical geometry compensates for declining cortical BMD, then these changes should correspond to one another locally within and between cross-sections of the forearm and leg. I expect to find high correlations between the regions where cortical bone distances from the centroid are greatest and BMD differences are greatest.

REFERENCES

Adel-Wahab, A. A., Alam, K., Silberschmidt, V. V. (2010). Analysis of anisotropic viscoelastoplastic properties of cortical bone tissues. Journal of the Mechanical Behavior of Biomedical Materials, 4(5):807-820.

Agarwal, S. C. (2021). What is normal bone health? A bioarchaeological perspective on meaningful measures and interpretations of bone strength, loss, and aging. American Journal of Human Biology, 33(5), e23647

Agostini, G., Holt, B. M., and Relethford, J. H. (2018). Bone functional adaptation does not erase neutral evolutionary information. Am J Phys Anthropol 166(3):708-729.

Allison, H., Holdsworth, G., & McNamara, L. M. (2020). Scl-Ab reverts pro-osteoclastogenic signalling and resorption in estrogen deficient osteocytes. BMC Cell Biology, 21(1), 1–78.

Almeida, M., O'Brien, C. A. (2013). Basic biology of skeletal aging: Role of stress response pathways. J Gerontol A Biol Sci Med Sci 68(10):1197-1208.

Almeida, M., Iyer, S., Martin-Milan, M., Bartell, S. M., Han, L., Ambrogini, E., Onal, M., Xiong, J., Weinstein, R. S., Jilka, R. L., O'Brien, C. A., Manolagas, S. C. (2012). Estrogen receptor-α signaling in osteoblast progenitors stimulates cortical bone accrual. Journal of Clinical Investigations 123(1): 394-404.

Andreasen, C. M., Delaisse, J.-M., van der Eerden, B. C., van Leeuwen, J. P., Ding, M., & Andersen, T. L. (2018). Understanding Age-Induced Cortical Porosity in Women: The Accumulation and Coalescence of Eroded Cavities Upon Existing Intracortical Canals Is the Main Contributor. Journal of Bone and Mineral Research, 33(4), 606–620.

Andreasen, C. M., Bakalova, L. P., Brüel, A., Hauge, E. M., Kiil, B. J., Delaisse, J.-M., Kersh, M. E., Thomsen, J. S., & Andersen, T. L. (2020). The generation of enlarged eroded pores upon existing intracortical canals is a major contributor to endocortical trabecularization. Bone, 130, 115127–115127.

Ascenzi, A., Bonucci, E. (1967). The tensile properties of single osteons. The Anatomical Record, 158(4), 375–386.

Beck, T. J., Ruff, C. B., Warden, K. E., Scott, W. W., Rao, G. U. (1990). Predicting femoral neck strength from bone mineral data: A structural approach. Invest Radiol 25:6–18.

Beck, T. J., Oreskovic, T. L., Stone, K. L., Ruff, C. B., Ensrud, K., Nevitt, M. C., Genant, H. K., & Cummings, S. R. (2001). Structural Adaptation to Changing Skeletal Load in the Progression Toward Hip Fragility: The Study of Osteoporotic Fractures. Journal of Bone and Mineral Research, 16(6), 1108–1119.

Biewener, A. A. (1989). Mammalian terrestrial locomotion and size. BioScience 39:776–783.

Bettis, T., Kim, B. J., Hamrick, M. W. (2018). Impact of muscle atrophy on bone metabolism and bone strength: implications for muscle-bone crosstalk with aging and disuse. Osteoporosis International 29: 1713-1720.

Birkhold, A.I., Razi, H., Duda, G.N., Checa, S., Willie, B. M. (2017). Tomography-based quantification of regional differences in cortical bone surface remodeling and mechano-response. Calcified Tissue International 100: 255-270.

Biver, E., Perréard Lopreno, G., Hars, M., van Rietbergen, B., Vallée, J. P., Ferrari, S., Besse, M., & Rizzoli, R. (2016). Occupation-dependent loading increases bone strength in men. Osteoporosis International, 27(3), 1169–1179.

Boivin, G., Farlay, D., Bala, Y., Doublier, A., Meunier, P. J., & Delmas, P. D. (2009). Influence of remodeling on the mineralization of bone tissue. Osteoporosis International, 20(6), 1023–1026.

Bord, S., Ireland, D. ., Beavan, S. ., Compston, J. (2003). The effects of estrogen on osteoprotegerin, RANKL, and estrogen receptor expression in human osteoblasts. Bone, 32(2), 136–141.

Burr, R. B., Allen, M. R. (2019). Basic and Applied Bone Biology (2nd edition). Academic Press. pp 125-140.

Carina, V., Della Bella, E., Costa, V. et al. (2020). Bone's Response to Mechanical Loading in Aging and Osteoporosis: Molecular Mechanisms. Calcif Tissue Int 107, 301–318.

Cauley, J. A. (2017). Osteoporosis: fracture epidemiology update 2016. Current Opinion in Rheumatology, 29(2): 150-156.

Chen, F., OuYang, Y., Ye, T., Ni, B., & Chen, A. (2014). Estrogen Inhibits RANKL-Induced Osteoclastic Differentiation by Increasing the Expression of TRPV5 Channel. Journal of Cellular Biochemistry, 115(4), 651–658.

Chen, J.-F., Lin, P.-W., Tsai, Y.-R., Yang, Y.-C., Kang, H.-Y. (2019). Androgens and Androgen Receptor Actions on Bone Health and Disease: From Androgen Deficiency to Androgen Therapy. Cells (Basel, Switzerland), 8(11), 1318.

Cheng, S., Xu, L., Nicholson, P. H., Tylavsky, F., Lyytikäinen, A., Wang, Q., Suominen, H., Kujala, U. M., Kröger, H., Alen, M. (2009). Low volumetric BMD is linked to upperlimb fracture in pubertal girls and persists into adulthood: a seven-year cohort study. Bone, 45:480–486.

Cowgill, L. W., Warrener, A., Pontzer, H., & Ocobock, C. (2010). Waddling and toddling: The biomechanical effects of an immature gait. American Journal of Physical Anthropology, 143(1), 52–61.

Currey, JD. (2006). Bones: structure and mechanics. Princeton, NJ: Princeton University Press.

Currey, J. D. (2012). The structure and mechanics of bone. Journal of Materials Science, 47(1), 41–54.

Damilakis, J., Adams, J. E., Guglielmi, G., & Link, T. M. (2010). Radiation exposure in X-ray-based imaging techniques used in osteoporosis. European Radiology, 20(11), 2707–2714.

Diaz Brinton, R. (2012). Minireview: Translational Animal Models of Human Menopause: Challenges and Emerging Opportunities. Endocrinology (Philadelphia), 153(8), 3571–3578.

Duan Y, Beck TJ, Wang X, Seeman E. (2003). Structural and biomechanical basis of sexual dimorphism in femoral neck fragility has its origins in growth and aging. Journal of Bone and Mineral Research 18(10): 1766-1774.

Farr JN, Xu M, Weivoda MM, Monroe DG, Fraser DG, Onken JL, Negley BA, Sfeir JG, Ogrodnik MB, Hachfeld CM, LaBrasseur NK, Drake MT, Pignolo RJ, Pirtskhalava T, Tchkonia T, Oursler MJ, Kirkland JL, Khosla S. (2017). Targeting cellular senescence prevents age-related bone loss in mice. Nature Medicine 23: 1072-1079.

Feik, S. A., Thomas, C. D. L., Bruns R., Clement J. G. (2000). Regional variations in cortical modeling in the femoral midshaft: sex and age differences. American Journal of Physical Anthropology 112:191-205.

Follet, H., Boivin, G., Rumelhart, C., & Meunier, P. . (2004). The degree of mineralization is a determinant of bone strength: a study on human calcanei. Bone (New York, N.Y.), 34(5), 783–789.

Frost, H. M. (1987). Bone “mass” and the “mechanostat”: a proposal. The Anatomical Record, 219(1):1-9.

Frost, H. M. (1997). On our age-related bone loss: insights from a new paradigm. Journal of Bone and Mineral Research, 12(10): 1539-1546.

Frost, H. M. (2003). Bone’s mechanostat: A 2003 update. The Anatomical Record, 275A(2), 1081–1101.

Gardiner, J. D. (2021). The diminishing returns of mechanical loading and potential mechanisms that desensitize osteocytes. Current Osteoporosis Reports 19:436-443.

Golding, P. H. (2022). Dual-energy X-ray absorptiometry (DXA) to measure bone mineral density (BMD) for diagnosis of osteoporosis - experimental data from artificial vertebrae confirms significant dependence on bone size. Bone Reports, 17: 101607.

Goldman, H. M., Mcfarlin, S. C., Cooper, D. M. L., Thomas, C. D. L., & Clement, J. G. (2009). Ontogenetic Patterning of Cortical Bone Microstructure and Geometry at the Human Mid-Shaft Femur. Anatomical Record, 292(1), 48–64.

Gosman JH, Stout SD, and Larsen CS. (2011). Skeletal biology over the life span: A view from the surfaces. American Journal of Physical Anthropology 146(S53):86-98.

Gosman J. H., Hubbell, Z. R., Shaw, C. N., & Ryan, T. M. (2013). Development of Cortical Bone Geometry in the Human Femoral and Tibial Diaphysis. Anatomical Record (Hoboken, N.J. : 2007), 296(5), 774–787.

Hemmatian, H., Bakker, A., Klein-Nulend, J., van Lenthe, G. (2017). Aging, osteocytes, and mechanotransduction. Current Osteoporosis Reports, 15(5), 401–411.

Hofbauer, L. C., Khosla, S. (1999). Androgen effects on bone metabolism: Recent progress and controversies. European Journal of Endocrinology, 140(4), 271–286.

Ho-Pham, L. T., Nguyen, N. D., & Nguyen, T. V. (2013). Quantification of the relative contribution of estrogen to bone mineral density in men and women. BMC Musculoskeletal Disorders, 14(1), 366–366.

Hughes, J. M., Petit, M. A. (2010). Biological underpinnings of Frost's mechanostat thresholds: the important role of osteocytes. Journal of Musculoskeletal and Neuronal Interactions, 10(2):128-135.

Ireland, A., Maden-Wilkinson, T., Ganse, B., Degens, H., & Rittweger, J. (2014). Effects of age and starting age upon side asymmetry in the arms of veteran tennis players: a cross-sectional study. Osteoporosis International, 25(4), 1389–1400.

Javaheri, B., Pitsillides, A. A. (2019). Aging and Mechanoadaptive Responsiveness of Bone. Current Osteoporosis Reports 17: 560-569.

Javaheri, B., Razi, H., Gohin, S., Wylie, S., Chang, Y.-M., Salmon, P., Lee, P. D., & Pitsillides, A. A. (2020). Lasting organ-level bone mechanoadaptation is unrelated to local strain. Science Advances, 6(10).

Johnell, O., Kanis, J. M. (2005). Epidemiology of osteoporotic fractures. Osteoporosis International, 16(Suppl 2): S3-7.

Kanis, J. M. (2002). Diagnosis of osteoporosis and assessment of fracture risk. The Lancet 359(9321): 1929-1936.

Keaveny, T. M., Morgan, E. F., Neibur, G. L., Yeh, O.C. (2001). Biomechanics of trabecular bone. Annu. Rev. Biomed. Eng., 3:307–333.

Khosla, S. (2013). Pathogenesis of age-related bone loss in humans. The Journals of Gerontology. Series A, Biological Sciences and Medical Sciences, 68(10), 1226–1235.

Khosla, S., Hofbauer, L. C. (2017). Osteoporosis treatment: recent developments and ongoing challenges. Osteoporosis 5(11): 898-907.

Kim, C.H., You, L., Yellowley, C. E., & Jacobs, C. R. (2006). Oscillatory fluid flow-induced shear stress decreases osteoclastogenesis through RANKL and OPG signaling. Bone (New York, N.Y.), 39(5), 1043–1047.

Korhonen M. T., Heinonen A., Siekkinen J., Isolehto J., Alén M., Kiviranta I., Suominen H. (2012). Bone density, structure and strength, and their determinants in aging sprint athletes. Medicine and Science in Sports and Exercise, 44(12): 2340-2349.

Lanyon, L., Skerry, T. (2001). Postmenopausal osteoporosis as a failure of bone's adaptation to functional loading: a hypothesis. Journal of Bone and Mineral Research 16(11): 1937-1947.

Lauretani F., Bandinelli S., Griswold M. E., Maggio M., Semba R., Guralnik J. M., Ferruci L. (2008). Longitudinal Changes in BMD and Bone Geometry in a Population-based study. Journal of Bone and Mineral Research 23(3): 400-408.

Lazenby, R. (1986). Porosity-geometry interaction in conservation of bone strength. Journal of Biomechanics, 19(3): 257-258.

Lieberman D.E., Pearson O.M., Polk J.D., Demes B., Crompton A.W. (2003). Optimization of bone growth and remodeling in response to loading in tapered mammalian limbs. Journal of Experimental Biology 206: 3125-3138.

Lorentzon, M., Johansson, H., Harvey, N. C., Liu, E., Vandenput, L., McCloskey, E. V., & Kanis, J. A. (2022). Osteoporosis and fractures in women: the burden of disease. Climacteric : the Journal of the International Menopause Society, 25(1), 4–10.

Luo, C. Y., Wang, L., Sun, C., Li, D. J. (2011). Estrogen enhances the functions of CD4+CD25+Foxp3+ regulatory T cells that suppress osteoclast differentiation and bone resorption in vitro. Cellular and Molecular Immunology 8: 50-58.

Ma, C., Geng, B., Zhang, X., Li, R., Yang, X., & Xia, Y. (2020). Fluid shear stress suppresses osteoclast differentiation in RAW264.7 cells through extracellular signal-regulated kinase 5 (ERK5) signaling pathway. Medical Science Monitor, 26, e918370–e918370.

Macdonald, H. M., Nishiyama, K. K., Kang, J., Hanley, D. A., & Boyd, S. K. (2011). Age-related patterns of trabecular and cortical bone loss differ between sexes and skeletal sites: A population-based HR-pQCT study. Journal of Bone and Mineral Research, 26(1), 50–62.

Manolagas, S. C., O'Brien, C. A., Almeida, M. (2013). The role of estrogen and androgen receptors in bone health and disease. Nature Reviews Endocrinology 9: 699-712.

Martin, R. B, Burr, D. B., Sharkey, N. A., & Fyhrie, D. P. (2015). Skeletal Tissue Mechanics (2nd ed. 2015.). Springer: New York.

McCalden, R. W., McGeough, J. A., Barker MB, Court-Brown CM. 1993. Age-related changes in the tensile properties of cortical bone. The relative importance of changes in porosity, mineralization, and microstructure. J Bone Joint Surg Am. 75(8): 1193-1205.

Melton, L. J. Chrischilles, E. A., Cooper, C., Lane, A. W., & Riggs, B. L. (1992). Perspective how many women have osteoporosis? Journal of Bone and Mineral Research, 7(9), 1005–1010.

Melton, L. J., Atkinson, E. J., O'Connor, M. K., O'Fallon, W. M., & Riggs, B. L. (1998). Bone Density and Fracture Risk in Men. Journal of Bone and Mineral Research, 13(12), 1915–1923.

Morgan, E. F., Unnikrisnan, G. U., & Hussein, A. I. (2018). Bone Mechanical Properties in Healthy and Diseased States. Annual Review of Biomedical Engineering, 20(1), 119–143.

Morrell, A. E., Brown, G. N., Robinson, S. T., Sattler, R. L., Baik, A. D., Zhen, G., Cao, X., Bonewald, L. F., Jin, W., Kam, L. C., Guo, X. E. (2018). Mechanically induced Ca2+ oscillations in osteocytes release extracellular vesicles and enhance bone formation. Bone Research 6(6).

Nadell, J. A., Shaw, C. N. (2016). Phenotypic plasticity and constraint along the upper and lower limb diaphyses of Homo sapiens. American Journal of Physical Anthropology, 159, 410–422.

Nicks, K. M., Amin, S., Atkinson, E. J., Riggs, B. L., Melton III, L. J., & Khosla, S. (2012). Relationship of age to bone microstructure independent of areal bone mineral density. Journal of Bone and Mineral Research, 27(3), 637–644.

Onal, M., Piemontese, M., Xiong, J., Wang, Y., Han, L., Ye, S., Komatsu, M., Selig, M., Weinstein, R. S., Zhao, H., Jilka, R. L., Almeida, M., Manolagas, S. C., & O'Brien, C. A. (2013). Suppression of Autophagy in Osteocytes Mimics Skeletal Aging. The Journal of Biological Chemistry, 288(24), 17432–17440.

Pearson, O. M., Lieberman, D. E. (2004). The aging of Wolff's "law": Ontogeny and responses to mechanical loading in cortical bone. American Journal of Physical Anthropology, 125(S39), 63–99.

Percival, M. (1997). Bone health and osteoporosis. Applied Nutritional Science Reports, 5(4): 1-6.

Perlman, R. L. (2016). Mouse models of human disease: An evolutionary perspective. Evolution, Medicine, and Public Health, 2016(1), 170–176.

Ramchand, S.K., Seeman, E. (2018). The Influence of Cortical Porosity on the Strength of Bone During Growth and Advancing Age. Curr Osteoporos Rep 16, 561–572.

Razi, H., Birkhold, A. I., Weinkamer, R., Duda, G. N., Willie, B. M., & Checa, S. (2015). Aging Leads to a Dysregulation in Mechanically Driven Bone Formation and Resorption. Journal of Bone and Mineral Research, 30(10), 1864–1873.

Reilly, D. T., Burstein, A. H. (1975). The elastic and ultimate properties of compact bone tissue. Journal of Biomechanics, 8(6), 393,IN9,397–396,IN11,405.

Riggs, B. L., Melton, L. J., Robb, R. A., Camp, J. J., Atkinson, E. J., Peterson, J. M., Rouleau, P. A., McCollough, C. H., Bouxsein, M. L., & Khosla, S. (2004). Population-Based Study of Age and Sex Differences in Bone Volumetric Density, Size, Geometry, and Structure at Different Skeletal Sites. Journal of Bone and Mineral Research, 19(12), 1945–1954.

Robling, A. G., Bellido, T., & Turner, C. H. (2006). Mechanical stimulation in vivo reduces osteocyte expression of sclerostin. Journal of Musculoskeletal & Neuronal Interactions, 6(4), 354–354.

Rubin, C. T., Bain, S. D., McLeod, K. J. (1992) Suppression of the osteogenic response in the aging skeleton. Calcified Tissue International, 50:306-313.

Ruff, C. B., Hayes, W. B. (1982). Subperiosteal expansion and cortical remodeling of the human femur and tibia with aging. Science 217(4563):945-948.

Ruff, C. B., Hayes, W. C. (1983). Cross-sectional geometry of Pecos Pueblo femora and tibiae: a biomechanical investigation. II. Sex, age, and side differences. Am J Phys Anthropol 60:383–400.

Ruff, C., Holt, B., & Trinkaus, E. (2006). Who's afraid of the big bad Wolff?: "Wolff's law" and bone functional adaptation. American Journal of Physical Anthropology, 129(4), 484–498.
Ruff, C. B. (2000). Body size, body shape, and long bone strength in modern humans. Journal of Human Evolution, 38(2): 269-290.

Schmidt, M., Fischer, M. (2008). Morphological integration in mammalian limb proportions: dissociation between function and development. Evolution 63(3):749-766.

Skedros, Holmes, J. L., Vajda, E. G., & Bloebaum, R. D. (2005). Cement lines of secondary osteons in human bone are not mineral-deficient: New data in a historical perspective. The Anatomical Record, 286A(1): 781–803.

Skerry, T. M. (2006). One mechanostat of many? Modifications of the site-specific response of bone to mechanical loading by nature and nurture. Journal of Musculoskeletal Neuronal Interactions 6(2): 122-127.

Springer,M. S., Murphy, W. J. (2007). Mammalian evolution and biomedicine: new views from phylogeny. Biological Reviews of the Cambridge Philosophical Society, 82(3), 375–392.

Stagi, S., Cavalli, L., Cavalli, T., De Martino, M., & Brandi, M. L. (2016). Peripheral quantitative computed tomography (pQCT) for the assessment of bone strength in most of bone affecting conditions in developmental age: A review. Italian Journal of Pediatrics, 42(1), 88–88.

Stenderup, K., Justesen, J., Clausen, C., Kassem, M. (2003). Aging is associated with decreased maximal life span and accelerated senescence of bone marrow stromal cells. Bone 33:919-926.

Streicher, C., Heyny, A., Andrukhova, O., Haigl, B., Slavic, S., Schüler, C., Kollmann, K., Kantner, I., Sexl, V., Kleiter, M., Hofbauer, L. C., Kostenuik, P. J., & Erben, R. G. (2017). Estrogen Regulates Bone Turnover by Targeting RANKL Expression in Bone Lining Cells. Scientific Reports, 7(1), 6460–14.

Taaffe, D. R., Cauley, J. A., Danielson, M., Nevitt, M. C., Lang, T. F., Bauer, D. C., Harris, T. B. (2001). Race and sex effects on the association between muscle strength, soft tissue, and bone mineral density in healthy elders: The Health, Aging, and Body Composition Study. Journal of Bone and Mineral Research 16(7): 1343-1352.

Tanaka, K., Nishimura, N., Kawai, Y. (2017). Adaptation to microgravity, deconditioning, and countermeasures. The Journal of Physiological Sciences, 67: 271-281.

Tatsumi, S., Ishii, K., Amizuka, N., Li, M., Kobayashi, T., Kohno, K., Ito, M., Takeshita, S., Ikeda, K. (2007). Targeted ablation of osteocytes induces osteoporosis with defective mechanotransduction. Cell Metabolism 5(6): 464–475.

Ucer, S., Iyer, S., Kim, H., Han, L., Rutlen, C., Allison, K., Thostenson, J. D., de Cabo, R., Jilka, R. L., O'Brien, C., Almeida, M., Manolagas, S. C. (2017). The effects of aging and sex steroid deficiency on the murine skeleton are independent and mechanistically distinct. Journal of Bone and Mineral Research 32(3): 560-574.

Vilayphiou, N., Boutroy, S., Sornay-Rendu, E., Van Rietbergen, B., & Chapurlat, R. (2016). Age-related changes in bone strength from HR-pQCT derived microarchitectural parameters with an emphasis on the role of cortical porosity. Bone (New York, N.Y.), 83, 233–240.

Wallace, I. J., Tommasini, S. M., Judex, S., Garland Jr, T., Demes, B. (2012). Genetic variations and physical activity as determinants of limb bone morphology: An experimental approach using a mouse model. Am J Phys Anthropol 148: 24-35.

Wallace, J. M. (2019). Skeletal Hard Tissue Mechanics. In: Editors, Burr, D. B., Allen, M. R., Basic and Applied Bone Biology (2nd edition). Academic Press. pp 125-140.

Wang L., You, X., Zhang, L., Zhang, C., & Zou, W. (2022). Mechanical regulation of bone remodeling. Bone Research, 10(1), 16–16.

Warden, S. J., Mantila Roosa, S. M., Kersh, M. E., Hurd, A. L., Fleisig, G. S., Pandy, M. G., Fuchs, R. K. (2014). Physical activity when young provides lifelong benefits to cortical bone size

and strength in men. Proceedings of the National Academy of Sciences, USA, 111(14): 5337-5342.

Weaver, C. M., Peacock, M. Skeletal Changes Across the Life Span. In: Burr DB, & Allen MR (editors). 2019. Basic and applied bone biology. Second edition. New York: Academic Press.

Wilson, L. A. B., De Groote, I., Humphrey L. T. (2020). Sex differences in the patterning of age-related bone loss in the human hallucal metatarsal in rural and urban populations. American Journal of Physical Anthropology 171(4): 628-644.

Woo, J., Kwok, T., Leung, J. C. S., Ohlsson, C., Vandenput, L., Leung, P. C. (2012). Sex steroids and bone health in older Chinese men. Osteoporosis International 23: 1553-1562.

Yan, Y., Sun, H., Gong, Y., Yan, Z., Zhang, X., Guo, Y., Wang, Y. (2016). Mechanical strain promotes osteoblastic differentiation through integrin-β1-mediated β-catenin signaling. International Journal of Molecular Medicine 38: 594-600.

Yang, H., Xu, X., Bullock, W., Main, R. (2019). Adaptive changes in micromechanical environments of cancellous and cortical bone in response to in vivo loading and disuse. Journal of Biomechanics 89: 85-94.

Yu, K., Sellman, D., Bahraini, A., Hagan, M., Elsherbini, A., Vanpelt, K., Marshall, P., Hamrick, M., McNeil, A., McNeil, P. et al. (2018). Mechanical loading disrupts osteocyte plasma membranes which initiates mechanosensation events in bone. Journal of Orthopaedic Research 36:653-662.

CHAPTER 2: LOCAL VARIATION IN AGE-RELATED CORTICAL EXPANSION WITHIN AND BETWEEN CROSS-SECTIONS OF DISTAL HUMAN LONG BONES

Publication statement: A version of this chapter is being prepared for publication by Greg J. Wehrman, Alice F. Gooding, Adam D. Sylvester, Dawnie Wolfe Steadman, Benjamin M. Auerbach as:

Wehrman, G. W., Gooding, A. F., Sylvester, A. D., Steadman D. W., Auerbach, B. M. (2023). Local variation in age-related cortical expansion within and between cross-sections of distal human long bones. *In preparation*.

This chapter constitutes novel research and regularly uses pronouns "we" and "our" to refer to the collective contributions of the co-authors. It should be noted, however, that in addition to conducting the majority of the research including data collection and analyses, I, Greg Wehrman, am the author in the ordinary sense.

ABSTRACT

Cortical bone expansion is an age-related process where, through endosteal resorption and periosteal apposition, cross-sectional diameter increases while cortical thickness decreases in long bone diaphyses. Local variation has been observed in this process between cross-sectional sites, but few studies have examined directional variation within cross-sections. In this study, we assess variation in age-related cortical expansion both within and between cross-sections using pQCT images of the tibia, radius, and ulna from a living sample of adults ages 40-80 years (n=126; 78 females, 48 males). Cross-sectional slices were generated at four locations along tibial and forearm length (20%, 35%, 50%, and 65%), while intra-slice variation was assessed through inter-landmark distances of endosteal and periosteal semi-landmarks along eight directional radii. Results demonstrate local variation in age-related differences of these geometric measurements both within and between cross-sections. Patterns of intra-slice variation of endosteal and periosteal distances to the centroid exhibit similarity, suggesting while variable at

different directions of the cross-section, age-related endosteal resorption and periosteal apposition are coupled. Finally, we observe shifting degrees and directional patterns of cortical expansion down the length of each bone, particularly in the radius. These results indicate that age-related cortical expansion occurs non-uniformly throughout distal elements, which suggests that systemic factors of aging (e.g. hormonal decline, decreased muscle strength, oxidative stress) are mediated by local factors.

INTRODUCTION

Bone loss in human limb long bones with advanced age is a concern associated with increased fracture risk and subsequent impacts on quality of life (Melton et al., 1998; Schuit et al., 2004; Siris et al., 2014; McCloskey et al., 2016). Bone loss can affect the macrostructure (size and shape), the microstructure (intracortical porosity, trabecular thinning/loss), or the material composition of bone (mineralization, collagen cross-linkage). Clinical approaches to the study of bone loss have focused on declining bone mineral density (BMD) (Johnell et al., 2005), which has some predictive accuracy for risk of fracture. However, research in the last two decades has indicated that fractures occur in individuals over the age of 60 with BMD in normal ranges for sex and age (Pasco et al., 2006; Bliuc et al., 2015; cf. Miller et al., 2002). This has led researchers to suggest that multiple processes other than BMD loss conspire to cause increased propensity for fracture risk, including changes in the microarchitecture of trabecular bone (McCloskey et al., 2015, 2016) and macroscopic loss of cortical bone (Bilezikian et al., 2019). Following the argument that many factors may contribute to age-related changes in limb long bone structure and composition, in this study we examine how cortical bone distribution and geometry differ in the distal major long bones of the limbs (radius, ulna, and tibia) among humans after the age of forty.

Age-related loss of bone in limb elements

It is unsurprising that changes in BMD alone are not responsible for increased fracture risk and bone fragility with age. This is because the clinical assessment of BMD encompasses several processes of bone loss without the capacity to distinguish between them through areal measures of bone density (e.g., DEXA or similar scanning methods) (Choski et al., 2018). Material composition and properties such as true density, elasticity, and anisotropy impact the capacity of a bone to withstand mechanical loading and resist fracture (Currey, 2006; Martin et al., 2015). Bone strength, moreover, is determined by both material properties and the geometric configuration of bone (Currey, 2006; Martin et al., 2015), and therefore both attributes of bone structure should be considered when assessing fracture risk. As changes in bone microarchitecture (e.g., osteopenia and osteoporosis) may lead to the alteration of bone macrostructure, since both are the product of bone remodeling, changes in bone material properties could directly relate to alterations in bone shape and size.

In studies of individuals over the age of 40, major limb long bones exhibit geometric changes that result in an expanded cortical diameter (Ruff and Hayes, 1982; Lauretani et al., 2008; Beck et al., 2001; Duan et al., 2003; Gooding, 2017). This expansion is a product of age-related changes in the inner (endosteal) and outer (periosteal) envelopes of long bones, where endosteal resorption and periosteal deposition move the outer table of long bones away from the centroid of the long bone in cross-section, which in turn theoretically increases resistance to bending and torsion in the long bone (Orwoll, 2003; Jepsen and Andarawis-Puri, 2012). Resorption primarily occurs on the endosteal surface, resulting in increased medullary area with age (Russo et al., 2003; Lauretani et al., 2008; Gosman et al., 2011). Concurrent with endosteal resorption,

deposition of bone occurs on the periosteal surface, increasing total cross-sectional area (Russo et al., 2003; Jepsen and Andarawis-Puri, 2012). The resulting cross-section becomes wider with age, but with thinner cortical walls.

Age-related cortical bone expansion has been characterized as being compensatory to bone loss since a net loss of cortical bone would necessitates redistribution of bone away from the neutral axis to maintain or even increase bending and torsional strength (Beck, 2001; Lauretani et al., 2008; Martin et al., 2015). Ruff and Hayes (1982) described such age-related changes, which increase second moments of area and section modulus, in the femora and tibiae of Native Americans buried at Pecos Pueblo. Similarly, in a longitudinal study of living females over the age of 65, Beck and colleagues (2001) found that as cortical area declined and subperiosteal width increased with age (and therefore total cross-sectional area increased), section modulus of the femoral neck and midshaft increased. Similar findings were reported by Lauretani and colleagues (2008) in a longitudinal study of older Italian adults.

Factors contributing to variation in cortical bone cross-sectional shape and size

While the pattern of age-related periosteal expansion in limb long bones is therefore well-established from skeletal remains and in living individuals, the causes remain unresolved. Researchers have favored declining systemic estrogen levels as contributing to endosteal resorption and periosteal deposition. During growth and development of long bones, estrogen has a restrictive effect on periosteal deposition while promoting accrual of bone on the endosteal surface (Duan et al., 2003; Manolagas et al., 2013). As estrogen declines, inhibitory effects on endosteal resorption and periosteal deposition are removed and cortical bone expansion occurs. The role of estrogen in maintenance of bone mass during adulthood is illustrated by the fact that

estrogen levels are the strongest hormonal predictor of bone loss in both females and males (Woo et al., 2012). In addition to effects of estrogen decline in advanced age, differential hormonal environments during growth establish sexual dimorphism among adults that later explains, in part, sex differences in relative bone loss and fracture risk. During adolescence, a greater proportion of androgens in males promotes periosteal growth of cortical bone, resulting in long bone diaphyses with increased diameter. In females, however, higher levels of estrogen are thought to constrain radial growth of the diaphysis (Gosman et al., 2011; Manolagas et al., 2013). As a result, female diaphyseal cortices have smaller total diameters than male cortices at skeletal maturity, despite similar cortical thickness throughout young adulthood (Duan et al. 2003). Thus, in addition to experiencing a comparatively rapid rate of bone loss post-menopause, declining bone mass in females has a disproportionate effect on bone strength compared to males; smaller diaphyseal cross-sections at the end of primary growth mean that cortical bone is positioned more closely to the central axis of a diaphysis, thereby impacting bending and torsional strength (Duan et al., 2003; Warden et al., 2014).

Cortical bone continues to respond to mechanical loading into advanced age, though attenuated in comparison with the responses in cortical bone at younger ages. Some of the most illustrative examples of bone functional adaptation later in life are those of senior athletes, whose continued training resulted in maintenance of adapted geometries achieved from sports-related loading at younger years (Korhonen et al., 2012; Warden et al., 2014). Given the continued response to loading in bone, cortical expansion may similarly be mediated by habitual activity and should therefore occur non-uniformly by location with age. Researchers have reported variation in age-related cortical expansion within the diaphyses of long bones among sites of clinical relevance, namely the distal tibia, distal radius, and femoral neck (Beck et al., 2001;

Lauretani et al., 2008). This is reflected in the study of individuals from Pecos Pueblo by Ruff and Hayes (1982), who noted variance in the loss in cortical area associated with cortical expansion along the lengths of the femur and tibia. Notably, in the midshaft of the femur cortical area remained statistically the same with age despite an increase in subperiosteal area. They attributed this to greater bending strain experienced at the diaphyseal midshaft compared to the more proximal and distal metaphyseal regions. Gooding (2017) similarly investigated age-related changes to cross-sectional properties at different sites along the length of long bone diaphyses and found that geometric changes occur non-uniformly both between and within long bone shafts. Thus, it appears that local factors mediate age-related geometric changes to cortical bone among diaphyses.

Few studies have examined local variation within long bone cross-sections to determine whether cortical bone expansion occurs uniformly in the axial dimension. To date, the analysis of local variation within cross-sections has been limited to skeletal samples and has not been compared at multiple points along the length of the bone. Feik and colleagues (2000) examined cortical thickness and total diameter of femoral midshafts from a modern Australian skeletal sample and found that periosteal deposition was greatest in the mediolateral axis and that endosteal resorption was greatest on the anterior aspect. Their study suggests that the location of periosteal expansion and endosteal resorption within a cross-section may not be the same, and therefore may be decoupled. Wilson and colleagues (2020) reported variation of the distribution of cortical bone change with age in mid-shaft cross-section of the first metatarsal among medieval and industrial English samples. Differences in their study were primarily between the sexes, while presumed differences in activity levels between rural and urban groups also affected patterns of bone loss. Together, these studies indicate that there may be structured variation in

the patterns of bone loss and apposition in long bone cross-sections with respect to age, arising from sex differences and activity, but the nature of this structure has not been established.

Our study expands on previous research by assessing local variation in age-related geometric differences in the long bone cortices of living humans both within cross-sections and at different slice locations along the length of each element. We examine these differences in three long bones: the radius, ulna, and tibia. Cortical bone expansion is characterized by age-related changes in cortical thickness and endosteal/periosteal distance from the centroid at different locations around a given cross-section's perimeter. Based on precedent, we anticipate sex differences in age-related cortical bone size, and so we first assess if this difference is present in our data. We then examine whether variation in cortical bone expansion is uniform, non-uniform but exhibiting discernable patterns, or is stochastic by slice location along the length of each bone. Finally, we investigate the effect of age and body mass index (BMI) at different slices and assess whether distance measurements associated with cortical bone expansion are influenced evenly or variably by these factors. We predict that:

1) Age-related changes in distance measurements (cortical thickness, endosteal distance, periosteal distance) will vary by slice location along the bone's length, following the precedent of various other studies cited above.
2) Age-related changes in distance measurements will significantly vary within cross-sectional slices, with greater endosteal resorption on the side of the bone cross-section on which the paired element is located, and greater periosteal expansion on the side opposite of the paired element. For example, in the tibia, endosteal resorption would be greatest on the lateral side (the side of the fibula), and periosteal expansion would be greatest on the medial side. This is because we hypothesize that load-sharing

between elements (e.g., Auerbach et al., 2017) would allow for a thinner cortical bone on the side adjacent to a within-segment paired element.

Through examination of local variation in age-related changes to bone geometry we gain a more thorough understanding of the interaction between systemic mechanisms of bone loss and the local factors that mediate them.

MATERIALS AND METHODS

Sample Composition

The sample for this study is composed of 126 living participants (78 females and 48 males) recruited from the southeastern United States, primarily Georgia and Tennessee (Table 1.1). Research was approved through IRB at both The University of Tennessee, Knoxville (IRB-22-06852-FB-RA) and Kennesaw State University (IRB-FY22-249). Data collection took place between June-December 2022 at the Bone Biomechanics Lab, directed by Dr. Alice Gooding at Kennesaw State University. Individuals were recruited from a list of registered donors to the University of Tennessee's Forensic Anthropology Center's body donation program, from nearby university communities, and through snowball sampling. Eligibility to participate was restricted to individuals between ages 40 and 80 years of age. Individuals with a history of cancer and radiation/chemotherapy treatment within the past 5 years were excluded due to known effects on bone remodeling (Guise, 2006). Individuals who have used certain medications for osteopenia/osteoporosis, like bisphosphonates, calcitonin, sclerostin inhibitors, and parathyroid hormone analog, were also excluded since the main effect of these drugs is to alter bone remodeling activity. Individuals with appendicular skeletal fractures in the past two years were excluded due to potential for atypical loading patterns between sides. Finally, individuals with a

BMI greater than 40 (Class III obese) and less than 18.5 (underweight) were excluded. Given the prevalence at which birth control and hormone replacement therapy (HRT) are used among American females, these were not considered exclusionary criteria but information on HRT was collected through a health and lifestyle questionnaire.

Data Collection

Study participants completed a self-administered questionnaire to survey demographic, medical, and lifestyle information. Survey questions are provided in the Supporting Information. Demographic information was comprised of age, biological sex, and self-identified race/ancestry. Height and weight were measured to the nearest millimeter and kilogram, respectively, before participants were scanned.

Bone property data from the forearm (ulna and radius) and leg (tibia and fibula) were acquired via use of a Stratec XCT 3000 peripheral quantitative computed tomography (pQCT) scanner, which allows for the collection of shape and density information from limb bones. G.J.W. obtained forearm and leg lengths of the self-reported non-dominant side, defined by the upper limb used for gross manipulation (e.g., lifting) and the lower limb on the same side as the dominant upper limb. The non-dominant side was chosen to reduce variation from disparate activity levels among individuals since cortical geometry is partly a product of repetitive loading (Ruff et al., 2006; Biver et al., 2016). Forearm length was measured as the length between the anterior midpoint between the humeral epicondyles and the anterior midpoint between the radial and ulnar styloid processes (Kushwaha et al., 2022). Leg length was measured as the length between the superior margin of the medial tibial condyle and the distal end of the medial malleolus (Sume, 2019). Total length for both measurements was taken to the nearest millimeter

using a tape measure. The locations for these bone landmarks were marked with a pen to aid in locating the extreme ends of the elements for determining total length within the pQCT scanner, which set the distal landmark as the alignment for initiating scans. Using these total lengths, participants were then scanned using the pQCT machine to obtain cross-sectional data at 20%, 35%, 50%, and 65% of total length for each limb segment, starting from the distal osteological feature (distal articular surface of radius, medial malleolus of tibia). Both forearm and leg scans required patients to insert their forearm/leg in a plane perpendicular to the scanner's ring, so that limb elements were scanned normal to the plane of the scanner's imaging sensor (see Figure 1.1). The forearm was placed in a pronated position for scanning. Despite the stereotypical placement of limbs within the scanning aperture, anatomical planes (e.g., coronal and parasagittal) were ascertained from skeletal cross-sectional morphology (see below). Scans were assessed for imaging artifacts and were repeated as needed.

Data Processing

Scan images were exported as bitmap (BMP) files for analysis. Image size dimensions were automatically established for each series of scans by the XCT software and these sizes were maintained to account for size variation within the sample. Visual inspection was performed to assure scan quality and unusable scans were excluded from analysis. The fibula was not included in our analysis due to insufficient image resolution. Data processing was conducted using custom MATLAB code (created by A.D.S. and G.J.W) that will be briefly summarized here. Cortical cross-sections were segmented from the surrounding soft tissue in each scan using pixel thresholding, resulting in binary images. Centroid location for each bone was determined and directional axes originating from the centroids were established from bone cross-sectional

morphology. For the forearm scan series, the 50% slice image was used to manually establish an element specific mediolateral axis for the radius and ulna using the interosseous crest. Thus, the ulnar interosseous crest served as a landmark for the lateral axis, while the radial interosseous crest was used to establish the medial axis. For the leg scan series, the most proximal scan slice of the tibia (65%) was used to establish the anteroposterior axis, using the anterior crest as a guide. These axes were translated to the other slices within a series by maintaining the vector angle from the original slice and originating it from each cross-section's centroid. Following earlier studies (Gosman et al., 2013; Wilson et al., 2020) eight equally spaced radial axes at forty-five degrees apart each were generated in MATLAB from the centroid, using the ascertained anteroposterior and mediolateral axes. Semi-landmarks were then set at the intersections of each axis with the endosteal and periosteal borders of the cortical bone in each cross-section (see Figure 1.2). The distances between the eight pairs of endosteal and periosteal semi-landmarks equaled cortical thicknesses, while the distances between each set of semi-landmarks and the centroid were the endosteal and periosteal distances to the nearest hundredth of a millimeter.

Statistical Analyses

Local age-related variation in cortical thickness, endosteal distance, and periosteal distance were assessed through redundancy analysis (RDA). A combination of multiple linear regression with principal component's analysis (PCA), RDA produces canonical axes (referred to as RDA1, RDA2, etc.) using linear combinations of explanatory variables (e.g. age, sex, BMI) that best describe variation among response variables (e.g. cortical thickness, endosteal distance) (Borcard et al., 2011). Further, RDAs provide scores for both explanatory and response variables that

describe the relative importance of these variables along the constrained axes. In this study, RDA models for each element were first constructed to examine the interaction between age and sex in explaining variance among cortical thickness, endosteal distance, and periosteal distance, henceforth collectively referred to as "distance measurements." Then, should sex differences significantly interact with age, sex-specific models are used to assess the variation explained by age, slice, and the interaction between age and slice on measurement distances across all slices within each element. Slice-specific models were tested to assess the effects of age and BMI on each distance measurement. The resulting scores for response variables along different axes were compared to assess whether the effects of age and/or BMI are uniform throughout a given cross-section. Throughout this study, we used a critical alpha of $p<0.05$.

The distance measurements described above were standardized by height$^{(3/2)}$ to account for differences in overall body size. Following inspection of distance measurements using D'Agostino normality tests, measurement data were log-transformed to conform with RDA assumptions of data normality more closely. Statistical significance of both constrained axes (RDAs) and explanatory variables within each model were tested through permutation ANOVAs (permutations = 9999; $\alpha = 0.05$).

RESULTS

Across the total sample, there is a significant interaction ($p<0.05$) between age and sex for some but not all RDAs in which we examined distance measurements. Significant interactions occur in all tibial distance measurements, as well as in radial cortical thickness and endosteal distance. In the ulna, there were no significant age-sex interactions. Despite differences between elements in the interaction between age and sex effect on measurement distances, significant

interaction effects in all tibial measurements and the radial cortical thickness and endosteal distance measurements suggest that age-related variation in these variables differ between biological females and males. Therefore, subsequent analyses are conducted separately between females and males to assess sex differences in age-related changes to cortical bone geometry.

We next examine whether distance measurements for each element differs with respect to age, slice location, and their interaction. Among females, variation within all distance measurements of the tibia significantly differ with age and among the four slice locations (Table 1.2). Similarly, males show significant differences with age and among slices for tibial cortical thickness and endosteal distance, but only slice location significantly differs in periosteal distances (Table 1.3). Radial cortical thickness and periosteal distances differ with age and slice locations among females (Table 1.2), and an age-slice interaction exists among endosteal distance for females (Table 1.2). Among males, cortical thickness and periosteal distance measurements of the radius differ with age and with slice locations, while only age is significant in explaining endosteal distance variation of the radius (Table 1.3). For both sexes, RDAs showed significant age and slice location effects in explaining variation among all ulnar distance measurements (Tables 1.2 and 1.3). Overall, these results suggest that distance measurements are not the same with age. Differences between slices within elements are unsurprising, as these results reflect distinctions in the size and shape of cross-sections throughout the length of the diaphysis in each element.

Given the differences in slice dimensions within each element, we focus our analyses on age-related differences within individual slices. Within slice-specific models, we include age and BMI as factors. No significant age or BMI effects on cortical thickness are detected in either the 20% slice or the 35% slice of the tibia for either sex (Table 1.4). Among females, variation in

cortical thickness in slices at 50% and 65% of diaphyseal length are not the same with age, while significant differences among ages in male occur only in the 65% slice (Table 1.4). For endosteal distance, both age and BMI significantly differ in the 35%, 50%, and 65% tibial slices among females, while in males, much like cortical thickness, only the 65% slice location differs with age (Table 1.5). Variation in tibial periosteal distances among females is more strongly related to BMI; all slices have significant BMI effects but not statistically significant age effects on periosteal distance (Table 1.6). Males exhibit no significant age or BMI effect on periosteal distances across tibial slices (Table 1.6).

These trends are more subtle in the distance measurements of the radius. Radial cortical thickness varies significantly with age at each slice location in females but not in males (Table S1.1). No significant differences in cortical thickness are associated with BMI for either sex. Endosteal distances differ significantly with age and BMI across all slice locations in the radii of the female subsample (Table S1.2), while the only difference among males occurs with age for the 35% slice (Table S1.2). Periosteal distances in females significantly differ by BMI at the 35%, 50%, and 65% radial slice locations (Table S1.3). No significant effects on periosteal distances of the radius are found in males (Table S1.3).

The pattern of variation in the ulna is similar to those we report for the radius. Cortical thickness in the ulna varies significantly with age at the 35% and 50% slice locations in females, but not in any slice locations in males (Table S1.4). Cortical thickness does not differ with BMI in either sex (Table S1.4). In contrast, endosteal distances significantly differ with age at every slice location of the ulna for both sexes (Table S1.5), and endosteal distances at the 35% and 50% slice locations in females and at the 65% slice location in males significantly differ with BMI (Table S1.5). Periosteal distance in the ulna varies significantly by age and BMI in females

at the 35% and 50% slice locations (Table S1.6). Among males, periosteal distance significantly differs with age for each ulnar slice location, but there are no significant BMI effects (Table S1.6).

Overall, these results show that distance measures broadly differ as individuals age for some slice locations within each element, while fewer differences are observed among individuals with different body mass indices. In most distance measures, females exhibit more significant relationships between differences in distance measurements and age than males. Effects of BMI are observed mainly for differences in periosteal distance, however this is not consistent across bones or slice locations. In most instances, variation in distance measurements is significantly explained by the first canonical axis, which in most instances reflect the majority of the variance in the linear combination of distance measures for each slice location. Given the more consistent effect of age on differences in distance measures, we focus our analyses on sex-specific intra-slice variation in distance measures by grouping ages into decadal groups (e.g., 40-49, 50-59 years old (y/o)).

Tibia: Intra-slice Differences with Age

In the tibia, based on the RDA results, we only examine cortical distance for the 50% and 65% slice locations using Tukey's HSD to compare among age groups. There are significant age-related differences between the 40-49 y/o group and the 70-79 y/o group along the anteromedial aspect at 50% length, and the lateral, medial, and anteromedial aspect of the 65% length among females (Table S1.7; Figure 1.3). Males have significant differences only at the lateral (between 50-59 & 70-79 y/o groups) and the posteromedial (between 40-49 & 70-79 y/o groups) aspects (Table S1.8). Mean percent difference between the youngest and oldest age

group also show that the greatest discrepancies in tibial cortical thickness among females occur at the 50% and 65% locations (Figure 1.3). At the 50% slice location, the greatest differences are in the posteromedial, medial, and anteromedial directions, while the anterior and anterolateral directions have the least differences (Figure 1.3). The 65% location has greater differences that are more evenly distributed across the directional radii, with the exception of the posterior and posteromedial directions (Figure 1.3). Among males, the greatest differences between the youngest and oldest age groups were in the medial direction for 50% length and the posteromedial direction for 65% length (Figure 1.3). In all instances of significant differences between age groups, cortical bone thickness is greater in the younger age group for both sexes.

Differences in endosteal and periosteal distances compliment the patterns observed in cortical thickness, with some notable exceptions. In almost all cases, endosteal and periosteal distances are greater in the older age groups (Figures 1.4 and 1.5). Significant age-related differences in endosteal distances of the tibia among females are at all slice locations and are more widely distributed across directional radii than cortical thickness differences (Table S1.9). Among males, significant differences between the 40-49 and 70-79 y/o groups are observed at the posterior and posteromedial aspects (Table S1.10). Periosteal distances differ significantly among females at the 20%, 50%, and 65% lengths, primarily between the 40-49 and 50-59 y/o groups (Table S1.11). Significant differences also occur between the 40-49 and 60-69 y/o groups at the anterolateral, lateral, and posteromedial directions of the 20% slice location and at the posterior and posteromedial directions of the 50% slice (Table S1.11). Males have significant age group differences in periosteal distances mainly at the 20% slice location, where differences are observed at the anterolateral, posterior, and posteromedial directions (Table S1.12). Differences in tibial endosteal and periosteal distances between the youngest and oldest age

groups for females are presented in Figure 1.4. The overall patterns of variation between endosteal and periosteal distances are similar, with greater differences being observed at the 50% and 65% slice at the posterior, posteromedial, medial, anteromedial, and anterior aspects of the bone (Figure 1.4). Across slice locations, the anterolateral, lateral, and posterolateral generally show smaller differences between the youngest and oldest age groups (Figure 1.4). Males have more concentrated differences along the posterior/posteromedial and anterior/anterolateral directions for both endosteal and periosteal distances at each slice location (Figure 1.5).

Radius: Intra-slice Differences with Age

Significant age-group differences in cortical thickness among females are observed broadly across directional radii for all slices of the radius (Table S1.13). No significant age-group differences are on the medial, anteromedial, and anterior directional radii at 20% length, the medial and anteromedial radii at 35% length, and the medial radii at 50% and 65% length (Table 18). Among males, age-related differences are primarily between the 50-59 and 70-79 y/o groups at 20% and 35% length, distributed somewhat evenly across directional radii (Table S1.14). The anteromedial direction shows differences between several age groups at the 20%, 35%, and 50% slice locations, while no significant age group differences are observed at the 65% location (Table S1.14). Proportional percent differences in radial cortical thickness by direction between 40-49 and 70-79 y/o groups show similar patterns between males and females, with females showing larger differences overall than males (Figure 1.6). At 20% radial length, the lateral direction exhibits the greatest age-related differences, followed by the posteromedial direction in females and the medial direction in males (Figure 1.6). At 35% of radial length, the anterolateral and posterior directions exhibit the most difference with age in both sexes (Figure 1.6). At 50%,

females exhibit large differences in cortical thickness at the anteromedial, anterior, anterolateral, and posteromedial directions, while the only substantial difference at midshaft among males is along the anterior direction (Figure 1.6). At 65% length, the medial direction exhibits the greatest difference between the youngest and oldest age groups in females, while the greatest difference among males is along the anterior direction (Figure 1.6).

Results from Tukey HSD tests comparing endosteal distances among females show significant age group differences across all directions and slice locations (Table S1.15). Differences are primarily between the 40-49 and 60-69 y/o groups and the 40-49 and 70-79 y/o groups. Among males, differences are in the anterior direction for the 35%, 50%, and 65% slice locations (Table S1.16). Tukey HSD test results for comparisons of periosteal distances indicate age group differences among females distributed variably across slices: at 20% of radial length, differences are mainly between 40-49 and 60-69 y/o groups along the anterior, lateral, and posterolateral directions; at 35% length, between both the 40-49 and 50-59 y/o groups as well as 40-49 and 60-69 y/o groups differences are along the anterolateral and lateral directions; at 50% length, differences are medial, anteromedial, anterior, lateral, and posterolateral between the 40-49 and 60-69 y/o groups and 40-49 and 70-79 y/o groups; and at 65% length, significant differences between the 40-49 and 60-69 y/o groups are at the anteromedial, anterior, posterior, and posteromedial directions (Table S1.17). Among males, fewer significant differences between age groups occur, with those that occur between the 40-49 and 70-79 y/o groups along the anterolateral and posterior directions at 50% of radial length and the posterior and posteromedial directions at 65% length (Table S1.18).

Percent differences in endosteal and periosteal distances of the radius among females mirror each other closely, with a few exceptions (Figure 1.7). At 35% of radial length, greater

differences in endosteal distance are along the anterior, posterior, and posteromedial directions while differences in these directions for periosteal distance are comparatively small relative to other directions (Figure 1.7). Additionally, the lateral and posterolateral directions have comparatively high differences relative to other directions for periosteal distances while these directions are somewhat middling for endosteal distance (Figure 1.7). Along the length of the bone, the pattern of differences by direction changes from the greatest differences at the medial, anteromedial, and anterior directions at the 50% and 65% locations, while the lateral, posterolateral, and posterior directions have the greatest differences at the 20% and 35% locations (Figure 1.7). Among males, patterns of difference between the youngest and oldest age groups are consistent between endosteal and periosteal distances: across all slices, the anterior, anterolateral, and posterior directions exhibit proportionally higher differences than other directional radii (Figure 1.8). The anteromedial direction also has high difference between youngest and oldest age groups at the 65% and 20% slice locations (Figure 1.8).

Ulna: Intra-slice Differences with Age

Tukey HSD test results of age group comparisons in ulnar cortical thickness among females indicate that most significant age groups differences are seen at 35% and 50% slice locations (Table S1.19). Between the youngest and oldest age groups, females have the highest percent difference in cortical thickness along the medial direction for the 65%, 50%, and 35% slice locations, and along the posteromedial direction of the 20% location (Figure 1.9). Among males, fewer significant age group differences are indicated and are mostly at in the anteromedial region of the 35% and 20% slice locations (Table S1.20). Notably, significantly greater cortical thickness differences are observed at the posterior direction between 40-49 and 50-59 y/o groups

and at the posteromedial direction between 40-49 and 60-69 y/o groups (Table S1.20). This difference in the posteromedial direction is also observed in the comparison of percent differences between youngest and oldest age groups by direction, particularly at the 50% slice location (Figure 1.9). Additionally, greater negative differences are observed at the 20% slice location compared to more proximal slices (Figure 1.9).

Tukey HSD test results for ulnar endosteal distance among females indicate differences observed across most directions at all slices, primarily between the 40-49 and 60-69 y/o groups and 40-49 and 70-79 y/o groups (Table S1.21). Among males, significant differences in ulnar endosteal distances occur between age groups except for the lateral, posterolateral, and posterior directions at the 20%, 35%, and 65% slices (Table S1.22). In contrast to endosteal patterns, significant differences in ulnar periosteal distance between age groups among females are in the posterior, posteromedial, and medial directions of the 20%, 35%, and 50% slice locations (Table S1.23). Similarly, significant differences in ulnar periosteal distances among males are in the posterior/posteromedial directions as well as anterior/anterolateral directions at all slice locations (Table S1.24).

The comparison of percent difference in ulnar endosteal distances between the youngest and oldest female age groups are similar to patterns of ulnar cortical thickness in females: the medial direction has the greatest difference at 65%, 50%, and 35% slices, while greatest difference at the 20% slice is in the posteromedial direction (Figure 1.10). Percent differences in ulnar periosteal distance among females are mostly similar to patterns in ulnar endosteal distances, though the posterolateral and anterior directions have the highest differences relative to other directional radii at 65% (Figure 1.10). Among males, the patterns of relative percent difference by direction between ulnar endosteal and periosteal distances are similar. At the 65% and 50% slice locations,

the anterolateral direction exhibits the greatest percent difference for both endosteal and periosteal distances, though the posteromedial direction has greater differences in periosteal distance than endosteal distance (Figure 1.10). At the 35% and 20% slice locations, the medial direction has the greatest percent difference for endosteal distance, while high percent differences for periosteal distance occur in the medial, lateral, and anterolateral directions (Figure 1.10).

DISCUSSION

The principal aims of this study were to examine measurements associated with cortical expansion to determine whether this age-related process occurs uniformly or varies locally by direction within a cross-section and whether these patterns are consistent across slice locations. Our results indicate that age-related differences in endosteal and periosteal distances have remarkably similar patterns within the same cross-section (Figures 1.4, 1.5, 1.7, 1.8, 1.10, and 1.11), suggesting that systemic factors are coupling the modeling of cortical bone in both the inner (endosteal) and outer (periosteal) envelopes with age. However, the degree of age-related changes in these measures varies by direction within a cross-section and these patterns of variation are not always consistent along the length of the bone. Shifting patterns of local variation in these measures are particularly marked in the radius and, to a lesser extent, the ulna (Figures 1.6-1.11). Local variation of age-related cortical geometric changes has been reported elsewhere (Ruff and Hayes, 1982; Feik et al., 2000; Wilson et al., 2020) and suggests that systemic processes implicated in aging are mediated by local factors. To better understand these patterns, it is important to understand the role of slice location on cortical bone geometry before considering this localized intra-slice variation.

The results of analyses examining effects of slice location on age-related geometric differences in the tibia, radius, and ulna support our first hypothesis and precedent in the literature (Shaw et al., 2014; Gooding, 2017) that differences in cross-sectional distributions of cortical bone will not be the same along the length of an element. RDA results indicate that variation in cortical thickness, endosteal distance, and periosteal distance for both females and males significantly differs among locations along the diaphyses of all elements except for endosteal distance of the radius in males (Tables 1.2 and 1.3). This result was expected given that bone morphology is not consistent along the length of the bone. For example, the tibia has a tapering shape from proximal to distal, so endosteal and periosteal distances will inherently be larger at more proximal slice locations. We found a significant interaction between age and slice location for endosteal distance of the radius among females, indicating that age-related differences in this measure are mediated by position along the length of the bone. A closer examination of the pattern of radial endosteal measures among females (Figure 1.7) shows a shift in the greatest differences located the lateral and posterior aspects of the cross-section in distal slices (20% and 35%) to greater differences in proximal slices (50% and 65%) at the anterior, anteromedial, and medial directions. Similar differences in patterns between age groups also appear in cortical thickness distributions in all three elements (Figures 1.3, 1.6, and 1.9) though there was no significant interaction between slice location and age for these distance measures. Thus, we conclude that though there is apparent coupling between endosteal resorption and periosteal deposition, the areas where these processes occur results in distinct directional changes in cortical bone distribution across age. When we performed slice-specific RDAs, however, age did not significantly explain variation in distance measurements at every slice, particularly for tibial and ulnar cortical thickness (Tables 1.4 and S1.4). Additionally, in examination of intra-

slice variation, we see clear differences in the magnitude of percent differences between the 40-49 y/o and 70-79 y/o groups along the length of each bone. This uneven pattern of differences is especially marked in the tibia where greater differences are present in cortical thickness and endosteal distance among females at the 65% and 50% slice locations compared to the 35% and 20% locations (Figures 1.3 and 1.4). Interestingly, greater change in the proximal tibia than more distal sites is also observed in ontogeny (Gosman et al., 2013) and from archaeological contexts (Ruff and Hayes, 1982).

Variation in age-related differences along the length of long bones adds support to the idea that these processes are best examined using a "whole bone" perspective (Gosman et al., 2013; Gooding, 2017). Clinically-oriented studies are often focused on sites of medical relevance, like the distal radius, femoral neck, and distal tibia (Beck et al., 2001; Lauretani et al., 2008). Meanwhile, biomechanical studies of cross-sectional geometry often regard the diaphyseal midshaft as the most representative region for demonstrating mechanically relevant cortical geometry (Ruff and Hayes 1982; Ruff et al., 1987; cf. Macintosh et al., 2013). This convention is borne from modeling bone as a hollow, uniformly cylindrical beam where maximum bending strain occurs at 50% length. Therefore, mechanically adaptive shape differences will be most marked at midshaft (Currey, 2006). However, human long bone morphology is often irregularly shaped and its morphology changes along its length, so strain is distributed unevenly throughout the bone. Additionally, since elements are shaped differently and undergo distinct and localized loading patterns, variation along the length of the bone will be further influenced by the bone in question. Our results suggest that, while the clinical and conventional biomechanical approaches are appropriate under different study contexts from those we use, researchers should be explicit about the assumptions made in restricting analyses to parts of diaphyses, as there is evidence that

age-related changes to cortical bone geometry are not equivalent throughout the shafts of at least the tibia, radius, and ulna.

While our study did not assess variables that might contribute to this local variation, mechanical loading is a possible candidate given its role in shaping bone geometry during growth through modeling (Lieberman et al., 2003; Pearson and Lieberman, 2004; Gosman et al., 2011). Following pubertal growth, bone becomes less responsive to mechanical loading through adaptive modeling (Leiberman et al., 2003). However, one posited explanation for local variation in age-related geometric changes to cortical bone is that bone is still responsive to loading, but through maintenance instead of modeling (Ruff and Hayes, 1987; Robling and Turner, 2009; Bergmann et al., 2011). In other words, as systemic bone loss occurs with aging, areas of skeletal elements that experience greater strain from loading are preferentially maintained compared to low-strain areas. This concept is supported by evidence from athlete studies demonstrating that continual activity into advanced age maintains cortical geometries adapted at younger ages through modeling (Korhonen et al., 2012; Warden et al., 2014). Similar results were reported by Biver and colleagues (2016), who found that individuals engaged in heavy-loading occupational activities had cross-sectional properties related to greater bone strength compared to those involved in less loading-intensive occupations.

If habitual activity does mediate changes in cortical bone with age through preferential maintenance, the results of this study suggest that the interaction of bone geometry and mechanical loading may not be easily linked to variation in age-related changes in cortical bone geometry. For example, the tibia is generally expected to experience loading primarily along the anteroposterior axis from normal activities (i.e. gait) (Cristofolini et al. 2013). In addition, as argued in Auerbach et al. (2017), the distribution of cortical bone in the tibia relates to the

position of the fibula, which shares load with the tibia (Funk et al., 2004). As we noted in the Introduction, we expected cortical bone to be thinner preferentially on the lateral side of the tibia on account of this load-sharing. However, our results indicate that age-related differences in endosteal and periosteal distance are lowest along the lateral aspect of the tibia and greatest along the posteromedial to anterior aspect (Figures 1.4 and 1.6). This result is contrary to an expectation of conservation at the anterior and posterior aspects, as well as the load-sharing that occurs with the fibula. Wallace and colleagues (2014) found similar results during an experimental study examining the osteogenic effects of exercise on sheep. Sheep tibiae had the highest strain along the anteroposterior axis, yet periosteal deposition in exercised subjects occurred primarily on the medial half of the cross-section (Wallace et al., 2014). Thus, it appears that while strain influences cortical bone geometry, the response to this relationship is complex and likely informed by other factors that make it difficult to interpret loading history by examining bone modeling or remodeling after the end of primary growth (Stewart et al. 2015).

Similarly, intra-slice differences among age groups in cortical dimensions in the radius and ulna are difficult to interpret. The upper limb is involved in a wider variety of movements (elbow flexion/extension, forearm pronation/supination, wrist movement) than the lower limb and is not weight-bearing, so typical loading patterns are not well-characterized for bones of the forearm (Burr and Martin, 1983; Hsu et al., 1993; Junno et al. 2011). Additionally, the radius and ulna are connected along their lengths by an interosseous membrane that plays an important role in load transmission between the two bones (Birbeck et al., 1997). Biomechanical studies assessing load sharing of the forearm among cadaveric specimens generally agree that when compressive loading is applied to the forearm, the distal radius receives about two thirds of the load compared to the ulna's one third, while proximally loads are evenly distributed between the two bones

(Birbeck et al., 1997; Shabaan et al., 2006). Further layers of complexities are introduced by various motions of the wrist and hand, such as wrist extension/flexion, radioulnar deviation, or a combination of these movements (McGregor, 2017). It is possible that the shifting patterns of variation in cortical thickness, endosteal distance, and periosteal distance within radial and ulnar cross-sections are reflective of the wide variety of loading patterns that result from these movements. Our radial results (Figures 1.7 and 1.8) are especially illustrative, as the greatest differences in endosteal and periosteal distances tend to occur in the medial and anterior aspects of the more proximal diaphysis, which are the sides of the radius that are adjacent to the ulna in supination and pronation. If load sharing is more equal between the proximal aspects of the forearm elements, then this fits our hypothesis. Yet, the ulna does not have a complimentary age-related difference, as greater differences in endosteal and periosteal distances occur on the medial side of the proximal ulna (Figures 1.10 and 1.11). Though biomechanical simulation of loading was not performed in our study, we tentatively conclude that factors other than load-generated strain are likely mediating cortical expansion.

What might be these other factors that affect the localized differences in patterns of cortical bone with age? Our results indicate that BMI has a significant effect on distance measures independent of age, though the relationship differs between the tibia and radius, where endosteal and periosteal distances have an inverse relationship with BMI, and the ulna. Other studies indicate that adiposity has less impact on cortical bone structure than lean mass (Pomeroy et al. 2018), though Reeves (2014) did report thicker cortical bone in the humerus, femur, tibia, and fibula of obese individuals. We assume that obesity would have systemic effects on bone geometry, but it is possible that a combination of different postures and mechanical loading patterns could have subtle effects that complicate our understanding of bone cross-sectional

shape in the three elements we examined. It is also possible that the expression of hormones and other factors responsible for bone maintenance (e.g., Watanabe-Takano et al., 2021; Wang et al., 2022) change with age, either due to expression or differences in mechanical loading patterns associated with aging. Disentangling the effects of mechanical loading, direct effects of body size, and regulatory factors on bone cortical geometry and its potential change with respect to age awaits future experimental studies.

This study has a few limitations beyond those we raise above. While our sample sizes are adequate to address our questions, the smaller number of males (especially younger males) is cause for concern that our sample is biased or more affected by outliers. This may explain why the male patterns were more attenuated in comparison with females. Our study is also limited by using a cross-sectional sampling approach instead of a longitudinal sample. We assume in this study that the mean patterns of cortical bone distance measures among individuals in different age groups is a good representation of how bone shape and structure would change in a population over time. It would be beneficial to assess this assumption by tracking changes in cross-sectional geometry in individuals over decades, though this was outside the scope possible in our study.

CONCLUSION

Our study contributes novel information to the growing model of diaphyseal cortical bone properties in human limb bones. As we noted in the Introduction, age-related cortical expansion has been well-documented in previous studies, but its consistency within a cross-section is not established. We show that cortical bone loss does not occur evenly throughout a diaphysis, both proximodistally and radially. The patterns vary, especially in the forearm bones. The unequal

thinning of cortical bone throughout a cross-section, as well as unequal periosteal deposition of bone, may contribute to the patterns of fracture risk that are not explained by loss of bone mineral content or its density. The fact that we found that thicker cortical bone and differences in the envelope distance measures do not appear to coincide with expected responses to mechanical loading or load-sharing deserves further consideration with respect to fracture risk. It may be that, while periosteal expansion of the diaphyses of limb long bones does happen, competing factors (or even competing sources of loading) may affect its occurrence within a bone slice or across an element. These multifactorial and likely overlapping influences on cortical bone geometry throughout aging offer an opportunity to refine current understanding of age-related bone loss and its clinical implications.

REFERENCES

Auerbach B.A, Gooding, A. F., Shaw, C. N., & Sylvester, A. D. (2017). The relative position of the human fibula to the tibia influences cross-sectional properties of the tibia. American Journal of Physical Anthropology, 163(1), 148–157.

Beck, T. J., Oreskovic, T. L., Stone, K. L., Ruff, C. B., Ensrud, K., Nevitt, M. C., Genant, H. K., & Cummings, S. R. (2001). Structural Adaptation to Changing Skeletal Load in the Progression Toward Hip Fragility: The Study of Osteoporotic Fractures. Journal of Bone and Mineral Research, 16(6), 1108–1119.

Bergmann P., Body, J. J., Boonen, S., Boutsen, Y., Devogelaer, J. P., Goemaere, S., Kaufman, J., Reginster, J. Y., & Rozenberg, S. (2011). Loading and Skeletal Development and Maintenance. Journal of Osteoporosis, 786752–15.

Bilezikian J. P., Lin, C. J. F., Brown, J. P., Wang, A. T., Yin, X., Ebeling, P. R., Fahrleitner-Pammer, A., Franek, E., Gilchrist, N., Miller, P. D., Simon, J. A., Valter, I., Zerbini, C. A. F., Libanati, C., & Chines, A. (2019). Long-term denosumab treatment restores cortical bone loss and reduces fracture risk at the forearm and humerus: analyses from the FREEDOM Extension cross-over group. Osteoporosis International, 30(9), 1855–1864.

Birkbeck, D. P., Failla, J. M., Hoshaw, S. J., Fyhrie, D. P., Schaffler, M. (1997). The interosseous membrane affects load distribution in the forearm. Journal of Hand Surgery, 22(6): 975-980.

Biver, E., Perréard Lopreno, G., Hars, M., van Rietbergen, B., Vallée, J. P., Ferrari, S., Besse, M., & Rizzoli, R. (2016). Occupation-dependent loading increases bone strength in men. Osteoporosis International, 27(3), 1169–1179.

Bliuc D., Alarkawi, D., Nguyen, T. V., Eisman, J. A., & Center, J. R. (2015). Risk of Subsequent Fractures and Mortality in Elderly Women and Men with Fragility Fractures with and without Osteoporotic Bone Density: The Dubbo Osteoporosis Epidemiology Study. Journal of Bone and Mineral Research, 30(4), 637–646.

Burr D. B., & Martin, R. B. (1983). The effects of composition, structure and age on the torsional properties of the human radius. Journal of Biomechanics, 16(8), 603–608.

Chen Y. Y., Fang W. H., Wang C. C., Kao T. W., Chang Y. W., Wu C. J., Zhou Y. C., Sun Y. S., Chen W. L. (2018). Body fat has stronger associations with bone mass density than body mass index in metabolically healthy obesity. PLOS ONE 13(11): e0206812.

Choksi, P., Jepsen, K.J. & Clines, G.A. (2018). The challenges of diagnosing osteoporosis and the limitations of currently available tools. Clin Diabetes Endocrinol 4, 12.

Coin, A., Sergi, G., Benincà, P., Lupoli, L., Cinti, G., Ferrara, L., Benedetti, G., Tomasi, G., Pisent, C., Enzi, G. (2000). Bone mineral density and body composition in underweight and normal elderly subjects. Osteoporosis International 11(12):1043-50.

Cristofolini, L., Angeli, E., Juszczyk, J. M., & Juszczyk, M. M. (2013). Shape and function of the diaphysis of the human tibia. Journal of Biomechanics, 46(11), 1882–1892.

Currey, J. D. (2006). Bones: structure and mechanics. Princeton, NJ: Princeton University Press.

Duan Y., Beck T. J., Wang X., Seeman E. (2003). Structural and biomechanical basis of sexual dimorphism in femoral neck fragility has its origins in growth and aging. Journal of Bone and Mineral Research 18(10): 1766-1774.

Feik, S. A., Thomas, C. D. L., Bruns R., Clement J. G. (2000). Regional variations in cortical modeling in the femoral midshaft: sex and age differences. American Journal of Physical Anthropology 112:191-205.

Funk, J. R., Rudd, R. W., Kerrigan, J. R., Crandall, J. R. (2004). The effect of tibial curvature and fibular loading on the tibia index. Traffic Injury Prevention, 5, 164-172.

Gooding, A. F. (2017). Variation in cortical bone distribution in the aging appendicular skeleton. Doctoral dissertation, The University of Tennessee – Knoxville.

Gosman J. H., Stout, S. D., and Larsen, C. S. (2011). Skeletal biology over the life span: A view from the surfaces. American Journal of Physical Anthropology 146(S53): 86-98.

Gosman J. H., Hubbell, Z. R., Shaw, C. N., & Ryan, T. M. (2013). Development of Cortical Bone Geometry in the Human Femoral and Tibial Diaphysis. Anatomical Record (Hoboken, N.J. : 2007), 296(5), 774–787.

Guise T. A. (2006). Bone loss and fracture risk associated with cancer therapy. Oncologist, 11(10):1121-31.

Hsu E. S., Patwardhan, A. G., Meade, K. P., Light, T. R., & Martin, W. R. (1993). Cross-sectional geometrical properties and bone mineral contents of the human radius and ulna. Journal of Biomechanics, 26(11), 1307,1311–1309,1318.

Jepsen, K. J., Andarawis-Puri, N. (2012). The amount of periosteal apposition required to maintain bone strength during aging depends on adult bone morphology and tissue-modulus degradation rate. Journal of Bone and Mineral Research, 27(9), 1916–1926.

Johnell, O., Kanis, J. A., Oden, A., et al. (2005). Predictive value of BMD for hip and other fractures. J Bone Miner Res., 20(7):1185–94.

Junno, J., Niinimäki, S., Niskanen, M., Nunez, M., & Tuukkanen, J. (2011). Cross sectional properties of the human radial tuberosity. Homo, 62(6), 459–465.

Korhonen M. T., Heinonen A., Siekkinen J., Isolehto J., Alén M., Kiviranta I., Suominen H. (2012). Bone density, structure and strength, and their determinants in aging sprint athletes. Medicine and Science in Sports and Exercise, 44(12): 2340-2349.

Kushwaha N. S., Verma V., Singh A., Sharma Y., Singh A. (2022). A study of factors associated with carrying angle of the human elbow in pediatric age group. Cureus; 14(5): e25478.

Lauretani F., Bandinelli S., Griswold M. E., Maggio M., Semba R., Guralnik J. M., Ferruci L. (2008). Longitudinal Changes in BMD and Bone Geometry in a Population-based study. Journal of Bone and Mineral Research 23(3): 400-408.

Lieberman, D. E., Pearson, O. M., Polk, J. D., Demes, B., Crompton, A. W. (2003). Optimization of bone growth and remodeling in response to loading in tapered mammalian limbs. Journal of Experimental Biology 206: 3125-3138.

Macintosh A. A., Davies, T. G., Ryan, T. M., Shaw, C. N., & Stock, J. T. (2013). Periosteal versus true cross-sectional geometry: A comparison along humeral, femoral, and tibial diaphyses. American Journal of Physical Anthropology, 150(3), 442–452.

Manolagas, S. C., O'Brien, C. A., Almeida, M. (2013). The role of estrogen and androgen receptors in bone health and disease. Nature Reviews Endocrinology 9: 699-712.

Martin, R. B, Burr, D. B., Sharkey, N. A., & Fyhrie, D. P. (2015). Skeletal Tissue Mechanics (2nd ed. 2015.). Springer New York.

McCloskey E. V., Odén, A., Harvey, N. C., Leslie, W. D., Hans, D., Johansson, H., & Kanis, J. A. (2015). Adjusting Fracture Probability by Trabecular Bone Score. Calcified Tissue International, 96(6), 500–509.

McCloskey E. V., Oden, A., Harvey, N., Leslie, W., Hans, D., Johansson, H., Barkmann, R., Boutroy, S., Brown, J., Chapurlat, R., Elders, P., Fujita, Y., Gluer, C., Goltzman, D., Iki, M., Karlsson, M., Kindmark, A., Kotowicz, M., Kurumatani, N., Kwok, T., Lamy, O., Leung, J., Lippuner, K., Ljunggren, O., Lorentzon, M., Mellstrom, D., Merlijn, T., Oei, L., Ohlsson, C., Pasco, J. A., Rivadeneira, F., Rosengren, B., Sornay-Rendu, E., Szulc, P., Tamaki, J., Kanis, J. (2016). A Meta-Analysis of Trabecular Bone Score in Fracture Risk Prediction and Its Relationship to FRAX. Journal of Bone and Mineral Research, 31(5), 940–948.

McGregor, M. E. (2017). A Biomechanical Investigation of Load Sharing at the Distal Forearm. Electronic Thesis and Dissertation Repository. 4944.
Melton L. J., Atkinson, E. J., O'Connor, M. K., O'Fallon, W. M., & Riggs, B. L. (1998). Bone Density and Fracture Risk in Men. Journal of Bone and Mineral Research, 13(12), 1915–1923.

Miller P.D., Siris, E. S., Barrett-Connor, E., Faulkner, K. G., Wehren, L. E., Abbott, T. A., Chen, Y., Berger, M. L., Santora, A. C., & Sherwood, L. M. (2002). Prediction of Fracture Risk in Postmenopausal White Women With Peripheral Bone Densitometry: Evidence From the National Osteoporosis Risk Assessment. Journal of Bone and Mineral Research, 17(12), 2222–2230.

Orwoll, E.S. (2003). Toward an Expanded Understanding of the Role of the Periosteum in Skeletal Health. Journal of Bone and Mineral Research, 18(6), 949–954.

Pasco J.A., Seeman, E., Henry, M. J., Merriman, E. N., Nicholson, G. C., & Kotowicz, M. A. (2006). The population burden of fractures originates in women with osteopenia, not osteoporosis. Osteoporosis International, 17(9), 1404–1409.

Pearson, O. M., Lieberman, D. E. (2004). The aging of Wolff's "law": Ontogeny and responses to mechanical loading in cortical bone. American Journal of Physical Anthropology, 125(S39), 63–99.

Pomeroy, E., Macintosh, A., Wells, J. C. K., Cole, T. J., & Stock, J. T. (2018). Relationship between body mass, lean mass, fat mass, and limb bone cross-sectional geometry: Implications for estimating body mass and physique from the skeleton. American Journal of Physical Anthropology, 166(1), 56–69.

Reeves, N. M. (2014). Augmenting functional adaptation : does obesity have a systemic effect on bone strength properties in humans? Doctoral Dissertation: The University of Tennessee, Knoxville.

Robling A. G., & Turner, C. H. (2009). Mechanical signaling for bone modeling and remodeling. Critical Reviews in Eukaryotic Gene Expression, 19(4), 319–338.

Ruff, C. B., Hayes, W. B. (1982). Subperiosteal expansion and cortical remodeling of the human femur and tibia with aging. Science 217(4563):945-948.

Ruff, C. B. (1987). Sexual dimorphism in human lower limb bone structure: relationship to subsistence strategy and sexual division of labor. Journal of Human Evolution, 16(5), 391–416.

Russo, C. R., Lauretani, F., Bandinelli, S., Bartali, B., Di Iorio, A., Volpato, S., Guralnik, J. M.,

Harris, T., & Ferrucci, L. (2003). Aging bone in men and women: Beyond changes in bone mineral density. Osteoporosis International, 14(7), 531–538.

Schuit S.C.E., van der Klift, M., Weel, A. E. A. ., de Laet, C. E. D. ., Burger, H., Seeman, E., Hofman, A., Uitterlinden, A. ., van Leeuwen, J. P. T. ., & Pols, H. A. (2004). Fracture incidence and association with bone mineral density in elderly men and women: the Rotterdam Study. Bone (New York, N.Y.), 34(1), 195–202.

Shaaban, H., Giakas, G., Bolton, M., Williams, R., Scheker, L. R., Lees, V. C. (2004). The distal radioulnar joint as a load-bearing mechanism - a biomechanical study. Journal of Hand Surgery, 29(1): 85-95.

Shaw, C. N., Stock, J. T., Davies, T. G., Ryan, T. M. (2014). Does the distribution and variation in cortical bone along lower limb diaphyses reflect selection for locomotor economy? In K. J. Carlson and D. Marchi (eds.), Reconstructing Mobility: Environmental, Behavioral, and Morphological Determinants. Springer, NY.

Siris E.S., Adler, R., Bilezikian, J., Bolognese, M., Dawson-Hughes, B., Favus, M. J., Harris, S. T., Jan de Beur, S. M., Khosla, S., Lane, N. E., Lindsay, R., Nana, A. D., Orwoll, E. S., Saag, K., Silverman, S., & Watts, N. B. (2014). The clinical diagnosis of osteoporosis: a position statement from the National Bone Health Alliance Working Group. Osteoporosis International, 25(5), 1439–1443.

Stewart M.C., Goliath, J. R., Stout, S. D., & Hubbe, M. (2015). Intraskeletal Variability of Relative Cortical Area in Humans. Anatomical Record (Hoboken, N.J. : 2007), 298(9), 1635–1643.

Sume, B. W. (2019). Estimation of body height from percutaneous length of tibia in Debre Markos University students, North West Ethiopia. Egypt J Forensic Sci; 9, 51.

Wallace I. J., Demes, B., Mongle, C., Pearson, O. M., Polk, J. D., & Lieberman, D. E. (2014). Exercise-induced bone formation is poorly linked to local strain magnitude in the sheep tibia. PloS One, 9(6), e99108–e99108.

Wang L., You, X., Zhang, L., Zhang, C., & Zou, W. (2022). Mechanical regulation of bone remodeling. Bone Research, 10(1), 16–16.

Warden, S. J., Mantila Roosa, S. M., Kersh, M. E., Hurd, A. L., Fleisig, G. S., Pandy, M. G., Fuchs, R. K. (2014). Physical activity when young provides lifelong benefits to cortical bone size and strength in men. Proceedings of the National Academy of Sciences, USA, 111(14): 5337-5342.

Watanabe-Takano, H., Ochi, H., Chiba, A., Matsuo, A., Kanai, Y., Fukuhara, S., Ito, N., Sako, K., Miyazaki, T., Tainaka, K., Harada, I., Sato, S., Sawada, Y., Minamino, N., Takeda, S., Ueda, H. R., Yasoda, A., & Mochizuki, N. (2021). Mechanical load regulates bone growth via periosteal Osteocrin. Cell Reports (Cambridge), 36(2), 109380–109380.

Wilson, L. A. B., De Groote, I., Humphrey L. T. (2020). Sex differences in the patterning of age-related bone loss in the human hallucal metatarsal in rural and urban populations. American Journal of Physical Anthropology 171(4): 628-644.

Woo J., Kwok T., Leung J. C. S., Ohlsson C., Vandenput L., Leung P. C. (2012). Sex steroids and bone health in older Chinese men. Osteoporosis International 23: 1553-1562.

APPENDIX 1

Table 1.1: Sex and age demographics of the sample used in this study.

Age Range	Female	Male	Female BMI (mean/standard deviation)	Male BMI (mean/standard deviation)
40-49 years	20	9	25.62/4.01	28.45/4.91
50-59 years	28	11	28.08/5.63	27.78/3.08
60-69 years	18	13	27.40/4.50	30.68/3.71
70-79 years	12	15	30.17/5.50	27.95/5.68
Total by sex	**78**	**48**	**27.61/5.10**	**28.76/4.52**

Table 1.2: RDA Results Summary: Variation in cortical thickness, endosteal distance, and periosteal distance by age and slice among females. Values in parentheses are percentage of total variance explained by RDA model for each element.

Cortical Thickness (tibia: 15.73%, radius: 12.22%, ulna: 35.21%)									
	RDA 1			RDA 2			RDA 3		
	Tibia	Radius	Ulna	Tibia	Radius	Ulna	Tibia	Radius	Ulna
Proportion Explained	77.44%	84.23%	96.81%	21.50%	10.22%	2.77%	1.05%	5.56%	0.42%
Age	**-0.539***	**-0.801***	**-0.177***	**0.771***	**0.546***	**0.970***	0.338	0.245	-0.164
Slice	**0.840***	**0.557***	**0.968***	**0.542***	**0.792***	**0.233***	0.023	0.199	-0.094
Age*Slice	0.566	0.217	0.775	0.824	0.969	0.558	-0.004	0.121	-.0298
Endosteal Distance (tibia: 15.02%; radius: 15.73%, ulna: 11.29%)									
	RDA 1			RDA 2			RDA 3		
	Tibia	Radius	Ulna	Tibia	Radius	Ulna	Tibia	Radius	Ulna
Proportion Explained	84.65%	92.89%	89.11%	15.04%	4.45%	9.81%	0.38%	2.66%	1.08%
Age	**-0.651***	-0.939**	**-0.985***	**0.744***	0.337	-0.171	0.152	-0.070	0.007
Slice	**-0.732***	0.215**	**0.083***	**-0.681***	0.777	-0.905	0.018	0.591	-0.416
Age*Slice	-0.931	**-0.190***	-0.324	-0.356	0.745	-0.801	-0.083	0.639	-0.504
Periosteal Distance (tibia: 29.34%; radius: 8.24%; ulna: 26.51%)									
	RDA 1			RDA 2			RDA 3		
	Tibia	Radius	Ulna	Tibia	Radius	Ulna	Tibia	Radius	Ulna
Proportion Explained	96.87%	75.71%	98.09%	2.92%	22.16%	1.66%	<0.01%	2.14%	0.25%
Age	**-0.186***	**0.859***	**-0.379***	0.978	**0.423***	-0.756	0.096	-0.288	0.534
Slice	**-0.977***	**0.487***	**-0.947***	-0.211	**-0.113***	0.297	-0.027	0.113	-0.121
Age*Slice	-0.975	0.790	-0.972	0.165	-0.595	0.050	-0.146	0.147	0.230

* Significant effect ($p < 0.05$) based on permutation ANOVA.

** If significant interaction effect is detected, permutation ANOVA does not consider individual variables.

Table 1.3: RDA Results Summary: Variation in cortical thickness, endosteal distance, and periosteal distance by age and slice among males. Values in parentheses are percentage of total variance explained by RDA model for each element.

Cortical Thickness (tibia: 13.61%, radius: 6.50%, ulna: 37.18%)									
	RDA 1			RDA 2			RDA 3		
	Tibia	Radius	Ulna	Tibia	Radius	Ulna	Tibia	Radius	Ulna
Proportion Explained	81.79%	81.95%	96.54%	15.94%	12.48%	3.28%	2.27%	5.58%	0.18%
Age	**0.059***	**-0.476***	**-0.090***	0.743	0.878	**0.994***	0.667	-0.048	-0.055
Slice	**0.994***	**0.871***	**0.996***	0.059	0.468	**0.084***	-0.088	0.151	-0.031
Age*Slice	0.893	0.639	0.873	0.448	0.767	0.476	0.055	-0.050	0.109
Endosteal Distance (tibia: 17.92%; radius: 7.61%, ulna: 12.83%)									
	RDA 1			RDA 2			RDA 3		
	Tibia	Radius	Ulna	Tibia	Radius	Ulna	Tibia	Radius	Ulna
Proportion Explained	96.6%	83.66%	63.91%	1.83%	13.02%	33.65%	1.57%	3.32%	2.44%
Age	**0.347***	**-0.944***	**-0.993***	0.936	0.325	**-0.117***	0.058	-0.057	-0.008
Slice	**0.943***	0.330	**0.122***	-0.310	0.940	**-0.991***	0.123	0.084	-0.048
Age*Slice	0.996	-0.046	-0.280	0.084	0.992	-0.953	-0.031	-0.115	0.113
Periosteal Distance (tibia: 32.50%; radius: 6.16%; ulna: 29.05%)									
	RDA 1			RDA 2			RDA 3		
	Tibia	Radius	Ulna	Tibia	Radius	Ulna	Tibia	Radius	Ulna
Proportion Explained	98.27%	65.95%	95.37%	0.01%	27.92%	3.44%	<0.01%	6.12%	1.20%
Age	0.182	**0.974***	**0.384***	0.023	**0.225***	0.917	0.983	0.007	-0.110
Slice	**0.990***	**0.215***	**0.921***	-0.016	**-0.977***	-0.380	-0.138	0.017	0.083
Age*Slice	0.956	0.566	0.981	0.160	-0.802	0.036	0.249	0.189	0.190

* Significant effect ($p < 0.05$) based on permutation ANOVA.

Table 1.4. Tibial RDA Results: Variation in cortical thickness by age and BMI.

	Female		Male	
Tibia: 20% Length (F: 5.51%; M: 3.05%)				
	RDA1	RDA2	RDA1	RDA2
Proportion Explained	80.23%	19.77%	76.98%	23.03%
Age	-0.529	-0.849	-0.849	0.528
BMI	0.686	-0.728	0.509	0.861
Tibia: 35% Length (F: 2.71%; M: 4.17%)				
	RDA1	RDA2	RDA1	RDA2
Proportion Explained	65.09%	34.91%	75.38%	24.62%
Age	0.836	0.548	-0.087	0.996
BMI	-0.303	0.953	0.994	0.110
Tibia: 50% Length (F: 8.41%; M: 5.92%)				
	RDA1	RDA2	RDA1	RDA2
Proportion Explained	86.79%	13.21%	76.30%	23.70%
Age	**-0.999***	-0.036	-0.641	0.768
BMI	-0.235	-0.972	0.753	0.658
Tibia: 65% Length (F:12.21%; M: 9.74%)				
	RDA1	RDA2	RDA1	RDA2
Proportion Explained	92.15%	7.85%	78.28%	21.72%
Age	**-0.999***	0.056	**-0.789***	0.615
BMI	0.077	0.786	0.597	0.803

* Significant effect ($p < 0.05$) based on permutation ANOVA.

Table 1.5. Tibial RDA Results: Variation in endosteal distance by age and BMI.

	Female		Male	
Tibia: 20% Length (F: 6.10%; M: 4.89%)				
	RDA1	RDA2	RDA1	RDA2
Proportion Explained	78.19%	21.81%	84.10%	15.90%
Age	-0.898	0.440	-0.895	0.447
BMI	-0.655	-0.756	0.427	0.905
Tibia: 35% Length (F: 9.56%; M: 6.16%)				
	RDA1	RDA2	RDA1	RDA2
Proportion Explained	90.48%	9.52%	87.05%	12.96%
Age	**-0.762***	0.648	-0.943	0.332
BMI	**-0.829***	-0.559	0.311	0.951
Tibia: 50% Length (F: 16.46%; M: 8.28%)				
	RDA1	RDA2	RDA1	RDA2
Proportion Explained	92.43%	7.57%	84.69%	15.31%
Age	**-0.890***	0.456	-0.899	0.437
BMI	**-0.678***	-0.735	0.417	0.909
Tibia: 65% Length (F:19.10%; M: 12.99%)				
	RDA1	RDA2	RDA1	RDA2
Proportion Explained	98.52%	1.48%	89.22%	10.78%
Age	**-0.892***	0.452	**-0.823***	0.567
BMI	**-0.665***	-0.746	0.549	0.836

* Significant effect ($p < 0.05$) based on permutation ANOVA.

Table 1.6. Tibial RDA Results: Variation in periosteal distance by age and BMI.

	Female		Male	
Tibia: 20% Length (F: 7.00%; M: 6.03%)				
	RDA1	RDA2	RDA1	RDA2
Proportion Explained	81.86%	18.14%	83.71%	16.29%
Age	-0.406	0.914	-0.975	0.222
BMI	**-0.987***	-0.160	0.200	0.980
Tibia: 35% Length (F: 10.81%; M: 6.24%)				
	RDA1	RDA2	RDA1	RDA2
Proportion Explained	90.71%	9.29%	68.44%	31.56%
Age	-0.433	0.902	-0.616	0.788
BMI	**-0.985***	-0.174	0.774	0.634
Tibia: 50% Length (F: 8.36%; M: 7.31%)				
	RDA1	RDA2	RDA1	RDA2
Proportion Explained	91.22%	8.78%	79.77%	20.23%
Age	-0.502	0.865	-0.420	0.907
BMI	**-0.968**	-0.251	0.898	0.441
Tibia: 65% Length (F: 10.83%; M: 7.06%)				
	RDA1	RDA2	RDA1	RDA2
Proportion Explained	92.38%	7.62%	84.64%	15.36%
Age	-0.718	0.696	-0.486	0.874
BMI	**-0.857***	-0.517	0.863	0.506

* Significant effect ($p < 0.05$) based on permutation ANOVA.

Figure 1.1. Positioning of participants in pQCT scanner. *Left*: Participant is seated with non-dominant leg in scanner with no visible leg rotation and foot vertical. *Right*: Participants non-dominant arm is abducted roughly 90 degrees with forearm pronated.

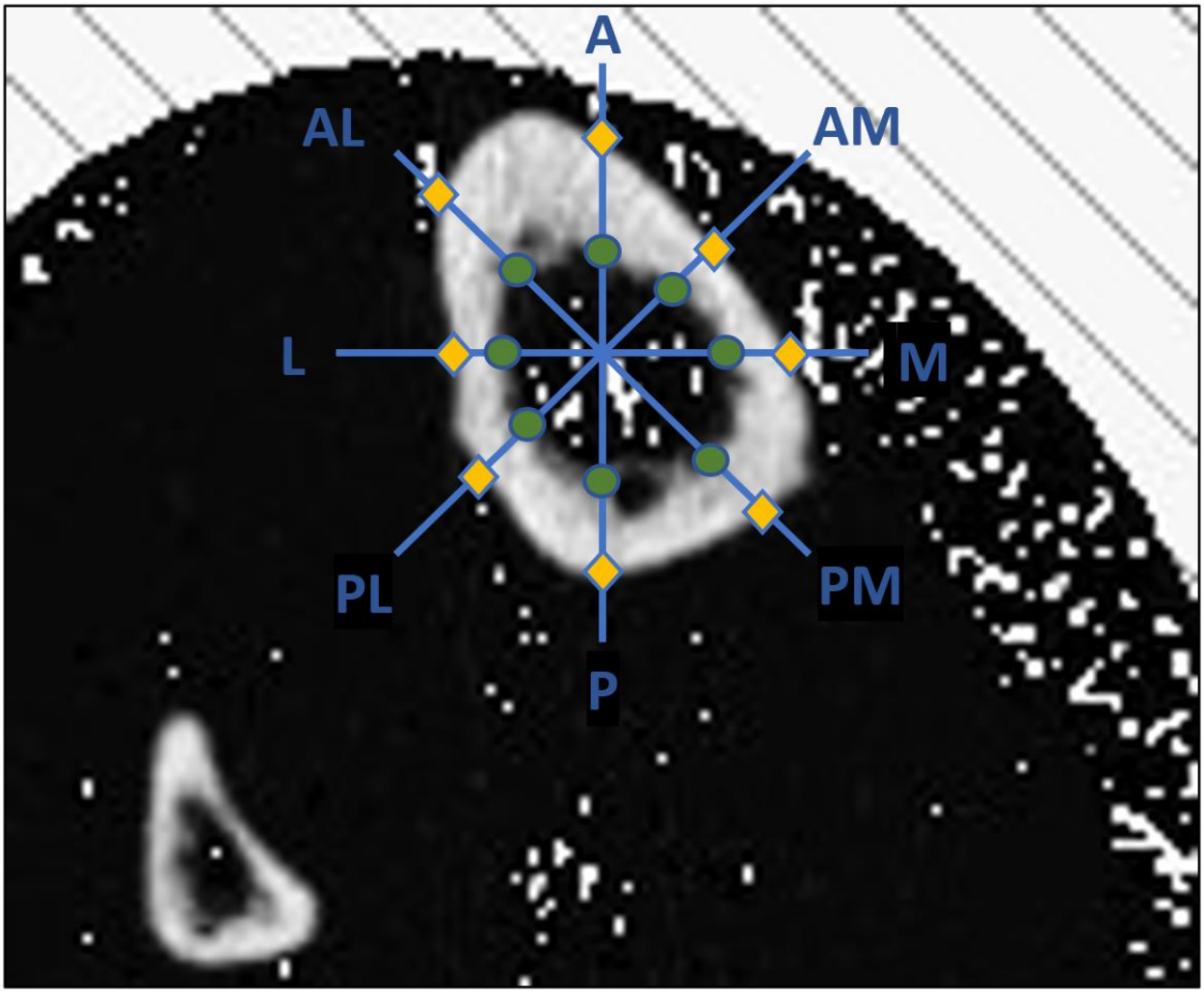

Figure 1.2. Schematic of eight equiangular radii originating from bone centroid of the tibia. Semi-landmarks are established where each radius intersects the endosteal (green circle) and periosteal (orange diamond) borders.

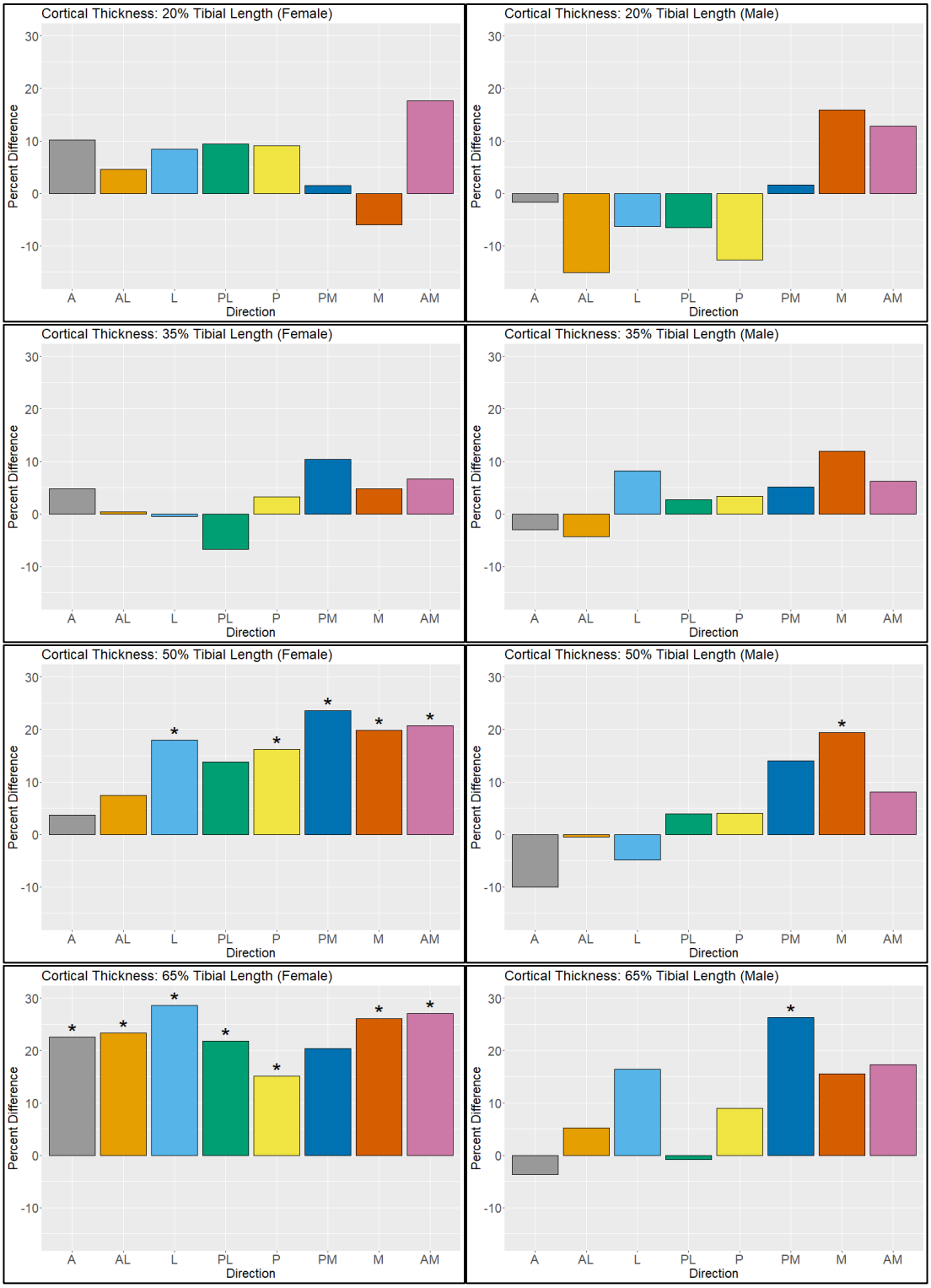

Figure 1.3. Percent difference in tibial cortical thickness between the youngest (40-49 year-old) and oldest (70-79 year old) age groups by direction (females left column, males right column). Positive percent differences reflect more cortical thickness in the younger age group, and negative values thinner cortical thicknesses in the younger age group. Significant differences are indicated with an asterisk (*).

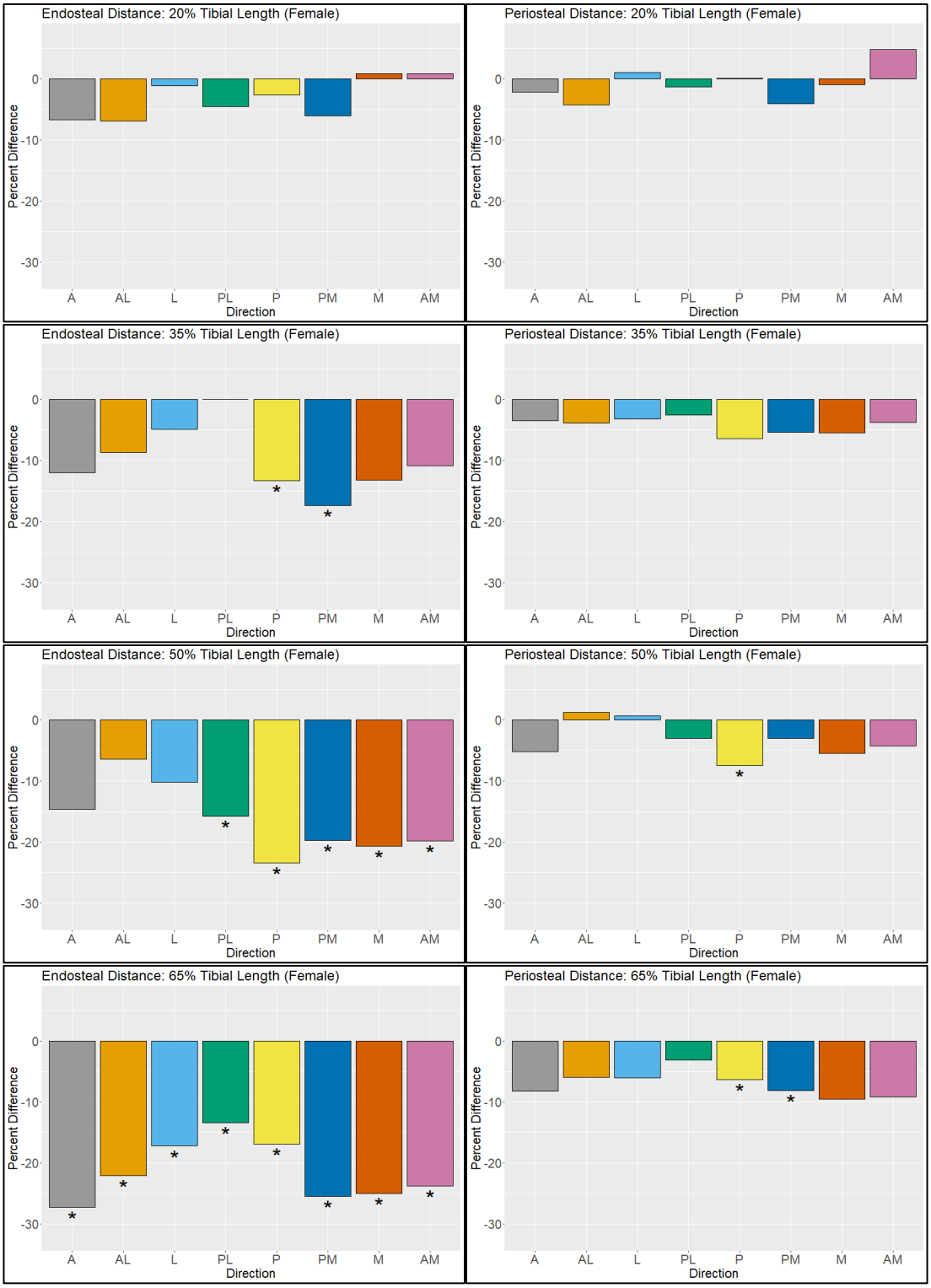

Figure 1.4. Percent difference in tibial endosteal distance and periosteal distance between the youngest (40-49 year-old) and oldest (70-79 year old) age groups by direction (females).

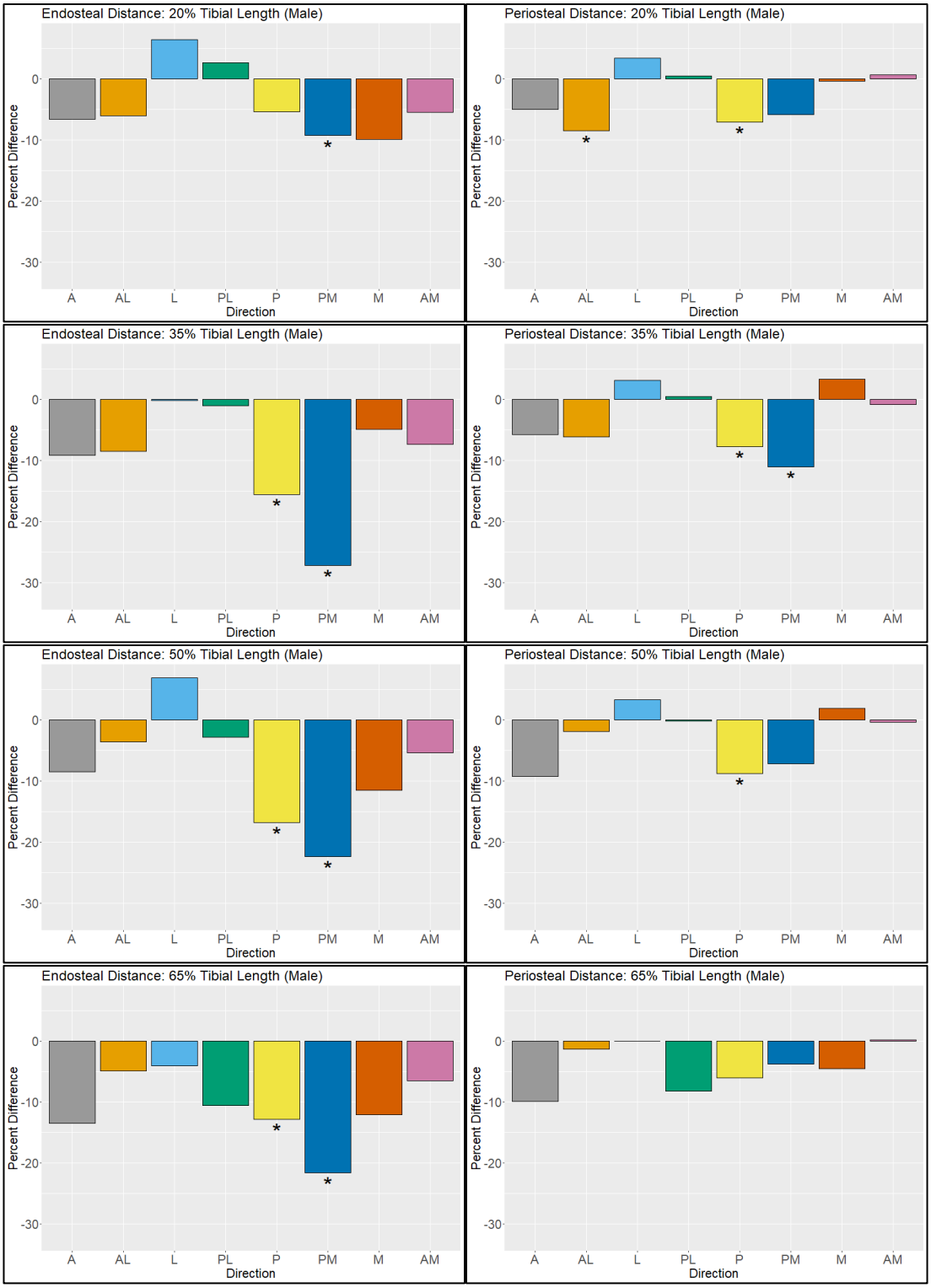

Figure 1.5. Percent difference in tibial endosteal distance and periosteal distance between the youngest (40-49 year-old) and oldest (70-79 year old) age groups by direction (males).

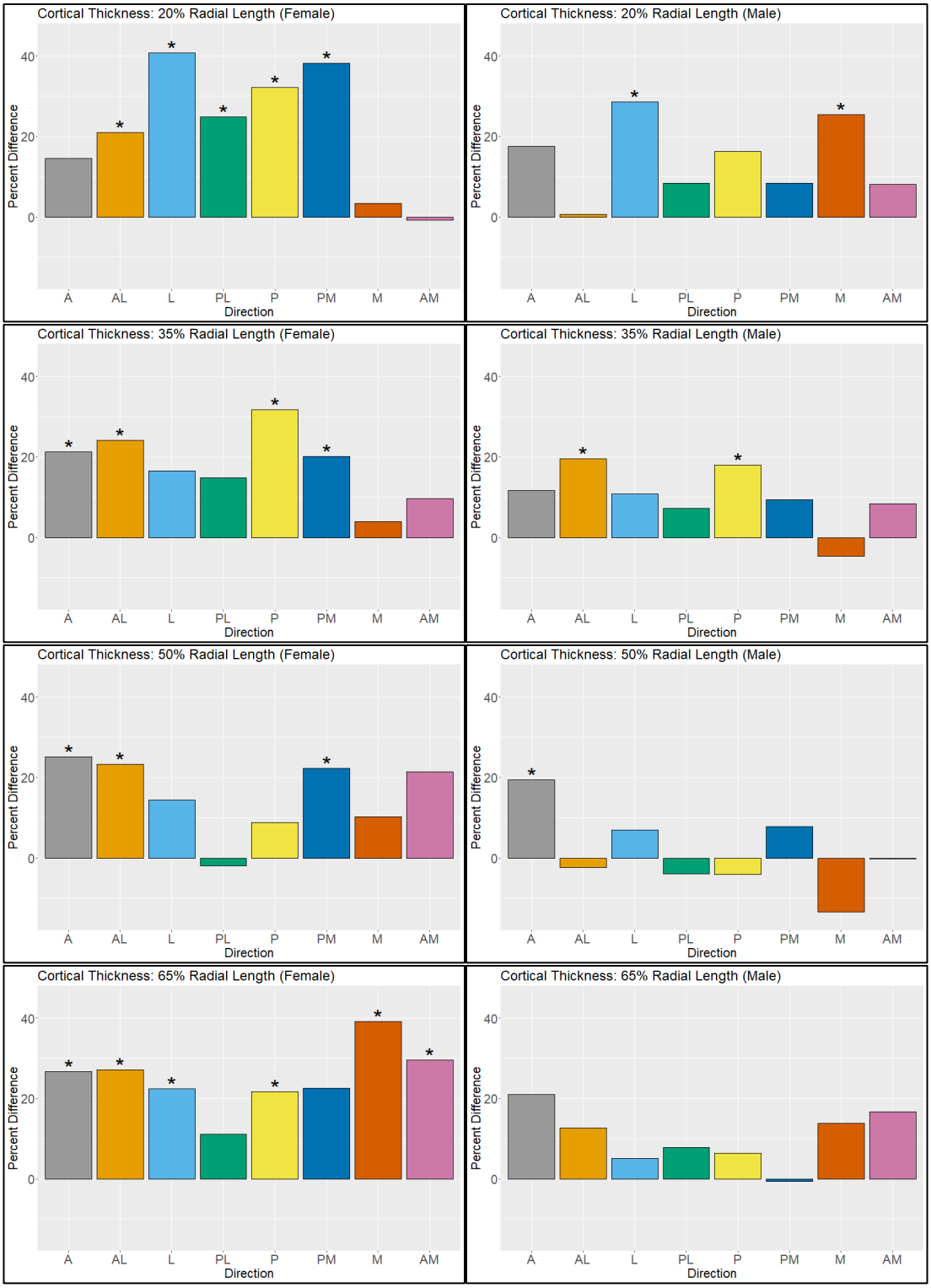

Figure 1.6. Percent difference in radial cortical thickness between the youngest (40-49 year-old) and oldest (70-79 year old) age groups by direction (females left column, males right column).

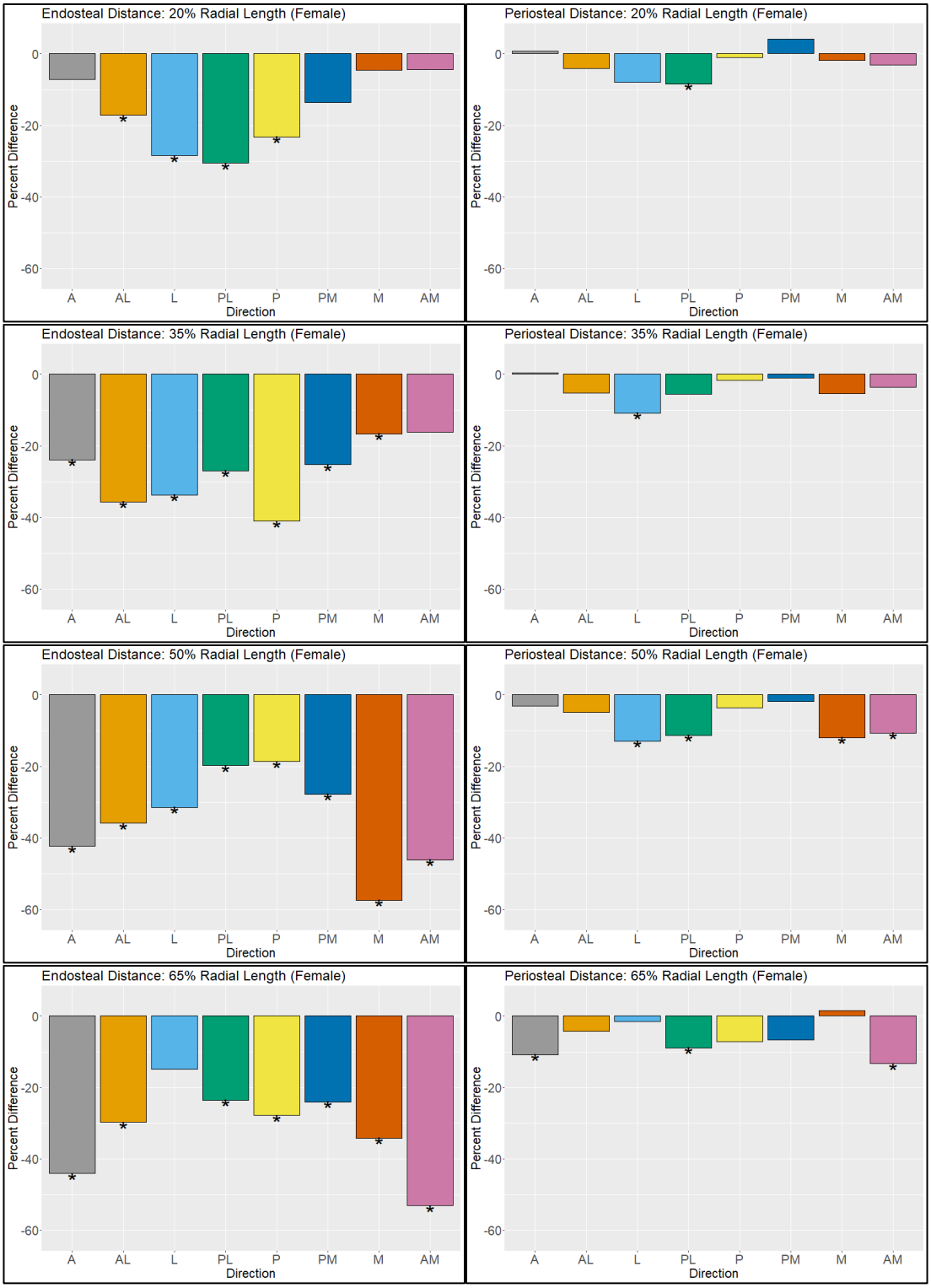

Figure 1.7. Percent difference in radial endosteal distance and periosteal distance between the youngest (40-49 year-old) and oldest (70-79 year old) age groups by direction (females).

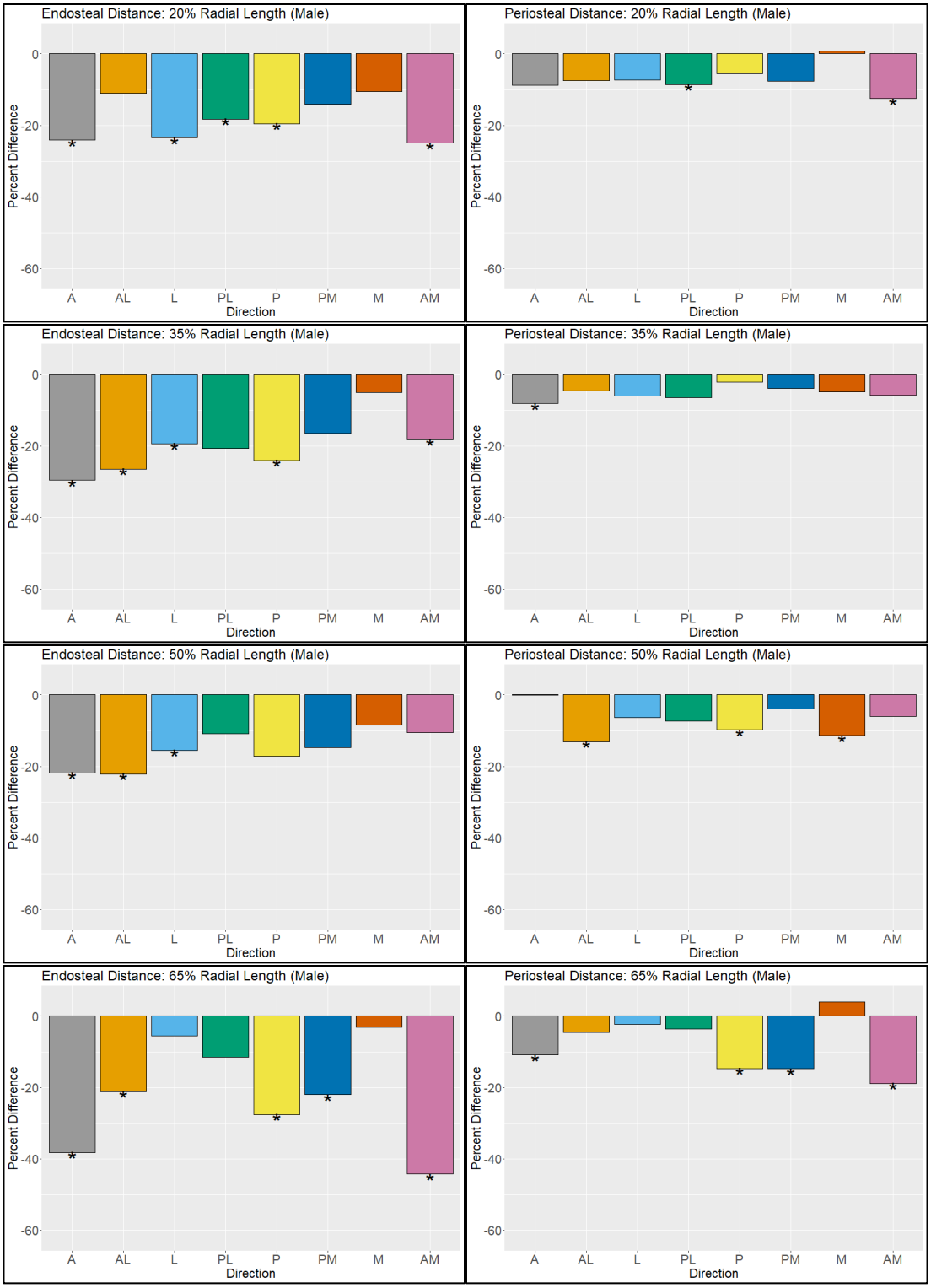

Figure 1.8. Percent difference in radial endosteal distance and periosteal distance between the youngest (40-49 year-old) and oldest (70-79 year old) age groups by direction (males).

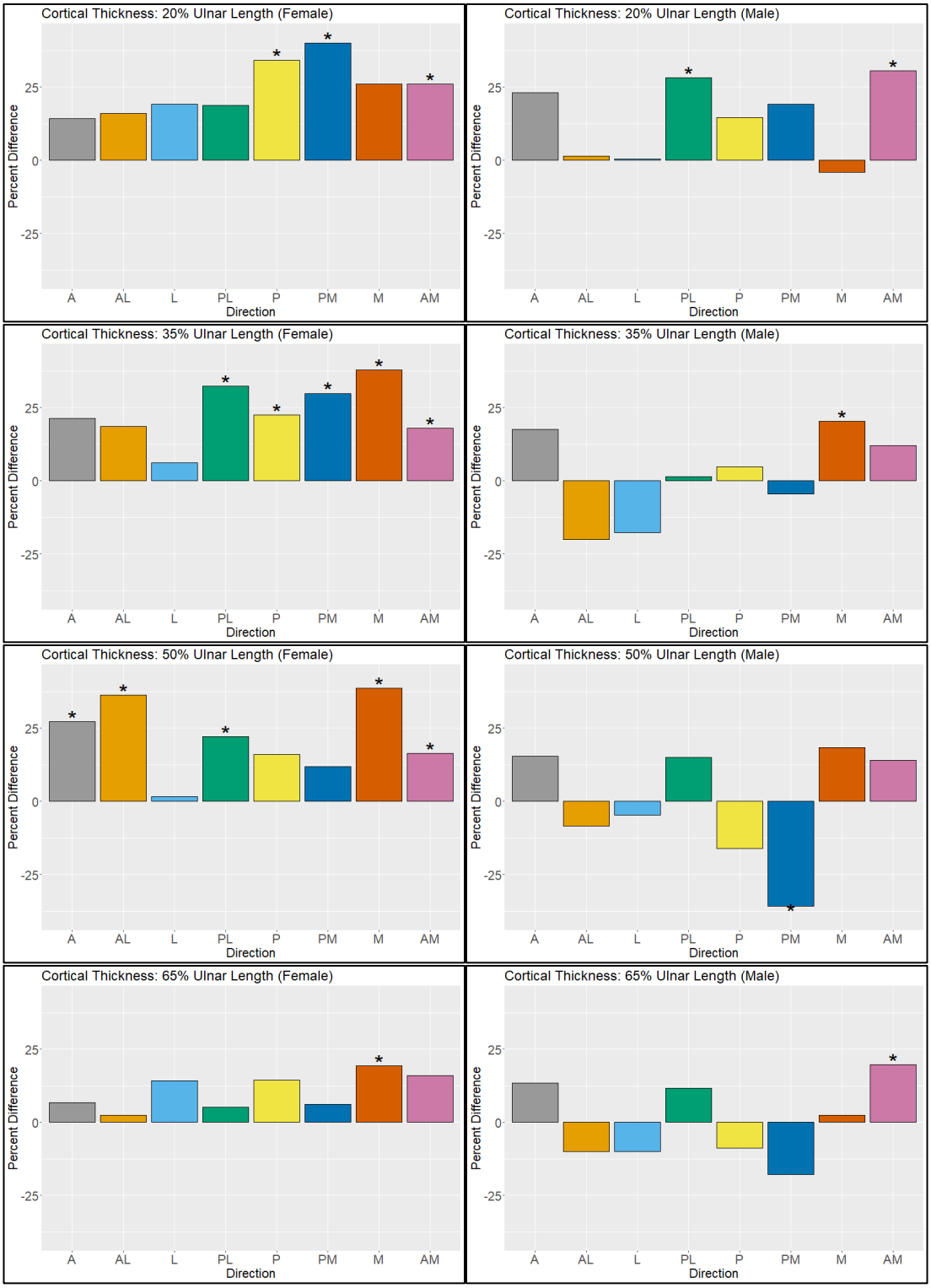

Figure 1.9. Percent difference in ulnar cortical thickness between the youngest (40-49 year-old) and oldest (70-79 year old) age groups by direction (females left column, males right column).

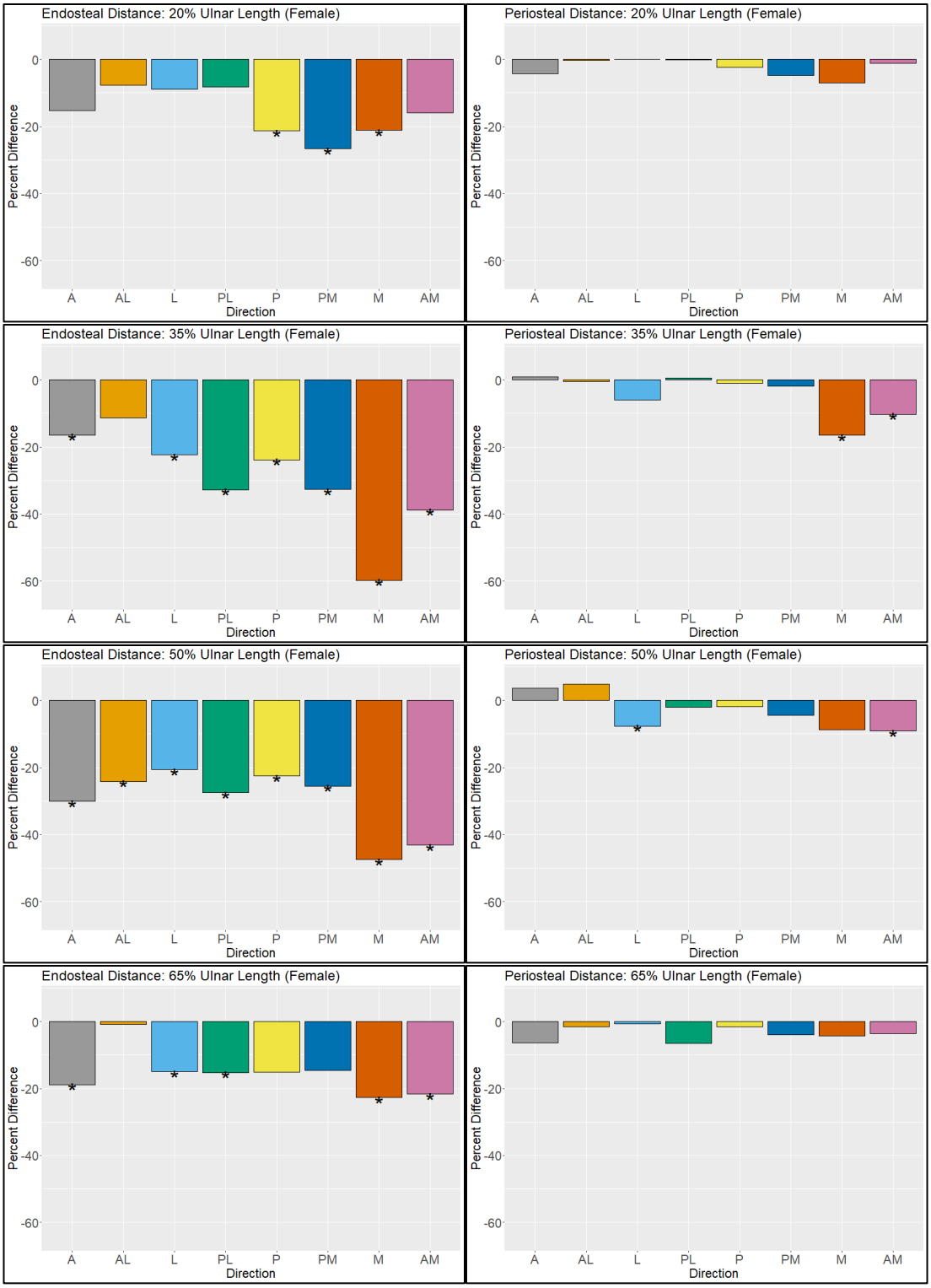

Figure 1.10. Percent difference in ulnar endosteal distance and periosteal distance between the youngest (40-49 year-old) and oldest (70-79 year old) age groups by direction (females).

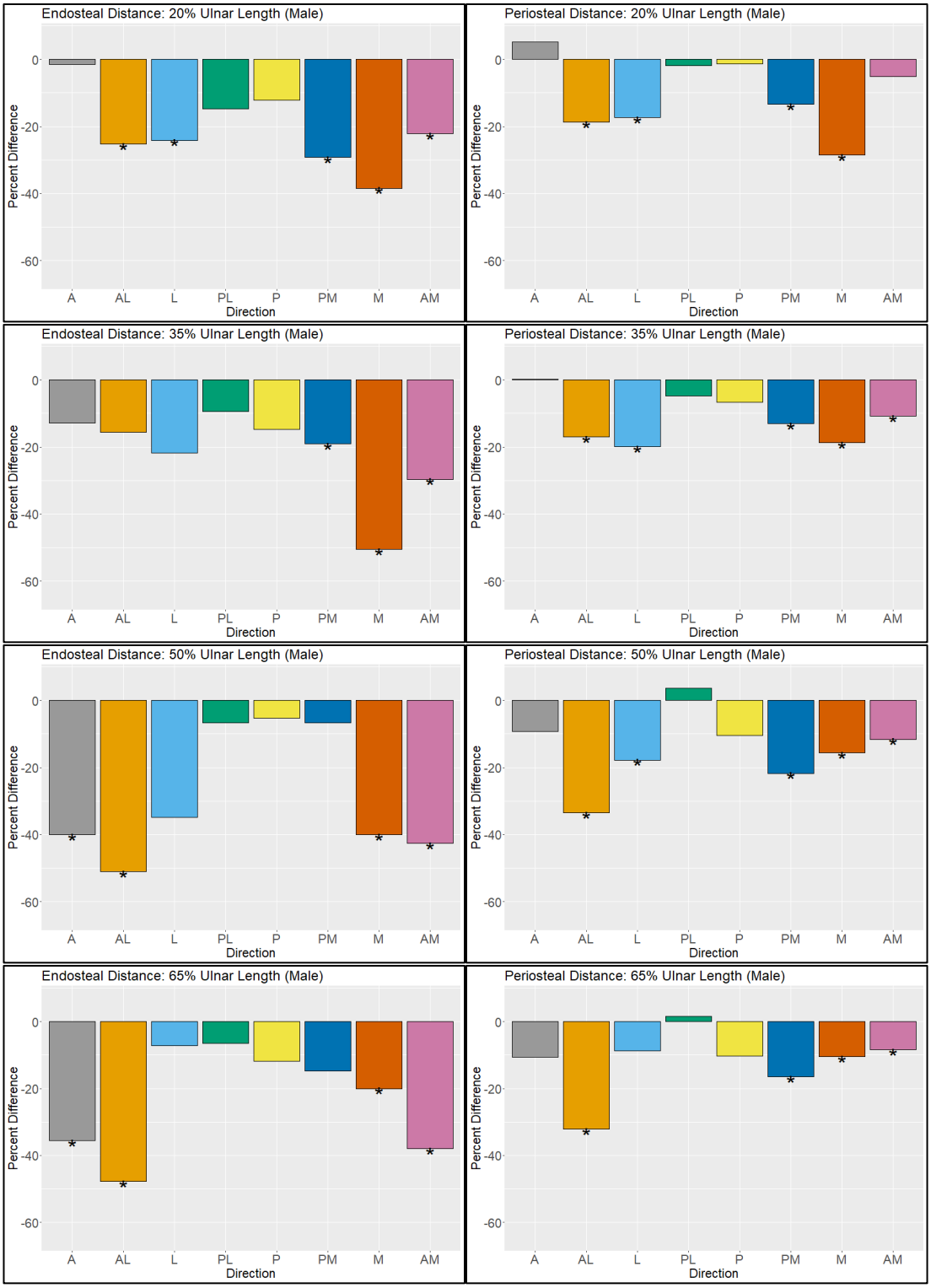

Figure 1.11. Percent difference in ulnar endosteal distance and periosteal distance between the youngest (40-49 year-old) and oldest (70-79 year old) age groups by direction (males).

SUPPLEMENTARY INFORMATION

Table S1.1. Radial RDA Results: Variation in cortical thickness by age and BMI.

	Female		Male	
Radius: 20% Length (F: 10.64%; M: 7.62%)				
	RDA1	RDA2	RDA1	RDA2
Proportion Explained	98.44%	1.56%	80.84%	19.16%
Age	**-0.970***	0.241	-0.999	-0.011
BMI	-0.471	-0.882	-0.014	-0.999
Radius: 35% Length (F: 10.44%; M: 6.04%)				
	RDA1	RDA2	RDA1	RDA2
Proportion Explained	92.84%	7.16%	89.19%	10.81%
Age	**-0.954***	0.300	-0.966	0.258
BMI	-0.545	-0.838	0.235	0.972
Radius: 50% Length (F: 10.08%; M: 4.00%)				
	RDA1	RDA2	RDA1	RDA2
Proportion Explained	94.26%	0.057%	74.74%	25.26%
Age	**-0.950***	-0.312	-0.942	0.335
BMI	-0.556	0.831	0.312	0.950
Radius: 65% Length (F:13.07%; M: 6.41%)				
	RDA1	RDA2	RDA1	RDA2
Proportion Explained	98.07%	1.94%	61.37%	38.63%
Age	**-0.972***	0.235	0.327	0.945
BMI	-0.445	-0.896	0.958	-0.289

* Significant effect ($p < 0.05$) based on permutation ANOVA.

Table S1.2. Radial RDA Results: Variation in endosteal distance by age and BMI.

	Female		Male	
Radius: 20% Length (F: 13.96%; M: 10.29%)				
	RDA1	RDA2	RDA1	RDA2
Proportion Explained	95.69%	4.31%	93.12%	6.89%
Age	**-0.874***	0.486	-0.997	-0.081
BMI	**-0.681***	-0.732	0.057	-0.998
Radius: 35% Length (F: 22.15%; M: 12.44%)				
	RDA1	RDA2	RDA1	RDA2
Proportion Explained	96.63%	3.37%	88.13%	11.87%
Age	**-0.864***	0.503	**-0.994***	-0.113
BMI	**-0.717***	-0.697	0.089	-0.996
Radius: 50% Length (F: 26.48%; M: 5.91%)				
	RDA1	RDA2	RDA1	RDA2
Proportion Explained	97.82%	2.18%	91.09%	8.91%
Age	**-0.872***	0.489	-0.995	0.105
BMI	**-0.705***	-0.709	-0.129	-0.992
Radius: 65% Length (F: 27.55%; M: 9.64%)				
	RDA1	RDA2	RDA1	RDA2
Proportion Explained	99.70%	0.30%	87.78%	12.22%
Age	**-0.936***	0.352	-0.973	-0.230
BMI	**-0.551***	-0.835	0.206	-0.979

* Significant effect ($p < 0.05$) based on permutation ANOVA.

Table S1.3. Radial RDA Results: Variation in periosteal distance by age and BMI.

	Female		Male	
Radius: 20% Length (F: 7.09%; M: 5.82%)				
	RDA1	RDA2	RDA1	RDA2
Proportion Explained	88.71%	11.29%	82.09%	17.91%
Age	-0.695	0.719	0.978	-0.210
BMI	-0.865	-0.503	-0.186	-0.983
Radius: 35% Length (F: 9.52%; M: 4.48%)				
	RDA1	RDA2	RDA1	RDA2
Proportion Explained	88.99%	11.01%	85.23%	14.77%
Age	-0.670	0.743	-0.999	-0.055
BMI	**-0.896***	-0.445	0.030	-0.999
Radius: 50% Length (F: 14.17%; M: 7.90%)				
	RDA1	RDA2	RDA1	RDA2
Proportion Explained	96.15%	3.85%	86.46%	13.54%
Age	**-0.813***	0.583	-0.974	0.228
BMI	**-0.780***	-0.626	0.204	0.979
Radius: 65% Length (F: 11.04%; M: 8.15%)				
	RDA1	RDA2	RDA1	RDA2
Proportion Explained	97.34%	2.66%	81.52%	18.48%
Age	**-0.829***	-0.559	-0.759	0.651
BMI	-0.729	0.685	0.632	0.775

* Significant effect ($p < 0.05$) based on permutation ANOVA.

Table S1.4. Ulnar RDA Results: Variation in cortical thickness by age and BMI.

	Female		Male	
Ulna: 20% Length (F: 2.38%; M: 5.04%)				
	RDA1	RDA2	RDA1	RDA2
Proportion Explained	64.65%	35.35%	82.00%	18.00%
Age	-0.596	-0.803	0.989	0.145
BMI	0.725	-0.689	0.252	-0.968
Ulna: 35% Length (F: 13.25%; M: 7.17%)				
	RDA1	RDA2	RDA1	RDA2
Proportion Explained	91.43%	8.57%	61.51%	38.49%
Age	**-0.966***	0.257	-0.708	-0.706
BMI	-0.506	-0.863	-0.738	0.675
Ulna: 50% Length (F: 11.14%; M 6.42%)				
	RDA1	RDA2	RDA1	RDA2
Proportion Explained	98.64%	1.36%	70.69%	29.31%
Age	**-0.964***	0.267	0.804	-0.595
BMI	-0.514	-0.858	-0.558	-0.830
Ulna: 65% Length (F: 4.76%; M 7.86%)				
	RDA1	RDA2	RDA1	RDA2
Proportion Explained	66.33%	33.67%	65.97%	34.03%
Age	0.940	0.342	0.339	-0.941
BMI	0.577	-0.817	-0.967	-0.253

* Significant effect ($p < 0.05$) based on permutation ANOVA.

Table S1.5. Ulnar RDA Results: Variation in endosteal distance by age and BMI.

	Female		Male	
Ulna: 20% Length (F: 11.81%; M: 12.30%)				
	RDA1	RDA2	RDA1	RDA2
Proportion Explained	98.82%	1.18%	94.43%	5.58%
Age	**0.963***	-0.269	**0.993***	-0.116
BMI	0.456	0.890	-0.073	-0.997
Ulna: 35% Length (F: 22.54%; M: 12.96%)				
	RDA1	RDA2	RDA1	RDA2
Proportion Explained	97.88%	2.12%	88.02%	11.98%
Age	**0.909***	-0.418	**-0.959***	-0.285
BMI	**0.647***	0.763	-0.329	0.944
Ulna: 50% Length (F: 21.91%; M 15.38%)				
	RDA1	RDA2	RDA1	RDA2
Proportion Explained	97.06%	2.94%	90.24%	9.76%
Age	**0.869***	-0.496	**-0.975***	-0.223
BMI	**0.711***	0.703	-0.268	0.964
Ulna: 65% Length (F: 12.18%; M 17.18%)				
	RDA1	RDA2	RDA1	RDA2
Proportion Explained	97.16%	2.84%	70.87%	29.13%
Age	**0.873***	-0.489	**-0.951***	**-0.309***
BMI	0.705	0.708	**-0.245***	**0.970***

* Significant effect ($p < 0.05$) based on permutation ANOVA.

Table S1.6. Ulnar RDA Results: Variation in periosteal distance by age and BMI.

	Female		Male	
Ulna: 20% Length (F: 5.31%; M: 11.91%)				
	RDA1	RDA2	RDA1	RDA2
Proportion Explained	94.80%	5.20%	95.23%	4.77%
Age	0.684	-0.730	**0.974***	-0.227
BMI	0.852	0.524	-0.185	-0.983
Ulna: 35% Length (F: 10.27%; M: 10.77%)				
	RDA1	RDA2	RDA1	RDA2
Proportion Explained	78.15%	21.85%	88.54%	11.46%
Age	**0.783***	-0.622	**0.984***	-0.177
BMI	**0.809***	0.587	-0.132	-0.991
Ulna: 50% Length (F: 7.93%; M 12.93%)				
	RDA1	RDA2	RDA1	RDA2
Proportion Explained	86.35%	13.65%	92.55%	7.45%
Age	**0.802***	-0.597	**0.971***	-0.239
BMI	**0.791***	0.612	-0.194	-0.981
Ulna: 65% Length (F: 5.43%; M 10.25%)				
	RDA1	RDA2	RDA1	RDA2
Proportion Explained	90.80%	9.20%	89.10%	10.90%
Age	0.746	-0.665	**0.903***	-0.430
BMI	0.842	0.540	-0.489	-0.872

* Significant effect ($p < 0.05$) based on permutation ANOVA.

Table S1.7. Tukey HSD results for age group comparisons in tibial cortical thickness by directional radii (female).

Slice	Age Group Comparison	A	AL	L	PL	P	PM	M	AM
20%	40-49 & 50-59								
	50-59 & 60-69								
	60-69 & 70-79								
	40-49 & 60-69								
	40-49 & 70-79								
	50-59 & 70-79								
35%	40-49 & 50-59								
	50-59 & 60-69								
	60-69 & 70-79								
	40-49 & 60-69								
	40-49 & 70-79								
	50-59 & 70-79								
50%	40-49 & 50-59								
	50-59 & 60-69								
	60-69 & 70-79								
	40-49 & 60-69								
	40-49 & 70-79								
	50-59 & 70-79								
65%	40-49 & 50-59								
	50-59 & 60-69								
	60-69 & 70-79								
	40-49 & 60-69								
	40-49 & 70-79								
	50-59 & 70-79								

Table S1.8. Tukey HSD results for age group comparisons in tibial cortical thickness by directional radii (male).

Slice	Age Group Comparison	A	AL	L	PL	P	PM	M	AM
20%	40-49 & 50-59								
	50-59 & 60-69								
	60-69 & 70-79								
	40-49 & 60-69								
	40-49 & 70-79								
	50-59 & 70-79								
35%	40-49 & 50-59								
	50-59 & 60-69								
	60-69 & 70-79								
	40-49 & 60-69								
	40-49 & 70-79								
	50-59 & 70-79								
50%	40-49 & 50-59								
	50-59 & 60-69								
	60-69 & 70-79								
	40-49 & 60-69								
	40-49 & 70-79								
	50-59 & 70-79								
65%	40-49 & 50-59								
	50-59 & 60-69								
	60-69 & 70-79								
	40-49 & 60-69								
	40-49 & 70-79								
	50-59 & 70-79								

Table S1.9. Tukey HSD results for age group comparisons in tibial endosteal distance by directional radii (female).

Slice	Age Group Comparison	A	AL	L	PL	P	PM	M	AM
20%	40-49 & 50-59						■		
	50-59 & 60-69								
	60-69 & 70-79								
	40-49 & 60-69	■	■	■			■		
	40-49 & 70-79								
	50-59 & 70-79								
35%	40-49 & 50-59						■		
	50-59 & 60-69								
	60-69 & 70-79								
	40-49 & 60-69	■	■	■			■		
	40-49 & 70-79						■		
	50-59 & 70-79								
50%	40-49 & 50-59					■	■		
	50-59 & 60-69								
	60-69 & 70-79								
	40-49 & 60-69		■	■	■	■	■	■	
	40-49 & 70-79					■	■	■	■
	50-59 & 70-79								
65%	40-49 & 50-59		■	■	■	■	■	■	■
	50-59 & 60-69								
	60-69 & 70-79								
	40-49 & 60-69	■	■	■		■	■	■	■
	40-49 & 70-79	■	■	■	■	■	■	■	■
	50-59 & 70-79								

Table S1.10. Tukey HSD results for age group comparisons in tibial endosteal distance by directional radii (male).

Slice	Age Group Comparison	A	AL	L	PL	P	PM	M	AM
20%	40-49 & 50-59								
	50-59 & 60-69								
	60-69 & 70-79								
	40-49 & 60-69								
	40-49 & 70-79								
	50-59 & 70-79								
35%	40-49 & 50-59								
	50-59 & 60-69								
	60-69 & 70-79								
	40-49 & 60-69								
	40-49 & 70-79								
	50-59 & 70-79								
50%	40-49 & 50-59								
	50-59 & 60-69								
	60-69 & 70-79								
	40-49 & 60-69								
	40-49 & 70-79								
	50-59 & 70-79								
65%	40-49 & 50-59								
	50-59 & 60-69								
	60-69 & 70-79								
	40-49 & 60-69								
	40-49 & 70-79								
	50-59 & 70-79								

Table S1.11. Tukey HSD results for age group comparisons in tibial periosteal distance by directional radii (female).

Slice	Age Group Comparison	A	AL	L	PL	P	PM	M	AM
20%	40-49 & 50-59								
	50-59 & 60-69								
	60-69 & 70-79								
	40-49 & 60-69								
	40-49 & 70-79								
	50-59 & 70-79								
35%	40-49 & 50-59								
	50-59 & 60-69								
	60-69 & 70-79								
	40-49 & 60-69								
	40-49 & 70-79								
	50-59 & 70-79								
50%	40-49 & 50-59								
	50-59 & 60-69								
	60-69 & 70-79								
	40-49 & 60-69								
	40-49 & 70-79								
	50-59 & 70-79								
65%	40-49 & 50-59								
	50-59 & 60-69								
	60-69 & 70-79								
	40-49 & 60-69								
	40-49 & 70-79								
	50-59 & 70-79								

Table S1.12. Tukey HSD results for age group comparisons in tibial periosteal distance by directional radii (male).

Slice	Age Group Comparison	A	AL	L	PL	P	PM	M	AM
20%	40-49 & 50-59								
	50-59 & 60-69								
	60-69 & 70-79								
	40-49 & 60-69								
	40-49 & 70-79								
	50-59 & 70-79								
35%	40-49 & 50-59								
	50-59 & 60-69								
	60-69 & 70-79								
	40-49 & 60-69								
	40-49 & 70-79								
	50-59 & 70-79								
50%	40-49 & 50-59								
	50-59 & 60-69								
	60-69 & 70-79								
	40-49 & 60-69								
	40-49 & 70-79								
	50-59 & 70-79								
65%	40-49 & 50-59								
	50-59 & 60-69								
	60-69 & 70-79								
	40-49 & 60-69								
	40-49 & 70-79								
	50-59 & 70-79								

Table S1.13. Tukey HSD results for age group comparisons in radial cortical thickness by directional radii (female).

Slice	Age Group Comparison	M	AM	A	AL	L	PL	P	PM
20%	40-49 & 50-59								
	50-59 & 60-69								
	60-69 & 70-79								
	40-49 & 60-69								
	40-49 & 70-79								
	50-59 & 70-79								
35%	40-49 & 50-59								
	50-59 & 60-69								
	60-69 & 70-79								
	40-49 & 60-69								
	40-49 & 70-79								
	50-59 & 70-79								
50%	40-49 & 50-59								
	50-59 & 60-69								
	60-69 & 70-79								
	40-49 & 60-69								
	40-49 & 70-79								
	50-59 & 70-79								
65%	40-49 & 50-59								
	50-59 & 60-69								
	60-69 & 70-79								
	40-49 & 60-69								
	40-49 & 70-79								
	50-59 & 70-79								

Table S1.14. Tukey HSD results for age group comparisons in radial cortical thickness by directional radii (male).

Slice	Age Group Comparison	M	AM	A	AL	L	PL	P	PM
20%	40-49 & 50-59								
	50-59 & 60-69								
	60-69 & 70-79								
	40-49 & 60-69								
	40-49 & 70-79								
	50-59 & 70-79								
35%	40-49 & 50-59								
	50-59 & 60-69								
	60-69 & 70-79								
	40-49 & 60-69								
	40-49 & 70-79								
	50-59 & 70-79								
50%	40-49 & 50-59								
	50-59 & 60-69								
	60-69 & 70-79								
	40-49 & 60-69								
	40-49 & 70-79								
	50-59 & 70-79								
65%	40-49 & 50-59								
	50-59 & 60-69								
	60-69 & 70-79								
	40-49 & 60-69								
	40-49 & 70-79								
	50-59 & 70-79								

Table S1.15. Tukey HSD results for age group comparisons in radial endosteal distance by directional radii (female).

Slice	Age Group Comparison	M	AM	A	AL	L	PL	P	PM
20%	40-49 & 50-59		■					■	■
	50-59 & 60-69					■			
	60-69 & 70-79								
	40-49 & 60-69			■	■	■	■	■	■
	40-49 & 70-79					■	■	■	
	50-59 & 70-79								
35%	40-49 & 50-59	■			■	■			
	50-59 & 60-69					■	■	■	■
	60-69 & 70-79								
	40-49 & 60-69	■	■	■	■	■	■	■	■
	40-49 & 70-79				■	■	■	■	■
	50-59 & 70-79								
50%	40-49 & 50-59	■	■	■		■			
	50-59 & 60-69							■	■
	60-69 & 70-79								
	40-49 & 60-69	■	■	■	■	■	■	■	■
	40-49 & 70-79	■	■	■	■	■	■		■
	50-59 & 70-79								
65%	40-49 & 50-59		■	■					
	50-59 & 60-69		■	■	■		■	■	■
	60-69 & 70-79								
	40-49 & 60-69	■	■	■	■	■	■	■	■
	40-49 & 70-79	■	■	■	■		■	■	■
	50-59 & 70-79								

Table S1.16. Tukey HSD results for age group comparisons in radial endosteal distance by directional radii (male).

Slice	Age Group Comparison	M	AM	A	AL	L	PL	P	PM
20%	40-49 & 50-59								
	50-59 & 60-69								
	60-69 & 70-79								
	40-49 & 60-69								
	40-49 & 70-79								
	50-59 & 70-79								
35%	40-49 & 50-59								
	50-59 & 60-69								
	60-69 & 70-79								
	40-49 & 60-69								
	40-49 & 70-79								
	50-59 & 70-79								
50%	40-49 & 50-59								
	50-59 & 60-69								
	60-69 & 70-79								
	40-49 & 60-69								
	40-49 & 70-79								
	50-59 & 70-79								
65%	40-49 & 50-59								
	50-59 & 60-69								
	60-69 & 70-79								
	40-49 & 60-69								
	40-49 & 70-79								
	50-59 & 70-79								

Table S1.17. Tukey HSD results for age group comparisons in radial periosteal distance by directional radii (female).

Slice	Age Group Comparison	M	AM	A	AL	L	PL	P	PM
20%	40-49 & 50-59								
	50-59 & 60-69								
	60-69 & 70-79								
	40-49 & 60-69			■		■	■		
	40-49 & 70-79						■		
	50-59 & 70-79								
35%	40-49 & 50-59				■	■			
	50-59 & 60-69								
	60-69 & 70-79								
	40-49 & 60-69				■	■			
	40-49 & 70-79					■			
	50-59 & 70-79								
50%	40-49 & 50-59	■				■			
	50-59 & 60-69								
	60-69 & 70-79								
	40-49 & 60-69	■	■	■		■	■		
	40-49 & 70-79	■	■			■	■		
	50-59 & 70-79								
65%	40-49 & 50-59			■					■
	50-59 & 60-69								
	60-69 & 70-79								
	40-49 & 60-69		■	■				■	■
	40-49 & 70-79		■						
	50-59 & 70-79								

Table S1.18. Tukey HSD results for age group comparisons in radial periosteal distance by directional radii (male).

Slice	Age Group Comparison	M	AM	A	AL	L	PL	P	PM
20%	40-49 & 50-59								
	50-59 & 60-69								
	60-69 & 70-79								
	40-49 & 60-69								
	40-49 & 70-79								
	50-59 & 70-79								
35%	40-49 & 50-59								
	50-59 & 60-69								
	60-69 & 70-79								
	40-49 & 60-69								
	40-49 & 70-79								
	50-59 & 70-79								
50%	40-49 & 50-59								
	50-59 & 60-69								
	60-69 & 70-79								
	40-49 & 60-69								
	40-49 & 70-79								
	50-59 & 70-79								
65%	40-49 & 50-59								
	50-59 & 60-69								
	60-69 & 70-79								
	40-49 & 60-69								
	40-49 & 70-79								
	50-59 & 70-79								

Table S1.19. Tukey HSD results for age group comparisons in ulnar cortical thickness by directional radii (female).

Slice	Age Group Comparison	L	PL	P	PM	M	AM	A	AL
20%	40-49 & 50-59								
	50-59 & 60-69								
	60-69 & 70-79								
	40-49 & 60-69								
	40-49 & 70-79								
	50-59 & 70-79								
35%	40-49 & 50-59								
	50-59 & 60-69								
	60-69 & 70-79								
	40-49 & 60-69								
	40-49 & 70-79								
	50-59 & 70-79								
50%	40-49 & 50-59								
	50-59 & 60-69								
	60-69 & 70-79								
	40-49 & 60-69								
	40-49 & 70-79								
	50-59 & 70-79								
65%	40-49 & 50-59								
	50-59 & 60-69								
	60-69 & 70-79								
	40-49 & 60-69								
	40-49 & 70-79								
	50-59 & 70-79								

Table S1.20. Tukey HSD results for age group comparisons in ulnar cortical thickness by directional radii (male).

Slice	Age Group Comparison	L	PL	P	PM	M	AM	A	AL
20%	40-49 & 50-59								
	50-59 & 60-69								
	60-69 & 70-79								
	40-49 & 60-69								
	40-49 & 70-79								
	50-59 & 70-79								
35%	40-49 & 50-59								
	50-59 & 60-69								
	60-69 & 70-79								
	40-49 & 60-69								
	40-49 & 70-79								
	50-59 & 70-79								
50%	40-49 & 50-59								
	50-59 & 60-69								
	60-69 & 70-79								
	40-49 & 60-69								
	40-49 & 70-79								
	50-59 & 70-79								
65%	40-49 & 50-59								
	50-59 & 60-69								
	60-69 & 70-79								
	40-49 & 60-69								
	40-49 & 70-79								
	50-59 & 70-79								

Table S1.21. Tukey HSD results for age group comparisons in ulnar endosteal distance by directional radii (female).

Slice	Age Group Comparison	L	PL	P	PM	M	AM	A	AL
20%	40-49 & 50-59	■	■		■	■			■
	50-59 & 60-69								
	60-69 & 70-79								
	40-49 & 60-69	■	■	■	■	■			
	40-49 & 70-79			■	■				
	50-59 & 70-79								
35%	40-49 & 50-59	■	■			■			
	50-59 & 60-69						■		
	60-69 & 70-79								
	40-49 & 60-69	■	■		■	■	■	■	
	40-49 & 70-79		■		■	■	■		
	50-59 & 70-79					■			
50%	40-49 & 50-59					■		■	
	50-59 & 60-69						■		
	60-69 & 70-79								
	40-49 & 60-69	■	■	■	■	■	■	■	■
	40-49 & 70-79		■	■	■	■	■	■	
	50-59 & 70-79								
65%	40-49 & 50-59								
	50-59 & 60-69			■	■				
	60-69 & 70-79								
	40-49 & 60-69	■	■	■	■	■	■	■	
	40-49 & 70-79					■	■		
	50-59 & 70-79								

Table S1.22. Tukey HSD results for age group comparisons in ulnar endosteal distance by directional radii (male).

Slice	Age Group Comparison	L	PL	P	PM	M	AM	A	AL
20%	40-49 & 50-59								
	50-59 & 60-69								
	60-69 & 70-79								
	40-49 & 60-69								
	40-49 & 70-79								
	50-59 & 70-79								
35%	40-49 & 50-59								
	50-59 & 60-69								
	60-69 & 70-79								
	40-49 & 60-69								
	40-49 & 70-79								
	50-59 & 70-79								
50%	40-49 & 50-59								
	50-59 & 60-69								
	60-69 & 70-79								
	40-49 & 60-69								
	40-49 & 70-79								
	50-59 & 70-79								
65%	40-49 & 50-59								
	50-59 & 60-69								
	60-69 & 70-79								
	40-49 & 60-69								
	40-49 & 70-79								
	50-59 & 70-79								

Table S1.23. Tukey HSD results for age group comparisons in ulnar periosteal distance by directional radii (female).

Slice	Age Group Comparison	L	PL	P	PM	M	AM	A	AL
20%	40-49 & 50-59								
	50-59 & 60-69								
	60-69 & 70-79								
	40-49 & 60-69								
	40-49 & 70-79								
	50-59 & 70-79								
35%	40-49 & 50-59								
	50-59 & 60-69								
	60-69 & 70-79								
	40-49 & 60-69								
	40-49 & 70-79								
	50-59 & 70-79								
50%	40-49 & 50-59								
	50-59 & 60-69								
	60-69 & 70-79								
	40-49 & 60-69								
	40-49 & 70-79								
	50-59 & 70-79								
65%	40-49 & 50-59								
	50-59 & 60-69								
	60-69 & 70-79								
	40-49 & 60-69								
	40-49 & 70-79								
	50-59 & 70-79								

Table S1.24. Tukey HSD results for age group comparisons in ulnar periosteal distance by directional radii (male).

Slice	Age Group Comparison	L	PL	P	PM	M	AM	A	AL
20%	40-49 & 50-59								
	50-59 & 60-69								
	60-69 & 70-79								
	40-49 & 60-69	■							
	40-49 & 70-79	■			■	■			■
	50-59 & 70-79					■			
35%	40-49 & 50-59								
	50-59 & 60-69								
	60-69 & 70-79								
	40-49 & 60-69								
	40-49 & 70-79	■				■			■
	50-59 & 70-79								
50%	40-49 & 50-59								■
	50-59 & 60-69								
	60-69 & 70-79								
	40-49 & 60-69								■
	40-49 & 70-79	■			■	■			■
	50-59 & 70-79								
65%	40-49 & 50-59								■
	50-59 & 60-69								
	60-69 & 70-79								
	40-49 & 60-69								■
	40-49 & 70-79				■				■
	50-59 & 70-79	■							

CHAPTER 3: DISTRIBUTION OF AGE-RELATED DIFFERENCES IN CORTICAL BONE MINERAL DENSITY WITHIN AND BETWEEN LONG BONE CROSS-SECTIONS

Publication statement: A version of this chapter is being prepared for publication by Greg J. Wehrman as:

Wehrman, G. W. (2023). Distribution of age-related changes in cortical bone mineral density within and between long bone cross-sections. *In preparation*.

ABSTRACT

Age-related bone loss and associated fracture risk is clinically assessed using bone mineral density (BMD), however this is a coarse areal measurement encompassing, but not distinguishing between, several processes of bone loss in trabecular and cortical bone. Cortical BMD (cBMD), specifically measuring the volumetric density of cortical bone, has been shown to vary regionally at sites throughout the skeleton, however its local variation within cross-sectional slices has been understudied in comparison and warrants further investigation. This study examines local variation of cBMD within and between diaphyseal cross-sections of the tibia, radius, and ulna from a sample of 126 living individuals (78 female, 48 male) between 40-80 years of age. Using a pQCT scanner, cross-sectional slices were created at 20%, 35%, 50%, and 65% length of the tibia and forearm. Eight directional sectors were established throughout the cross-section to assess average cBMD. Results show that cBMD differences with age are variable by location within and between cross-sections, and that greater differences occur in females than in males. Intra-slice cBMD variation of the tibia and distal radius suggest that load-sharing via interosseous membranes in the leg and forearm may partly shape local cBMD variation, however traditional mechanical expectations do not fully explain observed cBMD patterning. Having characterized cBMD distribution within cross-sections of these three distal limb elements, we conclude that a suite of factors, both global and local, are likely converging to produce local variation in cBMD differences with age.

INTRODUCTION

Bone loss is a pressing public health concern, as loss of bone content and density is associated with aging (Johnell et al., 2005; Weaver and Peacock, 2019) and life expectancy is greater than in the past (Medina et al., 2020). The problems posed by age-related bone loss reach beyond proximal consequences of fractures to secondary complications arising from reduced mobility, reduced quality of life, financial burden, and social stress (Harvey et al., 2010). Assessment of bone loss is clinically measured as bone mineral density (BMD), which is quantified as a T-score that describes existing bone mass in older individuals relative to healthy young adults and a Z-score that compares bone mass to an age- and sex-matched sample. Dual-energy x-ray absorptiometry (DEXA) is the most common method for BMD assessment, measuring overall BMD in either regional or whole-body scans as the amount of bone mass within an area of interest (Peterson, 2001). However, areal BMD measurement is not a true measure of density as it does not account for the three-dimensional configuration of bone, an important determining factor of bone strength (Currey, 2006). Additionally, area-based BMD does not distinguish between different processes involved in overall bone loss, which include trabecular loss (Riggs et al., 2009), endosteal resorption of cortical bone (Chen et al., 2014), or increasing intracortical porosity (Feik et al., 1997; Cooper et al., 2007). Thus, while areal BMD assessment through DEXA is clinically useful in predicting fracture risk, considering BMD decline with respect to specific processes offers a more accurate picture of its effect on bone strength and, potentially, provide opportunities to better understand the etiology of bone loss.

In a previous study (Chapter 2), colleagues and I used pQCT imaging of 126 adults aged between 40 and 80 to characterize the regionalization of cortical bone decline with age among four cross-sectional locations along the lengths of diaphyses of the tibia, radius, and ulna. We

examined differences in the distance measures of endosteal and periosteal envelopes from the cross-sectional centroid, as well as cortical thickness, along eight equidistant radii in each cross-section. Overall, we supported prior evidence for expansion of the periosteal envelope with age (Ruff and Hayes, 1982; Lauretani et al., 2008), and found that apparent bone loss in the endosteal envelope was mirrored by bone apposition in the periosteal envelope in the same radius. From our results we found significant differences between female and males in the distribution of cortical bone, especially in age-related differences of endosteal and periosteal distances. Moreover, we also showed that evident changes in cortical bone with age do not occur equally throughout the diaphysis, where bone loss appears to occur in some anatomical directions more than others, as well as differently long the length of the diaphysis. We concluded that factors in addition to mechanical loading of skeletal elements must be responsible for the heterogeneity of change in cortical bone. One possibility may be that localized changes in BMD could be contributing to the heterogeneity in cross-sectional geometric shifts with age, as other studies indicate that distribution of cortical porosity is associated with age-related changes in fracture risk (e.g, Ramchand and Seeman, 2018). In this study, given the results of our previous study and the need argued above to better characterize bone mineral density changes across a skeletal element, I examine heterogeneity in BMD loss with age across the cortical bone of diaphyses in the same sample as in Chapter 2.

Age-related Changes in Cortical BMD

Peripheral quantitative computed tomography (pQCT) allows for examination of age-related changes in cortical and trabecular bone that contribute to overall bone loss by visualizing both the density and geometry of bone. Researchers who examined population-based pQCT studies,

both cross-sectional and longitudinal, have argued that these different age-related changes are not contemporaneous (Riggs et al., 2008; Johannesdottir et al., 2013; Hung et al., 2015). Trabecular bone loss begins as early as the third decade in females and the fourth decade in males (Riggs et al., 2008). Loss of cortical bone is associated with menopause among females while males experience a more gradual cortical loss in the mid-sixties (Riggs et al., 2008; Lauretani et al, 2008). Biological sex also exerts a distinguishing effect on the characteristics of age-related bone loss. For trabecular loss, females experience a loss of trabecular number while males primarily experience trabecular thinning (Macdonald et al., 2011). Additionally, endosteal resorption of cortical bone occurs more rapidly in females than males (Lauretani et al, 2008), a pattern corroborated in Chapter 2. As noted above, patterns of cortical bone differences with age within the tibia, radius, and ulna also differ between females and males (Chapter 2), where the anatomical orientation under which bone loss occurs differs within elements between the biological sexes. Since age-related bone loss is a composite process of multiple changes happening across different bone surfaces and ages of occurrence, more specific measurements of bone mass with respect to bone geometry are warranted in characterizing age trends of these processes.

Cortical bone mineral density (cBMD) is reflective of both degree of mineralization and amount of intracortical porosity. After primary ossification, bone is maintained through functional adaptation (Frost, 2003; Ruff et al., 2006; Wang et al., 2022), where remodeling occurs in response to various factors (e.g., microcrack repair, increased strain, or calcium resorption) through synchronization of osteoclastic removal of bone and osteoblastic deposition of osteoid, which is then mineralized. Mineralization of osteoid in cortical bone is therefore reduced in newly remodeled bone, which has a relatively long duration of secondary

mineralization over the course of 2-3 years (Boivin et al., 2009). Accordingly, the mean degree of mineralization decreases more rapidly in females around menopause, a period of increased remodeling due, in part, to changes in systemic estrogen levels (Bergot et al., 2009). Age-related increases in intracortical porosity, on the other hand, are widely associated with dysregulation and asynchronicity of resorption relative to formation in remodeling that leads to a net loss of bone (Razi et al., 2015; Carina et al., 2020). Net-resorptive remodeling, coupled with greater overall rates of remodeling with age, is thought to result in more numerous pores that are wider in diameter due to proportionately less formation than resorption (Stein et al., 1999; Bakalova et al., 2018). However, recent research has argued that coalescence of resorption cones with existing Haversian canals contributes more to age-related cortical porosity than initiation of novel pores (Andreasen et al., 2018). Age-related increases in cortical porosity negatively affects the material strength of cortical bone and is associated with decreased bone strength, particularly among post-menopausal females (McCalden, 1993; Burghardt et al., 2010; Vilayphiou et al., 2016).

Age-related changes in cBMD exhibit regional variation throughout the skeleton. For example, MacDonald and colleagues (2011) found that the distal tibia experiences greater declines of cBMD and greater increases in cortical porosity compared to the distal radius. While cBMD decline has been studied between skeletal elements, usually at sites of clinical relevance (as exemplified in MacDonald et al., 2011), examination of variation within cortical cross-sections has been more targeted and is typically limited to a single region of a given element (Lai et al., 2005; Rantalainen et al., 2011). For instance, Lai and colleagues (2005) found greater cBMD in the posterior aspect of the distal tibia compared to the anterior, lateral, and medial aspects. In a small study, Rantalainen and colleagues (2011) found no significant differences in

cBMD by directional aspect of the tibia between young and old males but did detect decreased cBMD in the inner endocortical division and increased cBMD in the outer pericortical division in older individuals compared to younger individuals. While these studies demonstrate that cBMD varies locally in its age-related decline, no study to the author's knowledge has quantified directional variation in cortical BMD within cross-sections and whether this variation is consistent across the length of long bones.

Given the above context, the aim of this study is to characterize local variation in age-related cBMD decline in the shafts of the leg and forearm bones through pQCT imaging. I ask whether local variation can be observed in cBMD decline within diaphyseal cross-sections, between cross-sections along the length of a single element, and between the tibia, radius, and ulna. Based on a previous study of variation in cortical bone distribution within and between diaphyseal cross-sections (Chapter 2) and the few studies that have examined cBMD variation within diaphyseal cortical bone cross-sections, I predict that the distribution of age-related differences in cBMD will vary within a single cross-section. That is, age-related differences in cBMD, and thus bone porosity, will be nonrandom within cross-sections of these skeletal elements. The pattern of age-related differences in cBMD across cross-sections will not be the same between females and males, in part because of the effects of menopause, with females exhibiting greater differences in cBMD with age. Further, given structured differences with age and sex in cortical bone size and shape (Chapter 2), I predict that patterns of age-related differences in cBMD will differ along the diaphyseal length of each element.

MATERIALS AND METHODS

Sample Composition

Between June and December, 2022, 126 individuals (78 females, 48 males) participated in data collection for this study. Recruitment involved mailings sent to registered pre-donors to the University of Tennessee's Forensic Anthropology Center's body donation program, campus recruitment at Kennesaw State and The University of Tennessee, and through snowball sampling. Eligible individuals were between 40-80 years of age and did not meet exclusionary criteria, including no recent history of cancer, cancer treatment, appendicular bone fracture, and medication use affecting bone remodeling. Additionally, eligibility required that participants be between 18.5-40 BMI. Hormone replacement therapy and birth control were not considered exclusionary, however specific questioning in a questionnaire administered during each study visit asked for information about participant use of both.

Data Collection

A questionnaire soliciting demographic, medical, and lifestyle information was administered at the beginning of data collection. Demographic information included age, biological sex, and self-reported race. Lifestyle information included estimated hours per day of being sedentary, average time spent exercising per week, type of exercise performed (e.g. walking/running, weight training, exercise classes), and history and frequency of tobacco and alcohol consumption. Medical information included previously diagnosed conditions (e.g. malabsorption syndromes, liver disease, Paget's disease), current medication use (e.g. glucocorticoids, anticonvulsants), history or current use of HRT (both androgen and estrogen replacement) or birth control, fracture history, reproductive history, and recent weight gain or loss in the past two

years. Height and weight were measured to the nearest millimeter and kilogram, respectively, and a grip strength test was performed on the non-dominant side prior to scanning using a hand-held dynanometer.

Bone mineral density data of the tibia, radius, and ulna were collected using a Stratec XCT 3000 peripheral quantitative computed tomography (pQCT) scanner (voxel size = 0.5 mm). The scanner was calibrated for density measurement using a manufacturer-provided cone phantom to ensure consistent measurements between slices and individuals. Using the phantom, standard automated quality assurance tests were performed daily, while a more rigorous calibration was performed every 30 days, both using the manufacturer's scanner software. Total length of the non-dominant tibia and forearm were measured to the nearest millimeter (see Chapter 2 for more information about length measurements). A two-dimensional scout view was performed prior to scanning to determine the distal end point of the tibia and radius: a reference line was placed manually by the author at the level of the tibial medial malleolus and at the midpoint of the distal radius. The pQCT scanner then scanned the leg/forearm at 20%, 35%, 50%, and 65% of total length. Participant's leg/forearm were placed perpendicular to the scanner, and the forearm was pronated throughout scanning. The leg was placed with the foot oriented superiorly and with no obvious leg rotation. Scan images were examined by the author for imaging artifacts following scan completion and were repeated as needed.

Data Processing

Following a second round of visual inspection of scan images for artifacts (and exclusion of insufficient scans), images were processed using a custom MATLAB coding created by the author (Chapter 2). Images were binarized using a threshold (pixel value = 120) to isolate

cortical bone from trabecular bone and the remaining soft tissue. A primary set of equiangular directional radii (45 degrees apart) originating from the centroid were established using the 65% length slice for the tibia and the 50% slice for the radius and ulna. For the forearm series, the interosseous crests of the radius and ulna served as a landmark for the medial and lateral radii, respectively. Most leg series were already oriented such that the anterior aspect is pointing superiorly (i.e. the leg is horizontal), however in a few series the anterior crest was used as a guide for manual establishment of the anterior radii. These radii (anterior for tibia, medial for radius, lateral for ulna) were translated to the other slices within a series by maintaining the vector angle from the primary slice and originating it from each cross-sectional centroid. A second set of eight equiangular radii were generated offset from the primary directional radii by 22.5 degrees. These radii were then used divide each cross-section into eight sectors for localized cBMD assessment (Figure 2.1). The 22.5-degree offset of these sector boundaries mean that primary directional radii corresponding to standard anatomical directions (anterior, anterolateral, lateral, etc.) pass through the middle of each sector. Each sector's average cBMD value was assessed as the average pixel value from the original non-binarized scan image.

Statistical Analyses

cBMD data was log-transformed to better fit statistical assumptions of normality in subsequent statistical analyses. Local age-related variation in BMD was assessed through redundancy analysis (RDA), which examines the relative proportion of variation in dependent variables, like cBMD, explained by constrained independent variables (age, sex, slice, BMI). An initial analysis using a combined sex sample showed significant sex effects in explaining cBMD variation, so subsequent analyses were performed separately for each biological sex. Age, slice,

and the interaction between age and slice on bone mineral density were conducted on for each element across all slice locations combined. Then, for each individual slice, RDAs were performed assessing age and BMI effects on cBMD. Statistical significance of both constrained axes (RDAs) and independent variables within each model was tested through permutation ANOVAs (permutations = 9999; $\alpha = 0.05$).

To assess how cBMD by directional sector differs with age, the sample was divided into four decadal age groups and Tukey's Honestly Significant Difference test was performed to measure significant changes between age groups using a critical alpha (α) of $p = 0.05$. Welch's *t*-tests ($\alpha = 0.05$) were performed to assess whether significant differences exist between the mean cBMD values per sector of youngest (40-49 yr) and oldest (70-79 yr) age groups. These differences are presented as percent mean difference for each directional sector and are plotted as bar graphs to illustrate which directional sector experiences the greatest difference in BMD with age.

RESULTS

I first examined if the pattern of cBMD in each slice location along the length of the diaphysis (20%, 35%, 50%, or 65% of length) significantly differs with age, and to assess if age and cross-sectional slice location explain a significant amount of the variance in cBMD. Among females, RDAs performed on the combined slice data for each element indicate that both RDA1 and RDA2 are significant in explaining cBMD variation for the tibia, radius, and ulna (Table 2.1). In both the first and second components of the RDA, variance in cBMD in all bones is explained by both age and by location, though no interaction effect between age and slice location is detected among females (Table 2.1). Results of RDAs performed on all slices within each element among males indicate that RDA1 was significant for the tibia, radius, and ulna,

while RDA2 was significant for the radius only (Table 2.2). The tibial RDA showed a significant interaction between slice location and age for tibial slices, indicating that age-related changes in cBMD differ between slices (Table 2.2). For both the radius and ulna, slice location and age were both significant following permutation ANOVAs, though no significant interaction effect was observed (Table 2.2). These results suggest that age-related differences in cBMD are not the same for females and males, and that in females the pattern of bone density distribution throughout the diaphysis of all three elements under examination is consistent with age as overall cBMD decreases (see below). This is not the case for males, where pattern of higher or lower cBMD among diaphyseal cross-sectional locations relative to each other change with age in the tibia, and there is less of an age effect in explaining the variance in cBMD overall.

Even though there is a significant interaction between age and slice location for the male tibia, to better understand the patterns of cBMD difference among age groups each slice location was examined using RDA with age and BMI as covariates. With one exception in the male ulna noted below, BMI does not significantly explain any of the variance in cBMD, and so results focus on the relationship of age with cBMD among element cross-sectional locations. For slice-specific RDAs of the tibia, RDA1 is significant for all slice locations among females, and RDA1 is significant at the 65% slice among males (Table 2.3). These patterns are driven by intra-slice cBMD differences with age. Radial slice-specific RDAs show that RDA1 is significant for all slices among females and at 20%, 35%, and 50% slice locations among males (Table 2.4), with the variance significantly explained by age. Finally, RDA1 is significant at all ulnar slices among females and age has a significant effect at each location (Table 2.5). Among males, RDA1 is significant at the 50% and 65% slice locations; both RDA1 and RDA2 are significant at 35%

(Table 2.5). Age has a significant effect on cBMD variation at 50% and 65% slice locations, while both age and BMI are significant at the 35% location among males (Table 2.5).

It is therefore evident from these results that, especially among females, differences in cBMD occur both among diaphyseal cross-sectional slice locations and with age. Examining variation in the distribution of cBMD differences among directional sectors (Figure 2.1) in tibial slices, significant age group differences among females occur mostly between the 40-49 year-old (y/o) and 60-69 y/o group, as well as the 40-49 y/o and 70-79 y/o group (Table 2.6). Significant differences occur across all directional sectors at 20% and 35% slice locations, while differences are more consolidated at the posterior to anteromedial range of sectors at the 50% and 65% locations (Table 2.6). Patterns of apparent average cBMD differences within age groups at different directional sectors of tibial cross-sections are consistent between slice locations, with the greatest differences between youngest and oldest age groups seen at the lateral/posterolateral sectors as well as across the range of sectors from posteromedial to anterior (Figure 2.2). The magnitudes of cBMD differences between youngest and oldest age groups among males are smaller than those among females (Figure 2.2). Significant differences between male age groups are minimal and occur at the posterolateral and anteromedial sectors of 50% and 65% length (Table 2.7). Similarly, across tibial slice locations, males show a relatively higher difference in cBMD in the anteromedial sector, as well as the lateral and posterolateral sectors at the 50% and 65% slice locations (Figure 2.2).

These trends continue in comparisons of cBMD among directional sectors in the radius. Age group comparisons of the radius among females show significant differences in cBMD across most directional sectors for the 40-49/60-69 and 40-49/70/79 age-group comparisons (Table 2.8). The 20% and 65% slice locations showed significant differences in cBMD across sectors

between the 50-59 y/o and 60-69 y/o female age groups, and the 20% location also has significant differences between 50-59 y/o and 70-79 y/o groups (Table 2.8). Between the youngest and oldest age group, similar levels of difference are observed among all sectors for the 50% and 65% slice locations among females, while the 20% and 35% locations present a pattern where the medial and anterolateral sectors have the greatest differences in cBMD (Figure 2.3). Additionally, the posterior and posteromedial sectors show high levels of difference at the 20% slice location among females (Figure 2.3). Like the age-group comparison results for the tibia, fewer significant differences in cBMD between age groups were detected among males (Table 2.9). At the 65% slice location, males experienced the greatest differences between youngest and oldest age groups at the anteromedial, anterolateral, and posterior sectors, while a slightly different pattern is observed at 50%: anteromedial, anterior, and posterolateral sectors show the greatest differences (Figure 2.3). Slice locations for 20% and 35% length show more consistent patterns across directions with the anteromedial and medial sectors showing the least difference between age groups among males (Figure 2.3).

Unlike the tibia and radius, the ulna presents different patterns in both females and males. In Tukey HSD results, females between the 40-49/60-69 y/o and 40-49/70-79 y/o age groups exhibit differences in cBMD that are distributed more evenly across the 20% slice location, become more constrained between the posterolateral and anterolateral sectors at 35% and 50% locations, and are mostly absent at the 65% location (Table 2.10). Intra-slice variation in differences between youngest and oldest female age groups by sector show a higher difference at the medial sector for the 35%, 50%, and 65% slice locations and the posteromedial sector at 20% length, though differences between sectors are similar (Figure 2.4). Tukey HSD results among males show significant differences among all age groups are limited to the posteromedial to

anterolateral range of sectors, primarily at 20% and 35% slice locations (Table 2.11). Consistent patterns by directional sector are not observed between youngest and oldest age groups across slices (Figure 2.4).

DISCUSSION

The results of this study demonstrate that, as expected from previous studies, cBMD appears to decline with age, especially through the comparison of mean cBMD within each age group (Figures 2.2-2.4). Greater age-related differences in cBMD occur among females compared to males (Figures 2.2-2.4). However, significant age effects on cBMD distribution among and within diaphyseal cross-sections are unequal across the bone length, particularly among males where there is a significant age-slice interaction in the tibia and few significant age effects in slice-specific RDA results (Tables 2.2-2.5). In addition, the results also indicate that the average difference in cBMD varies by directional sector within cross-sections and that patterns of directional variation are not always consistent across the length of a bone (Figures 2.2-2.4), which supports the final prediction set out in the Introduction and mirrors the heterogeneity in the average change in cortical bone distribution within and across diaphyseal slices reported previously (Chapter 2).

The results indicating that age-related changes in cBMD do indeed vary by location within and between cross-sections can only be observed if local variation is assessed using a "whole bone" perspective (Gosman et al., 2013; Gooding, 2017), which in this study considers multiple slice locations along the length of a long bone to better characterize cortical bone density properties. Other studies have reported regional variation in cBMD decline between sites, such as between the femoral neck and shaft (Beck et al., 2001) or between the distal radius and tibia

(MacDonald et al., 2011; Alvarenga et al., 2017). Fewer studies have observed differential age-related changes within regions of a single cross-section (Kazakia et al., 2012; Weidauer et al., 2013). The causes of age-related cBMD variation are unclear, yet the lack of uniformity in this process has implications for the interpretation of the patterns and consequences of BMD decline.

As noted in the Introduction, cBMD represents both the cortical porosity of a given volume of bone and the degree of bone mineralization (MacDonald et al., 2011). Mineralization of remodeled bone, as previously discussed, is an ongoing process that occurs over years (Boivin et al., 2009), and so higher bone turnover through remodeling, especially in postmenopausal females, may result in a net decrease of mineralization in cortical bone. However, while mineralization is an important property relative to the stiffness of bone tissue (Follet et al., 2004), age-related changes in mineralization are generally quite small (McCalden et al., 1993; Granke et al., 2017). Thus, age-related changes in cBMD with age are thought to be reflective primarily of changes in cortical porosity, with one study estimating that porosity explains approximately 71% of cBMD variation (Bousson et al., 2001; Kontulainen et al., 2006; MacDonald et al., 2011). Therefore, while the resolution of the pQCT scans used in this study do not allow direct assessment of cortical porosity, it is reasonable that changes in cBMD are being primarily driven by changes in cortical porosity rather than lower mineralized bone content.

One possible explanation for variation in cortical porosity is that it results from targeted remodeling from mechanical loading (Lieberman et al., 2003; Wilks et al., 2009). Habitual loading leads to the accumulation of microdamage in areas of the bone that experience high strain, which in turn initiates remodeling to repair and reinforce the bone for similar activities in the future (Mori and Burr, 1993; Lieberman et al., 2003; Ramchand and Seeman, 2018; Wang et al., 2022). Thus, variation in cortical porosity and by proxy cBMD is partly mediated by

mechanical loading, however this relationship is somewhat unclear. Lai and colleagues (2006) asserted that greater cBMD in the posterior quadrant of the midshaft femur compared to the anterior quadrant might be related to that area of the cross-section experiencing compression during bending, however this is not tested experimentally in their study. Rantalainen and colleagues (2011), on the other hand, determined that while athletes in their sample had lower cBMD compared to control subjects, no differences were observed in the spatial distribution of density in tibial midshafts by direction. Instead of asserting a direct relationship between loading and bone density, they suggested that the distribution of cBMD within tibial cross-sections may be evolutionarily selected to distribute strain evenly and more predictably during bending (Rantalainen et al., 2011). This is consistent with other studies that have found higher values of cBMD and/or porosity at the posterior aspect of the tibia (Cooper et al., 2006; Weidauer et al., 2013). Haapasalo et al. (2000) similarly found that loading from athletic activity had a greater effect on bone geometry than density.

Contextualizing the results reported here with expected mechanical demands of each bone yields some possible interpretations. Among females, the greatest age-related difference in cBMD of the tibia is along the lateral/posterolateral directions and medial aspect of the cross-section at each slice location (Figure 2.2). Assuming primarily anteroposterior loading in the tibia from forward locomotion, age-related changes in tibial cBMD are consistent with the major axis of bending if the observed pattern is associated with bone density maintenance; regular loading in the anteroposterior direction would allow for lower bone density normal to that axis to occur with aging without affecting bone rigidity, especially if habitual loading of the tibia is sufficient to not trigger remodeling (Lazenby, 1986; Burr, 2010). The interpretation of the forearm element patterns are less clear. This is, in part, because habitual loading patterns of the

radius and ulna, particularly by direction within a cross-section, are ill-defined given the wide variety of movements performed by the forearm for elbow and wrist/hand movement. It is generally accepted that the proximal radius and ulna experience strains primarily through elbow flexion and extension, while the distal regions of these elements are comparatively subject to hand and wrist movement (Shaaban et al., 2006; McGregor, 2017). This may explain shifting patterns of intra-slice variation in radial and ulnar cross-sections (Figures 3 and 4), but it does not explain the differences between the female and male patterns. In both the radius and ulna, average cBMD differences are more generally distributed in females than in males, where the distribution in directionality of average cBMD differences among diaphyseal cross-sectional slices are more stochastic. Based on survey data, female and male participants in this study did not engage in significantly different habitual forearm loading such that the differences can be explained by loading activities alone. Thus, relating age-related differences in bone density to loading in the forearm is not straightforward. In the case of all elements, the relationship between habitual loading and loss of cBMD in advanced aging warrants experimental testing, either in a human sample or model animal (e.g., rabbits).

Another mechanical consideration is the fact that all bones studied here are joined along their lengths to another bone via an interosseous membrane. The interosseous membrane plays an important role in distributing loads between the two bones (Bader, 2011). For example, tibial cross-sectional geometry is influenced by the relative angle in the fibula's position to the tibia (Auerbach et al., 2017). This suggests that the orientation of the fibula, and therefore the interosseous membrane, may alter load-sharing with the tibia. For the radius and ulna, McGregor (2017) reported that while load sharing is fairly equal proximally, the radius takes on a greater share of the load distally, which makes intuitive sense given the greater cross-section of the distal

radius compared with the ulna. In both the forearm and leg, bones are not loaded in isolation and so adjacent anatomical relationships should be considered in interpreting mechanical effects on bone. Using this argument, effects associated with load-sharing would be expected on the posterolateral aspect of the tibia, the medial aspect of the radius, and the lateral aspect of the ulna. In both sexes, the posterior and posterior lateral directional sectors of the tibia exhibit among the greatest cBMD differences with age. The medial aspect has among the greatest cBMD differences with age in the distal radius of both sexes as well. In the ulna of both sexes a clear pattern is difficult to discern, though the medial sectors of the ulna tend to have the most differences. Together, these lend some support to the conclusion that cBMD loss with age could be tied, at least in the tibia and radius, to the aspect of the cortical bone adjacent to the other element in the limb segment. The reason for this pattern of cBMD distribution awaits further study, but shared loading or the presence of the interosseous membrane could be among the factors influencing change in bone mineral density.

Kazakia and colleagues (2012), further suggested that primary vasculature related to the interosseous membrane partially explained their findings of increased porosity in the posterolateral aspect of the tibia and medial aspect of the radius. While adjacent vessels do contribute to blood supply of the cortex (Lamas et al., 2009), nearby vasculature likely does not significantly explain variation in cBMD. If this were the case, one would expect that the periosteal surface, an important blood supply for cortical bone, would exhibit the most porosity compared to deeper layers of the cortex. Multiple studies have found the opposite pattern, with the endocortical region having the highest porosity and the pericortical region having the lowest (Kontulainen et al., 2006; Rantalainen et al., 2011; Nirody et al., 2016). Thus, the effects of age-related change in vascularization are not favored as an explanation for the patterns reported.

Beyond observing age-related variation in cBMD, results indicate that BMI is not adequate in explaining variation in cBMD within this sample. BMI was only significant in explaining cBMD at 35% ulnar length among males in slice-specific RDA (Table 2.5). The effects of BMI and obesity on bone health are mixed (Pomeroy et al., 2018), especially as BMI has been argued to be a poor index for adiposity (e.g., Wells, 2014). On one hand, BMI has been shown to have positive effects on cortical geometry and BMD, the prevailing idea being that greater mass leads to greater cross-sectional properties through increased loading (Reeves, 2014). On the other hand, high concentrations of visceral fat and associated comorbidities (diabetes mellitus, metabolic syndrome) are linked to low BMD (Palermo et al., 2016), though the fit of BMI to predict amounts of visceral fat is poor (Müller et al., 2016). Thus, the use of BMI is an imperfect proxy for adiposity. Moreover, the detrimental effects of BMI on fracture risk are generally concentrated at the extreme ends of BMI distributions within a population, and the exclusion of individuals below 18.5 and above 40 BMI may partly explain the lack of a significant signal with cBMD.

CONCLUSION

In conclusion, our results indicate that age-related differences in cBMD vary locally within and between cross-sections of the tibia, radius, and ulna. Previous research has linked variation in cBMD and cortical porosity with targeted remodeling as a result of differential strain distribution from loading. Patterns presented here in the tibia conform to these expectations, in that cBMD loss is concentrated along the mediolateral axis, pointing either to lower loading in that axis with age (i.e., more bone removal with lower strains) or load-sharing with the fibula. The patterns for the forearm are more mixed, though there is some indication that load-sharing in

the distal radius may be affecting its cBMD maintenance with age. These results provide provisional support for the argument that loading does contribute to local variation in changes to cBMD, as other studies suggest (Wilks et al., 2009; Haapsalo et al., 2000; Kazakia et al., 2013), though caution should be exercised as overall cortical bone geometry may better reflect local effects of loading and activity changes with age (Chapter 2). However, other factors associated with aging are likely interacting with mechanical signals that make local variation difficult to interpret. That there is variation at all suggests that aging effects on cortical bone remodeling is not entirely a global process and that with aging certain areas of the cortical bone experience greater differences in bone density and distribution than others. Variability in age-related changes to cBMD has implications for clinical approaches toward age-related bone loss treatment and prevention, however further characterization of this variation and the factors that shape it is needed.

REFERENCES

Alvarenga, J. C., Fuller, H., Pasoto, S. G., & Pereira, R. M. R. (2017). Age-related reference curves of volumetric bone density, structure, and biomechanical parameters adjusted for weight and height in a population of healthy women: an HR-pQCT study. Osteoporosis International, 28(4), 1335–1346.

Andreasen, C. M., Delaisse, J.-M., van der Eerden, B. C., van Leeuwen, J. P., Ding, M., & Andersen, T. L. (2018). Understanding Age-Induced Cortical Porosity in Women: The Accumulation and Coalescence of Eroded Cavities Upon Existing Intracortical Canals Is the Main Contributor. Journal of Bone and Mineral Research, 33(4), 606–620.

Auerbach B.A, Gooding, A. F., Shaw, C. N., & Sylvester, A. D. (2017). The relative position of the human fibula to the tibia influences cross-sectional properties of the tibia. American Journal of Physical Anthropology, 163(1), 148–157.

Bader, J. S. (2011). Distal Radioulnar Joint Biomechanics and Forearm Muscle Activity. Doctoral Dissertation, University of Kentucky. 825.

Bakalova, L. P., Andreasen, C. M., Thomsen, J. S., Brüel, A., Hauge, E., Kiil, B. J., Delaisse, J., Andersen, T. L., & Kersh, M. E. (2018). Intracortical Bone Mechanics Are Related to Pore Morphology and Remodeling in Human Bone. Journal of Bone and Mineral Research, 33(12), 2177–2185.

Beck, T. J., Oreskovic, T. L., Stone, K. L., Ruff, C. B., Ensrud, K., Nevitt, M. C., Genant, H. K., & Cummings, S. R. (2001). Structural Adaptation to Changing Skeletal Load in the Progression Toward Hip Fragility: The Study of Osteoporotic Fractures. Journal of Bone and Mineral Research, 16(6), 1108–1119.

Bergot, C., Wu, Y., Jolivet, E., Zhou, L. ., Laredo, J. ., & Bousson, V. (2009). The degree and distribution of cortical bone mineralization in the human femoral shaft change with age and sex in a microradiographic study. Bone (New York, N.Y.), 45(3), 435–442.

Boivin, G., Farlay, D., Bala, Y., Doublier, A., Meunier, P. J., & Delmas, P. D. (2009). Influence of remodeling on the mineralization of bone tissue. Osteoporosis International, 20(6), 1023–1026.

Bousson, V., Meunier, A., Bergot, C., Vicaut, É., Rocha, M. A., Morais, M. H., Laval-Jeantet, A., & Laredo, J. (2001). Distribution of Intracortical Porosity in Human Midfemoral Cortex by Age and Gender. Journal of Bone and Mineral Research, 16(7), 1308–1317.

Burghardt, A., Kazakia, G. J., Ramachandran, S., Link, T. M., & Majumdar, S. (2010). Age- and gender-related differences in the geometric properties and biomechanical significance of intracortical porosity in the distal radius and tibia. Journal of Bone and Mineral Research, 25(5), 983–993.

Burr, D. B. (2010). Cortical bone: a target for fracture prevention? The Lancet (British Edition), 375(9727), 1672–1673.

Carina, V., Della Bella, E., Costa, V. et al. (2020). Bone's Response to Mechanical Loading in Aging and Osteoporosis: Molecular Mechanisms. Calcif Tissue Int 107, 301–318.

Chen, F., OuYang, Y., Ye, T., Ni, B., & Chen, A. (2014). Estrogen Inhibits RANKL-Induced Osteoclastic Differentiation by Increasing the Expression of TRPV5 Channel. Journal of Cellular Biochemistry, 115(4), 651–658.

Cooper, D. M. L., Thomas, C. D. L., Clement, J. G., Turinsky, A. L., Sensen, C. W., & Hallgrímsson, B. (2007). Age-dependent change in the 3D structure of cortical porosity at the human femoral midshaft. Bone (New York, N.Y.), 40(4), 957–965.

Currey, JD. (2006). Bones: structure and mechanics. Princeton, NJ: Princeton University Press. Feik SA, Thomas CD, Clement JG. (1997). Age-related changes in cortical porosity of the midshaft of the human femur. J Anat., 191(3): 407-16.

Follet, H., Boivin, G., Rumelhart, C., & Meunier, P. . (2004). The degree of mineralization is a determinant of bone strength: a study on human calcanei. Bone (New York, N.Y.), 34(5), 783–789.

Frost, H. M. (2003). Bone’s mechanostat: A 2003 update. The Anatomical Record, 275A(2), 1081–1101.

Gooding, A. F. (2017). Variation in cortical bone distribution in the aging appendicular skeleton. Doctoral dissertation, The University of Tennessee – Knoxville.

Gosman J. H., Hubbell, Z. R., Shaw, C. N., & Ryan, T. M. (2013). Development of Cortical Bone Geometry in the Human Femoral and Tibial Diaphysis. Anatomical Record (Hoboken, N.J. : 2007), 296(5), 774–787.

Granke, M., Makowski, A. J., Uppuganti, S., & Nyman, J. S. (2016). Prevalent role of porosity and osteonal area over mineralization heterogeneity in the fracture toughness of human cortical bone. Journal of Biomechanics, 49(13), 2748–2755.

Haapasalo, H., Kontulainen, S., Sievänen, H., Kannus, P., Järvinen, M., & Vuori, I. (2000). Exercise-induced bone gain is due to enlargement in bone size without a change in volumetric

bone density: a peripheral quantitative computed tomography study of the upper arms of male tennis players. Bone (New York, N.Y.), 27(3), 351–357.

Harvey, N., Dennison, E., Cooper, C. (2010). Osteoporosis: impact on health and economics. Nat Rev Rheumatol., 6(2): 99-105.

Hung, V.W.Y., Zhu, T.Y., Cheung, WH. et al. (2015). Age-related differences in volumetric bone mineral density, microarchitecture, and bone strength of distal radius and tibia in Chinese women: a high-resolution pQCT reference database study. Osteoporos Int 26, 1691–1703.

Johannesdottir, F., Aspelund, T., Reeve, J., Poole, K. E., Sigurdsson, S., Harris, T. B., Gudnason, V. G., & Sigurdsson, G. (2013). Similarities and differences between sexes in regional loss of cortical and trabecular bone in the mid-femoral neck: The AGES-Reykjavik longitudinal study. Journal of Bone and Mineral Research, 28(10), 2165–2176.

Johnell, O., Kanis, J. A., Oden, A., et al. (2005). Predictive value of BMD for hip and other fractures. J Bone Miner Res., 20(7): 1185–94.

Kazakia, G. J., Nirody, J. A., Bernstein, G., Sode, M., Burghardt, A. J., & Majumdar, S. (2013). Age- and gender-related differences in cortical geometry and microstructure: Improved sensitivity by regional analysis. Bone (New York, N.Y.), 52(2), 623–631.

Kontulainen, S., Sievänen, H., Kannus, P., Pasanen, M., & Vuori, I. (2003). Effect of Long-Term Impact-Loading on Mass, Size, and Estimated Strength of Humerus and Radius of Female Racquet-Sports Players: A Peripheral Quantitative Computed Tomography Study Between Young and Old Starters and Controls. Journal of Bone and Mineral Research, 18(2), 352–359.

Lai, Qin, L., Hung, V. W. Y., & Chan, K. M. (2005). Regional differences in cortical bone mineral density in the weight-bearing long bone shaft—A pQCT study. Bone (New York, N.Y.), 36(3), 465–471.

Lamas, C., Llusà, M., Méndez, A., Proubasta, I., Carrera, A., & Forcada, P. (2009). Intraosseous Vascularity of the Distal Radius: Anatomy and Clinical Implications in Distal Radius Fractures. Hand (New York, N.Y.), 4(4), 418–423.

Lauretani F., Bandinelli S., Griswold M. E., Maggio M., Semba R., Guralnik J. M., Ferruci L. (2008). Longitudinal Changes in BMD and Bone Geometry in a Population-based study. Journal of Bone and Mineral Research 23(3): 400-408.

Lazenby, R. (1986). Porosity-geometry interaction in conservation of bone strength. Journal of Biomechanics, 19(3): 257:258.

Lieberman, D. E., Pearson, O. M., Polk, J. D., Demes, B., Crompton, A. W. (2003). Optimization of bone growth and remodeling in response to loading in tapered mammalian limbs. Journal of Experimental Biology 206: 3125-3138.

Macdonald, H. M., Nishiyama, K. K., Kang, J., Hanley, D. A., & Boyd, S. K. (2011). Age-related patterns of trabecular and cortical bone loss differ between sexes and skeletal sites: A population-based HR-pQCT study. Journal of Bone and Mineral Research, 26(1), 50–62.

McCalden, R. W., McGeough, J. A., Barker MB, Court-Brown CM. 1993. Age-related changes in the tensile properties of cortical bone. The relative importance of changes in porosity, mineralization, and microstructure. J Bone Joint Surg Am. 75(8): 1193-1205.

McGregor, M. E. (2017). A Biomechanical Investigation of Load Sharing at the Distal Forearm. Electronic Thesis and Dissertation Repository. 4944.

Medina, L., Sabo, S., Vespa, J. 2020. Living Longer: Historical and Projected Life Expectancy in the United States, 1960 to 2060. Census Report P25-1145.

Mori, S., Burr, D. B. (1993). Increased intracortical remodeling following fatigue damage. Bone, 14: 103–109.

Müller, M. J., Braun, W., Enderle, J., & Bosy-Westphal, A. (2016). Beyond BMI: Conceptual Issues Related to Overweight and Obese Patients. Obesity Facts, 9(3), 193–205.

Nirody, J. A., Cheng, K. P., Parrish, R. M., Burghardt, A. J., Majumdar, S., Link, T. M., & Kazakia, G. J. (2015). Spatial distribution of intracortical porosity varies across age and sex. Bone (New York, N.Y.), 75, 88–95.

Peterson, J. A. (2001). Osteoporosis overview. Geriatric Nursing, 22(1), 17–23.
Pomeroy, E., Macintosh, A., Wells, J. C. K., Cole, T. J., & Stock, J. T. (2018). Relationship between body mass, lean mass, fat mass, and limb bone cross-sectional geometry: Implications for estimating body mass and physique from the skeleton. American Journal of Physical Anthropology, 166(1), 56–69.

Ramchand, S.K., Seeman, E. (2018). The Influence of Cortical Porosity on the Strength of Bone During Growth and Advancing Age. Curr Osteoporos Rep 16, 561–572.

Rantalainen, T., Nikander, R., Daly, R. ., Heinonen, A., & Sievänen, H. (2011). Exercise loading and cortical bone distribution at the tibial shaft. Bone (New York, N.Y.), 48(4), 786–791.

Razi, H., Birkhold, A. I., Weinkamer, R., Duda, G. N., Willie, B. M., & Checa, S. (2015). Aging Leads to a Dysregulation in Mechanically Driven Bone Formation and Resorption. Journal of Bone and Mineral Research, 30(10), 1864–1873.

Riggs, B. L., Melton, L. J., Robb, R. A., Camp, J. J., Atkinson, E. J., McDaniel, L., Amin, S., Rouleau, P. A., & Khosla, S. (2008). A Population-Based Assessment of Rates of Bone Loss at Multiple Skeletal Sites: Evidence for Substantial Trabecular Bone Loss in Young Adult Women and Men. Journal of Bone and Mineral Research, 23(2), 205–214.

Ruff, C. B., Hayes, W. B. (1982). Subperiosteal expansion and cortical remodeling of the human femur and tibia with aging. Science 217(4563):945-948.

Ruff, C., Holt, B., & Trinkaus, E. (2006). Who's afraid of the big bad Wolff?: "Wolff's law" and bone functional adaptation. American Journal of Physical Anthropology, 129(4), 484–498.

Shaaban, H., Giakas, G., Bolton, M., Williams, R., Wicks, P., Scheker, L. R., & Lees, V. C. (2006). The load-bearing characteristics of the forearm: pattern of axial and bending force transmitted through ulna and radius. Journal of Hand Surgery, British Volume, 31(3), 274–279.

Stein, M., Feik, S. A., Thomas, C. D. L., Clement, J. G., & Wark, J. D. (1999). An Automated Analysis of Intracortical Porosity in Human Femoral Bone Across Age. Journal of Bone and Mineral Research, 14(4), 624–632.

Vilayphiou, N., Boutroy, S., Sornay-Rendu, E., Van Rietbergen, B., & Chapurlat, R. (2016). Age-related changes in bone strength from HR-pQCT derived microarchitectural parameters with an emphasis on the role of cortical porosity. Bone (New York, N.Y.), 83, 233–240.

Wang L., You, X., Zhang, L., Zhang, C., & Zou, W. (2022). Mechanical regulation of bone remodeling. Bone Research, 10(1), 16.

Weaver, C. M., Peacock, M. Skeletal Changes Across the Life Span. In: Burr DB, & Allen MR (editors). 2019. Basic and applied bone biology. Second edition. New York: Academic Press.

Weidauer, L. A., Binkley, T. L., Berry, R., Specker, B. L. (2013). Variation in cortical density within the cortical shell of individuals across a range in densities and ages. J Musculoskelet Neuronal Interact, 13(1):89-96.

Wells, J. C. K. (2014). Commentary: The paradox of body mass index in obesity assessment: not a good index of adiposity, but not a bad index of cardio-metabolic risk. International Journal of Epidemiology, 43(3), 672–674.

Wilks, D. C., Winwood, K., Gilliver, S. ., Kwiet, A., Chatfield, M., Michaelis, I., Sun, L. ., Ferretti, J. ., Sargeant, A. ., Felsenberg, D., & Rittweger, J. (2009). Bone mass and geometry of the tibia and the radius of master sprinters, middle and long distance runners, race-walkers and sedentary control participants: A pQCT study. Bone (New York, N.Y.), 45(1), 91–97.

APPENDIX 2

Table 2.1. RDA Results Summary: Variation in cortical BMD by age and slice among females. Values in parentheses are percentage of total variance explained by RDA model for each element.

	RDA 1			RDA 2			RDA 3		
Bone Mineral Density (tibia: 20.69%; radius: 20.20%; ulna: 16.98%)									
	Tibia	Radius	Ulna	Tibia	Radius	Ulna	Tibia	Radius	Ulna
Proportion Explained	90.21%	88.26%	88.28%	8.59%	10.50%	10.38%	1.21%	1.99%	1.33%
Age	**-0.964***	**-0.938***	**-0.740***	**0.243***	**0.338***	**-0.632***	-0.110	0.080	0.232
Slice	**-0.227***	**-0.365***	**0.605***	**-0.969***	**-0.902***	**-0.793***	0.096	-0.231	0.073
Age*Slice	-0.540	-0.678	0.265	-0.835	-0.735	-0.915	-0.103	-0.027	0.304

* Significant effect ($p < 0.05$) based on permutation ANOVA.

Table 2.2. RDA Results Summary: Variation in cortical BMD by age and slice among males. Values in parentheses are percentage of total variance explained by RDA model for each element.

	RDA 1			RDA 2			RDA 3		
Bone Mineral Density (tibia: 19.92%; radius: 12.89%; ulna: 10.04%)									
	Tibia	Radius	Ulna	Tibia	Radius	Ulna	Tibia	Radius	Ulna
Proportion Explained	94.74%	80.84%	80.75%	4.78%	16.63%	16.82%	0.48%	2.54%	2.43%
Age	0.463**	**0.633***	**-0.522***	0.851	**-0.730***	0.756	-0.247	-0.257	0.395
Slice	0.857**	**0.765***	**0.855***	-0.474	**0.629***	0.450	0.205	0.136	0.258
Age*Slice	**0.990***	0.929	0.573	-0.078	0.344	0.781	0.120	-0.138	0.249

* Significant effect ($p < 0.05$) based on permutation ANOVA.

** If significant interaction effect is detected, permutation ANOVA does not consider individual variables.

Table 2.3. Tibial RDA Results: Variation in BMD by age and BMI.

	Female		Male	
Tibia: 20% Length (F: 28.57%; M: 7.33%)				
	RDA1	RDA2	RDA1	RDA2
Proportion Explained	96.08%	3.93%	85.93%	14.07%
Age	**-0.999***	0.050	0.375	0.927
BMI	-0.276	-0.961	0.854	-0.521
Tibia: 35% Length (F: 19.79%; M: 9.53%)				
	RDA1	RDA2	RDA1	RDA2
Proportion Explained	95.69%	4.31%	78.53%	21.47%
Age	**-0.993***	0.116	0.757	0.654
BMI	-0.278	-0.961	0.537	-0.844
Tibia: 50% Length (F: 19.86%; M: 8.40%)				
	RDA1	RDA2	RDA1	RDA2
Proportion Explained	96.76%	3.24%	85.93%	14.07%
Age	**-0.969***	0.249	-0.998	0.064
BMI	-0.462	-0.887	-0.090	-0.996
Tibia: 65% Length (F: 26.09%; M: 17.19%)				
	RDA1	RDA2	RDA1	RDA2
Proportion Explained	99.08%	0.93%	84.12%	15.88%
Age	**-0.920***	0.392	**-0.977***	0.214
BMI	-0.614	-0.789	-0.268	-0.963

* Significant effect ($p < 0.05$) based on permutation ANOVA.

Table 2.4. Radial RDA Results: Variation in BMD by age and BMI.

	Female		Male	
Radius: 20% Length (F: 27.86%; M: 15.14%)				
	RDA1	RDA2	RDA1	RDA2
Proportion Explained	95.69%	4.31%	87.90%	12.10%
Age	**-0.989***	0.148	**-0.992***	0.123
BMI	-0.455	-0.890	-0.171	-0.985
Radius: 35% Length (F: 17.08%; M: 9.82%)				
	RDA1	RDA2	RDA1	RDA2
Proportion Explained	98.06%	1.94%	93.49%	6.51%
Age	**-0.989***	0.148	**-0.925***	0.380
BMI	-0.377	-0.926	-0.441	-0.897
Radius: 50% Length (F: 20.89%; M: 12.29%)				
	RDA1	RDA2	RDA1	RDA2
Proportion Explained	94.83%	5.17%	84.50%	15.50%
Age	**-0.969***	0.246	**-0.985***	0.172
BMI	-0.511	-0.859	0.170	0.985
Radius: 65% Length (F: 16.86%; M: 5.46%)				
	RDA1	RDA2	RDA1	RDA2
Proportion Explained	97.79%	2.21%	89.62%	10.38%
Age	**-0.997***	0.072	-0.979	0.204
BMI	-0.205	-0.979	-0.150	-0.989

Table 2.5. Ulnar RDA Results: Variation in BMD by age and BMI.

	Female		Male	
Ulna: 20% Length (F: 20.55%; M: 6.08%)				
	RDA1	RDA2	RDA1	RDA2
Proportion Explained	93.51%	6.49%	83.78%	16.22%
Age	**0.995***	-0.103	-0.929	-0.371
BMI	0.080	-0.997	-0.367	0.930
Ulna: 35% Length (F: 20.13%; M: 12.45%)				
	RDA1	RDA2	RDA1	RDA2
Proportion Explained	99.35%	0.65%	61.00%	39.00%
Age	**0.972***	0.236	**-0.785***	**-0.620***
BMI	0.486	-0.874	**-0.649***	**0.761***
Ulna: 50% Length (F: 16.29%; M: 12.92%)				
	RDA1	RDA2	RDA1	RDA2
Proportion Explained	94.21%	5.79%	80.26%	19.74%
Age	**0.956***	0.292	**-0.995***	-0.101
BMI	0.545	-0.838	-0.125	0.992
Ulna: 65% Length (F: 6.23%; M 11.83%)				
	RDA1	RDA2	RDA1	RDA2
Proportion Explained	91.24%	8.76%	70.00%	30.00%
Age	**0.960***	-0.281	**0.925***	-0.381
BMI	0.489	0.873	-0.416	-0.910

Table 2.6. Tukey HSD results for age group comparisons in tibial cBMD by directional radii (female).

Slice	Age Group Comparison	A	AL	L	PL	P	PM	M	AM
20%	40-49 & 50-59	■						■	
	50-59 & 60-69				■	■			
	60-69 & 70-79								
	40-49 & 60-69	■	■	■	■	■	■	■	■
	40-49 & 70-79	■		■	■	■	■	■	■
	50-59 & 70-79			■					■
35%	40-49 & 50-59			■					■
	50-59 & 60-69								
	60-69 & 70-79								
	40-49 & 60-69	■		■		■	■		■
	40-49 & 70-79	■		■	■		■	■	■
	50-59 & 70-79				■				
50%	40-49 & 50-59	■			■			■	
	50-59 & 60-69								
	60-69 & 70-79								
	40-49 & 60-69	■			■			■	
	40-49 & 70-79	■			■		■	■	■
	50-59 & 70-79								
65%	40-49 & 50-59		■			■			
	50-59 & 60-69						■		
	60-69 & 70-79								
	40-49 & 60-69					■	■	■	
	40-49 & 70-79			■		■	■	■	■
	50-59 & 70-79			■					

Table 2.7. Tukey HSD results for age group comparisons in tibial cBMD by directional radii (male).

Slice	Age Group Comparison	A	AL	L	PL	P	PM	M	AM
20%	40-49 & 50-59								
	50-59 & 60-69								
	60-69 & 70-79								
	40-49 & 60-69								
	40-49 & 70-79								
	50-59 & 70-79								
35%	40-49 & 50-59								
	50-59 & 60-69								
	60-69 & 70-79								
	40-49 & 60-69								
	40-49 & 70-79								
	50-59 & 70-79								
50%	40-49 & 50-59								
	50-59 & 60-69								
	60-69 & 70-79								
	40-49 & 60-69								
	40-49 & 70-79								
	50-59 & 70-79								
65%	40-49 & 50-59								
	50-59 & 60-69								
	60-69 & 70-79								
	40-49 & 60-69								
	40-49 & 70-79								
	50-59 & 70-79								

Table 2.8. Tukey HSD results for age group comparisons in radial cBMD by directional radii (female).

Slice	Age Group Comparison	M	AM	A	AL	L	PL	P	PM
20%	40-49 & 50-59								
	50-59 & 60-69								
	60-69 & 70-79								
	40-49 & 60-69								
	40-49 & 70-79								
	50-59 & 70-79								
35%	40-49 & 50-59								
	50-59 & 60-69								
	60-69 & 70-79								
	40-49 & 60-69								
	40-49 & 70-79								
	50-59 & 70-79								
50%	40-49 & 50-59								
	50-59 & 60-69								
	60-69 & 70-79								
	40-49 & 60-69								
	40-49 & 70-79								
	50-59 & 70-79								
65%	40-49 & 50-59								
	50-59 & 60-69								
	60-69 & 70-79								
	40-49 & 60-69								
	40-49 & 70-79								
	50-59 & 70-79								

Table 2.9. Tukey HSD results for age group comparisons in radial cBMD by directional radii (male).

Slice	Age Group Comparison	M	AM	A	AL	L	PL	P	PM
20%	40-49 & 50-59								
	50-59 & 60-69								
	60-69 & 70-79								
	40-49 & 60-69								
	40-49 & 70-79								
	50-59 & 70-79								
35%	40-49 & 50-59								
	50-59 & 60-69								
	60-69 & 70-79								
	40-49 & 60-69								
	40-49 & 70-79								
	50-59 & 70-79								
50%	40-49 & 50-59								
	50-59 & 60-69								
	60-69 & 70-79								
	40-49 & 60-69								
	40-49 & 70-79								
	50-59 & 70-79								
65%	40-49 & 50-59								
	50-59 & 60-69								
	60-69 & 70-79								
	40-49 & 60-69								
	40-49 & 70-79								
	50-59 & 70-79								

Table 2.10. Tukey HSD results for age group comparisons in ulnar cBMD by directional radii (female).

Slice	Age Group Comparison	L	PL	P	PM	M	AM	A	AL
20%	40-49 & 50-59								
	50-59 & 60-69								
	60-69 & 70-79								
	40-49 & 60-69								
	40-49 & 70-79								
	50-59 & 70-79								
35%	40-49 & 50-59								
	50-59 & 60-69								
	60-69 & 70-79								
	40-49 & 60-69								
	40-49 & 70-79								
	50-59 & 70-79								
50%	40-49 & 50-59								
	50-59 & 60-69								
	60-69 & 70-79								
	40-49 & 60-69								
	40-49 & 70-79								
	50-59 & 70-79								
65%	40-49 & 50-59								
	50-59 & 60-69								
	60-69 & 70-79								
	40-49 & 60-69								
	40-49 & 70-79								
	50-59 & 70-79								

Table 2.11. Tukey HSD results for age group comparisons in ulnar cBMD by directional radii (male).

Slice	Age Group Comparison	L	PL	P	PM	M	AM	A	AL
20%	40-49 & 50-59								
	50-59 & 60-69								
	60-69 & 70-79								
	40-49 & 60-69								
	40-49 & 70-79								
	50-59 & 70-79								
35%	40-49 & 50-59								
	50-59 & 60-69								
	60-69 & 70-79								
	40-49 & 60-69								
	40-49 & 70-79								
	50-59 & 70-79								
50%	40-49 & 50-59								
	50-59 & 60-69								
	60-69 & 70-79								
	40-49 & 60-69								
	40-49 & 70-79								
	50-59 & 70-79								
65%	40-49 & 50-59								
	50-59 & 60-69								
	60-69 & 70-79								
	40-49 & 60-69								
	40-49 & 70-79								
	50-59 & 70-79								

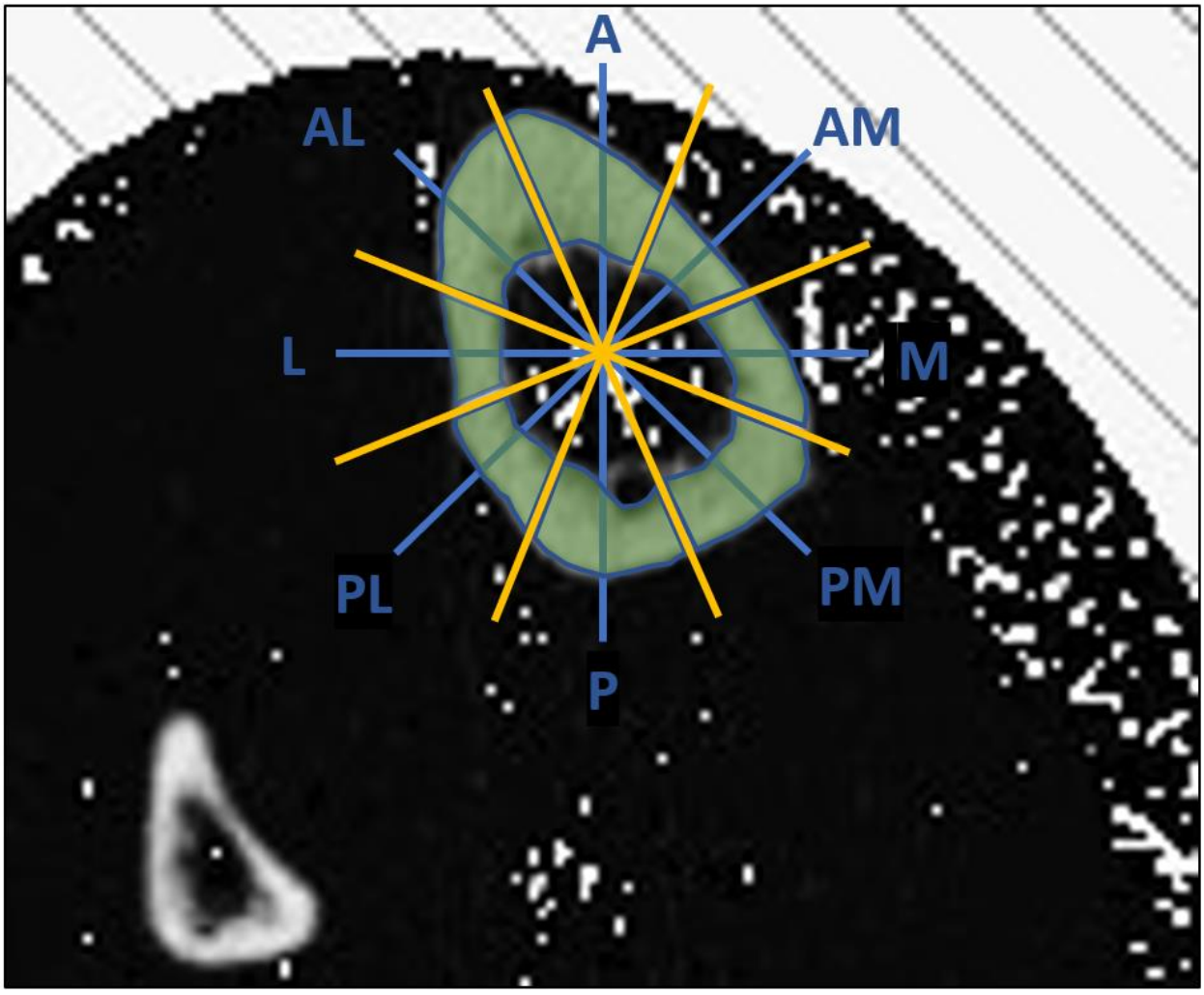

Figure 2.1. Schematic showing how sectors sampled for average cBMD (light green) correspond to directional radii (blue). Eight directional radii were established originating from the cross-sectional centroid. A second set of radii (yellow) were generated at a 22.5 degree offset to serve as boundaries for cBMD sectors.

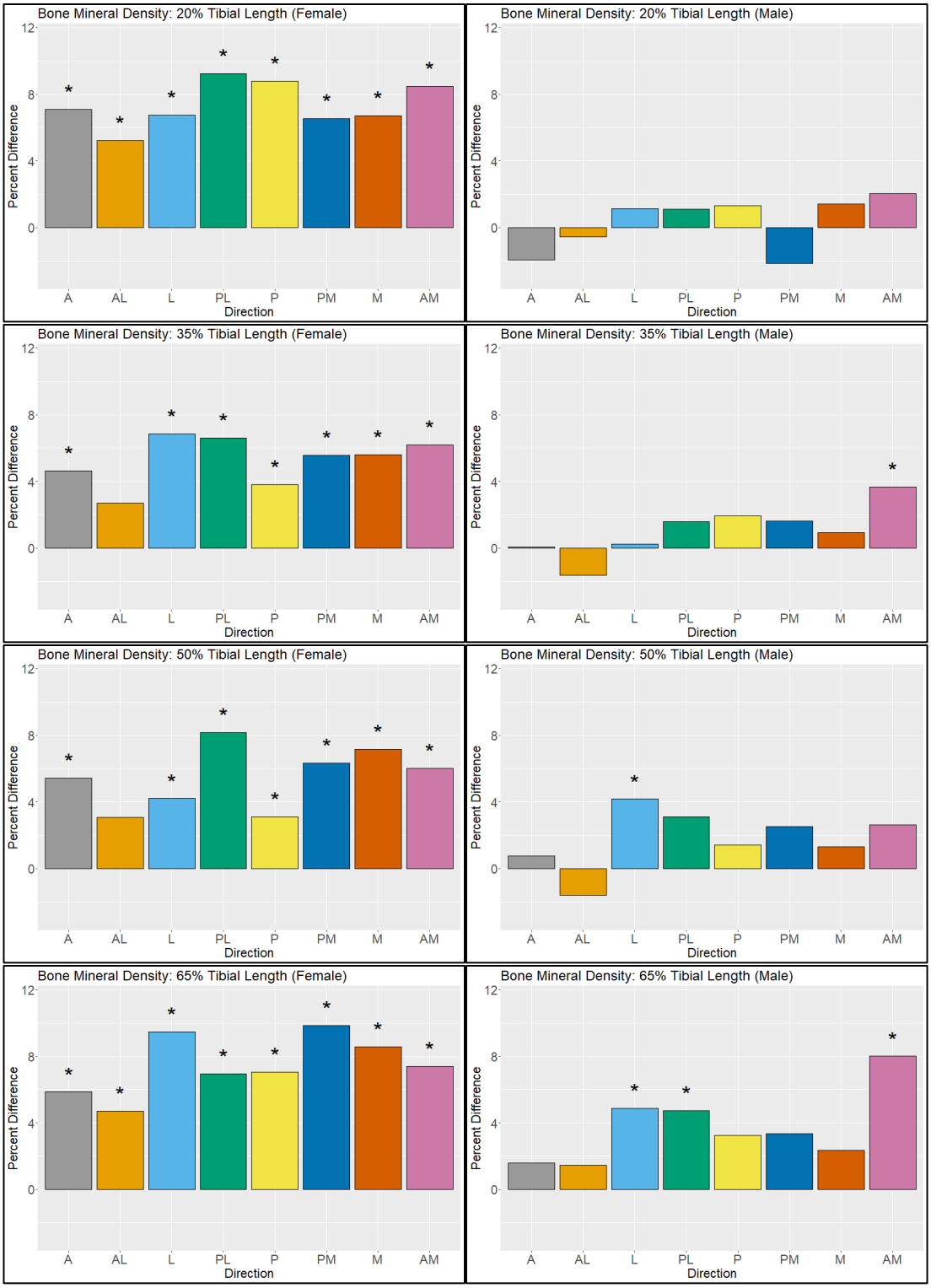

Figure 2.2. Percent difference in tibial cBMD between the youngest (40-49 year-old) and oldest (70-79 year-old) age groups by direction (females left column, males right column). Positive percent differences reflect more cBMD in the younger age group, while negative percent difference reflect less cBMD in the younger age group. Significant differences are indicated with an asterisk (*).

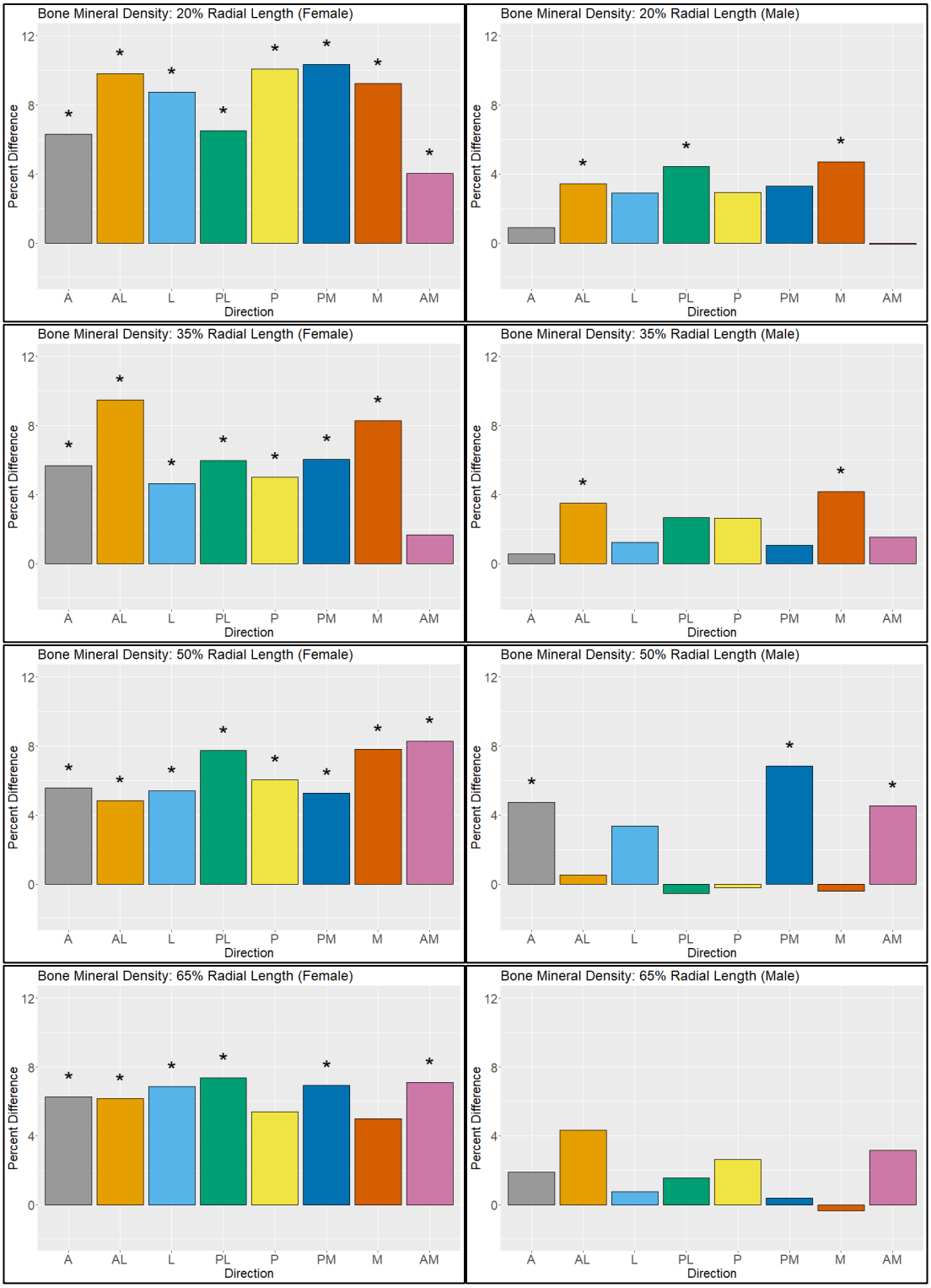

Figure 2.3. Percent difference in radial cBMD between youngest (40-49 year-old) and oldest (70-79 year-old) age groups by direction (females left, males right).

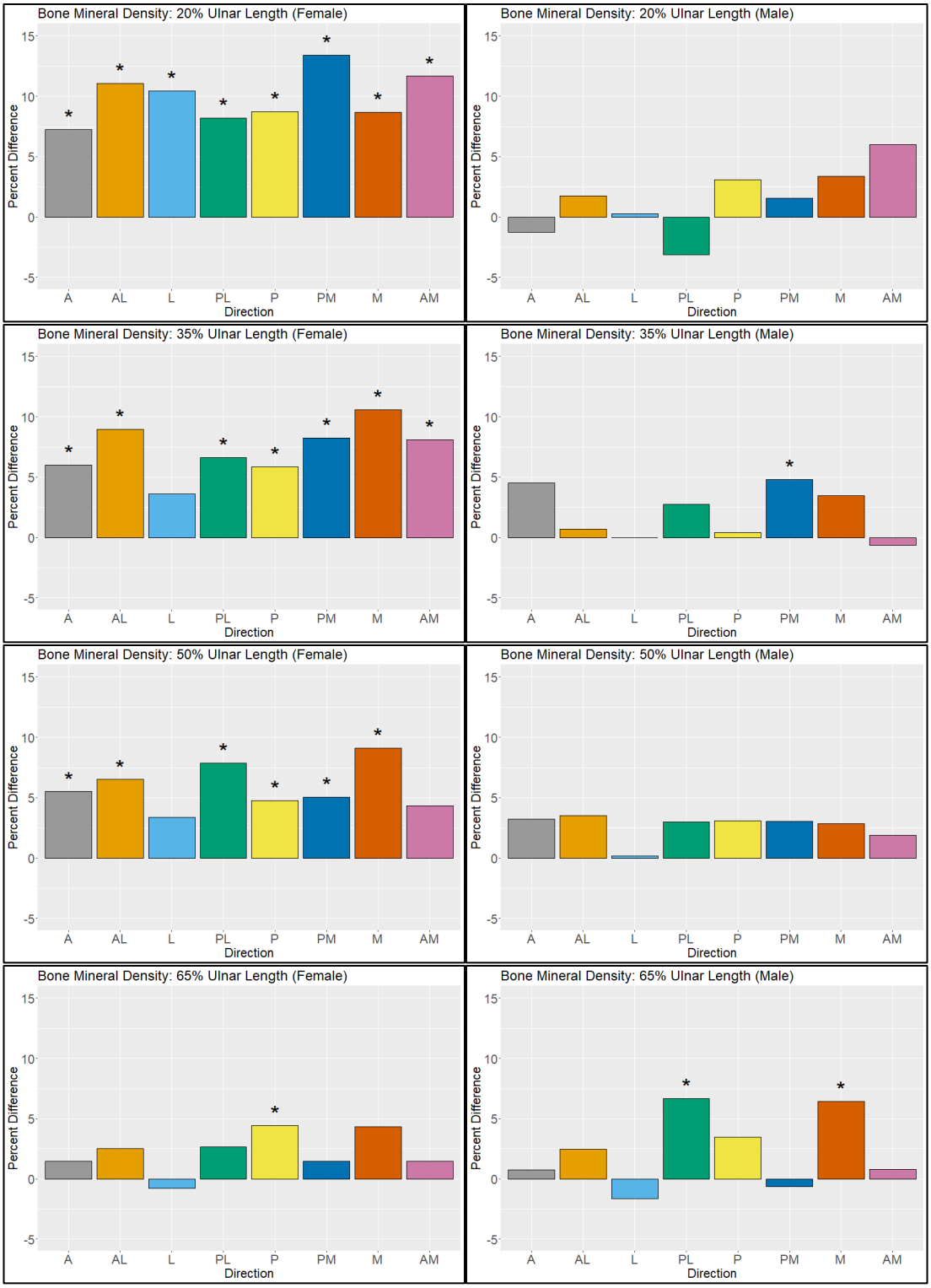

Figure 2.4. Percent difference in ulnar cBMD between youngest (40-49 year-old) and oldest (70-79 year-old) age groups by direction (females left, males right).

CHAPTER 4: AGE-RELATED CHANGES TO CORTICAL GEOMETRY AND CORTICAL BONE MINERAL DENSITY HAVE LOW CORRELATIONS IN HUMAN LONG BONES

Publication statement: A version of this chapter is being prepared for publication by Greg J. Wehrman, Alice F. Gooding, Adam D. Sylvester, Dawnie Wolfe Steadman, Benjamin M. Auerbach as:

Wehrman, G. W., Sylvester, A. D., Gooding, A. F., Steadman D. W., Auerbach, B. M. (2023). Age-related changes to cortical geometry and cortical bone mineral density have low correlations in human long bones. *In preparation*.

This chapter constitutes novel research and regularly uses pronouns "we" and "our" to refer to the collective contributions of the co-authors. It should be noted, however, that in addition to conducting the majority of the research including data collection and analyses, I, Greg Wehrman, am the author in the ordinary sense.

ABSTRACT

Objectives:

From a mechanical standpoint, macrostructure and microstructure of bone should interact to maintain bone strength, however both of these attributes undergo age-related changes that may increase fracture risk. Additionally, the relationship between localized changes in bone macrostructure and microstructure is not well defined. This study, therefore examines correlations between age-related differences in geometric and cortical bone mineral density (cBMD) within and between cross-sections of the tibia, radius, and ulna.

Materials and Methods:

Peripheral quantitative computed tomography (pQCT) scans of 126 living individuals (78 female, 48 male) were performed at 20%, 35%, 50%, and 65% tibial and forearm length. Within these cross-sections, local relationships between directional geometric measurements (cortical thickness, endosteal/periosteal distance to the centroid) and corresponding directional cBMD

sectors was assessed using Spearman's rho correlation coefficients. Additionally, age-related differences in cross-sectional properties of bone strength (I_x, I_y, J, and Z_p) were examined using multi-factor and one-way ANOVAs.

Results:

Results show that geometric measurements and cBMD are not strongly correlated, with the strongest correlations to cBMD being with cortical thickness and endosteal distance. Local patterns of these correlations appear to be driven by the magnitude of age-related differences in endosteal distance from the centroid. Furthermore, cross-sectional properties show very few significant differences with age.

Conclusions:

Correlations between geometric measurements associated with cortical expansion and cBMD are low to moderate at best. The strength of correlations between cBMD and cortical thickness/endosteal distance are likely reflective of the local degree of resorption, which can be observed as a gradation between intracortical and endosteal envelopes. Finally, age-related periosteal expansion is sufficient in maintaining bending and torsional strength with age despite locally non-uniform differences in cortical thickness and cBMD.

INTRODUCTION

Age-related changes to modeling and remodeling of bone, when bone functional adaptation is thought to be less active compared to at younger ages (Pivonka et al., 2018; Carina et al., 2019; Weaver and Peacock, 2019), is well-established as a pattern in primates and laboratory model organisms (Carter and Orr, 1992; Pearson and Lieberman, 2004; Ireland et al., 2014; Meakin et al., 2014). Modeling involves addition or removal of bone on different surfaces,

thereby altering bone macrostructure (Martin et al., 2015; Barak, 2020). Remodeling, meanwhile, is the removal and subsequent addition of bone at the microstructural level. Frost's mechanostat model of bone functional adaptation implicated modeling and remodeling as the mechanisms by which bone responds to signals from mechanical loading (Frost, 1987, 1997, 2003), and that these processes are present throughout the entire lifespan. Since its inception, a number of studies have largely corroborated the core premise of Frost's mechanostat, that bone adapts to its mechanical environment through changes in its macro- and microstructure (Rubin, 1992; Kannus et al., 1995; Lieberman et al., 2003; Ruff et al., 2006; Yang et al., 2019; Wang et al., 2022). However, several inconsistencies and unexpected patterns in bone response to loading, especially those related to aging, have prompted calls for refinement of the model to consider non-mechanical factors shaping bone structure (Beaupré et al., 1990; Pearson and Lieberman, 2004; Skerry, 2006; Agostini et al., 2018). These patterns occur in both bone geometry (the macrostructural scale) and in bone mineral density and porosity (the microstructural scale), so reconciling the relationship between these with respect to mechanical loading is important to creating accurate models of bone functional adaptation. This study examines cortical bone in human limb elements to contextualize the relationship between these two scales with respect to advanced aging.

As individuals get older, bone becomes progressively less capable of anabolic modeling in response to loading (Lieberman et al., 2003; Ireland et al., 2014). However, a continual age-related pattern of cortical expansion accelerates as the skeleton loses bone mass (Ruff and Hayes, 1982; Lauretani et al., 2008; Gosman et al., 2011). Cortical expansion involves removal of bone on the inner endosteal surface and addition of bone on the outer periosteal surface, resulting in cross-sections that increase in diameter while decreasing in cortical thickness. Cortical expansion

is thought to be primarily a result of estrogen decline, which serves to restrict periosteal deposition and maintain endosteal mass during growth and young adulthood (Duan et al., 2003; Khosla et al., 2012; Manolagas et al., 2013). Despite a net loss of bone, this redistribution of bone mass away from the cross-sectional centroid bolsters properties related to bone strength in bending and torsion (Ruff and Hayes, 1982; Beck et al., 2001; Gosman et al., 2011), as bone rigidity and resistance to bending are, in part, determined by the overall distribution of bone away from the neutral axis of strains (Ruff and Hayes, 1983).

In addition to bone loss and apposition at the endosteal and periosteal envelopes of cortical bone within limb elements, bone is also lost within the cortex through accelerated remodeling. Measured as cortical bone mineral density (cBMD), or more precisely as parameters related to intracortical porosity, remodeling appears to increase globally throughout the skeleton with age compared to younger adulthood. In addition to greater remodeling activity, resorption and formation become dysregulated and uncoupled with age so that proportionally more bone is being removed than replaced (Razi et al., 2015; Andreasen et al., 2018). As a result, pores become larger in diameter and begin to coalesce to further increase overall porosity of the bone (Andreasen et al., 2018; Andreasen et al., 2020). Increased intracortical porosity with age has a detrimental effect on bone strength (Vilayphiou et al., 2016), accounting for approximately 76% of age-related decline in bone strength (McCalden et al., 1993).

Local variation occurs in age-related changes to both macrostructure and microstructure. Cortical expansion does not occur uniformly throughout the cross-section (Feik et al., 2000; Wilson et al., 2020; Wehrman et al., Chapter 2), and local variation has been observed in the distribution of porosity (Thomas et al., 2005; Kazakia et al., 2013) and cBMD (Wiedauer et al., 2013). These observations suggest that local factors, potentially related to mechanical loading,

may be shaping variation in an otherwise global age-related process. What is unclear is whether changes in cortical geometry and microstructure are locally correlated.

Some research has suggested that bone macrostructure and microstructure are spatially related in a way that maximizes mechanical competence (Lazenby, 1986; Haapasalo et al., 2000; Burr, 2010). Greater concentrations of intracortical porosity are located in regions of the cross-section that correspond with the neutral axis of bending, where bone is expected to experience the least strain from loading (Lazenby et al., 1986). Additionally, multiple studies have demonstrated that porosity is lower closer to the periosteal surface, where bending and torsional strains are the highest (e.g., Thomas et al., 2005; Rantalainen et al., 2011). The idea that porosity occurs at low-strain regions is somewhat at odds with evidence that greater porosity from remodeling is also associated with high strain areas as a response to the accumulation of microdamage from loading (Burr and Martin, 1993; Burr, 2014). Still others have observed no discernable relationship between cortical geometry and microstructure (Rosenbaum-Chau et al., 2007; Skedros et al., 2013; Eleazer and Jankauskas, 2016). Thus, the spatial relationships between cortical bone geometry and microstructure warrant further investigation.

In prior studies, Wehrman (Chapter 3) and Wehrman et al. (Chapter 2) investigated age-related differences in the distribution of cortical bone and in cBMD variation across multiple locations in the diaphyses of human tibiae, radii, and ulnae, sampled from living participants. Both studies corroborated the findings reported above—older individuals exhibit periosteal expansion, endosteal resorption, and increased porosity in the form of decreased cBMD. These trends were stronger in females, and most notable in comparisons of individuals in their 40s with individuals in their 70s (the oldest individual in the studies was 79). Unique to these studies was the finding that neither cortical bone or cBMD decreased evenly throughout long bone

diaphyses, either along the lengths of the elements or within cross-sectional slices. While areas of greater cortical bone difference did present a pattern, these patterns are not easily interpretable from a mechanical perspective. In contrast, increased porosity, as estimated by cBMD, may be occurring within cross-sectional slices along anatomical axes that are under less habitual loading or experience load-sharing with the other element in the leg and forearm (supporting arguments like those in Lazenby et al., 1986). These results indicate that macrostructure and microstructure may not relate to each other among individuals in these analyses, however, this was not examined directly in either of these prior studies.

The central aim of this study, then, is to assess how local variation in age-related changes to cortical bone macrostructure relates to local variation in microstructure, measured as cBMD. To this end, we use geometric and cBMD data gathered from pQCT scans of the tibia, radius, and ulna from a cross-sectional sample of adults ages 40-80 years from the southeastern United States. Our predictions, based on precedent in the literature and previous studies of this sample, are as follows:

1) Correlations between distance measurements associated with cortical expansion (cortical thickness, endosteal distance, and periosteal distance) and cBMD at corresponding locations within the cross-section will not be uniform within cross-sections.
2) Patterns of correlations between distance measurements and cBMD at corresponding locations within the cross-section will be non-uniform between cross-sections along the length of a given bone.
3) Females will show stronger correlations between distance measurements associated with cortical expansion (cortical thickness, endosteal distance, and periosteal distance) and cBMD due to more rapid age-related bone loss associated with menopause.

In addition to the relationship between cortical bone macro- and microstructure, we also test whether age-related changes in cortical geometry affect total cross-sectional geometric properties of bone strength and rigidity. In so doing, we relate the effects of local variation in cortical expansion to age-related changes in geometric properties of bone strength.

MATERIALS AND METHODS

Sample and Data Acquisition

To assess correlations between local cBMD and distance measurements associated with cortical expansion, 126 participants (78 females, 48 males) from the southeastern United States, mainly Georgia and Tennessee, were recruited to undergo scanning using a Stratec XCT 3000 peripheral quantitative computed tomography (pQCT) scanner. Participants were between 40-80 years of age and met a series of inclusion criteria meant to reduce variation from altered bone remodeling (either pathologically or medication-induced), loading patterns (recent bone fracture), or body mass index (BMI). For a more detailed summary of inclusion criteria, see Wehrman et al. (Chapter 2) and Wehrman (Chapter 3).

Details for the scanning procedure are outlined in Wehrman et al. (Chapter 2) and Wehrman (Chapter 3), but we provide a summary here. Four cross-sectional slices were generated from the pQCT scanner along the length of the leg and forearm (20%, 35%, 50%, and 65% length). Manufacturer provided software provided calculations of cross-sectional geometric properties for the tibia, radius, and ulna, including second moments of area (I_x, I_y), polar second moments of area (J), and polar section modulus (Z_p) (Stratec Medizinteknik). Scans were assessed for imaging artifacts before undergoing processing through custom Matlab coding (created by

G.J.W). This procedure made use of equiangular radii originating from the cross-sectional centroid to establish measures of cortical thickness, endosteal distance from the centroid, and periosteal distance from the centroid along different directions (anterior, anterolateral, lateral, etc.). Additionally, a second series of radii were offset at 22.5 degrees from those generating distance measurements to segment the cross-section into eight sectors for cBMD sampling. Thus, the radii used for generating distance measurements correspond and run through the angular center of a corresponding cBMD sector.

Statistical Analyses

Measures of cortical thickness, endosteal distance, and periosteal distance were standardized by height$^{(3/2)}$ to account for differences in body size among individuals. It is preferable to standardize cross-sectional geometric properties using an estimate of lean body mass (Ruff et al., 2000), so total body mass for individuals who widely varied in BMI is not an accurate way to account for overall size difference as it relates to bone geometry. For this reason, the linear dimensions were scaled to stature without body mass, following Auerbach and Sylvester (2011). Cross-sectional properties related to bending strength were standardized by the product of body mass and total element length, following convention established by Ruff (2008). In the absence of total radial and ulnar lengths, forearm length was used for standardization of both elements.

All statistical analyses were performed using RStudio, version 2022.12.0+353. Following d'Agostino normality tests to assess whether variables were normally distributed, both distance measurements and cBMD values were log-transformed to more closely conform to statistical assumptions of data normality. Correlations between local cBMD and cortical thickness, endosteal distance to the centroid, and periosteal distance to the centroid were assessed using

Spearman correlation coefficients. Spearman correlation was selected to measure association between these variables because it does not assume a linear relationship between variables and is less sensitive to non-normal data. Correlations were calculated between direction-paired cBMD and distance measurements (e.g. anterior cBMD – anterior cortical thickness). Correlations were performed separately between males and females due to established differences in age-related changes to bone geometry and microstructure between sexes (Riggs et al., 2004; Lauretani et al., 2008; Macdonald et al., 2011). Additionally, correlations were performed using both an age-pooled sample and using decadal age subsets to assess whether relationships between distance measurements and cBMD are consistent across the age range used in this study.

To assess age related differences among cross-sectional geometric properties, multi-factor ANOVAs were performed on the combined sample to assess whether second moments of area, polar second moments of area, and polar section modulus varies by sex, age group, slice location, and interaction terms of these factors (critical $\alpha = 0.05$). Multi-factor ANOVAs were chosen over MANOVAs to assess individual cross-sectional geometric properties, even though multi-factor ANOVAs have less statistical power. One-way ANOVAs were then performed on individual sex-specific slice locations with age as the factor of interest. If a significant age effect was detected by these ANOVAs, Tukey's Honestly Significant Difference (HSD) tests were performed to determine which age group differences were driving the effect.

RESULTS

Correlations between cBMD and cortical bone distance measures

Broadly, Spearman's rho correlations between cBMD and distance measurements associated with cortical expansion exhibit more consistent patterns when performed on a combined age

sample (see Tables 3.1-3.6) than constrained to decadal age groups (Tables S2.1-S2.24). This is likely due to increased statistical power and because changes in both distance measures and cBMD are correlated with age; by pooling age groups, the covariation with aging is taken into account in the statistical model. The overarching trend across elements is that correlations between cortical thickness and cBMD exhibit positive correlations of low to moderate values ($\rho \cong 0.1$ to 0.6), while endosteal distance and cBMD exhibit negative low to moderate correlations ($\rho \cong -0.1$ to -0.7). Meanwhile, periosteal distance and cBMD show comparatively low value correlations that are mixed between positive and negative.

In the tibia, females exhibit higher correlations, particularly for cortical thickness and endosteal distance relative to cBMD (Table 3.1). Correlations between endosteal distance and cBMD among females are highest at 65% and 50% length along most directions except for lateral and posterolateral (Table 3.1). At 35% length, no clear patterns emerge, however at 20% length correlations in endosteal distance are highest from the anterior to posterolateral directions, and again along the posteromedial direction (Table 3.1). Male tibiae show less consistent directional patterns in correlations between cBMD and distance measurements (Table 3.2). Correlations between periosteal distances and cBMD among males are more likely to be positive than those among females, however they remain fairly low in magnitude (Table 3.2).

Similar to the tibia, female radii also exhibit the higher directional trends in correlations for cortical thickness and endosteal distance with cBMD (Table 3.3 and 3.4). At the 65% and 50% slice locations, endosteal distance and cortical thickness correlations are highest from the anteromedial to lateral directions along the anterior aspect of the bone (Table 3.3). More distally at 35% and 20% length, we observe a shift where the directions with the highest correlation

coefficients are from the anterolateral to posteromedial directions along the posterior aspect (Table 3.3). A similar but muted pattern is observed among male radii (Table 3.4).

The ulnar patterns differ from those reported above for the tibia and radius. Ulnar correlations between cBMD and distance measurements among females are more evenly distributed across directions (Table 3.5). An area of highest correlations in cortical thickness and endosteal distance with cBMD is observed at the medial and anteromedial directions at 50% length, and spanning more broadly between posteromedial and anterolateral directions at 35% and 20% length (Table 3.5). Among males, a similar pattern to females occurs at 35% and 20% length, dissipating to no discernable trends at 50% and 65% length (Table 3.6). Correlations between periosteal distance and cBMD become distinctly more positive at 65% length in both males and females, specifically in the posterolateral direction and the anterior aspect spanning from anteromedial to anterolateral directions (Tables 3.5 and 3.6).

Multi-factor ANOVA results for cross-sectional geometric properties

We first examined if there are differences in cross-sectional geometric properties (I_x, I_y, J, and Z_p) with respect to age group, sex, and diaphyseal location using multi-factor ANOVAs. Significant sex-age interaction effects were found for all cross-sectional properties of the tibia, while significant sex-slice interactions were found for I_y and J (Table 3.7). Significant sex-age interaction effects indicate that the pattern of sex differences in cross-sectional geometric properties across age groups are not consistent, while significant sex-slice interactions for the anteroposterior second moment and polar moment of area indicate that variation in these have different relationships among slice locations between the sexes. Like the results for the tibia, there are significant interaction effects between sex and age groups for all cross-sectional

geometric properties of the radius (Table 3.8), as well as for all properties of the ulna (Table 3.9). While no significant interactions occur between sex and slice location in the radius, all cross-sectional geometric properties in the ulna except Z_p have significantly different patterns of variation among slices between sexes (Table 3.9).

Because of the interaction effects reported in multi-factor ANOVAs above, we examined differences among age groups in cross-sectional geometric properties within sex- and slice-specific one-factor ANOVAs. No significant age effects were detected in either males or females for any slice of the tibia or radius (Tables 3.10 and 3.11). The ulna showed significant age effects on all cross-sectional geometric properties at the 20% slice location for females, while a significant age effect for males was detected at the 65% slice location for I_y and Z_p (Table 3.12). Post-hoc Tukey HSD test results showed that differences between the 40-49 year old (y/o) group and the 60-69 y/o and 70-79 y/o group were responsible for age effects at the 20% ulnar slice among females, with the older groups showing higher values for all properties. For the significant age effect among males at 65% ulnar length, I_y was higher in the 50-59 y/o, 60-69 y/o, and 70-79 y/o groups relative to the 40-49 y/o group, while the age effect for Z_p was driven by an increase between the 50-59 y/o and 60-69 y/o groups. Thus, when significant age effects were detected, in all cases older age groups presented increased resistance to bending rigidity. Examining general trends in cross-sectional geometric properties, most of these increased with age group in the ulna, as reflected in *F*-values greater than 1 (Tables 3.10-3.12). Increases in these properties were restricted to the distal radius in both sexes and were more mixed in the tibia, with greater differences present among females than males and in the distal tibia.

DISCUSSION

Our results collectively indicate that the relationship of cross-sectional geometric properties to overall age-related differences in cortical bone distribution and mineral density are complex but not unrelated. In both females and males, there is evidence for cortical expansion to occur with increasing age unevenly throughout the diaphysis and by directional radii within cross-sectional slices (I_x and I_y values in Tables 3.7-3.9; Wehrman et al., Chapter 2). However, the correlations between periosteal distances and bone porosity as indicated by cBMD are low. As we explore in more detail below, variation in cBMD more closely relates to endosteal distance and cortical thickness, which both generally decrease with age (Wehrman et al., Chapter 2). We first consider the relationship between bone porosity and cortical bone distribution before returning to examine cross-sectional geometric properties in the context of these results.

Influence of Location on Relationships Between Cortical Macro- and Microstructure

Correlations between cBMD and distance measurements associated with cortical expansion are at best moderate, indicating that age-related changes in geometry are not strongly coupled with cBMD changes. Our results show low-to-moderate correlations for cortical thickness and endosteal distance as they relate to cBMD, with cBMD-cortical thickness correlations being positively correlated and cBMD-endosteal distance correlations being negatively correlated (Tables 3.1-3.6). In other words, on average, as cBMD decreases, the thickness of cortical sections decreases and the endosteal distances increase. Correlations between cBMD and periosteal distance were low and were not consistently positive or negative (Tables 3.1-3.6). These low correlations may be explained by our previous finding that variation in periosteal

distance within this sample is not strongly influenced by age and is more related to BMI (Wehrman et al., Chapter 2).

The correlations between cBMD and distance measurements in our sample are varied by location both within and between elements. Similar findings were reported by Ural and Vashishth (2006), in their investigation of spatial relationships between geometric and microstructural parameters at different sites on male tibiae. They concluded that cortical area and subperiosteal area were correlated with porosity parameters at the distal mid-diaphysis (3.5 cm distal to midshaft) but not at the proximal mid-diaphysis (Ural and Vashishth, 2006). Goldman and colleagues (2014) also found that relationships between robusticity measures (total area/bone length) and porosity differ between sites of the tibial diaphysis, with greater porosity at the more proximal location. They posit that this regional difference may be a result of a biological mechanism that regulates remodeling relative to site-specific robusticity, thereby balancing the need for repair through remodeling with local geometric strength and metabolic expenditure of the tissue (Goldman et al., 2014). In the context of our analyses, we observe greater correlations between cBMD and cortical thickness/endosteal distance more proximally than distally among females, potentially corroborating this idea given the tapered morphology of the tibia (Table 3.1). However, no such pattern is observed among males (Table 3.2), though this may be in part due to lower statistical power.

While our results show that slice location influences correlations between geometric distance measurements and cBMD, these relationships vary further by the directional aspect within the cross-section. Some authors have reported that relationships between geometry and microstructural changes with age are not especially predictable based on mechanical loading patterns (Rosenbaum-Chau, 2008; Kazakia et al., 2013; Carina et al., 2019). Kazakia and

colleagues (2013) found that, while some correspondence was shown between cortical thickness and cortical porosity, in other areas age-related changes were relatively independent, such as the distal tibia showing greatest difference in porosity at the anterior aspect while the greatest difference in cortical thickness occurred at the lateral aspect. In this study, directional correlations between cBMD and distance values similarly do not exhibit patterns that are easily interpretable in a mechanical context, except that, generally, bone density appears to decrease with endosteal resorption and cortical thinning. However, cortical thinning is also related to periosteal expansion and broadly evident increases in cross-sectional geometric properties with age.

Variation in the locations of higher correlation between cBMD and cortical bone dimensions throughout all three skeletal elements highlights the fact that long bones are morphologically complex throughout their diaphyses, so that strain distribution will not be well-characterized by unimodal models of loading, which thereby complicates interpretations (Demes et al., 2001; Skedros, 2012; Wallace et al., 2014). As we noted in the Introduction, other researchers have argued that porosity distributions should occur in the context of biomechanical efficacy (Lazenby, 1986; Thomas et al, 2005; Burr, 2010). Among these studies, remodeling is thought to increase near the endosteal surface (Thomas et al., 2005; Rantalainen et al., 2011) and would often be located along the neutral axis of bending (Lazenby, 1986). From these models we would hypothesize that bone is lost through remodeling in areas that experience the least strain and where decreased mass is less consequential to resistance to failure. Conversely, targeted remodeling due to accumulation of microdamage implies that local patterns of remodeling will result in porosity concentrations in areas experiencing high strain (Burr et al., 1993). It is likely

that observed distributions of porosity are an amalgam of superimposed signals shaped by microdamage, strain distribution, the effects of aging, and other factors (Goldman et al., 2014).

Our results support this synthesis. Higher correlations between cBMD and both cortical thickness and endosteal distance measures occur in different directions among slices throughout diaphyses of all three elements. For example, in the female tibia, at 50% of the diaphyseal length (where we would expect most loading to be along the anteroposterior axis), the highest correlations are anterior, medial, and lateral for cortical thickness. In Wehrman et al. (Chapter 2), we reported that the greatest differences on average in cortical thickness with age occur in the posterior to medial aspect of the tibia, with the greatest amount toward the medial side, and the lowest on the anterior aspect. If higher porosity were motivated by remodeling in response to microdamage (Burr et al., 1993), we would expect the correlation between cBMD and cortical thickness to be roughly along the anteroposterior axis. We observe similar patterns in other slice locations and in the other elements. Our results do not discount remodeling in response to the formation of microcracks, but the effects of aging may complicate this relationship. Thus, we conclude that researchers should 1) be cautious about the relationship between remodeling patterns and their relationships with strain and microdamage, and 2) be aware that these relationships change with age, as evidenced by the interactions in our multi-factor ANOVAs between sex and slice with age.

Age-Related Bone Loss and the Relationships Between Geometry and cBMD

The clearest patterns in correlations between geometric and density measurements are observed when correlations are performed on sex-specific age-pooled samples. When samples are subset into decadal age ranges, correlation directions and magnitudes vary widely between

slices and directions (Tables S2.1-S2.24), which we attribute to an inability to observe sufficient age-related changes over a decade. Since cortical expansion and cBMD decline are both highly correlated with age, their correlation with each other is dependent on a strong age signal. Similarly, females show greater magnitudes in correlations than males, and clearer patterns of variation in these correlations within and between slices of a bone (Tables 3.1-3.6). Greater correlations among females are likely a result of greater differences in these properties with age due to menopausal bone loss. During menopause, estrogen decline leads to a period of rapid bone loss through elevated net-resorptive remodeling before returning post-menopause to similar levels as age-matched men (Iqbal and Zaidi, 2009). This accelerated menopausal bone loss results in greater observable age-related bone loss among females, which in turn can be observed as stronger correlations with clearer local patterning.

Unlike the inconsistent locations we observed with respect to where cBMD and cortical bone geometry are highest in directional sector among slices in each element, average decreases in endosteal bone have a clearer relationship with cBMD. When local correlations between endosteal distance and cBMD are compared with local variation in age-related differences in endosteal distance (see Wehrman et al., Chapter 2), the patterns of variation roughly match each other. Greater differences in endosteal distance with age are associated with stronger correlations between endosteal distance and cBMD. “Trabecularization” of the cortex may partly explain this observation. Several studies have found that porosity is highest near the endosteal border of the cortex throughout life (Rantalainen et al., 2011; Thomas et al., 2005; Nirody et al., 2015; Andreasen et al., 2020). With age, pores increase in diameter due to incomplete filling and coalesce so that what was formerly compact cortical bone more closely resembles trabecular morphology in advanced age (Andreasen et al., 2018). Since remodeling in part depends on

available surface area, a positive feedback occurs where resorption increases the amount of surfaces available for remodeling (Szulc and Seeman, 2009). Thus, a continuum of resorption from the endosteal surface to remodeling within the adjacent intracortical regions exists such that these processes are linked.

We do not observe such clear relationships between cBMD and areas of increase in the periosteal envelope. In both sexes and among all three elements, the correlations are lowest between the periosteal dimensions and cBMD. This makes sense if we consider bone apposition in the subperiosteal area of the diaphysis to be a form of modeling, where bone is not being removed along the envelope (Thomas et al., 2005; Russo et al., 2006; Seeman, 2013), even though there is a correspondence between the areas of the diaphysis that show endosteal bone decreases and periosteal bone increases (Wehrman et al., Chapter 2).

Cortical Expansion and Measures of Bone Strength

As we noted in the Results and at the beginning of this Discussion, age-related differences in cross-sectional geometric properties relate to periosteal expansion in our sample, and while differences with age in these properties are not the same between females and males in most properties (Tables 3.7-3.9), once we separated the sexes we found that *I*, *J*, and *Z* do not significantly differ with age. This suggests that periosteal expansion is largely preserving bone rigidity in our sample. In many cases, resistance to bending rigidity appears to increase slightly with age, as *F*-values greater than 1 implies that more of the variance in cross-sectional geometric properties is explained positively with age than within age groups. We tentatively conclude that, while not statistically significant, the overall geometry of all three elements remains stable if not increases slightly with age in our sample.

Such patterns are achieved through the age-related shift in cortical bone farther from the bone centroid, which bolsters bending and torsional strength despite lower cortical mass. Similar findings were reported by other studies, both cross-sectional and longitudinal (Ruff and Hayes, 1982; Lauretani et al., 2008; Gooding, 2017). It is possible, however, that deleterious effects on bone strength as measured by these properties occur at later ages. Gooding (2017) specifically found little age-related change in parameters of bone rigidity until late in life (80+ years). Thus, it may be that significant age-related changes were not detected in these analyses due to a more constrained age range of 40-80 years of age.

CONCLUSIONS

As we previously reported local variation in distance measurements associated with cortical expansion (Wehrman et al., Chapter 2) and cortical BMD (Wehrman, Chapter 3), this study provides the relationships between these variables and places them into the context of cross-sectional geometric properties. We asked if the strength of correlations between cBMD and distance measurements varies by location within and between cross-sections of the tibia, radius, and ulna. Correlations with cBMD were strongest between cortical thickness and endosteal distance. Patterns of cBMD correlations with cortical thickness do not clearly match either models of high remodeling in response to microdamage in areas of high strain or models of high remodeling in areas of low strain/low consequence. These results point toward the need for more nuanced models of bone strain throughout the diaphysis and a better understanding of the relationships between bone porosity and loading, especially in individuals of advancing age. Patterns of correlation strength do roughly mirror those observed in age-related differences in endosteal distance. We suggest that this may reflect a gradation between intracortical porosity

and trabecularization along the endosteal surface. Finally, we note again that bone strength does not appear to significantly differ with age, which we interpret to be a consequence of maintenance of bone strength and rigidity with apposition of bone on the periosteal envelope of the diaphyses of all three elements. While we broadly consider biomechanical explanations for this variation, our results are not easily explained in this context, which suggest that non-mechanical factors may influence the relationship between cortical bone geometry and microstructure with aging. Disentanglement of these factors will rely on future studies with larger samples and experimental contexts for examining the relationships between mechanical loads, bone mineral density change, and the effects of aging on cortical bone.

REFERENCES

Agostini, G., Holt, B. M., Relethford, J. H. (2018). Bone functional adaptation does not erase neutral evolutionary information. American Journal of Physical Anthropology 166(3):708-729.

Andreasen, C. M., Delaisse, J.-M., van der Eerden, B. C., van Leeuwen, J. P., Ding, M., & Andersen, T. L. (2018). Understanding Age-Induced Cortical Porosity in Women: The Accumulation and Coalescence of Eroded Cavities Upon Existing Intracortical Canals Is the Main Contributor. Journal of Bone and Mineral Research, 33(4), 606–620.

Andreasen, C. M., Bakalova, L. P., Brüel, A., Hauge, E. M., Kiil, B. J., Delaisse, J.-M., Kersh, M. E., Thomsen, J. S., & Andersen, T. L. (2020). The generation of enlarged eroded pores upon existing intracortical canals is a major contributor to endocortical trabecularization. Bone, 130, 115127–115127.

Auerbach, B. M., Sylvester, A. D. (2011). Allometry and apparent paradoxes in human limb proportions: Implications for scaling factors. American Journal of Physical Anthropology, 144(3), 382–391.

Barak, M.M. (2020) Bone modeling or bone remodeling: That is the question. American Journal of Physical Anthropology, 172(2): 153-155.

Beaupré, G. S., Orr, T. E., Carter, D. R. (1990). An approach for time-dependent bone modeling and remodeling—theoretical development. J. Orthop. Res., 8: 651-661.

Beck, T. J., Oreskovic, T. L., Stone, K. L., Ruff, C. B., Ensrud, K., Nevitt, M. C., Genant, H. K., & Cummings, S. R. (2001). Structural Adaptation to Changing Skeletal Load in the Progression Toward Hip Fragility: The Study of Osteoporotic Fractures. Journal of Bone and Mineral Research, 16(6), 1108–1119.

Burr, D. B., Martin, R. B. (1993). Calculating the probability that microcracks initiate resorption spaces. Journal of Biomechanics, 26(4), 613–616.

Burr, D. B. (2014). Repair mechanisms for microdamage in bone. Journal of Bone and Mineral Research, 29(12), 2534–2536.

Burr, D. B. (2010). Cortical bone: a target for fracture prevention? The Lancet (British Edition), 375(9727), 1672–1673.

Carina, V., Della Bella, E., Costa, V. et al. (2020). Bone's response to mechanical loading in aging and osteoporosis: molecular mechanisms. Calcif Tissue Int 107, 301–318.

Carter, D. R., Orr, T. E. (1992). Skeletal development and bone functional adaptation. Journal of Bone and Mineral Research, 7(S2), S389–S395.

Demes, B., Qin, Y.-X., Stern Jr, J. T., Larson, S. G., & Rubin, C. T. (2001). Patterns of strain in the macaque tibia during functional activity. American Journal of Physical Anthropology, 116(4), 257–265.
Duan Y, Beck TJ, Wang X, Seeman E. (2003). Structural and biomechanical basis of sexual dimorphism in femoral neck fragility has its origins in growth and aging. Journal of Bone and Mineral Research 18(10): 1766-1774.

Eleazer, C. D., Jankauskas, R. (2016). Mechanical and metabolic interactions in cortical bone development. American Journal of Physical Anthropology 160:317-333.

Feik, S. A., Thomas, C. D. L., Bruns R., Clement J. G. (2000). Regional variations in cortical modeling in the femoral midshaft: sex and age differences. American Journal of Physical Anthropology 112:191-205.

Frost, H. M. (1987). Bone "mass" and the "mechanostat": a proposal. The Anatomical Record, 219(1):1-9.

Frost, H. M. (1997). On our age-related bone loss: insights from a new paradigm. Journal of Bone and Mineral Research, 12(10): 1539-1546.

Frost, H. M. (2003). Bone's mechanostat: A 2003 update. The Anatomical Record, 275A(2), 1081–1101.

Goldman, H. M., Hampson, N. A., Guth, J. J., Lin, D., & Jepsen, K. J. (2014). Intracortical remodeling parameters are associated with measures of bone robustness. Anatomical Record, 297(10), 1817–1828.

Gooding, A. F. (2017). Variation in cortical bone distribution in the aging appendicular skeleton. Doctoral dissertation, The University of Tennessee – Knoxville.

Gosman JH, Stout SD, and Larsen CS. (2011). Skeletal biology over the life span: A view from the surfaces. American Journal of Physical Anthropology 146(S53):86-98.

Haapasalo, H., Kontulainen, S., Sievänen, H., Kannus, P., Järvinen, M., & Vuori, I. (2000). Exercise-induced bone gain is due to enlargement in bone size without a change in volumetric bone density: a peripheral quantitative computed tomography study of the upper arms of male tennis players. Bone, 27(3), 351–357.

Iqbal, J., Zaidi, M. (2009). Understanding Estrogen Action during Menopause. Endocrinology, 150(8), 3443–3445.

Ireland, A., Maden-Wilkinson, T., Ganse, B., Degens, H., & Rittweger, J. (2014). Effects of age and starting age upon side asymmetry in the arms of veteran tennis players: a cross-sectional study. Osteoporosis International, 25(4), 1389–1400.

Kannus, P., Haapasalo, H., Sankelo, M., Sievänen, H., Pasanen, M., Heinonen, A., Oja, P., & Vuori, I. (1995). Effect of starting age of physical activity on bone mass in the dominant arm of tennis and squash players. Annals of Internal Medicine, 123(1), 27–31.

Kazakia, G. J., Nirody, J. A., Bernstein, G., Sode, M., Burghardt, A. J., & Majumdar, S. (2013). Age- and gender-related differences in cortical geometry and microstructure: Improved sensitivity by regional analysis. Bone, 52(2), 623–631.

Khosla, S. (2013). Pathogenesis of age-related bone loss in humans. The Journals of Gerontology. Series A, Biological Sciences and Medical Sciences, 68(10), 1226–1235.

Lauretani F., Bandinelli S., Griswold M. E., Maggio M., Semba R., Guralnik J. M., Ferruci L. (2008). Longitudinal Changes in BMD and Bone Geometry in a Population-based study. Journal of Bone and Mineral Research 23(3): 400-408.

Lazenby, R. (1986). Porosity-geometry interaction in conservation of bone strength. Journal of Biomechanics, 19(3): 257:258.

Lieberman D.E., Pearson O.M., Polk J.D., Demes B., Crompton A.W. (2003). Optimization of bone growth and remodeling in response to loading in tapered mammalian limbs. Journal of Experimental Biology 206: 3125-3138.

Macdonald, H. M., Nishiyama, K. K., Kang, J., Hanley, D. A., & Boyd, S. K. (2011). Age-related patterns of trabecular and cortical bone loss differ between sexes and skeletal sites: A population-based HR-pQCT study. Journal of Bone and Mineral Research, 26(1), 50–62.

Manolagas, S. C., O'Brien, C. A., Almeida, M. (2013). The role of estrogen and androgen receptors in bone health and disease. Nature Reviews Endocrinology 9: 699-712.

McCalden, R. W., McGeough, J. A., Barker MB, Court-Brown CM. 1993. Age-related changes in the tensile properties of cortical bone. The relative importance of changes in porosity, mineralization, and microstructure. J Bone Joint Surg Am. 75(8): 1193-1205.

Meakin, L. B., Galea, G. L., Sugiyama, T., Lanyon, L. E., & Price, J. S. (2014). Age-related impairment of bones' adaptive response to loading in mice is associated with sex-related deficiencies in osteoblasts but no change in osteocytes. Journal of Bone and Mineral Research, 29(8), 1859–1871.

Nirody, J. A., Cheng, K. P., Parrish, R. M., Burghardt, A. J., Majumdar, S., Link, T. M., & Kazakia, G. J. (2015). Spatial distribution of intracortical porosity varies across age and sex. Bone, 75, 88–95.

Pearson, O. M., Lieberman, D. E. (2004). The aging of Wolff's "law": Ontogeny and responses to mechanical loading in cortical bone. American Journal of Physical Anthropology, 125(S39), 63–99.

Pivonka P, Park A, and Forwood MR. (2018). Functional adaptation of bone: the mechanostat and beyond. In (Pivonka P, editor): Multiscale Mechanobiology of Bone Remodeling and Adaptation. Springer. pp. 1-60.

Rantalainen, T., Nikander, R., Daly, R. ., Heinonen, A., & Sievänen, H. (2011). Exercise loading and cortical bone distribution at the tibial shaft. Bone, 48(4), 786–791.

Razi, H., Birkhold, A. I., Weinkamer, R., Duda, G. N., Willie, B. M., & Checa, S. (2015). Aging leads to a dysregulation in mechanically driven bone formation and resorption. Journal of Bone and Mineral Research, 30(10), 1864–1873.

Riggs, B. L., Melton, L. J., Robb, R. A., Camp, J. J., Atkinson, E. J., McDaniel, L., Amin, S., Rouleau, P. A., & Khosla, S. (2008). A population-based assessment of rates of bone loss at multiple skeletal sites: Evidence for substantial trabecular bone loss in young adult women and Men. Journal of Bone and Mineral Research, 23(2), 205–214.

Rosenbaum Chou, T. G., Child, J. R., Naughtin, R. J., Rigdon, R. R., Schumann, C., & Bloebaum, R. D. (2008). The relationship between femoral periprosthetic cortical bone geometry and porosity after total hip arthroplasty. Journal of Biomedical Materials Research. Part A, 87A(1), 107–115.

Rubin, C. T., Bain, S. D., McLeod, K. J. (1992) Suppression of the osteogenic response in the aging skeleton. Calcified Tissue International, 50:306-313.

Ruff, C. B., Hayes, W. B. (1982). Subperiosteal expansion and cortical remodeling of the human femur and tibia with aging. Science 217(4563):945-948.

Ruff, C. B., Hayes, W. C. (1983). Cross-sectional geometry of Pecos Pueblo femora and tibiae: a biomechanical investigation. II. Sex, age, and side differences. Am J Phys Anthropol 60:383–400.

Ruff, C., Holt, B., & Trinkaus, E. (2006). Who's afraid of the big bad Wolff?: "Wolff's law" and bone functional adaptation. American Journal of Physical Anthropology, 129(4), 484–498.

Ruff, C. B. (2000). Body size, body shape, and long bone strength in modern humans. Journal of Human Evolution, 38(2): 269-290.

Ruff, C. B. (2008). Biomechanical Analyses of Archaeological Human Skeletons. In: Katzenburg, M. A., Grauer, A. L. editors. Biological Anthropology of the Human Skeleton, 3rd edition. Hoboken, NJ: John Wiley & Sons, Inc. pp. 189-224.

Russo, C. R., Lauretani, F., Seeman, E., Bartali, B., Bandinelli, S., Di Iorio, A., Guralnik, J., & Ferrucci, L. (2006). Structural adaptations to bone loss in aging men and women. Bone, 38(1), 112–118.

Seeman, E. (2013). Age- and menopause-related bone loss compromise cortical and trabecular microstructure. The Journals of Gerontology. Series A, Biological Sciences and Medical Sciences, 68(10), 1218–1225.

Skedros, J. G., Knight, A. N., Clark, G. C., Crowder, C. M., Dominguez, V. M., Qiu, S., Mulhern, D. M., Donahue, S. W., Busse, B., Hulsey, B. I., Zedda, M., & Sorenson, S. M. (2013). Scaling of Haversian canal surface area to secondary osteon bone volume in ribs and limb bones. American Journal of Physical Anthropology, 151(2), 230–244.

Skedros, J. G. (2012). Interpreting load history in limb-bone diaphyses: important considerations and their biomechanical foundations. In: Crowder C, Stout S, editors. Bone histology: an anthropological perspective. Boca Raton, FL: CRC Press. pp. 153–220.

Skerry, T. M. (2006). One mechanostat of many? Modifications of the site-specific response of bone to mechanical loading by nature and nurture. Journal of Musculoskeletal Neuronal Interactions 6(2): 122-127.

Szulc, P., Seeman, E. (2009). Thinking inside and outside the envelopes of bone: Dedicated to PDD. Osteoporosis international, 20(8): 1281-1288.

Thomas, C. D., Feik, S. A., & Clement, J. G. (2005). Regional variation of intracortical porosity in the midshaft of the human femur: age and sex differences. Journal of Anatomy, 206(2), 115–125.

Ural, A., Vashishth, D. (2006). Interactions between microstructural and geometrical adaptation in human cortical bone. Journal of Orthopaedic Research, 24(7), 1489–1498.

Vilayphiou, N., Boutroy, S., Sornay-Rendu, E., Van Rietbergen, B., & Chapurlat, R. (2016). Age-related changes in bone strength from HR-pQCT derived microarchitectural parameters with an emphasis on the role of cortical porosity. Bone, 83, 233–240.

Wallace I. J., Demes, B., Mongle, C., Pearson, O. M., Polk, J. D., & Lieberman, D. E. (2014). Exercise-induced bone formation is poorly linked to local strain magnitude in the sheep tibia. PloS One, 9(6), e99108–e99108.

Wang L., You, X., Zhang, L., Zhang, C., & Zou, W. (2022). Mechanical regulation of bone remodeling. Bone Research, 10(1), 16–16.

Weaver, C. M., Peacock, M. Skeletal Changes Across the Life Span. In: Burr DB, & Allen MR (editors). 2019. Basic and applied bone biology. Second edition. New York: Academic Press.

Weidauer, L. A., Binkley, T. L., Berry, R., Specker, B. L. (2013). Variation in cortical density within the cortical shell of individuals across a range in densities and ages. J Musculoskelet Neuronal Interact, 13(1):89-96.

Wilson, L. A. B., De Groote, I., Humphrey L. T. (2020). Sex differences in the patterning of age-related bone loss in the human hallucal metatarsal in rural and urban populations. American Journal of Physical Anthropology 171(4): 628-644.

Yang, H., Xu, X., Bullock, W., Main, R. (2019). Adaptive changes in micromechanical environments of cancellous and cortical bone in response to in vivo loading and disuse. Journal of Biomechanics 89: 85-94.

APPENDIX 3

Table 3.1. Spearman's ρ correlations between female, age-pooled cBMD and distance measures within cortical cross-sections of the tibia. Directional sector abbreviations are: A, anterior; AL, anterior lateral; L, lateral; PL, posterior lateral; P, posterior; PM, posterior medial; M, medial; AM, anterior medial. Green denotes positive correlations; red denotes negative correlations.

Slice	Distance measure	Directional sector within cortical slice							
		A	AL	L	PL	P	PM	M	AM
20%	Cortical thickness	0.484	0.594	0.463	0.413	0.309	0.463	0.228	0.314
	Endosteal distance	-0.383	-0.335	-0.367	-0.452	-0.253	-0.491	-0.226	-0.211
	Periosteal distance	-0.137	-0.033	-0.215	-0.127	-0.114	-0.131	-0.049	-0.057
35%	Cortical thickness	0.219	0.259	0.433	0.232	0.332	0.155	0.343	0.465
	Endosteal distance	-0.114	-0.219	-0.188	-0.182	-0.449	-0.275	-0.253	-0.265
	Periosteal distance	0.026	0.072	0.093	-0.035	-0.184	-0.124	0.018	-0.031
50%	Cortical thickness	0.511	0.259	0.507	0.381	0.352	0.27	0.535	0.511
	Endosteal distance	-0.494	-0.426	-0.291	-0.288	-0.435	-0.315	-0.361	-0.253
	Periosteal distance	0.007	-0.069	0.057	0.082	-0.078	-0.01	-0.012	0.075
65%	Cortical thickness	0.573	0.377	0.606	0.433	0.399	0.293	0.511	0.575
	Endosteal distance	-0.436	-0.467	-0.308	-0.31	-0.452	-0.412	-0.434	-0.422
	Periosteal distance	0.002	-0.175	-0.029	-0.028	-0.129	-0.25	-0.261	-0.109

Table 3.2. Spearman's ρ correlations between male, age-pooled cBMD and distance measures within cortical cross-sections of the tibia. Directional sector abbreviations are: A, anterior; AL, anterolateral; L, lateral; PL, posterolateral; P, posterior; PM, posteromedial; M, medial; AM, anteromedial. Green denotes positive correlations; red denotes negative correlations.

Slice	Distance measure	Directional sector within cortical slice							
		A	AL	L	PL	P	PM	M	AM
20%	Cortical thickness	0.376	0.153	0.163	0.525	0.155	0.317	0.203	0.289
	Endosteal distance	-0.497	-0.27	-0.272	-0.412	-0.153	-0.348	-0.187	-0.426
	Periosteal distance	-0.272	-0.15	-0.22	0.102	-0.03	-0.036	-0.015	-0.231
35%	Cortical thickness	0.107	0.255	0.349	0.251	0.413	-0.101	0.303	0.32
	Endosteal distance	-0.296	-0.336	-0.484	-0.139	-0.238	-0.033	-0.21	-0.267
	Periosteal distance	-0.235	-0.092	-0.221	-0.005	0.09	-0.121	0.168	0.101
50%	Cortical thickness	0.435	0.293	0.286	0.357	0.367	-0.103	0.18	0.184
	Endosteal distance	-0.478	-0.367	-0.021	-0.094	-0.283	-0.12	0.024	-0.214
	Periosteal distance	0.046	-0.075	0.196	0.156	0.159	-0.237	0.237	-0.039
65%	Cortical thickness	0.22	0.238	0.47	0.052	0.444	0.124	0.386	0.485
	Endosteal distance	-0.234	-0.469	-0.084	0.056	-0.338	-0.141	-0.084	-0.148
	Periosteal distance	-0.044	-0.273	0.112	0.021	0.208	-0.051	0.104	0.118

Table 3.3. Spearman's ρ correlations between female, age-pooled cBMD and distance measures within cortical cross-sections of the radius. Directional sector abbreviations are: A, anterior; AL, anterior lateral; L, lateral; PL, posterior lateral; P, posterior; PM, posterior medial; M, medial; AM, anterior medial. Green denotes positive correlations; red denotes negative correlations.

Slice	Distance measure	Directional sector within cortical slice							
		A	AL	L	PL	P	PM	M	AM
20%	Cortical thickness	0.255	0.515	0.657	0.523	0.582	0.58	0.468	0.103
	Endosteal distance	-0.206	-0.509	-0.45	-0.558	-0.569	-0.206	-0.499	-0.138
	Periosteal distance	-0.054	-0.27	-0.147	-0.379	-0.227	0.284	-0.174	-0.087
35%	Cortical thickness	0.43	0.641	0.359	0.619	0.492	0.452	0.4	0.186
	Endosteal distance	-0.384	-0.594	-0.398	-0.592	-0.473	-0.48	-0.453	-0.261
	Periosteal distance	0.019	-0.121	-0.146	-0.082	-0.13	-0.042	0.005	-0.056
50%	Cortical thickness	0.583	0.621	0.598	0.135	0.366	0.538	0.136	0.592
	Endosteal distance	-0.572	-0.555	-0.546	-0.357	-0.372	-0.523	-0.537	-0.62
	Periosteal distance	-0.111	-0.037	-0.229	-0.186	-0.044	0.005	-0.336	-0.186
65%	Cortical thickness	0.683	0.699	0.475	0.479	0.674	0.417	0.351	0.55
	Endosteal distance	-0.562	-0.676	-0.471	-0.35	-0.469	-0.41	-0.398	-0.227
	Periosteal distance	-0.04	-0.156	-0.119	-0.033	-0.043	-0.031	-0.043	0.264

Table 3.4. Spearman's ρ correlations between male, age-pooled cBMD and distance measures within cortical cross-sections of the radius. Directional sector abbreviations are: A, anterior; AL, anterior lateral; L, lateral; PL, posterior lateral; P, posterior; PM, posterior medial; M, medial; AM, anterior medial. Green denotes positive correlations; red denotes negative correlations.

Slice	Distance measure	Directional sector within cortical slice							
		A	AL	L	PL	P	PM	M	AM
20%	Cortical thickness	0.243	0.489	0.61	0.347	0.618	0.515	0.301	0.489
	Endosteal distance	-0.108	-0.391	-0.584	-0.255	-0.467	-0.472	-0.335	-0.259
	Periosteal distance	0.167	-0.224	-0.388	-0.069	0.144	-0.122	-0.141	0.078
35%	Cortical thickness	0.533	0.319	0.633	0.215	0.363	0.438	0.319	0.434
	Endosteal distance	-0.323	-0.541	-0.358	-0.309	-0.461	-0.149	-0.465	-0.311
	Periosteal distance	0.243	-0.338	0.247	-0.006	0.002	0.33	-0.158	0.033
50%	Cortical thickness	0.486	0.432	0.582	0.114	0.1	0.417	-0.081	0.15
	Endosteal distance	-0.453	-0.415	-0.355	-0.014	-0.108	-0.414	-0.193	-0.302
	Periosteal distance	0.084	-0.055	0.09	0.125	-0.047	-0.04	-0.299	-0.114
65%	Cortical thickness	0.433	0.312	0.446	0.289	0.487	0.388	0.072	0.483
	Endosteal distance	-0.239	-0.433	-0.088	-0.352	-0.127	-0.18	-0.049	-0.458
	Periosteal distance	0.061	-0.233	0.239	-0.138	0.179	0.02	-0.101	-0.07

Table 3.5. Spearman's ρ correlations between female, age-pooled cBMD and distance measures within cortical cross-sections of the ulna. Directional sector abbreviations are: A, anterior; AL, anterior lateral; L, lateral; PL, posterior lateral; P, posterior; PM, posterior medial; M, medial; AM, anterior medial. Green denotes positive correlations; red denotes negative correlations.

Slice	Distance measure	Directional sector within cortical slice							
		A	AL	L	PL	P	PM	M	AM
20%	Cortical thickness	0.466	0.427	0.337	0.245	0.44	0.431	0.514	0.406
	Endosteal distance	-0.427	-0.174	-0.381	-0.341	-0.219	-0.351	-0.426	-0.468
	Periosteal distance	-0.146	0.178	-0.059	-0.098	0.014	-0.018	-0.123	-0.228
35%	Cortical thickness	0.553	0.508	0.317	0.519	0.445	0.61	0.651	0.469
	Endosteal distance	-0.481	-0.397	-0.474	-0.311	-0.31	-0.489	-0.599	-0.469
	Periosteal distance	0.119	0.057	-0.204	0.112	-0.03	0.026	-0.222	-0.149
50%	Cortical thickness	0.411	0.593	0.112	0.503	0.369	0.26	0.692	0.304
	Endosteal distance	-0.21	-0.072	-0.349	-0.331	-0.296	-0.464	-0.632	-0.408
	Periosteal distance	0.184	0.34	-0.313	0.133	0.035	-0.137	-0.01	-0.18
65%	Cortical thickness	0.403	0.459	0.011	0.509	0.373	0.16	0.316	0.463
	Endosteal distance	-0.057	0.039	-0.22	-0.151	-0.269	-0.207	-0.399	-0.167
	Periosteal distance	0.144	0.259	-0.371	0.157	0.02	-0.081	-0.104	0.244

Table 3.6. Spearman's ρ correlations between male, age-pooled cBMD and distance measures within cortical cross-sections of the ulna. Directional sector abbreviations are: A, anterior; AL, anterolateral; L, lateral; PL, posterolateral; P, posterior; PM, posteromedial; M, medial; AM, anteromedial. Green denotes positive correlations; red denotes negative correlations.

Slice	Distance measure	Directional sector within cortical slice							
		A	AL	L	PL	P	PM	M	AM
20%	Cortical thickness	0.505	0.4	0.301	0.328	0.586	0.406	0.427	0.564
	Endosteal distance	-0.628	-0.282	-0.292	-0.163	-0.603	-0.225	-0.383	-0.435
	Periosteal distance	-0.105	-0.081	-0.14	0.005	-0.035	0.069	-0.012	-0.167
35%	Cortical thickness	0.45	0.456	0.43	0.248	0.205	0.401	0.423	0.498
	Endosteal distance	-0.51	-0.367	-0.365	-0.243	-0.012	-0.232	-0.494	-0.367
	Periosteal distance	0.03	0.142	0	0.106	0.292	0.186	-0.241	-0.036
50%	Cortical thickness	0.119	0.436	0.238	0.209	0.155	0.276	0.187	0.116
	Endosteal distance	-0.242	-0.155	-0.294	-0.056	-0.112	-0.134	-0.393	-0.127
	Periosteal distance	-0.091	0.136	-0.049	0.098	0.118	0.206	-0.321	0.011
65%	Cortical thickness	0.362	0.352	0.091	0.499	0.467	0.29	0.236	0.433
	Endosteal distance	0.085	0.185	-0.441	0.038	-0.471	-0.383	-0.306	-0.159
	Periosteal distance	0.261	0.331	-0.183	0.356	0.144	0.031	-0.092	0.224

Table 3.7. Multi-factor ANOVA *F*-values for the tibia examining the effects of sex, age, and diaphyseal slice location on cross-sectional geometric properties. Significant results ($p<0.05$) are indicated in **bold**.

Cross-sectional geometric property	Factors				
	Sex	Age	Slice	Sex*Age	Sex*Slice
I_x	**21.743**	**3.582**	**318.652**	**3.348**	2.213
I_y	**100.925**	0.754	**107.980**	**8.677**	**7.806**
J	**59.707**	2.269	**277.952**	**5.636**	**5.163**
Z_p	1.447	2.294	**148.567**	**4.500**	0.843

Table 3.8. Multi-factor ANOVA *F*-values for the radius examining the effects of sex, age, and diaphyseal slice location on cross-sectional geometric properties. Significant results ($p<0.05$) are indicated in **bold**.

Cross-sectional geometric property	Factors				
	Sex	Age	Slice	Sex*Age	Sex*Slice
I_x	**82.214**	**2.952**	**8.603**	**8.474**	0.677
I_y	**48.617**	**2.798**	**21.938**	**3.50**	0.081
J	**68.944**	2.576	**16.484**	**5.867***	0.257
Z_p	**7.753**	**4.375**	**12.399**	**6.858***	0.151

Table 3.9. Multi-factor ANOVA *F*-values for the ulna examining the effects of sex, age, and diaphyseal slice location on cross-sectional geometric properties. Significant results ($p<0.05$) are indicated in **bold**.

Cross-sectional geometric property	Factors				
	Sex	Age	Slice	Sex*Age	Sex*Slice
I_x	**96.423**	**2.951**	**174.497**	**8.192**	**3.518**
I_y	**126.298**	**6.944**	**219.631**	**8.811**	**7.685**
J	**141.278**	**5.582**	**249.432**	**9.983**	**6.738**
Z_p	**29.015**	**7.017**	**175.652**	**7.610**	0.476

Table 3.10. ANOVA results for the tibia examining the effects of age on cross-sectional properties at 20%, 35%, 50%, and 65% slice locations. *F*-values are presented with *p*-values in parentheses. Significant results are **bold.**

Cross-sectional geometric property	*F* (*p*-value)	*F* (*p*-value)
	Females	Males
20% of length		
$\boldsymbol{I_x}$	1.633 (0.19)	1.707 (0.18)
$\boldsymbol{I_y}$	2.259 (0.08)	0.437 (0.73)
$\boldsymbol{J}$	2.079 (0.11)	0.935 (0.43)
$\boldsymbol{Z_p}$	1.795 (0.16)	0.787 (0.51)
35% of length		
$\boldsymbol{I_x}$	0.673 (0.57)	1.368 (0.27)
$\boldsymbol{I_y}$	1.065 (0.37)	1.299 (0.29)
$\boldsymbol{J}$	0.896 (0.45)	1.087 (0.37)
$\boldsymbol{Z_p}$	0.679 (0.57)	0.553 (0.65)
50% of length		
$\boldsymbol{I_x}$	0.979 (0.41)	1.227 (0.31)
$\boldsymbol{I_y}$	1.784 (0.16)	0.653 (0.59)
$\boldsymbol{J}$	1.361 (0.26)	0.808 (0.50)
$\boldsymbol{Z_p}$	1.098 (0.36)	0.52 (0.67)
65% of length		
$\boldsymbol{I_x}$	0.766 (0.52)	0.973 (0.42)
$\boldsymbol{I_y}$	1.730 (0.17)	1.419 (0.25)
$\boldsymbol{J}$	1.122 (0.35)	0.991 (0.41)
$\boldsymbol{Z_p}$	1.097 (0.36)	0.906 (0.45)

Table 3.11. ANOVA results for the radius examining the effects of age on cross-sectional properties at 20%, 35%, 50%, and 65% slice locations. *F*-values are presented with *p*-values in parentheses. Significant results are **bold.**

Cross-sectional geometric property	*F* (*p*-value)	*F* (*p*-value)
	Females	Males
20% of length		
I_x	1.09 (0.36)	1.34 (0.27)
I_y	2.105 (0.11)	0.494 (0.69)
J	1.794 (0.16)	0.595 (0.62)
Z_p	1.812 (0.15)	1.656 (0.19)
35% of length		
I_x	1.65 (0.19)	1.469 (0.24)
I_y	1.981 (0.12)	0.645 (0.59)
J	1.953 (0.13)	0.981 (0.41)
Z_p	1.492 (0.22)	1.398 (0.26)
50% of length		
I_x	0.573 (0.64)	1.959 (0.14)
I_y	0.809 (0.49)	1.36 (0.27)
J	0.784 (0.51)	1.532 (0.22)
Z_p	0.849 (0.47)	1.605 (0.21)
65% of length		
I_x	0.736 (0.53)	1.22 (0.31)
I_y	0.865 (0.46)	0.578 (0.63)
J	0.71 (0.55)	0.928 (0.44)
Z_p	0.773 (0.51)	1.552 (0.22)

Table 3.12. ANOVA results for the ulna examining the effects of age on cross-sectional properties at 20%, 35%, 50%, and 65% slice locations. *F*-values are presented with *p*-values in parentheses. Significant results are **bold.**

Cross-sectional geometric property	*F* (*p*-value) Females	*F* (*p*-value) Males
20% of length		
I_x	**4.204 (0.01)**	1.158 (0.34)
I_y	**3.554 (0.02)**	0.924/ (0.44)
J	**4.209 (0.01)**	1.102/ (0.36)
Z_p	**4.301 (0.01)**	1.344/ (0.27)
35% of length		
I_x	1.685 (0.18)	1.506/ (0.23)
I_y	0.696 (0.56)	2.101/ (0.11)
J	1.526 (0.22)	2.055/ (0.12)
Z_p	1.561 (0.21)	1.297/ (0.29)
50% of length		
I_x	2.111 (0.11)	0.813/ (0.49)
I_y	1.405 (0.25)	2.309/ (0.09)
J	2.22 (0.09)	1.556/ (0.21)
Z_p	1.829 (0.15)	1.133/ (0.35)
65% of length		
I_x	2.098 (0.11)	1.51/ (0.23)
I_y	1.878 (0.15)	3.922/ (**0.01)**
J	2.152 (0.10)	2.731/ (0.06)
Z_p	1.242 (0.30)	4.278/ (**0.01)**

SUPPLEMENTARY INFORMATION

Table S2.1. Spearman's ρ correlations between female (ages 40-49) cBMD and distance measures within cortical cross-sections of the tibia. Directional sector abbreviations are: A, anterior; AL, anterolateral; L, lateral; PL, posterolateral; P, posterior; PM, posteromedial; M, medial; AM, anteromedial. Green denotes positive correlations; red denotes negative correlations.

Slice	Distance measure	Directional sector within cortical slice							
		A	AL	L	PL	P	PM	M	AM
20%	Cortical thickness	0.45	0.632	0.421	0.193	0.486	0.357	-0.032	0.182
	Endosteal distance	-0.332	-0.254	-0.136	0.107	0.293	-0.571	0.207	0.057
	Periosteal distance	-0.168	0.354	0.046	0.15	0.407	-0.257	0.279	0.118
35%	Cortical thickness	-0.109	0.024	0.594	0.088	0.444	-0.229	-0.303	0.435
	Endosteal distance	0.347	-0.065	-0.376	-0.05	-0.215	0.197	0.432	-0.009
	Periosteal distance	0.244	-0.153	0.288	0.003	0.132	-0.1	0.359	0.279
50%	Cortical thickness	-0.399	-0.232	0.02	0.323	0.531	-0.236	0.187	-0.195
	Endosteal distance	-0.362	-0.34	0.16	0.009	0.079	0.364	0.476	0.141
	Periosteal distance	0.098	-0.451	0.224	0.137	0.585	0.292	0.618	-0.034
65%	Cortical thickness	0.486	-0.007	0.754	0.376	0.385	0.156	0.235	0.433
	Endosteal distance	-0.09	-0.442	-0.218	0.196	-0.081	-0.152	-0.319	0.046
	Periosteal distance	0.262	-0.305	0.191	0.49	0.332	-0.042	-0.284	0.376

Table S2.2. Spearman's ρ correlations between female (ages 50-59) cBMD and distance measures within cortical cross-sections of the tibia. Directional sector abbreviations are: A, anterior; AL, anterolateral; L, lateral; PL, posterolateral; P, posterior; PM, posteromedial; M, medial; AM, anteromedial. Green denotes positive correlations; red denotes negative correlations.

Slice	Distance measure	Directional sector within cortical slice							
		A	AL	L	PL	P	PM	M	AM
20%	Cortical thickness	0.427	0.379	-0.043	0.244	0.071	0.216	0.252	0.129
	Endosteal distance	-0.425	-0.283	0.071	-0.179	-0.466	-0.419	-0.299	-0.035
	Periosteal distance	-0.119	-0.174	0.099	-0.073	-0.273	-0.145	-0.084	0.035
35%	Cortical thickness	0.18	0.227	0.458	0.085	0.267	0.081	0.58	0.369
	Endosteal distance	-0.063	-0.159	0.042	0.145	-0.669	0.077	-0.541	-0.112
	Periosteal distance	0.08	0.084	0.327	0.053	-0.327	-0.015	-0.04	0.024
50%	Cortical thickness	-0.427	0.306	0.499	0.472	0.16	0.127	0.394	0.664
	Endosteal distance	-0.372	-0.305	-0.156	-0.073	-0.33	-0.156	-0.2	-0.286
	Periosteal distance	0.013	-0.052	0.107	0.29	-0.027	0.202	-0.029	0.149
65%	Cortical thickness	0.396	0.384	0.349	0.309	0.233	0.001	0.44	0.484
	Endosteal distance	-0.232	-0.301	-0.356	-0.186	-0.523	-0.171	-0.161	-0.271
	Periosteal distance	-0.078	-0.111	-0.243	-0.06	-0.432	-0.332	-0.042	-0.094

Table S2.3. Spearman's ρ correlations between female (ages 60-69) cBMD and distance measures within cortical cross-sections of the tibia. Directional sector abbreviations are: A, anterior; AL, anterolateral; L, lateral; PL, posterolateral; P, posterior; PM, posteromedial; M, medial; AM, anteromedial. Green denotes positive correlations; red denotes negative correlations.

Slice	Distance measure	Directional sector within cortical slice							
		A	AL	L	PL	P	PM	M	AM
20%	Cortical thickness	0.539	0.566	0.664	0.657	0.275	0.828	0.292	0.039
	Endosteal distance	-0.118	0.01	-0.605	-0.642	-0.142	-0.37	-0.037	-0.238
	Periosteal distance	0.118	0.265	-0.382	-0.137	0.098	0.142	0.304	-0.297
35%	Cortical thickness	0.507	0.674	0.314	0.757	0.417	0.539	0.49	0.647
	Endosteal distance	-0.485	-0.385	0.037	-0.446	-0.409	-0.223	-0.385	-0.635
	Periosteal distance	-0.049	0.404	0.35	0.061	-0.27	0.35	0.076	-0.203
50%	Cortical thickness	-0.596	0.629	0.721	0.046	0.254	0.654	0.564	0.482
	Endosteal distance	-0.461	-0.571	-0.329	0.075	-0.396	-0.571	-0.329	-0.404
	Periosteal distance	0.236	0.211	0.086	0.307	-0.371	0.225	0.175	-0.146
65%	Cortical thickness	0.637	0.352	0.566	0.291	0.511	0.396	0.456	0.582
	Endosteal distance	-0.648	-0.401	-0.033	-0.698	-0.39	-0.615	-0.599	-0.341
	Periosteal distance	0.027	0.016	0.511	-0.527	0.28	-0.269	-0.538	-0.137

Table S2.4. Spearman's ρ correlations between female (ages 70-79) cBMD and distance measures within cortical cross-sections of the tibia. Directional sector abbreviations are: A, anterior; AL, anterolateral; L, lateral; PL, posterolateral; P, posterior; PM, posteromedial; M, medial; AM, anteromedial. Green denotes positive correlations; red denotes negative correlations.

Slice	Distance measure	Directional sector within cortical slice							
		A	AL	L	PL	P	PM	M	AM
20%	Cortical thickness	0.071	0.024	0.524	-0.167	0.167	0.286	-0.071	0.095
	Endosteal distance	0.286	0.405	-0.429	-0.071	-0.667	-0.119	0.071	0
	Periosteal distance	0.5	0.333	-0.048	-0.238	-0.452	0.071	-0.024	0.167
35%	Cortical thickness	0	0.071	0.119	0.167	-0.048	0.214	0.476	0.738
	Endosteal distance	-0.238	-0.333	-0.048	0	0.238	0.214	-0.071	-0.095
	Periosteal distance	-0.333	-0.048	-0.333	-0.286	0.167	0.095	0.048	0.143
50%	Cortical thickness	-0.571	0.381	0.381	0.238	0.524	0.452	0.976	0.762
	Endosteal distance	-0.357	-0.143	-0.429	-0.024	-0.595	-0.5	-0.738	-0.119
	Periosteal distance	0.286	0.5	-0.143	0.19	0.071	-0.119	-0.024	-0.071
65%	Cortical thickness	0.771	0.486	0.829	0.2	0.371	0.6	0.771	0.886
	Endosteal distance	-0.886	-0.257	0.086	0.029	-0.371	-0.6	-0.086	-0.257
	Periosteal distance	-0.143	-0.086	0.371	0.029	0.143	-0.429	0.086	-0.2

Table S2.5. Spearman's ρ correlations between male (ages 40-49) cBMD and distance measures within cortical cross-sections of the tibia. Directional sector abbreviations are: A, anterior; AL, anterolateral; L, lateral; PL, posterolateral; P, posterior; PM, posteromedial; M, medial; AM, anteromedial. Green denotes positive correlations; red denotes negative correlations.

Slice	Distance measure	Directional sector within cortical slice							
		A	AL	L	PL	P	PM	M	AM
20%	Cortical thickness	0.214	-0.119	-0.31	0.095	-0.524	0.357	-0.19	-0.048
	Endosteal distance	-0.381	-0.452	-0.143	-0.095	-0.024	0.143	0.095	-0.143
	Periosteal distance	-0.31	-0.929	-0.333	-0.214	-0.071	0.405	-0.262	-0.024
35%	Cortical thickness	-0.714	0.333	-0.262	-0.381	0.19	-0.5	-0.31	-0.238
	Endosteal distance	-0.071	-0.381	-0.167	0.095	0.071	0.381	-0.167	0.31
	Periosteal distance	-0.524	-0.048	-0.357	-0.619	0.214	-0.429	-0.024	0.143
50%	Cortical thickness	0.095	0.238	0.048	0.238	0.762	-0.571	-0.214	-0.357
	Endosteal distance	-0.048	-0.452	-0.548	0.095	-0.643	0.595	0.048	-0.071
	Periosteal distance	-0.048	-0.381	-0.238	0.143	-0.214	-0.5	-0.286	-0.405
65%	Cortical thickness	-0.405	0.214	0.714	-0.119	0.476	0.286	0.333	0.381
	Endosteal distance	-0.238	-0.262	-0.19	0	-0.119	-0.69	-0.071	0.048
	Periosteal distance	-0.643	-0.19	-0.095	-0.286	0.357	-0.262	0.262	0.238

Table S2.6. Spearman's ρ correlations between male (ages 50-59) cBMD and distance measures within cortical cross-sections of the tibia. Directional sector abbreviations are: A, anterior; AL, anterolateral; L, lateral; PL, posterolateral; P, posterior; PM, posteromedial; M, medial; AM, anteromedial. Green denotes positive correlations; red denotes negative correlations.

Slice	Distance measure	Directional sector within cortical slice							
		A	AL	L	PL	P	PM	M	AM
20%	Cortical thickness	0.333	0.31	0.405	0.214	0.024	0.69	0.238	0.19
	Endosteal distance	-0.524	-0.024	-0.071	-0.619	-0.071	-0.381	-0.5	-0.81
	Periosteal distance	-0.405	-0.048	-0.095	-0.571	-0.31	0.119	-0.5	-0.667
35%	Cortical thickness	0.183	0.167	0.783	0.283	0.533	0.083	0.517	0.433
	Endosteal distance	-0.133	0.217	-0.467	0.167	-0.217	0.133	-0.767	-0.217
	Periosteal distance	0.1	-0.067	0.317	0.283	0.317	-0.067	-0.25	0.033
50%	Cortical thickness	-0.017	0.15	0.433	-0.083	0.533	-0.033	0.8	0.717
	Endosteal distance	-0.667	-0.333	0.35	0.45	-0.667	-0.2	-0.05	-0.083
	Periosteal distance	-0.133	-0.15	0.583	0.15	0.367	-0.167	0.6	0.383
65%	Cortical thickness	-0.19	0.286	0.333	0.31	0.238	0.524	0.238	0.381
	Endosteal distance	0.143	-0.143	0.548	0.333	0.31	-0.071	0.19	0.548
	Periosteal distance	0.095	0.405	0.548	0.238	0.095	0.595	0.167	0.524

Table S2.7. Spearman's ρ correlations between male (ages 60-69) cBMD and distance measures within cortical cross-sections of the tibia. Directional sector abbreviations are: A, anterior; AL, anterolateral; L, lateral; PL, posterolateral; P, posterior; PM, posteromedial; M, medial; AM, anteromedial. Green denotes positive correlations; red denotes negative correlations.

Slice	Distance measure	Directional sector within cortical slice							
		A	AL	L	PL	P	PM	M	AM
20%	Cortical thickness	0.445	0.491	0.091	0.773	-0.082	0.691	0.1	0.364
	Endosteal distance	-0.591	-0.518	-0.409	-0.682	-0.082	-0.764	-0.209	-0.436
	Periosteal distance	-0.336	-0.527	-0.409	-0.145	-0.318	-0.5	-0.255	-0.173
35%	Cortical thickness	0.497	-0.091	-0.07	0.469	0.308	0.378	0.042	-0.252
	Endosteal distance	-0.566	-0.252	-0.853	-0.713	-0.587	-0.126	-0.168	-0.231
	Periosteal distance	-0.14	-0.441	-0.909	-0.364	-0.105	0.217	0.098	-0.133
50%	Cortical thickness	-0.626	-0.209	0.225	0.516	0.33	-0.33	0.104	-0.022
	Endosteal distance	-0.632	0.044	0.264	-0.093	-0.066	-0.236	-0.066	-0.302
	Periosteal distance	0.027	-0.165	0.291	0.181	0.72	-0.604	-0.005	-0.154
65%	Cortical thickness	0.678	0.112	0.126	0.021	0.846	-0.161	0.266	0.797
	Endosteal distance	-0.175	-0.441	-0.182	0.538	-0.42	0.021	0.056	-0.364
	Periosteal distance	0.448	-0.503	-0.056	0.42	0.573	-0.573	0.021	0.147

Table S2.8. Spearman's ρ correlations between male (ages 70-79) cBMD and distance measures within cortical cross-sections of the tibia. Directional sector abbreviations are: A, anterior; AL, anterolateral; L, lateral; PL, posterolateral; P, posterior; PM, posteromedial; M, medial; AM, anteromedial. Green denotes positive correlations; red denotes negative correlations.

Slice	Distance measure	Directional sector within cortical slice							
		A	AL	L	PL	P	PM	M	AM
20%	Cortical thickness	0.3	0.345	0.333	0.773	0.2	0.136	0.345	0.036
	Endosteal distance	-0.7	-0.382	-0.291	-0.473	-0.236	-0.773	0.173	-0.118
	Periosteal distance	-0.382	-0.009	-0.209	0.536	0.055	-0.727	0.364	0.064
35%	Cortical thickness	-0.077	0.549	0.637	0.209	0.555	-0.473	0.663	0.729
	Endosteal distance	-0.28	-0.604	-0.467	0.038	0.049	0.115	0.005	-0.527
	Periosteal distance	-0.478	0.143	0.088	0.022	0.341	-0.495	0.379	0.258
50%	Cortical thickness	-0.588	0.824	0.692	0.473	0.253	-0.374	0.115	0.226
	Endosteal distance	-0.39	-0.615	-0.363	-0.445	-0.396	0.027	0.571	-0.302
	Periosteal distance	0.22	0.313	0.038	-0.121	0.022	-0.346	0.412	-0.198
65%	Cortical thickness	-0.064	0.193	0.282	-0.25	0.007	-0.329	0.427	0.3
	Endosteal distance	-0.146	-0.589	-0.336	0.243	-0.014	0.311	0.025	0.021
	Periosteal distance	-0.182	-0.386	-0.229	-0.154	0.225	0.018	0.329	0.129

Table S2.9. Spearman's ρ correlations between female (ages 40-49) cBMD and distance measures within cortical cross-sections of the radius. Directional sector abbreviations are: A, anterior; AL, anterolateral; L, lateral; PL, posterolateral; P, posterior; PM, posteromedial; M, medial; AM, anteromedial. Green denotes positive correlations; red denotes negative correlations.

Slice	Distance measure	Directional sector within cortical slice							
		A	AL	L	PL	P	PM	M	AM
20%	Cortical thickness	0.005	0.703	0.775	0.179	0.792	0.62	0.73	0.505
	Endosteal distance	0.037	-0.625	-0.233	-0.338	-0.672	-0.255	-0.765	-0.38
	Periosteal distance	0.054	-0.216	0.527	-0.417	-0.223	0.265	-0.194	0.029
35%	Cortical thickness	0.464	0.538	-0.011	0.007	-0.037	0.407	0.648	-0.196
	Endosteal distance	-0.631	-0.345	0.042	0.007	-0.112	-0.442	-0.354	-0.033
	Periosteal distance	0.037	0.24	0.182	0.068	-0.121	0.116	0.538	-0.108
50%	Cortical thickness	0.462	0.424	0.211	0.195	0.406	0.368	0.093	0.371
	Endosteal distance	-0.46	-0.472	-0.126	-0.038	-0.059	-0.104	0.09	-0.021
	Periosteal distance	0.002	0.03	-0.06	0.182	0.302	0.341	-0.364	0.268
65%	Cortical thickness	0.424	0.547	0.182	0.468	0.727	0.077	0.16	0.332
	Endosteal distance	-0.376	-0.618	-0.196	0.314	-0.31	-0.081	-0.402	0.174
	Periosteal distance	0.024	-0.081	0.121	0.552	0.143	0.086	-0.345	0.596

Table S2.10. Spearman's ρ correlations between female (ages 50-59) cBMD and distance measures within cortical cross-sections of the radius. Directional sector abbreviations are: A, anterior; AL, anterolateral; L, lateral; PL, posterolateral; P, posterior; PM, posteromedial; M, medial; AM, anteromedial. Green denotes positive correlations; red denotes negative correlations.

Slice	Distance measure	Directional sector within cortical slice							
		A	AL	L	PL	P	PM	M	AM
20%	Cortical thickness	0.086	-0.031	0.363	0.419	0.346	0.309	0.295	-0.128
	Endosteal distance	-0.081	-0.316	-0.262	-0.278	-0.328	0.327	-0.373	-0.16
	Periosteal distance	0.035	-0.424	-0.099	0.01	0.144	0.561	-0.114	-0.193
35%	Cortical thickness	0.328	0.367	0.543	0.38	0.256	0.317	-0.101	-0.02
	Endosteal distance	-0.062	-0.313	-0.32	-0.256	-0.22	-0.13	-0.136	-0.056
	Periosteal distance	0.239	-0.123	0.078	0.023	-0.008	0.183	-0.185	-0.078
50%	Cortical thickness	0.316	0.265	0.706	-0.132	0.39	0.473	-0.149	0.557
	Endosteal distance	-0.29	-0.285	-0.506	-0.131	-0.112	-0.319	-0.467	-0.397
	Periosteal distance	0.008	-0.003	-0.118	-0.305	0.305	0.225	-0.239	-0.048
65%	Cortical thickness	0.466	0.392	0.084	0.12	0.466	0.194	0.287	0.343
	Endosteal distance	-0.338	-0.406	-0.185	-0.251	-0.501	-0.099	-0.29	0.132
	Periosteal distance	-0.107	0.077	0.015	-0.123	-0.048	0.059	0.144	0.71

Table S2.11. Spearman's ρ correlations between female (ages 60-69) cBMD and distance measures within cortical cross-sections of the radius. Directional sector abbreviations are: A, anterior; AL, anterolateral; L, lateral; PL, posterolateral; P, posterior; PM, posteromedial; M, medial; AM, anteromedial. Green denotes positive correlations; red denotes negative correlations.

Slice	Distance measure	Directional sector within cortical slice							
		A	AL	L	PL	P	PM	M	AM
20%	Cortical thickness	0.482	0.521	0.554	0.836	0.6	0.738	0.382	0.204
	Endosteal distance	-0.479	-0.425	-0.496	-0.846	-0.743	-0.563	-0.35	-0.45
	Periosteal distance	-0.204	-0.379	-0.332	-0.729	-0.325	0.113	-0.2	-0.332
35%	Cortical thickness	0.55	0.674	0.337	0.643	0.742	0.567	0.709	0.362
	Endosteal distance	-0.564	-0.602	-0.439	-0.536	-0.616	-0.482	-0.501	-0.34
	Periosteal distance	-0.104	0.038	-0.09	0.143	-0.03	-0.065	0.294	0.222
50%	Cortical thickness	0.804	0.627	0.608	-0.078	0.377	0.65	-0.113	0.801
	Endosteal distance	-0.441	-0.485	-0.446	0.123	-0.123	-0.463	-0.654	-0.547
	Periosteal distance	0.385	-0.051	-0.076	0.039	0.135	0	-0.235	0.275
65%	Cortical thickness	0.491	0.774	0.653	0.726	0.762	0.447	0.256	0.735
	Endosteal distance	-0.168	-0.453	-0.285	-0.479	-0.5	0.026	-0.185	-0.191
	Periosteal distance	0.274	0.212	0.129	-0.021	-0.097	0.409	0.15	0.441

Table S2.12. Spearman's ρ correlations between female (ages 70-79) cBMD and distance measures within cortical cross-sections of the radius. Directional sector abbreviations are: A, anterior; AL, anterolateral; L, lateral; PL, posterolateral; P, posterior; PM, posteromedial; M, medial; AM, anteromedial. Green denotes positive correlations; red denotes negative correlations.

Slice	Distance measure	Directional sector within cortical slice							
		A	AL	L	PL	P	PM	M	AM
20%	Cortical thickness	0.571	0.75	0.143	0.5	0.429	0.214	0.429	-0.071
	Endosteal distance	-0.179	-0.393	-0.429	-0.214	-0.464	0.107	-0.357	-0.107
	Periosteal distance	0.5	0.429	-0.214	-0.143	-0.071	0.714	-0.357	-0.143
35%	Cortical thickness	0.273	0.536	0.164	0.764	0.227	0.173	0.627	0.727
	Endosteal distance	-0.136	-0.764	-0.345	-0.764	-0.445	-0.336	-0.636	-0.418
	Periosteal distance	0.164	-0.418	-0.236	-0.345	-0.318	-0.245	0.118	0.236
50%	Cortical thickness	0.545	0.491	0.682	0.482	0.082	0.482	-0.173	0.291
	Endosteal distance	-0.682	-0.5	-0.682	-0.645	-0.773	-0.573	-0.227	-0.427
	Periosteal distance	-0.473	0.155	-0.418	-0.264	-0.864	-0.4	-0.109	-0.373
65%	Cortical thickness	0.881	0.452	0.714	0.429	0.548	0.429	0.286	0.214
	Endosteal distance	-0.738	-0.19	-0.357	-0.643	-0.19	0.095	-0.571	0.19
	Periosteal distance	-0.024	-0.214	-0.143	0.143	0.167	0.381	-0.19	0.571

Table S2.13. Spearman's ρ correlations between male (ages 40-49) cBMD and distance measures within cortical cross-sections of the radius. Directional sector abbreviations are: A, anterior; AL, anterolateral; L, lateral; PL, posterolateral; P, posterior; PM, posteromedial; M, medial; AM, anteromedial. Green denotes positive correlations; red denotes negative correlations.

Slice	Distance measure	Directional sector within cortical slice							
		A	AL	L	PL	P	PM	M	AM
20%	Cortical thickness	0.617	0.233	0.367	-0.251	0.435	0.117	0.433	0.217
	Endosteal distance	-0.1	-0.233	-0.633	0.067	-0.833	-0.667	-0.65	-0.517
	Periosteal distance	0.367	-0.317	-0.467	0	-0.283	-0.583	-0.267	-0.067
35%	Cortical thickness	0.775	-0.252	0.179	0.214	-0.143	-0.054	0.5	0.357
	Endosteal distance	-0.321	-0.357	-0.357	-0.786	-0.107	-0.143	-0.857	0.107
	Periosteal distance	0.607	-0.607	0.143	-0.393	0.036	-0.179	-0.429	0.321
50%	Cortical thickness	0.238	-0.071	0.619	-0.143	0.119	0.262	0.31	0.31
	Endosteal distance	-0.119	-0.048	-0.905	-0.286	-0.429	-0.571	-0.429	-0.214
	Periosteal distance	0.286	0.238	-0.381	-0.19	-0.024	-0.333	-0.286	0
65%	Cortical thickness	0.133	-0.45	0.033	0.833	-0.268	0.317	0.017	0.067
	Endosteal distance	0.083	-0.267	0.183	-0.333	0.65	0.067	-0.25	0.333
	Periosteal distance	0.117	-0.417	-0.167	0.317	0.25	0.317	-0.333	0.117

Table S2.14. Spearman's ρ correlations between male (ages 50-59) cBMD and distance measures within cortical cross-sections of the radius. Directional sector abbreviations are: A, anterior; AL, anterolateral; L, lateral; PL, posterolateral; P, posterior; PM, posteromedial; M, medial; AM, anteromedial. Green denotes positive correlations; red denotes negative correlations.

Slice	Distance measure	Directional sector within cortical slice							
		A	AL	L	PL	P	PM	M	AM
20%	Cortical thickness	0.183	0.4	0.683	0.1	0.733	0.867	0.25	0.519
	Endosteal distance	-0.017	-0.417	-0.933	0.133	-0.483	-0.483	-0.083	-0.35
	Periosteal distance	0.533	-0.3	-0.583	-0.1	0.283	0.033	0.2	-0.15
35%	Cortical thickness	-0.118	0.036	0.791	0.3	0.136	0.282	-0.555	0.1
	Endosteal distance	0.218	-0.127	-0.191	0.036	-0.618	0.136	-0.6	-0.118
	Periosteal distance	0.318	-0.1	0.627	0.245	-0.264	0.464	-0.764	-0.064
50%	Cortical thickness	0.358	0.479	0.77	0.188	0.139	0.636	0.2	0.103
	Endosteal distance	0.333	-0.806	0.042	-0.673	0.224	-0.576	-0.37	-0.224
	Periosteal distance	0.406	-0.467	0.636	-0.212	0.394	0.091	-0.697	-0.442
65%	Cortical thickness	0.336	-0.009	0.391	-0.345	0.864	0.132	-0.282	0.718
	Endosteal distance	0.127	-0.409	0.045	-0.445	-0.3	-0.227	0.327	-0.209
	Periosteal distance	0.527	-0.536	0.4	-0.455	0.255	-0.264	0.436	0.564

Table S2.15. Spearman's ρ correlations between male (ages 60-69) cBMD and distance measures within cortical cross-sections of the radius. Directional sector abbreviations are: A, anterior; AL, anterolateral; L, lateral; PL, posterolateral; P, posterior; PM, posteromedial; M, medial; AM, anteromedial. Green denotes positive correlations; red denotes negative correlations.

Slice	Distance measure	Directional sector within cortical slice							
		A	AL	L	PL	P	PM	M	AM
20%	Cortical thickness	0.345	0.691	0.727	0.564	0.645	0.318	0.509	0.582
	Endosteal distance	-0.218	-0.5	-0.455	-0.182	-0.427	-0.245	-0.427	0.045
	Periosteal distance	-0.064	-0.209	-0.173	0.109	0.218	-0.1	-0.118	0.382
35%	Cortical thickness	0.655	0.091	0.709	-0.4	0.136	0.773	0.2	0.718
	Endosteal distance	-0.382	-0.373	-0.236	-0.236	-0.491	-0.264	-0.045	-0.5
	Periosteal distance	0.373	-0.518	0.227	-0.445	-0.209	0.591	0.064	-0.045
50%	Cortical thickness	0.483	0.6	0.567	0.2	0.167	-0.133	0.25	0.067
	Endosteal distance	-0.617	-0.683	-0.233	-0.567	-0.167	0.25	-0.067	0.2
	Periosteal distance	-0.283	-0.283	0.167	-0.3	-0.183	0.017	-0.35	0.1
65%	Cortical thickness	0.713	0.608	0.573	0.315	0.566	0.699	0.049	0.049
	Endosteal distance	-0.503	-0.392	0	-0.294	-0.315	-0.021	0.189	-0.497
	Periosteal distance	-0.049	-0.14	0.273	-0.063	0.028	0.14	-0.14	-0.399

Table S2.16. Spearman's ρ correlations between male (ages 70-79) cBMD and distance measures within cortical cross-sections of the radius. Directional sector abbreviations are: A, anterior; AL, anterolateral; L, lateral; PL, posterolateral; P, posterior; PM, posteromedial; M, medial; AM, anteromedial. Green denotes positive correlations; red denotes negative correlations.

Slice	Distance measure	Directional sector within cortical slice							
		A	AL	L	PL	P	PM	M	AM
20%	Cortical thickness	0.028	0.343	0.175	0.524	0.413	0.629	-0.168	0.42
	Endosteal distance	-0.028	-0.014	-0.608	-0.245	-0.154	-0.385	0.21	-0.259
	Periosteal distance	-0.091	0.189	-0.587	0.14	0.378	0.266	0.042	-0.266
35%	Cortical thickness	0.308	0.082	0.363	0.352	0.473	0.258	0.72	0.209
	Endosteal distance	-0.286	-0.396	-0.159	-0.049	-0.082	-0.016	-0.379	-0.088
	Periosteal distance	0.159	-0.346	0.275	0.242	0.544	0.39	0.126	0.115
50%	Cortical thickness	0.684	0.125	0.512	-0.033	0.209	0.385	0.033	0.323
	Endosteal distance	-0.574	0.037	-0.459	0.429	-0.103	-0.398	-0.042	-0.38
	Periosteal distance	0.108	0.02	-0.108	0.481	-0.046	0.037	-0.218	0.073
65%	Cortical thickness	0.063	0.706	0.476	0.252	0.35	0.245	0.084	0.673
	Endosteal distance	-0.462	-0.399	-0.175	-0.399	0.301	-0.497	0.154	-0.51
	Periosteal distance	-0.378	0.28	0.042	-0.161	0.476	-0.336	0.552	-0.098

Table S2.17. Spearman's ρ correlations between female (ages 40-49) cBMD and distance measures within cortical cross-sections of the ulna. Directional sector abbreviations are: A, anterior; AL, anterolateral; L, lateral; PL, posterolateral; P, posterior; PM, posteromedial; M, medial; AM, anteromedial. Green denotes positive correlations; red denotes negative correlations.

Slice	Distance measure	Directional sector within cortical slice							
		A	AL	L	PL	P	PM	M	AM
20%	Cortical thickness	0.547	0.779	0.218	0.262	0.371	0.271	0.765	0.347
	Endosteal distance	-0.144	-0.438	-0.221	-0.115	0.032	-0.256	-0.368	-0.559
	Periosteal distance	0.318	0.3	0.012	0.082	0.241	0.035	0.485	-0.485
35%	Cortical thickness	0.568	0.443	0.054	0.307	0.314	0.596	0.354	0.357
	Endosteal distance	-0.539	-0.182	-0.418	0.125	0.018	-0.332	-0.332	-0.254
	Periosteal distance	0.196	0.257	-0.5	0.332	0.361	0.289	0.086	0.046
50%	Cortical thickness	0.349	0.481	-0.184	0.495	0.381	-0.109	0.693	0.025
	Endosteal distance	0.142	0.235	-0.246	0.132	-0.114	-0.196	-0.447	-0.009
	Periosteal distance	0.474	0.661	-0.049	0.437	0.17	-0.318	0.374	-0.047
65%	Cortical thickness	0.481	0.552	-0.046	0.473	0.363	0.284	0.27	0.53
	Endosteal distance	-0.059	0.165	-0.464	-0.323	0.297	-0.534	-0.42	0.024
	Periosteal distance	0.305	0.31	-0.538	0.244	0.385	-0.002	-0.081	0.543

Table S2.18. Spearman's ρ correlations between female (ages 50-59) cBMD and distance measures within cortical cross-sections of the ulna. Directional sector abbreviations are: A, anterior; AL, anterolateral; L, lateral; PL, posterolateral; P, posterior; PM, posteromedial; M, medial; AM, anteromedial. Green denotes positive correlations; red denotes negative correlations.

Slice	Distance measure	Directional sector within cortical slice							
		A	AL	L	PL	P	PM	M	AM
20%	Cortical thickness	0.532	0.388	0.289	0.271	0.258	0.541	0.268	0.402
	Endosteal distance	-0.633	-0.03	-0.462	-0.338	-0.069	-0.211	-0.177	-0.468
	Periosteal distance	-0.457	0.125	-0.066	-0.012	0.024	0.247	-0.018	-0.268
35%	Cortical thickness	0.465	0.379	0.531	0.298	0.264	0.588	0.404	0.286
	Endosteal distance	-0.347	-0.576	-0.539	-0.27	-0.339	-0.339	-0.289	-0.404
	Periosteal distance	0.134	-0.115	-0.078	-0.153	-0.231	0.288	-0.173	-0.233
50%	Cortical thickness	0.329	0.486	0.239	0.439	0.319	0.125	0.421	0.111
	Endosteal distance	-0.19	0.402	-0.245	-0.182	-0.081	-0.332	-0.205	-0.196
	Periosteal distance	0.151	0.545	-0.338	0.19	0.077	-0.035	0.062	-0.127
65%	Cortical thickness	0.317	0.613	-0.037	0.492	0.063	0.069	0.086	-0.08
	Endosteal distance	-0.03	0.141	-0.009	0.055	-0.016	-0.158	-0.016	-0.078
	Periosteal distance	0.132	0.432	-0.324	0.206	0.066	-0.111	0.219	-0.163

Table S2.19. Spearman's ρ correlations between female (ages 60-69) cBMD and distance measures within cortical cross-sections of the ulna. Directional sector abbreviations are: A, anterior; AL, anterolateral; L, lateral; PL, posterolateral; P, posterior; PM, posteromedial; M, medial; AM, anteromedial. Green denotes positive correlations; red denotes negative correlations.

Slice	Distance measure	Directional sector within cortical slice							
		A	AL	L	PL	P	PM	M	AM
20%	Cortical thickness	0.503	0.648	0.442	-0.139	0.588	0.067	0.673	0.37
	Endosteal distance	-0.576	-0.127	-0.224	-0.503	-0.297	0.2	-0.648	-0.164
	Periosteal distance	-0.261	0.491	0.37	-0.37	-0.103	0.2	-0.115	0.152
35%	Cortical thickness	0.144	0.597	0.144	0.491	0.588	0.494	0.747	0.585
	Endosteal distance	-0.229	-0.097	-0.468	-0.012	-0.347	-0.424	-0.374	-0.244
	Periosteal distance	-0.203	0.332	-0.326	0.471	0.041	0.174	0.321	-0.029
50%	Cortical thickness	0.409	0.535	-0.338	0.403	0.268	0.582	0.632	0.679
	Endosteal distance	-0.226	-0.115	-0.365	-0.268	-0.115	-0.559	-0.506	-0.312
	Periosteal distance	-0.05	0.079	-0.147	-0.006	0.141	0.038	0.244	0.065
65%	Cortical thickness	0.326	0.485	-0.056	0.397	0.571	0.047	0.243	0.667
	Endosteal distance	-0.262	-0.061	-0.176	-0.152	-0.453	0.176	-0.029	-0.368
	Periosteal distance	-0.189	0.15	-0.422	0.091	-0.076	0.164	0.385	0.321

Table S2.20. Spearman's ρ correlations between female (ages 70-79) cBMD and distance measures within cortical cross-sections of the ulna. Directional sector abbreviations are: A, anterior; AL, anterolateral; L, lateral; PL, posterolateral; P, posterior; PM, posteromedial; M, medial; AM, anteromedial. Green denotes positive correlations; red denotes negative correlations.

Slice	Distance measure	Directional sector within cortical slice							
		A	AL	L	PL	P	PM	M	AM
20%	Cortical thickness	-0.8	-0.4	0.6	-0.2	0.8	0.6	0.4	0.8
	Endosteal distance	0.6	-0.4	-0.8	0.4	-0.4	0.8	0.2	-0.8
	Periosteal distance	-0.2	-0.4	0	0.4	0.2	0.8	0.4	-0.8
35%	Cortical thickness	0.741	0.685	0.315	0.566	0.245	0.51	0.713	0.413
	Endosteal distance	-0.587	-0.594	-0.462	-0.524	-0.28	-0.517	-0.783	-0.196
	Periosteal distance	0.448	0.084	0.245	0.399	-0.105	-0.343	0.035	0.077
50%	Cortical thickness	-0.045	0.636	-0.291	0.609	0.382	0.282	0.945	0.5
	Endosteal distance	-0.1	-0.2	-0.509	-0.709	-0.255	-0.264	-0.727	-0.236
	Periosteal distance	-0.036	0.127	-0.309	0.027	0.045	-0.064	0.373	0.064
65%	Cortical thickness	0.75	-0.05	0.333	0.517	0.383	0.383	0.6	0.8
	Endosteal distance	-0.05	0.167	-0.733	-0.767	-0.55	-0.233	-0.833	0.267
	Periosteal distance	0.35	0.017	-0.417	0	-0.133	0.067	-0.7	0.65

Table S2.21. Spearman's ρ correlations between male (ages 40-49) cBMD and distance measures within cortical cross-sections of the ulna. Directional sector abbreviations are: A, anterior; AL, anterolateral; L, lateral; PL, posterolateral; P, posterior; PM, posteromedial; M, medial; AM, anteromedial. Green denotes positive correlations; red denotes negative correlations.

Slice	Distance measure	Directional sector within cortical slice							
		A	AL	L	PL	P	PM	M	AM
20%	Cortical thickness	0.643	-0.072	-0.071	-0.429	0.179	0.143	0.143	0.643
	Endosteal distance	-0.714	-0.571	-0.036	-0.107	-0.929	0.643	-0.321	-0.429
	Periosteal distance	-0.643	-0.5	-0.464	-0.321	-0.5	0.75	-0.214	-0.286
35%	Cortical thickness	-0.048	0.524	0.333	0.024	-0.381	0.048	0.024	0.476
	Endosteal distance	-0.238	-0.571	-0.381	-0.405	0.452	-0.286	0.548	-0.69
	Periosteal distance	-0.381	-0.119	-0.333	-0.143	0.19	-0.214	0.429	-0.524
50%	Cortical thickness	-0.119	0.238	-0.286	0.168	0.381	-0.048	-0.024	-0.667
	Endosteal distance	-0.357	0.333	-0.167	-0.108	0.167	0.31	-0.333	0.81
	Periosteal distance	-0.571	0.143	0.143	0.443	0.548	0.357	-0.429	0.048
65%	Cortical thickness	0.19	-0.738	-0.119	0.738	0.286	0.429	0.024	0.143
	Endosteal distance	-0.238	-0.429	-0.571	0.19	-0.476	-0.81	0.262	-0.238
	Periosteal distance	0.19	-0.452	-0.381	0.619	-0.143	-0.429	0.262	0.024

Table S2.22. Spearman's ρ correlations between male (ages 50-59) cBMD and distance measures within cortical cross-sections of the ulna. Directional sector abbreviations are: A, anterior; AL, anterolateral; L, lateral; PL, posterolateral; P, posterior; PM, posteromedial; M, medial; AM, anteromedial. Green denotes positive correlations; red denotes negative correlations.

Slice	Distance measure	Directional sector within cortical slice							
		A	AL	L	PL	P	PM	M	AM
20%	Cortical thickness	0.405	0.738	0.429	0.024	0.667	0.85	0.262	0.515
	Endosteal distance	0.119	0.119	-0.667	-0.333	-0.667	-0.643	-0.167	-0.19
	Periosteal distance	0.667	0.167	-0.381	-0.214	-0.429	0.357	-0.214	0.024
35%	Cortical thickness	0.291	0.136	0.109	0.245	0.264	0.136	0.5	0.255
	Endosteal distance	-0.309	-0.218	-0.164	-0.373	-0.473	0.164	-0.436	0.182
	Periosteal distance	0.018	0.036	-0.082	0.045	0.109	0.2	-0.082	0.473
50%	Cortical thickness	0.333	0.091	-0.479	0.127	0.394	0.212	-0.091	-0.03
	Endosteal distance	-0.37	-0.382	-0.539	0.091	0.442	-0.139	-0.382	-0.248
	Periosteal distance	-0.079	-0.139	0.03	0.164	0.648	-0.018	-0.261	-0.212
65%	Cortical thickness	0.264	0.3	0.291	-0.045	0.845	0.591	0.3	0.645
	Endosteal distance	0.173	-0.336	-0.155	-0.027	-0.645	-0.545	-0.455	-0.055
	Periosteal distance	0.427	-0.164	0.273	-0.164	0.6	0.2	-0.255	0.691

Table S2.23. Spearman's ρ correlations between male (ages 60-69) cBMD and distance measures within cortical cross-sections of the ulna. Directional sector abbreviations are: A, anterior; AL, anterolateral; L, lateral; PL, posterolateral; P, posterior; PM, posteromedial; M, medial; AM, anteromedial. Green denotes positive correlations; red denotes negative correlations.

Slice	Distance measure	Directional sector within cortical slice							
		A	AL	L	PL	P	PM	M	AM
20%	Cortical thickness	0.618	0.218	0.173	0.464	0.873	0.182	0.355	0.691
	Endosteal distance	-0.655	-0.073	-0.409	-0.518	-0.327	-0.473	-0.555	-0.3
	Periosteal distance	-0.045	0.136	-0.273	-0.173	0.564	-0.491	0.055	0.227
35%	Cortical thickness	0.727	0.573	-0.009	-0.009	0.218	0.618	0.4	0.4
	Endosteal distance	-0.673	-0.318	-0.164	-0.5	-0.218	-0.709	-0.582	-0.564
	Periosteal distance	0.245	0.345	-0.045	-0.336	0.236	-0.055	-0.282	-0.345
50%	Cortical thickness	0.167	0.143	-0.071	0.071	-0.048	0.429	0.5	0.167
	Endosteal distance	-0.69	0.048	-0.31	0.357	0.048	-0.167	-0.405	0.214
	Periosteal distance	-0.119	0.429	-0.167	0.095	-0.167	0.333	-0.333	0.238
65%	Cortical thickness	0.764	0.309	0.318	0.464	0.155	0.109	-0.273	0.764
	Endosteal distance	0	0.1	-0.1	-0.255	-0.336	0.327	0.109	-0.082
	Periosteal distance	0.245	0.136	-0.073	0.109	-0.245	0.345	-0.1	0.591

Table S2.24. Spearman's ρ correlations between male (ages 70-79) cBMD and distance measures within cortical cross-sections of the ulna. Directional sector abbreviations are: A, anterior; AL, anterolateral; L, lateral; PL, posterolateral; P, posterior; PM, posteromedial; M, medial; AM, anteromedial. Green denotes positive correlations; red denotes negative correlations.

Slice	Distance measure	Directional sector within cortical slice							
		A	AL	L	PL	P	PM	M	AM
20%	Cortical thickness	0.607	0.75	0.536	0.5	0.571	0.607	0.25	0.071
	Endosteal distance	-0.143	-0.5	-0.143	0.357	-0.607	-0.071	0.214	-0.75
	Periosteal distance	0.286	-0.036	0.321	0.429	0.143	0.107	0.536	-0.714
35%	Cortical thickness	0.418	0.648	0.659	0.286	0.225	0.44	-0.527	0.549
	Endosteal distance	-0.385	-0.22	-0.313	0.22	0.115	0.313	0.225	-0.352
	Periosteal distance	0.066	0.412	0.275	0.566	0.538	0.824	-0.264	-0.044
50%	Cortical thickness	0.022	0.687	0.044	0.049	0.077	0.253	0.159	0.225
	Endosteal distance	0.176	-0.269	-0.016	0.093	-0.396	-0.104	0.016	-0.308
	Periosteal distance	0.258	0.275	-0.121	0.126	-0.115	0.242	0.049	-0.022
65%	Cortical thickness	0.267	0.283	0.083	0.383	0.2	0.133	0.55	0.517
	Endosteal distance	0.25	-0.117	-0.55	0.067	-0.8	-0.367	-0.033	-0.483
	Periosteal distance	0.283	0.233	-0.167	0.1	-0.25	0.067	0.233	-0.05

CHAPTER 5: DISCUSSION AND CONCLUSIONS

Summary of Findings

The preceding chapters of this dissertation explored the spatial variation of cortical geometry and cortical bone mineral density (cBMD) with respect to age in distal human long bones. Using a modified "whole bone" approach, where changes in cortical bone are observed throughout the diaphysis instead of a single location (e.g., 50% of diaphyseal length), this variation was characterized between and within cross-sectional slices of the tibia, radius, and ulna. Few studies have examined the relationship of cBMD and cortical bone geometry, as explored in Chapters 1 and 4, especially across a sample of older adults. Cortical bone mineral density has been well-studied in both humans and model organisms, but these studies have had a clinical focus on fracture risk and osteoporosis. Furthermore, while other studies have examined cortical bone cross-sectional geometric properties in aging individuals (Gooding, 2017), none have examined the distribution of cortical bone within diaphyseal slices and paired this with bone density. Thus, while there are decades of precedent in published studies for the research performed in this dissertation, the research performed here is unique and contributes new insights about aging and cortical bone in human limb long bones.

There are many implications for the results reported in Chapters 2-4. Before considering these, it is useful to review the primary findings of each topic of study. The main findings were:

1) The degree and direction of age-related differences in cortical bone that indicate periosteal expansion and endosteal resorption occurs non-uniformly within cross-sectional slices. Patterns of local variation in this geometric change vary along the length of the bone, particularly in the bones of the forearm (Chapter 2).

2) Patterns of local age-related variation in cortical expansion do not easily conform to expectations based on mechanical loading and load-sharing between paired bones of the leg or forearm, suggesting other factors influence this variation (Chapter 2).
3) Local variation is observed in cBMD differences between age groups both within and between diaphyseal cross-sections. Likewise, cBMD differences corroborate previous findings of average density loss with age and these patterns are more pronounced in females, likely reflecting differences in hormone production and sensitivity between males and postmenopausal females (Chapter 3).
4) Age-related measures of cortical thickness and endosteal distance to the centroid are more strongly correlated with measures of cBMD than periosteal distance to the centroid (Chapter 4).
5) Correlations between distance measurements associated with cortical expansion and cBMD vary based on location within and between cross-sections. The strength of these correlations is driven largely by greater age-related differences in directional distance measurements, specifically cortical thickness and endosteal distance (Chapter 4).

Below I discuss these findings and their context with current and past research on age-related bone loss and bone biomechanics. Additionally, limitations to these studies and future directions are considered.

Local Variation of Age-related Changes to Cortical Geometry

The findings of non-uniform cortical expansion during advanced age reported in this dissertation echo a few other studies examining local variation in this process. Ruff and Hayes

(1982) observed cortical expansion varying across the length of the tibia and femur among Native American individuals from the Pecos Pueblo archaeological site. Among their chief findings was that age-related changes in cortical area of the midshaft femur were nonsignificant in their sample, despite significant increases in medullary area and total cross-sectional area which indicates that cortical area is maintained through cortical expansion (Ruff and Hayes, 1982). Additionally, the degree of cortical expansion was varied throughout the femoral and tibial shafts, with the greatest differences in these measures being at the femoral midshaft and the tibial mid-distal region. While the authors mentioned the relationship is likely complex, these patterns and their differences between males and females were largely attributed to differences in in vivo mechanical loading, such as gendered differences in habitual activity and dimorphic pelvic morphology (Ruff and Hayes, 1982). Similar findings were reported by Wilson and colleagues (2020), who attributed spatial variation of cortical expansion in the 1st metatarsal midshaft to greater agriculture-related activity among a rural medieval English sample compared to an urban post-industrial sample from London. Using a modern Australian sample, Feik and colleagues (2000) credited greater age-related periosteal apposition along the mediolateral axis of the midshaft femur to changes in gait patterns with age. The common explanation among these studies is that local differences in cortical expansion are likely mediated by mechanical stimuli, and that this relationship is relatively straightforward. As explored in Chapters 2 and 4, however, the results in this study complicate this relationship, suggesting that there may be more factors than mechanical loading that lead to localized variation in cross-sectional cortical bone in adults over the age of 40.

Cross-sectional geometry is indeed responsive to mechanical loading, especially at younger ages (Ruff et al., 1994; Lieberman et al., 2003; Goldman et al., 2009; Gosman et al., 2013). For

instance, several studies have characterized a shift from more mediolaterally reinforced femoral midshaft in juveniles, especially individuals younger than 2 years, to an adult morphology that is reinforced anteroposteriorly (Goldman et al., 2009; Gosman et al., 2013; Cowgill et al., 2012). This shift is closely associated with gait patterns shifting from more of a waddling, side-to-side locomotion to one that is directed more anteriorly (Cowgill et al., 2012). Furthermore, modeling response is especially high during puberty (Kannus et al., 1995; Macdonald et al., 2006; Bradney et al., 2009) and begins to attenuate approaching young adulthood (Kontulainen et al., 2009). For example, among female racquet-sport players, the dominant arm of individuals who started training pre- or peri-menarche exhibited increased cortical area and torsional strength compared to those who started after menarche (Kontulainen et al., 2009).

While the capacity for mechanically induced modeling diminishes during adulthood, it is reasonable to expect that mechanical signals still have a role, if muted, in advanced age. Ruff and Hayes (1982) postulated that loading results in conservation of bone mass during adulthood rather than an anabolic response. This appears to be borne out in literature examining senior athletes, who maintain adapted geometries and lose less bone mass than non-athlete controls with age (Korhonen et al., 2012; Warden et al., 2014; Wilks et al., 2009; Harding et al., 2020). However, Wilks and colleagues (2009) observed that the greater cross-sectional benefits afforded by running decline with age, becoming similar to sedentary controls above 80 years of age. This concurs with the broader pattern of bone loss that occurs after the eight decade reported in Gooding (2017), who showed that, while some cross-sectional geometric properties in limb bones may be maintained in some individuals into their 70s, with advanced age all individuals show a decline in cross-sectional geometric properties regardless of activity. Therefore, elevated

activity in old age has a measurable effect in slowing but not outright preventing age-related bone loss.

Given evidence that mechanical loading remains influential to bone geometry into advanced age, it is likely that the variation in age-related changes to cortical geometry observed in Chapter 2 is in part reflective of habitual activity. However, patterns of this variation in the tibia, for example, do not meet expectations based on anteroposterior loading (Cristofolini et al., 2013) or expected maintenance of cortical thickness in the tibia, radius, and ulna due to load-sharing (Chapter 2). Load-sharing between the tibia and fibula is complex (Auerbach et al., 2017), but, as discussed in Chapter 2, a preferential decrease with age in cortical bone on the posterior lateral aspect of the tibia would be expected if the fibula were able to share loading and thus compensate for bone loss; this is not clearly the case, as more bone decreases occur in the anterior and medial margins. One possibility for this lack of a coherent mechanical footprint is that bone cross-sectional morphology, while influenced by mechanical signaling, does not consistently reflect habitual activity (Lieberman et al., 2004; Demes et al., 2001; Wallace et al., 2014). Lieberman and colleagues (2004) illustrated that, because the neutral axis of bending is shifted away from the center of a long bone toward the endosteal envelope under tension, cross-sectional properties of bone are not always consistent with the direction of load distribution. Indeed, *in vivo* strain direction did not correspond with maximum second moments of area in sheep (Wallace et al., 2014) or macaques (Demes et al., 2001). Recently, mouse models have shown that a consideration of the lacunocanilicular network refines expectations of geometric responses to in vivo strain (van Tol et al., 2020), but this approach is likely difficult to apply to humans.

The idea that we should expect to observe more bone in areas that experience greater strain assumes that the mechanoadaptive response serves to minimize strain (Frost, 1987, 1997, 2003). Rather than exclusively lowering strain, functional adaptation instead may, in part, keep strains within a predictable range, which may explain why most long bones exhibit curvature (Bertram and Beiwener, 1988; Lanyon, 1996). A straight long bone, while quite strong under purely axial loading, is not necessarily strong in other loading directions such as the combination of bending, compression, and torsion that long bones experience. On the other hand, bone curvature keeps strains in a predictable range and direction, at the expense of heightening strain magnitude (Lanyon, 1996). One recent study of the murine tibia shows that this may indeed be the case; Javaheri and colleagues (2020) proposed that adaptive geometric changes to long bone diaphyses may deviate from expectations based on strain magnitude to regulate bone curvature. They found that under both acute and chronic loading conditions, geometric responses of bone were linear in the proximal tibia but non-linear in the mid-distal region (Javaheri et al., 2020). Additionally, load-induced geometric changes in the mid-distal region were conserved, while those in the proximal region were reversed after acute loading was complete, suggesting that management of whole bone shape competes with local variation in strain magnitude (Javaheri et al., 2020). In the context of the results reported here, this may explain why greater age-related differences are observed in both sexes at 65% and 50% length of the tibia than at the more distal 35% and 20% slice locations (Chapter 2).

The geometric age-related changes observed in this dissertation are consistent with the evidence that responses in bone shape to mechanical loading are not always straightforward particularly with age, when the adaptive capability of bone to loading is muted. However, as evidenced by the analysis of cross-sectional properties of bone strength in Chapter 4, resistance

to bending and torsion does not change significantly over the age range of this sample. This suggests that variation in age-related differences in endosteal distance may not be as important as the changes in periosteal distance for cross-sectional estimates of bending/torsional strength. This also corroborates the general maintenance of cross-sectional geometric properties into the eighth decade as observed in Gooding (2017). Nonetheless, clear differences in cortical thickness were observed with age (Chapter 2) and the degree of these differences varied locally. This increases local risk for buckling, particularly in areas of bone under compression (Beck et al., 2001). Additionally, bone strength is further informed by age-related changes to bone microstructure.

Local Variation in Cortical BMD and Intracortical Porosity

The analyses reported in this dissertation demonstrate local variation in cBMD distribution during advanced age, in concurrence with other studies (Carballio-Gamio et al., 2013; Kazakia et al., 2013; Weidauer et al., 2016). This suggests that changes in cBMD are not solely related to global factors of aging, but are instead mediated locally by some signal(s). In Chapter 3, I reviewed that cBMD reflects the overall degree of cortical bone mineralization and its porosity. Changes in cBMD are more likely a result of intracortical porosity than age-related changes in mineralization (McCalden et al., 1993; Macdonald et al., 2011). In theory, mineralization decreases with age due to age-related increases in remodeling and associated period of secondary mineralization, which can last two to three years (Bousson et al., Martin et al., 2015; Boivin et al., 2009). Contrary to these remodeling-based expectations, mineralization appears to increase slightly with age and become more homogenous (Currey et al., 1996; Grynpas et al., 1993; Augut and Schorlemmer, 2006), but does not significantly affect bone strength (Martin and

Ishida, 1989; McCalden et al., 1993). Intracortical porosity, however, is well-documented to decline with age and detrimentally impact bone strength (McCalden et al., 1993; Cooper et al., 2007; Macdonald et al., 2011; Andreasen et al., 2018; Ramchand and Seeman, 2018). Therefore, I focus here on spatial variation in age-related changes to cBMD on intracortical porosity.

Intracortical porosity can be measured as the number of pores, their density, or their overall size (Cooper et al., 2007; Andreasen et al., 2018). Multiple studies have shown that age-related increases in intracortical porosity are primarily due to widening of pore diameters and coalescence of existing pores, not increased pore number (Bousson et al., 2001; Cooper et al., 2007; Lerebours et al., 2015; Andreasen et al., 2018). Andreasen and colleague (2018) detailed this process by developing a novel classification scheme to characterize erosion of existing pore surfaces by new resorption cavities. Their results demonstrated that age-related increases in porosity are primarily driven by this erosion, which can extend beyond the cement line of the original osteon and even connect adjacent osteons (Andreasen et al., 2018). Their study also supported the notion that age-related remodeling is characterized by a delayed formation phase, perhaps from a disruption of the reversal phase (Delaisse, 2014; Jensen et al., 2015), since most of these eroding pores were not quiescent (Andreasen et al., 2018). These findings add nuance to my conception of net-resorptive remodeling with age, suggesting that instead of simply decreased formation capacity alone there is an age-related dysregulation between the otherwise coupled resorption and formation phases, possibly leading to a prolonged period of infilling of resorption cavities.

Global remodeling is known to increase during advanced age in both sexes and is particularly marked during and after menopause in females (Seeman, 2013, Martin et al., 2015). Thus, there is a systemic effect that would suggest elevated remodeling throughout the skeleton. Age-related

increases in remodeling are likely associated with declines of estrogen, which normally inhibits remodeling through RANKL regulation (Khosla, 2012; Striecher et al., 2017). Additionally, the effects of cellular senescence and oxidative stress contributing to osteocyte apoptosis (also not unrelated to estrogen decline) may contribute to elevated remodeling during this period (Almeida and O'Brien, 2013; Farr et al., 2014). While the Chapter 3 results indicate overall decrease in cBMD with age, particularly among females, this does not explain the variation observed within and between cross-sections.

One possible explanation for localized variation in remodeling is the repair of accumulated microdamage from loading (Burr et al., 1985; Mori and Burr, 1993). Microdamage occurs when bone undergoes high strain from loading. The two main types of microdamage are linear microcracks (50–100 μm in length) and diffuse damage, which are small groups of sublamellar cracks (Seref-Ferlengez et al., 2015). Linear microcracks are thought to initiate osteonal remodeling by causing osteocyte apoptosis, which in turn signals osteoclasts to initiate the resorption phase of remodeling. Diffuse damage, on the other hand, does not appear to cause osteocyte apopotosis or initiate remodeling (Herman et al., 2010), but heals nonetheless (Seref-Ferlengez et al., 2014; Burr et al., 2014). The mechanism for local healing of diffuse damage is unknown, though Burr (2014) speculated that this could be due to local direct mediation of mineral or organic bone matrix by osteocytes. However, diffuse damage does not appear to have much of an age-related distribution, in contrast with linear microdamage which increases significantly with age (Schaffler et al., 1995; Seref-Ferlengez et al., 2015). Thus, a possible explanation for spatial variation in cortical porosity is that it is guided in part by mechanical loading as a repair mechanism for microdamage.

At odds with this explanation, however, is the observation that porosity is often concentrated in areas of cortical bone that are subjected to the least strain. Lazenby (1986) reported that cortical porosity of the femur is most concentrated along the axis of greatest resistance to bending. Additionally, multiple studies have reported that porosity is greatest along the endocortical circumference and is the least along the periosteal envelope (Thomas et al., 2005; Rantalainen et al., 2011; Nirody et al., 2015), corresponding to where torsional and bending strains will be at their smallest and greatest values radially along cortical bone. The idea that porosity is somewhat restricted to areas where its presence is least mechanically consequential fits well with optimization arguments that posit bone morphology and composition chiefly balances mechanical competency with metabolic demands (Pearson and Lieberman, 2004). My results partly lend support to this expectation, with age-related differences in cBMD consistently greatest along the lateral and posterolateral aspects of the tibia among females, conforming to expectations based on primarily anteroposterior loading. However, similar signals were not observed in the radius and ulna (Chapter 3). Similarly, Thomas and colleagues (2005) observed the least porosity along medial and lateral aspects of the femur, seemingly opposite to the findings of Lazenby (1985). As mentioned before, strain patterns may not be reflected predictably in cross-sectional geometry and caution should be exercised with such interpretations.

The idea that intracortical remodeling is stimulated by both high and low strain is seemingly paradoxical. Martin (2000) proposed a theory to account for this inconsistency based on a common signaling through osteocytes. In this framework, bone lining cells by default will initiate resorption through recruitment of osteoclasts unless they receive an inhibitory signal (Martin, 2000). Osteocytes supply this inhibitory signal through the canalicular network but this

signal can be interrupted through osteocyte apoptosis (Martin, 2000; Cardoso et al., 2009). Since osteocyte apoptosis can occur via microcrack damage or in periods of disuse, remodeling is initiated in both circumstances (Martin, 2000). The signal as Martin (2000) described is similar to the ATP-mediated "find me" signal discussed by Bolomperti and colleagues (2022). Additionally, neighboring osteocytes express anti-apoptotic factors, further localizing resorption activity to the affected area (Hughes and Petit, 2010). It seems plausible, then, that remodeling is responsive to both low and high strain environments through similar signaling pathways.

This logically leads to the question: which of these processes is most likely to be influencing local variation in porosity and cBMD in old age? In the United States, physical activity declines with age following a plateau period during middle age, with a steeper decline in moderate/high physical activity than light activity (Takagi et al., 2015; Varma et al., 2017). During advanced age, males tend to engage in lower amounts of physical activity than females (Varma et al., 2017). Reduced activity levels suggest that perhaps targeted remodeling is less important during old age, however microdamage can accumulate from fairly low strain rates through daily activity (Burr et al., 2009; Seref-Ferlengez et al., 2015). Additionally, age-related accumulation of microdamage indicates that while it is indeed occurring, the repair mechanism through targeted remodeling may be impaired (Schaffler et al., 1995). On the other hand, from a standpoint of mechanical optimization, it would make more sense that age-related variation in porosity is driven by lower strain environments than higher ones, where porosity is allowed in areas that its mechanical effect is least impactful. The most likely but least satisfying explanation, however, is that these factors guiding remodeling with age are probably overlapping, thereby obscuring interpretation of local variation. Longitudinal experimental studies are needed to parse out

differential mechanical factors in remodeling against the backdrop of systemic increases in intracortical porosity.

Interaction Between Macro- and Microstructure with Age

Thus far, I have discussed age-related changes in cortical bone geometry and microstructure separately. Since both attributes contribute to overall bone strength, it is prudent to consider interactions between them. Results from Chapter 4 of this dissertation demonstrated low-to-moderate correlations between cortical thickness and endosteal distance relative to cBMD. Furthermore, the strength of these correlations varied within and between cross-sections and appear to be a result of the magnitude of age-related differences in geometric distance measurements (Chapter 4). In other words, greater differences by directional radii resulted in stronger correlations with cBMD within corresponding directional sectors. This also explains why patterns of correlations among females are stronger than those among males, given greater differences in cBMD decline and geometric measurements associated with cortical expansion.

Stronger correlations between cBMD and cortical thickness/endosteal distance are likely reflecting age-related resorption acting on both endosteal and intracortical surfaces. While bone surfaces are typically categorized by envelopes (Gosman et al., 2011), age-related resorption is probably not envelope-specific, at least along trabecular, endosteal, and intracortical surfaces. Instead, resorption depends largely on the surface available to be resorbed. This explains why most of bone loss in advanced age is cortical and not trabecular; enough trabecular loss has occurred during adulthood that less surface area for resorption is available later in life (Riggs et al., 2004). Thus, intracortical porosity and endosteal resorption are linked. This connection can be observed in the gradation of porosity that increases from pericortical to endocortical regions

of the cross-section (Thomas et al., 2005; Rantalainen et al., 2011) and the eventual "trabecularization" of the endocortical region when pores become larger and coalesce (Andreasen et al., 2020).

Bone geometry appears to interact with the material properties of bone as well. Tommasini and colleagues (2009) demonstrated such an interaction between robusticity and material properties of the tibia. Specifically, slender tibiae were associated with greater measures of brittleness (post-yield strain, total energy to failure) than wider counterparts (Tommasini et al., 2009). The authors suggest that some signal of robusticity interacts with material properties of bone to compensate for smaller geometric cross-sectional properties, however this is a double-edged sword in extreme conditions as brittle bones are more prone to microdamage accumulation (Tommasini et al., 2008; Tommasini et al., 2009). Robusticity also appears to influence intracortical porosity, with larger, more proximal sites of the tibia having more numerous osteons with greater diameter than smaller distal sites (Goldman et al., 2014). Miszkiewicz and Mahoney (2019) similarly found that pore number was positively associated with robusticity in the femur but reported narrower pores in contrast to tibial results reported by Goldman and colleagues (2014). The authors attributed this discrepancy to possible differences in local load-mediated variability, given they only examined the posterior quadrant of the femur and not the whole cross-section as in the tibial study by Goldman and colleagues (2014). In summary, there appears to be a size effect on material properties and microstructure, however it is unclear how this relationship might be affected by age.

While the aforementioned studies suggest a link between macrostructure and microstructure of bone, as proposed by Frost (1987, 2003), my results demonstrate that this relationship is not especially strong during old age. What might explain this? As discussed, the process of

remodeling becomes less coordinated with age, ultimately leading to incomplete osteonal remodeling (Andreasen et al., 2018). Additionally, physical activity and muscle strength decline with age, making mechanical signals (already somewhat complicated, see Skedros et al., 2012; Wallace et al., 2014) less influential in shaping geometry and potentially microstructure than at younger ages (Varma et al., 2017; Bettis et al., 2018). Systemic factors like declines in sex and growth hormones promotes a less mechanosensitive (Hemmatian et al., 2017; McNamara, 2021) and more resorptive (Chung et al., 2014; Chen et al., 2014) bony environment, along with the effects of oxidative stress and cellular senescence. Interactions between bone and soft tissue may introduce further noise in the milieu of aging factors (Bettis et al., 2018; Rinonapoli et al., 2021). In short, there is no concise answer, though by considering these many processes and factors together—changes in activity compounded over decades of skeletal loading, coupled with shifts in tissue composition, hormonal and other factor shifts, and overlaid with the multiple pathways responsible for instigating bone resorption and deposition—we arrive at a potential model.

In their seminal work on phenotypic covariation as it relates to morphological integration, Hallgrímmsson and colleagues (2009) metaphorically described the problem of interpreting the relationships among developmental processes as a palimpsest, a document that has been repeatedly written over so much so that the many erased messages leave vestiges on the final document. I suggest that aging similarly serves as a palimpsest in interpreting changes to cortical bone. Throughout this dissertation, a number possible explanations for the variation observed in cortical bone macro- and microstructure with age have been explored, but none of these have been able to explain the overarching patterns observed in the results reported here. Additionally, it is clear that aging is not a purely systemic suite of signals and that this process is mediated on the local level as well. I suggest that this is due to overlapping and likely interacting age-related

factors that complicate interpretation of the aging experience from cortical bone. The proposed palimpsest of aging poses a problem for clinical approaches to bone loss, as these approaches likely need to be intensive, multipronged, and instigated early in adulthood. One silver lining of the results in Chapters 2 and 4 is that, while average loss in local bone regions could lead to more frailty in some loading directions over others, global cross-sectional geometric properties among slice locations in all three limb elements do not significantly decrease between the fifth and eighth decades of life. It may be possible that interventions—including active loading, hormone therapies, and other approaches to improve bone retention—during any of these decades may have a positive effect on bone strength. This hypothesis requires further clinical assessment. Additionally, anthropological investigations of cross-sectional geometry in older adults must exercise further caution in interpretations of the effects of activity, mobility, diet, and more on cortical bone. Future studies are necessary for untangling the effects of aging on cortical bone, but this dissertation shows that relying on any one factor as the reason for bone loss with aging is likely to miss other important contributors.

Limitations

The research set forth in this dissertation has limitations that require further consideration. First, the study is cross-sectional by design, meaning age-related changes were not observable, only differences in cortical geometry and cBMD across ages. A longitudinal study is impractical for doctoral research, and so the cross-sectional sampling is justified, but its use does introduce restrictions. Since cross-sectional studies are surveying many individuals to observe patterns, considerable noise is likely clouding patterns in the data. Several factors may contribute to this noise, including differences in genetic background, developmental history, physiological

differences, current and past activity patterns, and environmental factors, to name a few. Some effort was made to mitigate variation due to health conditions, medication, and BMI by establishing eligibility requirements, however these criteria were broadly set to promote wider participation in the study. I have confidence that the trends observed represent decadal means for cortical bone geometry and porosity, but idiosyncrasies among study participants' lifestyles and biology present caution in the variances analyzed in statistical comparisons among groups.

Another limitation is an overall small sample size. Sample sizes were particularly low among males and females between 70-79 years of age, thereby reducing statistical power when participants were subdivided into decadal age groups. This was in part why RDA was chosen for testing age, slice, and BMI effects on cortical distance measurements and cBMD (Chapters 2 and 3), since RDA allowed for age to be treated as a continuous variable over the entire age range, thereby increasing statistical power. When comparing age groups, however, small sample sizes increase the risk of Type II error. Additionally, the sample for this study was mostly white, limiting the studies applicability for non-white individuals. Future studies examining these age-related changes will benefit from a larger, more representative sample size.

Relatedly, I made a conscious decision at the outset of the study to only sample individuals up to 80 years of age. This was set to capture data from pre-, peri-, and postmenopausal women, especially, as well as an age-matched male sample. As I noted above and in other chapters, however, Gooding (2017) indicated that many cross-sectional geometric properties do not significantly decrease by age until advanced decades, namely after 75. Even though her sample of humans was deceased and skeletonized, the general demographics were similar to mine, in that the individuals largely represented white individuals living in the southeastern U.S. Thus,

were the sample to have been extended to individuals in their 80s and 90s, I might have observed significant trends that were not present in my pool of participants.

Additionally, there may have been error introduced during the scanning procedure. As mentioned, the forearms of participants were pronated for scanning of the radius and ulna, but the degree of pronation may have varied among individuals. Additionally, the ulna is relatively perpendicular to the scanner in pronation however the radius is generally at a slight angle given its position, meaning radial scans may not be exactly axial cross-sections. Finally, imaging artifacts may have been introduced from movement or beam hardening. Quality inspection of scans occurred on-site following their completion and repeat scans were performed as needed. Additionally, scan images were inspected for artifacts a second time prior to data processing. However, it is possible that, despite these efforts, some error was introduced through imaging artifacts that were not screened out during quality inspection.

Future Directions

The complicated picture aging presents for cortical bone macrostructure, microstructure, and their interaction opens several avenues for further inquiry. For example, a long-term longitudinal study examining geometry-microstructure interaction at a local level would be beneficial. In such a study, age-related changes within individuals would be observed rather than patterns across a sample. Additionally, longitudinal analysis would reduce inter-individual variation and therefore a clearer pattern might be observed. Further, the extended time period of contact between researchers and participants afforded by a longitudinal study presents an opportunity for a clearer picture of health, activity, and lifestyle habits. For example, the more widespread usage of

smartwatches might be a relatively easy way to measure aspects of activity rather than relying on participant recall of average trends.

This dissertation made use of cBMD to infer microstructural parameters of porosity in our sample. While cortical porosity explains a high amount of cBMD variance (Bousson et al., 2001), this is a coarse measure of microstructure that is likely prone to error from partial volume effects. Future studies would make use of high-resolution CT (or pQCT) imaging to observe porosity more directly. While a longitudinal sampling strategy and higher-resolution scanning might pose higher radiation risk, newer CT technologies have made high resolution, short duration scanning, and low dosage possible. It would be especially interesting to see if local relationship between intracortical porosity and endosteal distance suggested here is observable when porosity is more effectively visualized.

While ontogenetic growth of cortical bone geometry and microstructure was not discussed in detail, there is evidence that patterns established during development carry over to inform bone strength in advanced age (Duan et al., 2003; Oliver et al., 2007; Dennison et al., 2013). It would therefore be interesting to translate local variation during growth (Goldman et al., 2009; Gosman et al., 2013) to the changes observed later in life, particularly since the cortical expansion occurring in old age can be thought of as a continuation of the expansion observed during growth. Additionally, it would be elucidating to see whether patterns in porosity distribution are similar or different to those observed at older ages.

Conclusions

Bone strength is modeled as a product of its geometric configuration and material properties. Both attributes change with age: cortical expansion increases bone diameter while decreasing

cortical thickness, while cBMD declines primarily due to increasing cortical porosity. Local variation has been observed in these age-related changes, however the interaction between macro- and microstructural changes has been relatively understudied. Following a "whole bone" approach, this dissertation examined age-related differences in cortical geometry and cBMD along the length of the tibia, radius, and ulna. Local variation of these properties was also assessed within cross-sectional slices, and the relationships between geometric and density measures were examined through correlation analysis.

Importantly, this dissertation demonstrates that cortical expansion does not occur uniformly throughout a cross-section or at different sites along the length of the long bones. In the tibia, greater changes in endosteal and periosteal distance are seen at more proximal and midshaft slices compared to distally (Chapter 2). Additionally, patterns of intra-slice variation by direction shift along the length of the radius, and to a lesser extent in the ulna (Chapter 2). Local variation is also observed in age-related differences of cBMD within and between cross-sections (Chapter 3). This local variation suggests that local factors mediate systemic processes of aging, possibly through mechanical loading through activity or load-sharing between elements, though, as mentioned, this relationship is not always straightforward. It is also likely that non-mechanical factors are influencing cortical bone shape and microstructure, though that is beyond the scope of this dissertation and should be investigated in future research.

Importantly, the results from Chapter 4 indicate that age-related changes in macrostructure and microstructure are not tightly coupled. The relationships between age-related differences in geometry and microstructure also vary spatially (Chapter 4). Low to moderate correlations are observed between cBMD and cortical thickness/endosteal distance, while differences in periosteal distance appear fairly unrelated to those in cBMD (Chapter 4). Additionally, the

strength of correlations with cortical thickness and endosteal distance mirror patterns of local variation in endosteal distance observed in Chapter 2. This indicates that greater endosteal loss with age is locally linked to lesser average cBMD measurements, likely a result of a continuum of local resorption from the intracortical to endosteal envelopes.

Taken together, this dissertation shows that 1) skeletal aging does not occur evenly in distal limb long bones, and 2) the non-uniformity of skeletal aging is not easily explained by systemic or mechanical explanations alone. The variation in cortical bone properties observed here illustrate how aging is a variable process that is multifactorial, shaped by genetic, developmental, environmental, and behavioral processes. Future research may decipher the layered and likely interacting factors shaping cortical bone in advanced age.

REFERENCES

Agostini, G., Holt, B. M., Relethford, J. H. (2018). Bone functional adaptation does not erase neutral evolutionary information. American Journal of Physical Anthropology 166(3):708-729.

Andreasen, C. M., Delaisse, J.-M., van der Eerden, B. C., van Leeuwen, J. P., Ding, M., & Andersen, T. L. (2018). Understanding Age-Induced Cortical Porosity in Women: The Accumulation and Coalescence of Eroded Cavities Upon Existing Intracortical Canals Is the Main Contributor. Journal of Bone and Mineral Research, 33(4), 606–620.

Andreasen, C. M., Bakalova, L. P., Brüel, A., Hauge, E. M., Kiil, B. J., Delaisse, J.-M., Kersh, M. E., Thomsen, J. S., & Andersen, T. L. (2020). The generation of enlarged eroded pores upon existing intracortical canals is a major contributor to endocortical trabecularization. Bone, 130, 115127–115127.

Auerbach, B. M., Sylvester, A. D. (2011). Allometry and apparent paradoxes in human limb proportions: Implications for scaling factors. American Journal of Physical Anthropology, 144(3), 382–391.

Beaupré, G. S., Orr, T. E., Carter, D. R. (1990). An approach for time-dependent bone modeling and remodeling—theoretical development. J. Orthop. Res., 8: 651-661.

Beck, T. J., Oreskovic, T. L., Stone, K. L., Ruff, C. B., Ensrud, K., Nevitt, M. C., Genant, H. K., & Cummings, S. R. (2001). Structural Adaptation to Changing Skeletal Load in the Progression Toward Hip Fragility: The Study of Osteoporotic Fractures. Journal of Bone and Mineral Research, 16(6), 1108–1119.

Burr, D. B., Martin, R. B. (1993). Calculating the probability that microcracks initiate resorption spaces. Journal of Biomechanics, 26(4), 613–616.

Burr, D. B. (2014). Repair Mechanisms for Microdamage in Bone. Journal of Bone and Mineral Research, 29(12), 2534–2536.

Burr, D. B. (2010). Cortical bone: a target for fracture prevention? The Lancet (British Edition), 375(9727), 1672–1673.

Carina, V., Della Bella, E., Costa, V. et al. (2020). Bone's Response to Mechanical Loading in Aging and Osteoporosis: Molecular Mechanisms. Calcif Tissue Int 107, 301–318.

Carter, D. R., Orr, T. E. (1992). Skeletal development and bone functional adaptation. Journal of Bone and Mineral Research, 7(S2), S389–S395.

Demes, B., Qin, Y.-X., Stern Jr, J. T., Larson, S. G., & Rubin, C. T. (2001). Patterns of strain in the macaque tibia during functional activity. American Journal of Physical Anthropology, 116(4), 257–265.

Duan Y, Beck TJ, Wang X, Seeman E. (2003). Structural and biomechanical basis of sexual dimorphism in femoral neck fragility has its origins in growth and aging. Journal of Bone and Mineral Research 18(10): 1766-1774.

Eleazer, C. D., Jankauskas, R. (2016). Mechanical and metabolic interactions in cortical bone development. American Journal of Physical Anthropology 160: 317-333.

Feik, S. A., Thomas, C. D. L., Bruns R., Clement J. G. (2000). Regional variations in cortical modeling in the femoral midshaft: sex and age differences. American Journal of Physical Anthropology 112:191-205.

Frost, H. M. (1987). Bone "mass" and the "mechanostat": a proposal. The Anatomical Record, 219(1):1-9.

Frost, H. M. (1997). On our age-related bone loss: insights from a new paradigm. Journal of Bone and Mineral Research, 12(10): 1539-1546.

Frost, H. M. (2003). Bone's mechanostat: A 2003 update. The Anatomical Record, 275A(2), 1081–1101.

Goldman, H. M., Hampson, N. A., Guth, J. J., Lin, D., & Jepsen, K. J. (2014). Intracortical Remodeling Parameters Are Associated With Measures of Bone Robustness. Anatomical Record, 297(10): 1817–1828.

Gooding, A. F. (2017). Variation in cortical bone distribution in the aging appendicular skeleton. Doctoral dissertation, The University of Tennessee – Knoxville.

Gosman JH, Stout SD, and Larsen CS. (2011). Skeletal biology over the life span: A view from the surfaces. American Journal of Physical Anthropology, 146(S53):86-98.

Haapasalo, H., Kontulainen, S., Sievänen, H., Kannus, P., Järvinen, M., & Vuori, I. (2000). Exercise-induced bone gain is due to enlargement in bone size without a change in volumetric bone density: a peripheral quantitative computed tomography study of the upper arms of male tennis players. Bone, 27(3), 351–357.

Iqbal, J., Zaidi, M. (2009). Understanding Estrogen Action during Menopause. Endocrinology, 150(8), 3443–3445.

Ireland, A., Maden-Wilkinson, T., Ganse, B., Degens, H., & Rittweger, J. (2014). Effects of age and starting age upon side asymmetry in the arms of veteran tennis players: a cross-sectional study. Osteoporosis International, 25(4), 1389–1400.

Kannus, P., Haapasalo, H., Sankelo, M., Sievänen, H., Pasanen, M., Heinonen, A., Oja, P., & Vuori, I. (1995). Effect of starting age of physical activity on bone mass in the dominant arm of tennis and squash players. Annals of Internal Medicine, 123(1), 27–31.

Kazakia, G. J., Nirody, J. A., Bernstein, G., Sode, M., Burghardt, A. J., & Majumdar, S. (2013). Age- and gender-related differences in cortical geometry and microstructure: Improved sensitivity by regional analysis. Bone, 52(2), 623–631.

Khosla, S. (2013). Pathogenesis of age-related bone loss in humans. The Journals of Gerontology. Series A, Biological Sciences and Medical Sciences, 68(10), 1226–1235.

Lauretani F., Bandinelli S., Griswold M. E., Maggio M., Semba R., Guralnik J. M., Ferruci L. (2008). Longitudinal Changes in BMD and Bone Geometry in a Population-based study. Journal of Bone and Mineral Research 23(3): 400-408.

Lazenby, R. (1986). Porosity-geometry interaction in conservation of bone strength. Journal of Biomechanics, 19(3): 257:258.

Lieberman D.E., Pearson O.M., Polk J.D., Demes B., Crompton A.W. (2003). Optimization of bone growth and remodeling in response to loading in tapered mammalian limbs. Journal of Experimental Biology, 206: 3125-3138.

Macdonald, H. M., Nishiyama, K. K., Kang, J., Hanley, D. A., & Boyd, S. K. (2011). Age-related patterns of trabecular and cortical bone loss differ between sexes and skeletal sites: A population-based HR-pQCT study. Journal of Bone and Mineral Research, 26(1), 50–62.

Manolagas, S. C., O'Brien, C. A., Almeida, M. (2013). The role of estrogen and androgen receptors in bone health and disease. Nature Reviews Endocrinology, 9: 699-712.

McCalden, R. W., McGeough, J. A., Barker MB, Court-Brown CM. 1993. Age-related changes in the tensile properties of cortical bone. The relative importance of changes in porosity, mineralization, and microstructure. J Bone Joint Surg Am., 75(8): 1193-1205.

Meakin, L. B., Galea, G. L., Sugiyama, T., Lanyon, L. E., & Price, J. S. (2014). Age-Related Impairment of Bones' Adaptive Response to Loading in Mice Is Associated With Sex-Related Deficiencies in Osteoblasts but No Change in Osteocytes. Journal of Bone and Mineral Research, 29(8), 1859–1871.

Nirody, J. A., Cheng, K. P., Parrish, R. M., Burghardt, A. J., Majumdar, S., Link, T. M., & Kazakia, G. J. (2015). Spatial distribution of intracortical porosity varies across age and sex. Bone, 75, 88–95.

Pearson, O. M., Lieberman, D. E. (2004). The aging of Wolff's "law": Ontogeny and responses to mechanical loading in cortical bone. American Journal of Physical Anthropology, 125(S39), 63–99.

Pivonka P, Park A, and Forwood MR. (2018). Functional Adaptation of Bone: The Mechanostat and Beyond. In (Pivonka P, editor): Multiscale Mechanobiology of Bone Remodeling and Adaptation. Springer. pp. 1-60.

Rantalainen, T., Nikander, R., Daly, R. ., Heinonen, A., & Sievänen, H. (2011). Exercise loading and cortical bone distribution at the tibial shaft. Bone (New York, N.Y.), 48(4), 786–791.

Razi, H., Birkhold, A. I., Weinkamer, R., Duda, G. N., Willie, B. M., & Checa, S. (2015). Aging Leads to a Dysregulation in Mechanically Driven Bone Formation and Resorption. Journal of Bone and Mineral Research, 30(10), 1864–1873.

Riggs, B. L., Melton, L. J., Robb, R. A., Camp, J. J., Atkinson, E. J., McDaniel, L., Amin, S., Rouleau, P. A., & Khosla, S. (2008). A Population-Based Assessment of Rates of Bone Loss at Multiple Skeletal Sites: Evidence for Substantial Trabecular Bone Loss in Young Adult Women and Men. Journal of Bone and Mineral Research, 23(2), 205–214.

Rosenbaum Chou, T. G., Child, J. R., Naughtin, R. J., Rigdon, R. R., Schumann, C., & Bloebaum, R. D. (2008). The relationship between femoral periprosthetic cortical bone geometry and porosity after total hip arthroplasty. Journal of Biomedical Materials Research. Part A, 87A(1), 107–115.

Rubin, C. T., Bain, S. D., McLeod, K. J. (1992) Suppression of the osteogenic response in the aging skeleton. Calcified Tissue International, 50:306-313.

Ruff, C. B., Hayes, W. B. (1982). Subperiosteal expansion and cortical remodeling of the human femur and tibia with aging. Science 217(4563):945-948.

Ruff, C. B., Hayes, W. C. (1983). Cross-sectional geometry of Pecos Pueblo femora and tibiae: a biomechanical investigation. II. Sex, age, and side differences. Am J Phys Anthropol 60:383–400.

Ruff, C. B. (2000). Body size, body shape, and long bone strength in modern humans. Journal of Human Evolution, 38(2): 269-290.

Ruff, C., Holt, B., & Trinkaus, E. (2006). Who's afraid of the big bad Wolff?: "Wolff's law" and bone functional adaptation. American Journal of Physical Anthropology, 129(4), 484–498.

Russo, C. R., Lauretani, F., Seeman, E., Bartali, B., Bandinelli, S., Di Iorio, A., Guralnik, J., & Ferrucci, L. (2006). Structural adaptations to bone loss in aging men and women. Bone (New York, N.Y.), 38(1), 112–118.

Seeman, E. (2013). Age- and menopause-related bone loss compromise cortical and trabecular microstructure. The Journals of Gerontology. Series A, Biological Sciences and Medical Sciences, 68(10), 1218–1225.

Skedros, J. G., Knight, A. N., Clark, G. C., Crowder, C. M., Dominguez, V. M., Qiu, S., Mulhern, D. M., Donahue, S. W., Busse, B., Hulsey, B. I., Zedda, M., & Sorenson, S. M. (2013). Scaling of Haversian canal surface area to secondary osteon bone volume in ribs and limb bones. American Journal of Physical Anthropology, 151(2), 230–244.

Skedros, J. G. (2012). Interpreting load history in limb-bone diaphyses: important considerations and their biomechanical foundations. In: Crowder C, Stout S, editors. Bone histology: an anthropological perspective. Boca Raton, FL: CRC Press. pp. 153–220.

Skerry, T. M. (2006). One mechanostat of many? Modifications of the site-specific response of bone to mechanical loading by nature and nurture. Journal of Musculoskeletal Neuronal Interactions 6(2): 122-127.

Szulc, P., Seeman, E. (2009). Thinking inside and outside the envelopes of bone: Dedicated to PDD. Osteoporosis international, 20(8): 1281-1288.

Thomas, C. D., Feik, S. A., Clement, J. G. (2005). Regional variation of intracortical porosity in the midshaft of the human femur: age and sex differences. Journal of Anatomy, 206(2), 115–125.

Ural, A., Vashishth, D. (2006). Interactions between microstructural and geometrical adaptation in human cortical bone. Journal of Orthopaedic Research, 24(7), 1489–1498.

Vilayphiou, N., Boutroy, S., Sornay-Rendu, E., Van Rietbergen, B., & Chapurlat, R. (2016). Age-related changes in bone strength from HR-pQCT derived microarchitectural parameters with an emphasis on the role of cortical porosity. Bone, 83, 233–240.

Wallace I. J., Demes, B., Mongle, C., Pearson, O. M., Polk, J. D., & Lieberman, D. E. (2014). Exercise-induced bone formation is poorly linked to local strain magnitude in the sheep tibia. PloS One, 9(6), e99108–e99108.

Wang L., You, X., Zhang, L., Zhang, C., & Zou, W. (2022). Mechanical regulation of bone remodeling. Bone Research, 10(1), 16–16.

Weaver, C. M., Peacock, M. Skeletal Changes Across the Life Span. In: Burr DB, & Allen MR (editors). 2019. Basic and applied bone biology. Second edition. New York: Academic Press.
Weidauer, L. A., Binkley, T. L., Berry, R., Specker, B. L. (2013). Variation in cortical density within the cortical shell of individuals across a range in densities and ages. J Musculoskelet Neuronal Interact, 13(1):89-96.

Wilson, L. A. B., De Groote, I., Humphrey L. T. (2020). Sex differences in the patterning of age-related bone loss in the human hallucal metatarsal in rural and urban populations. American Journal of Physical Anthropology 171(4): 628-644.

Yang, H., Xu, X., Bullock, W., Main, R. (2019). Adaptive changes in micromechanical environments of cancellous and cortical bone in response to in vivo loading and disuse. Journal of Biomechanics 89: 85-94.

VITA

Greg Wehrman grew up in Seneca, South Carolina and received his undergraduate degree in Anthropology from the University of South Carolina in 2014. Following graduation, he attended The University of Tennessee, Knoxville (UTK) to pursue a Master's of Arts in biological anthropology. His M.A. thesis focused on morphometric assessment of cranial modification in bioarchaeological contexts. Greg remained at UTK for his doctoral studies, shifting his research focus to functional anatomy and biomechanics. In 2022, he received a Doctoral Dissertation Research Improvement Grant from the National Science Foundation, allowing him to conduct the dissertation research here using a living sample. Outside of research, Greg cultivated skills and experience in human anatomy education through his teaching assistantship at UTK as well as outside opportunities through Ross University School of Medicine and Marist College. In August 2023, Greg received his PhD in biological anthropology and is joining the faculty at Rowan-Virtua School of Osteopathic Medicine to continue teaching and research.